Design and experimental development of thermoelectric generators for shallow geothermal anomalies of volcanic origin

Ph. D. Dissertation prepared to

obtain the Doctor degree by

Leyre Catalán Ros

upna

Universidad Pública de Navarra
Nafarroako Unibertsitate Publikoa

Supervisors

David Astrain Ulibarrena
Patricia Aranguren Garacochea

Pamplona, 1st September 2020
Engineering Department
Public University of Navarre

Compendium of Publications

The present Ph. D. dissertation is a compendium of the following publications:

- L. Catalan, P. Aranguren, M. Araiz, G. Perez, D. Astrain. **New opportunities for electricity generation in shallow hot dry rock fields: A study of thermoelectric generators with different heat exchangers**. *Energy Conversion and Management* 200 (2019) 112061. DOI: 10.1016/j.enconman.2019.112061
- L. Catalan, M. Araiz, P. Aranguren, D. Astrain. **Computational study of geothermal thermoelectric generators with phase change heat exchangers**. *Energy Conversion and Management* 221 (2020) 113120. DOI: 10.1016/j.enconman.2020.113120
- L. Catalan, M. Araiz, P. Aranguren, G.D. Padilla, P.A. Hernandez, N.M. Perez, C. Garcia de la Noceda, J.F. Albert, D. Astrain. **Prospects of Autonomous Volcanic Monitoring Stations: Experimental Investigation on Thermoelectric Generation from Fumaroles**. *Sensors* 20 (2020) 3547. DOI: 10.3390/s20123547
- L. Catalan, A. Garacochea, A. Casi, M. Araiz, P. Aranguren, D. Astrain. **Experimental evidence of the viability of thermoelectric generators to power volcanic monitoring stations**. *Sensors* 20 (2020) 4839. DOI: 10.3390/s20174839

All the articles have been published in high-quality JCR journals, whose quality indicators are summarized as follows:

- *Energy Conversion and Management*

  Impact factor (2019): 8.208

  Category: Thermodynamics

  Rank: 2/61

  Quartile: Q1

- *Sensors*

  Impact factor (2019): 3.275

  Category: Instruments & Instrumentation

  Rank: 15/64

  Quartile: Q1

Furthermore, since the articles have been performed in co-authorship, the author contributions are detailed below:

- L. Catalan, P. Aranguren, M. Araiz, G. Perez, D. Astrain. **New opportunities for electricity generation in shallow hot dry rock fields: A study of thermoelectric generators with different heat exchangers**. *Energy Conversion and Management* 200 (2019) 112061. DOI: 10.1016/j.enconman.2019.112061

  Leyre Catalan: Methodology, Investigation, Data Curation, Writing - Original Draft, Writing - Review & Editing, Visualization

  Patricia Aranguren: Methodology, Writing - Review & Editing, Supervision

  Miguel Araiz: Methodology, Visualization

  Gurutze Perez: Writing - Review & Editing

  David Astrain: Conceptualization, Writing - Review & Editing, Supervision

- L. Catalan, M. Araiz, P. Aranguren, D. Astrain. **Computational study of geothermal thermoelectric generators with phase change heat exchangers**. *Energy Conversion and Management* 221 (2020) 113120. DOI: 10.1016/j.enconman.2020.113120

  Leyre Catalan: Methodology, Software, Validation, Formal analysis, Investigation, Writing – Original Draft, Writing – Review & Edition, Visualization

  Miguel Araiz: Methodology, Software, Writing – Review & Edition

  Patricia Aranguren: Writing – Review & Edition, Supervision

  David Astrain: Conceptualization, Writing – Review & Edition, Supervision

- L. Catalan, M. Araiz, P. Aranguren, G.D. Padilla, P.A. Hernandez, N.M. Perez, C. Garcia de la Noceda, J.F. Albert, D. Astrain. **Prospects of Autonomous Volcanic Monitoring Stations: Experimental Investigation on Thermoelectric Generation from Fumaroles**. *Sensors* 20 (2020) 3547. DOI: 10.3390/s20123547

  Leyre Catalan: Conceptualization, Data curation, Investigation, Methodology, Software, Visualization, Writing – Original Draft, Writing – Review & Edition

Miguel Araiz: Conceptualization, Investigation, Methodology

Patricia Aranguren: Conceptualization, Writing – Review & Edition

Germán D. Padilla: Methodology, Project administration

Pedro A. Hernandez: Funding acquisition, Project administration

Nemesio M. Perez: Funding acquisition, Project administration

Celestino Garcia de la Noceda: Funding acquisition

Jose F. Albert: Conceptualization, Funding acquisition

David Astrain: Conceptualization, Data curation, Funding acquisition, Methodology, Supervision, Writing – Review & Edition

- L. Catalan, A. Garacochea, A. Casi, M. Araiz, P. Aranguren, D. Astrain. **Experimental evidence of the viability of thermoelectric generators to power volcanic monitoring stations**. *Sensors* 20 (2020) 4839. DOI: 10.3390/s20174839

  Leyre Catalan: Conceptualization, Investigation, Construction and Characterization, Monitoring and Communication Systems, Software, Installation, Analysis of Results, Writing – Original Draft, Writing – Review & Edition

  Amaia Garacochea: Conceptualization, Investigation, Construction and Characterization, Monitoring and Communication Systems, Software, Installation, Analysis of Results

  Alvaro Casi: Conceptualization, Investigation, Construction and Characterization, Installation

  Miguel Araiz: Conceptualization, Investigation, Construction and Characterization, Installation

  Patricia Aranguren: Conceptualization, Writing – Review & Edition

  David Astrain: Conceptualization, Installation, Analysis of Results, Supervision, Writing – Review & Edition

Abstract

In the current energy situation, characterized by an unceasing growing demand and a large dependence on fossil fuels, it is essential to promote efficient systems based on renewable energies that contribute to better exploitation of the resources and are environmentally friendly. In this sense, geothermal energy stands out among other renewable sources due to its permanent nature, being independent of weather conditions. Nevertheless, its contribution to the global energy system is minimal, especially towards electricity generation.

As an alternative to the traditional cycles used for geothermal power generation, the present Ph. D. dissertation proposes the use of thermoelectric generators due to their multiple advantages such as reliability, durability, and scalability. More specifically, this thesis focuses on shallow geothermal anomalies of volcanic origin for two different applications: medium–scale power generation from hot dry rock fields, and stand–alone power supply of remote volcanic vigilance stations.

Due to the importance of the heat exchangers in the total efficiency of thermoelectric generators, initially, a deep study to determine which heat exchangers are more appropriate has been conducted. In both applications, it has been experimentally demonstrated that the most suitable heat exchangers are those based on phase change, since apart from presenting low values of thermal resistance, do not require moving parts nor auxiliary equipment, thus minimizing maintenance.

Additionally, it has also been of great importance to develop a quick and reliable computational model that takes into account the heat exchangers and the heat reservoirs, that does not neglect any thermoelectric effect, and that considers the thermal and electrical contacts as well as the influence of temperature on the properties. This model, programmed based on the finite difference method or thermal–electrical analogy, has become a true design and optimization tool for the two applications subject of study in this Ph. D. dissertation, thanks to its relative error of less than 8 %.

The first studied application focuses on the medium–scale power generation in hot dry rock fields. The utilization of thermoelectric generators with phase change heat exchangers in this type of geothermal fields entails a more environmentally friendly alternative in comparison with enhanced geothermal systems, the only technique existing nowadays, which requires rock fracture and as a result, it is not used. Taking as reference the shallow geothermal anomalies located at Timanfaya National Park (Canary Islands, Spain), it has been experimentally demonstrated the viability of the proposed technology, with a generation of 3.3 W per module, 54 % more than with fin dissipators, evincing that the developed heat exchangers permit maximizing the temperature difference between the sides of the thermoelectric modules, approaching it to the available one between the heat source and sink and therefore, maximizing the efficiency. This result has served as basis for the optimization and construction of a new prototype with promising potential, being able to produce more than 680 MWh per year thanks to its scalability.

On a completely different scale, the second application aims the stand–alone power supply of volcanic vigilance stations. These stations become indispensable in order to predict future eruptions and therefore, reduce their risks. Nevertheless, due to their remoteness, obtaining autonomous, robust, and resistant power sources is an absolute challenge. This Ph. D. dissertation has demonstrated that thermoelectric generators can solve these problems, transforming the heat emitted by volcanic fumaroles directly into electricity reliably and without maintenance requirements, being able to generate up to 0.75 W in 83 °C fumaroles with the proposed design. This generation is enough to power the sensors used to detect the precursors of the volcanic eruptions, as has been evinced with the system installed at Teide volcano (Canary Islands, Spain), which has been in operation without signs of degradation for more than 8 months, monitoring several variables and emitting their data every 4 minutes to a center located 14 km away, just with the energy produced by only one thermoelectric module.

The results derived from this Ph. D. dissertation demonstrate that thermoelectricity can solve the power supply issues in hot dry rock fields and volcanic monitoring stations, two unprecedented applications of thermoelectric generation that can make this technology finally become a reality in the civil sphere.

Resumen

En el contexto energético actual, caracterizado por un incesante aumento en el consumo de energía y una gran dependencia de los combustibles fósiles, resulta imprescindible apostar por sistemas eficientes y basados en energías renovables que contribuyan a un mejor aprovechamiento de los recursos y sean respetuosos con el medio ambiente. En este sentido, la energía geotérmica destaca entre otras fuentes renovables por su carácter permanente, al no depender de las condiciones meteorológicas. Sin embargo, su contribución al sistema energético mundial es mínimo, sobre todo en generación de electricidad.

Como alternativa a los ciclos que tradicionalmente se emplean para la generación eléctrica geotérmica, esta tesis doctoral propone la utilización de generadores termoeléctricos debido a sus numerosas ventajas tales como fiabilidad, durabilidad y escalabilidad. Concretamente, la tesis se centra en anomalías geotérmicas superficiales de origen volcánico para dos aplicaciones distintas: la generación eléctrica de media escala en yacimientos de roca caliente seca y el abastecimiento autónomo de estaciones de vigilancia volcánica.

Dada la importancia de los intercambiadores de calor en la eficiencia total del sistema, en ambas aplicaciones se ha realizado un profundo estudio para determinar qué tipo de intercambiadores de calor son los más adecuados. En ambos casos, se ha demostrado experimentalmente que los intercambiadores de calor más propicios son aquellos basados en el cambio de fase, ya que aparte de presentar bajas resistencias térmicas, no tienen partes móviles ni requieren de equipos auxiliares, minimizando así el mantenimiento.

Asimismo, también ha resultado de gran importancia el desarrollo de un modelo computacional rápido y fiable que tenga en cuenta los intercambiadores de calor, la fuente de calor y el sumidero, sin despreciar ningún efecto termoeléctrico, y considerando los contactos térmicos y eléctricos y la influencia de la temperatura en las propiedades. Este modelo, programado en base al método de las diferencias finitas, se ha convertido en una verdadera herramienta de diseño y optimización para las dos aplicaciones objeto de estudio en esta tesis doctoral, gracias a su error relativo menor al 8%.

La primera aplicación estudiada se centra en la generación eléctrica de media escala en yacimientos de roca caliente seca. La utilización de generadores termoeléctricos con intercambiadores de calor bifásicos en este tipo de yacimientos supone una alternativa más respetuosa con el medio ambiente que la única técnica existente en la actualidad, que requiere fracturar la roca y por tanto no se emplea. Tomando como referencia las anomalías geotérmicas superficiales del Parque Nacional de Timanfaya (Islas Canarias, España), se ha demostrado experimentalmente la viabilidad de la tecnología propuesta, con una generación por módulo de 3,3 W, un 54% más que si se empleasen disipadores de aletas, poniendo de manifiesto que los intercambiadores de calor desarrollados permiten maximizar el salto térmico entre las caras de los módulos termoeléctricos, acercándolo al disponible entre focos y maximizando la eficiencia. Este resultado ha servido de base para la optimización y construcción de un nuevo prototipo que presenta un potencial muy prometedor, pudiendo generar más de 680 MWh al año gracias a su escalabilidad.

En otra escala completamente diferente, la segunda aplicación tiene como objeto el abastecimiento autónomo de estaciones de vigilancia volcánica. Este tipo de estaciones resultan imprescindibles para la predicción de futuras erupciones y por consiguiente, la reducción de sus daños. Sin embargo, dado su carácter remoto, el abastecimiento de energía de manera autónoma, robusta y resistente a todo tipo de condiciones meteorológicas supone un auténtico reto. Esta tesis ha demostrado que los generadores termoeléctricos son capaces de resolver esta problemática, transformando el calor emitido por las fumarolas volcánicas directamente en electricidad de manera fiable y sin necesidades de mantenimiento, pudiendo proporcionar con el diseño propuesto una potencia de hasta 0,75 W por módulo en fumarolas a 83 °C. Esta generación es suficiente para abastecer los sensores empleados para detectar los precursores de erupciones volcánicas, tal y como ha evidenciado el sistema instalado en el volcán del Teide (Islas Canarias, España), el cual lleva en funcionamiento más de 8 meses sin signo alguno de degradación, monitorizando diferentes variables y emitiéndolas cada 4 minutos a un centro ubicado a más de 14 kilómetros de distancia, todo ello con la energía generada por un único módulo termoeléctrico.

De esta manera, los resultados derivados de esta tesis doctoral demuestran que la termoelectricidad puede solucionar las problemáticas de generación eléctrica en los yacimientos de roca caliente seca y en las estaciones de monitorización volcánica, dos aplicaciones inéditas de generación termoeléctrica que pueden hacer que esta tecnología se convierta por fin en una realidad en el ámbito civil.

Agradecimientos

"Si quieres ir rápido camina solo, si quieres llegar lejos ve acompañado". En mi caso, he tenido la suerte de estar muy bien acompañada a lo largo de estos tres apasionantes años, rodeándome de magníficas personas a las cuales no puedo dejar de dedicarles unas líneas de agradecimiento.

A mis directores de tesis, David y Patricia, por la relación de confianza y afecto que hemos mantenido durante la tesis y por vuestro apoyo en los aspectos técnicos, especialmente en los momentos más complicados de la investigación.

A mis compañeros de grupo ITF por todos los momentos que hemos pasado dentro y fuera del laboratorio, que hacen que trabajar con vosotros sea un auténtico placer. En especial me gustaría destacar a Miguel por ser el mejor espejo en el que mirarse, a Álvaro Casi por ser el mejor maestro montador que puede haber, a Amaia Garacochea, por contagiar tu energía y pasión allá dónde vas, no rendirte y creer en lo imposible, a Amaya Merino, por ser mi *Pon* durante el tiempo que nos acompañaste, y a Patricia Alegría, por tu incesante esfuerzo para hacer que los prototipos fuesen una realidad.

A las grandes actrices de la obra "Yo quiero ser científica". Edurne, Aránzazu, Gurutze, Idoia, Alicia, Marisol, Silvia, Patricia y Nora, sois la mejor inspiración que se puede tener.

A los miembros del grupo Ingeper, por hacerme una más del grupo y acogerme en todos los planes, y a los compañeros de APERNA, por hacer que la universidad sea algo más que un lugar de estudio y trabajo.

A Pepe Albert por embarcarnos a todos en esta gran aventura y nunca dejar de soñar.

A mis compañeros canarios, especiamente a Vidal, por ser más amigo que compañero, hacerme que me enamorase de Guayota y de las afortunadas Islas Canarias, y contagiarme la pasión por el software y la atención a los detalles.

A mis amigas por las grandes expectativas que tienen en mi y por los buenos momentos que pasamos juntas y que son tan necesarios para afrontar con motivación cada nueva

semana.

A Alberto por ser mi apoyo día a día, compartir mis días buenos y los no tan buenos, creer en mi, y hacerme ver las cosas desde otras perspectivas. Eres el mejor compañero de vida que se puede tener.

Y por último, pero no menos importante, a mi familia, en especial a mis padres. Soy quien soy gracias a vosotros, y sin vuestro ejemplo, cariño y apoyo esta tesis no habría sido posible.

Muchas gracias.

Contents

List of Acronyms

CHE	Cold–side Heat Exchanger
EGS	Enhanced Geothermal System
FD	Fin Dissipator
GTEG	Geothermal Thermoelectric Generator
HDR	Hot Dry Rock
HHE	Hot–side Heat Exchanger
IoT	Internet of Things
LPWAN	Low Power Wide Area Network
LT	Loop Thermosyphon
MPPT	Maximum Power Point Tracker
ORC	Organic Rankine Cycle
RTG	Radioisotope Thermoelectric Generator
TEG	Thermoelectric Generator
TEM	Thermoelectric Module
TPCT	Two Phase Closed Thermosyphon

Chapter 1

State of the Art and Objectives

1.1 Introduction

Despite the efforts made all over the world, society still depends enormously on fossil fuels. According to the International Energy Agency, 81.2 % of the world's total primary energy supply came from fossil fuels in 2018 [IEA2020a]. This percentage share has barely changed since the 1970s, when fossil fuels accounted for 86.3 %. However, the net supply has unceasingly increased, reaching 14 282 Mtoe in 2018, more than 2.5 times the supply in 1971 [IEA2020a]. Both the growing demand and the large dependence on limited resources are the key aspects responsible for the actual energy problem. A complex issue that encompasses traits of scientific, technological, economic, environmental, sociological, and political nature.

Considering this scenario, two main trends have emerged in the last decades. On the one hand, there has been increasing awareness regarding the necessity of making a rational use of energy, avoiding its wasting. In this sense, different *energy efficiency* policies have been implemented. As a result, in the last years, a reduction in the global energy intensity has been detected, i.e. it has been possible to improve the gross domestic product of the countries per unit of consumed energy. Without the adopted measures, in 2018, the energy–related greenhouse gas emissions would have been more than 15 % higher [IEA2019].

On the other hand, the use of *renewable energies* has been encouraged, promoting a sustainable and decentralized energy system that is independent of exporting countries or price fluctuations and therefore more competitive. Nevertheless, although these energies have expanded at a fast pace during the last years, nowadays they just account for less than 14 % of global energy production, mainly due to biofuels and waste (9.3 %) and hydropower

(2.5 %) [IEA2020a]. It is towards electricity generation that they have a larger, but still insufficient, contribution: 26 % [IEA2020b].

Taking into account the future perspectives of renewable energies, the present Ph. D. dissertation concentrates on one of the largest renewable sources [UN2000]: *geothermal energy*, or in other words, the heat contained within the Earth. In comparison with other sustainable sources, geothermal energy stands out because it can provide both heat and electricity, it is unaffected by weather, it is stable, it has a high capacity factor, it can be used as base–load power, and it has a high thermal efficiency. However, despite these advantages, it is still positioned behind other renewable energies, especially in electricity generation, with only 13.9 GW installed accounting for less than 0.4 % of global electricity production [REN21-2020].

Li et al. identified that the reasons causing the low growth rate of geothermal power are the high initial investment, the long payback and construction time, as well as the difficulties assessing the resource and modularizing [Li2015]. In order to speed up its growth, they pointed out three possible directions: co–produced geothermal power from oil/gas fields, enhanced geothermal systems, as well as development and utilization of new technologies such as thermoelectric generators. The present Ph. D. dissertation focuses on the latter, developing a novel and alternative generating system to transform geothermal heat into electricity.

Thermoelectricity is the branch of thermodynamics that deals with the study of phenomena in which heat and electricity take part at the same time, and it is based in a series of interactions that were discovered in the 19^{th} century: Joule, Seebeck, Peltier, Thomson, Hall, Nernst, Ettingshausen and Righi–Leduc. Nonetheless, only the first four cause a significant macroscopic influence [Rowe2006].

Joule effect is the well–known interaction between an electric phenomenon (the conducting of an electric current) and its associated thermal one (the heating of the conductive material where the current flows). Matter offers some resistance to the movement of electrons, which release kinetic energy in the successive collisions. This energy is dissipated as heat and it is proportional to the internal electrical resistance of the material R_0 and the square of the intensity of the current I, as indicated in Equation 1.1.

$$\dot{Q}_{Joule} = R_0 \cdot I^2 \tag{1.1}$$

Seebeck effect denotes that given a circuit formed by two different materials, "A" and "B", connected by their ends, if these unions are maintained at a different temperature,

an electromotive force (Et) appears. This electromotive force depends on the Seebeck coefficient (α) of each of the materials as well as on the temperature difference between the unions, as depicted in Equation 1.2.

$$\frac{dEt}{dT} = \alpha_A - \alpha_B \tag{1.2}$$

In contrast to the Seebeck effect, *Peltier effect* consists in the cooling or heating of the union between two materials when an electric current is flowing. This cooling or heating depends on the Seebeck coefficient of each material, the current intensity, and the temperature of the union, according to Equation 1.3.

$$\dot{Q}_{Peltier} = \pm I \cdot T \left(\alpha_A - \alpha_B\right) \tag{1.3}$$

Lastly, *Thomson effect* deals with the absorption or generation of heat in a material presenting a temperature gradient and in which there is an electric current flowing. Its value is indicated by Equation 1.4, where σ is the Thomson coefficient.

$$\dot{Q}_{Thomson} = -\sigma \vec{I} \left(\overrightarrow{\Delta T}\right) \tag{1.4}$$

This Thomson coefficient is related with Seebeck effect by means of the Kelvin relation shown in Equation 1.5.

$$\sigma = T \cdot \frac{\partial \alpha}{\partial T} \tag{1.5}$$

Based on the previous interactions, thermoelectric devices are capable of directly transforming heat into electricity, which is known as *thermoelectric generation* and it is of interest in the present Ph. D. dissertation, or conducting the inverse process, converting electricity into heat, which receives the name of *thermoelectric cooling*. The devices belonging to both lines resemble conventional thermal machines destined for cooling, heating, or electricity generation (air conditioning devices, refrigerators, heat pumps, or motors), with the difference that in this case, an electron current acts as working fluid. This characteristic, in conjunction with the absence of moving parts, converts them into robust, compact, and noiseless equipment, capable of operating in any position.

The transformation itself occurs in the thermoelectric modules. As shown in Figure 1.1, a conventional thermoelectric module is made up of various thermocouples connected electrically in series to increase the operating voltage, and thermally in parallel to increase the thermal conductance. Each couple itself is typically composed of two semiconductor

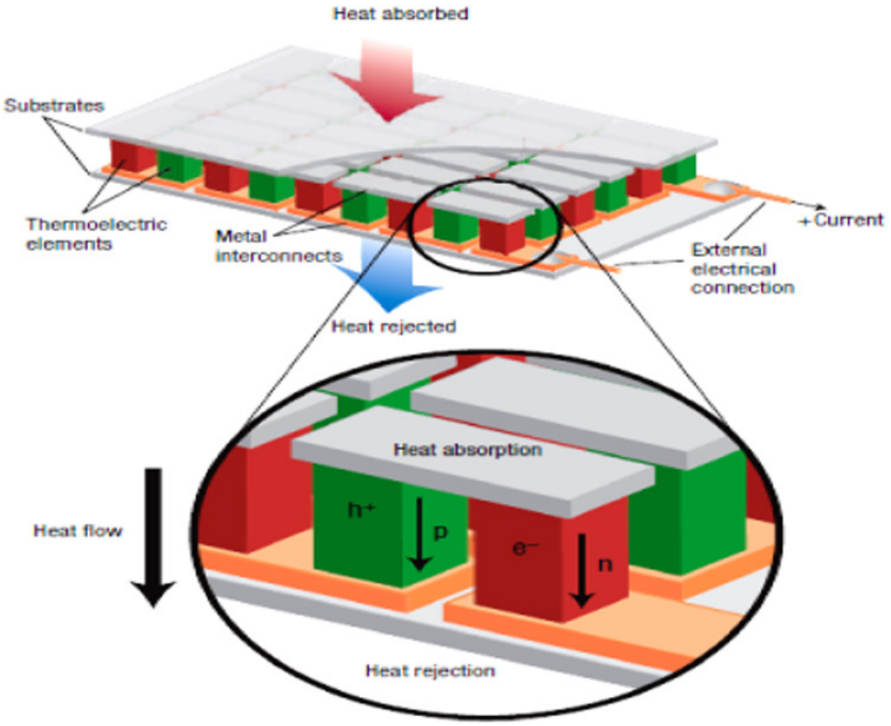

Figure 1.1: Thermoelectric module and thermocouple. *Reprinted with the permission from [Dey2016], in turn adapted from [Snyder2008].*

thermoelements (an n–type one, in which free electrons predominate, and a p–type one, dominated by free holes) connected by a metal conductor. Two rigid substrates of ceramic material provide mechanical firmness to the whole system and isolate the internal circuit.

Neglecting the effect of the union between semiconductors, the efficiency of a thermocouple, defined as the ratio between the electric power generated P and the absorbed heat flux $\dot{Q}$, can be approximated by the following relation for an optimal electric load [Rowe2006]:

$$\eta_{max} = \frac{P}{\dot{Q}} = \frac{T_H - T_C}{T_H} \cdot \frac{\sqrt{1+ZT}-1}{\sqrt{1+ZT}+\frac{T_C}{T_H}} \tag{1.6}$$

where T represents the working temperature of the thermocouple, average between the temperature of the hot and the cold sides T_H and T_C respectively; and Z is the figure of merit defined by Equation 1.7, which is a function of the Seebeck coefficient α, the thermal conductivity k (both lattice and carrier) and the electrical resistivity ρ of the material.

$$Z = \frac{\alpha^2}{k \cdot \rho} \tag{1.7}$$

As can be observed, the maximum efficiency of a thermocouple is basically the product of Carnot efficiency and a factor in which the dimensionless parameter ZT is the most important element. Hence, the efficiency of a thermocouple, and by extension of a thermoelectric module, is directly related to the capability of the material as energy converter. The ideal thermoelectric material should present a high Seebeck coefficient, thus permitting an elevated voltage; low electrical resistivity, in order to minimize Joule effect; and low thermal conductivity, so that the thermal gradient between the sides of the thermoelectric module is maximized. Nevertheless, this is not an easy task as the three parameters that define Z closely depend on one another, being strongly coupled through the carrier concentration [Zhou2018].

Figure 1.2 depicts the typical values of thermoelectric efficiency for different values of ZT. Currently available thermoelectric materials present a ZT of around 1 [Champier2017]. Therefore, only efficiencies lower than 10 % can be achieved. In the figure, it can also be observed that the efficiency of the system increases with the temperature difference across the thermoelectric modules. Hence, as shown in Figure 1.3, thermoelectric generators also include heat exchangers at both sides of the thermoelectric modules, with the purpose of approaching the temperatures of their sides, T_H and T_C, to the ones of the heat source and sink respectively, thus increasing the temperature difference between the sides of the thermoelectric modules, ΔT_{TEM}, and therefore the generated power P.

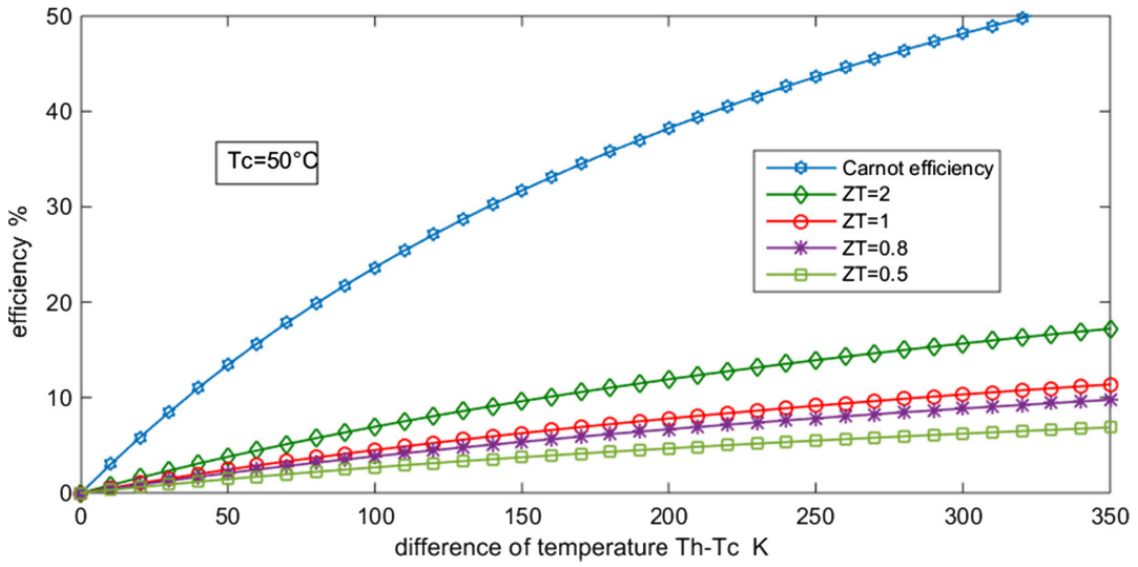

Figure 1.2: Typical values of thermoelectric efficiency for different values of ZT. *Reprinted with the permission from [Champier2017].*

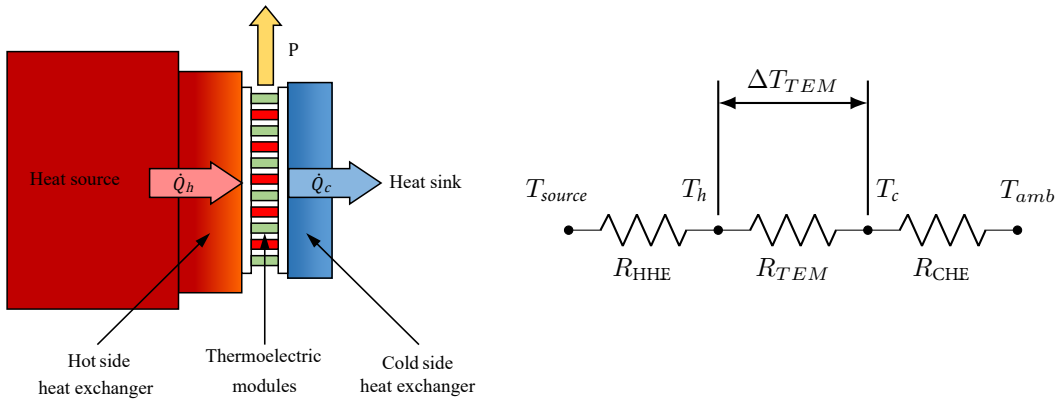

Figure 1.3: Schematics of a thermoelectric generator and its electrical analogy.

The low efficiency characteristic of thermoelectric generators has limited their use in commercial applications. Nevertheless, there exist some cases in which these devices can become the best alternative due to their well–known advantages, such as reliability, robustness, durability, lack of maintenance, and scalability [Champier2017]. This is the case of the two applications to be analyzed in this Ph. D. dissertation, which are specifically focused on shallow geothermal anomalies of volcanic origin.

The first application deals with medium to large scale geothermal power generation from Hot Dry Rock fields (HDR). Traditionally, in order to generate power from the heat contained within the Earth, a geothermal system is required (Figure 1.4). Geothermal systems are characterized by three elements: a heat source, which is normally caused by a magmatic intrusion; a fluid that acts as heat carrier, typically meteoric water from rainfalls either in liquid or vapor state; and a reservoir from which the circulating fluids extract heat [Dickson2004]. The essence of electricity generation from geothermal systems is the conventional expansion of vapor in a turbine, producing a rotational movement that generates electricity in an alternator. Depending on the temperature of the geothermal system, conventional Rankine cycles (either directly with dry steam plants or after flash vaporization), organic Rankine cycles (ORC) or Kalina cycles are used.

Hot dry rock fields, as indicated by their name, are characterized by a body of compact and hot rocks. Thus, both the fluid that acts as heat carrier and the reservoir are absent. Nowadays, there only exists one methodology for power generation from these fields, which consists in the artificial implementation of the lacking elements, leading to

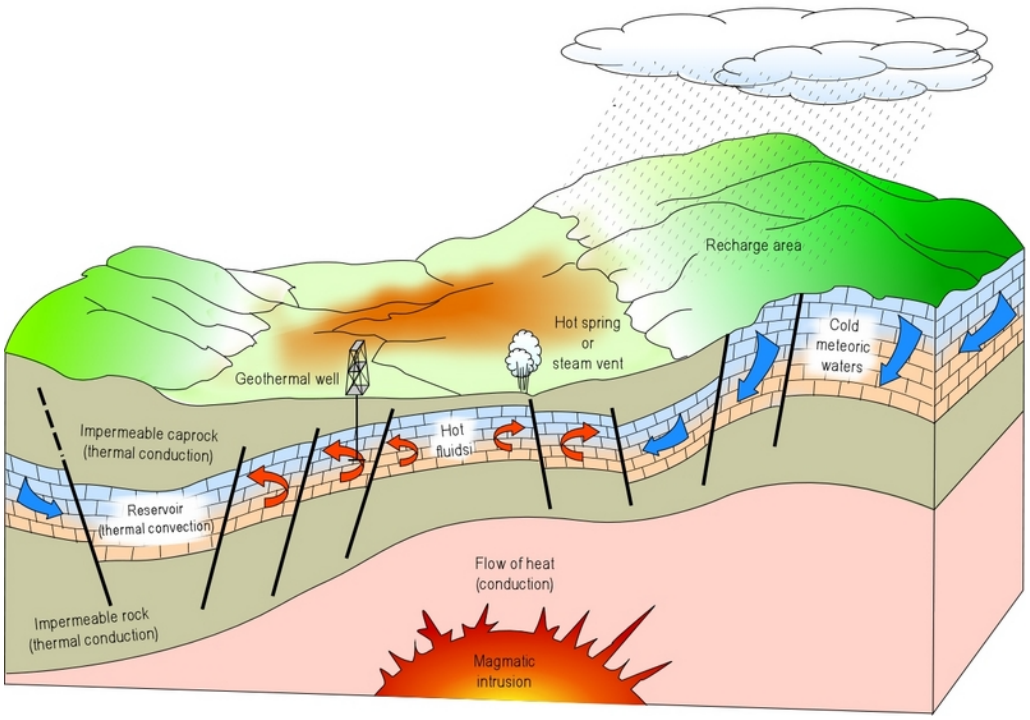

Figure 1.4: Schematic representation of a traditional geothermal system. *Source: International Geothermal Association* [Dickson2004].

an Enhanced Geothermal System (EGS). In these systems, firstly, high–pressure water is pumped through a specially drilled well into the body of rocks causing its hydraulic fracturing and creating a human–made reservoir. After that, the injection of the fluid at high enough pressures holds open the interconnected network of joints created against the earth stresses and forces its circulation in order to effectively exchange heat. The most critical issue associated with this method is the induction of seismicities. As an alternative with less environmental impact, the present Ph. D. dissertation studies, for the first time, the use of geothermal thermoelectric generators from those HDR that are considered shallow.

On another scale, the second application of this Ph. D. dissertation is oriented to the stand–alone power supply of remote volcanic monitoring stations. Since volcanoes are one of the most dangerous natural hazards, their vigilance results indispensable so that the precursors of volcanic eruptions are detected and their damage can be minimized. For this purpose, it is necessary to install several data acquisition and communication equipment in remote locations where normally there is no power grid. Nowadays, the power supply is obtained by means of photovoltaic panels and batteries. However, this solution does not guarantee a permanent energy supply in all locations due to the severe conditions characteristic of some volcanoes, with long snow periods that can cover the

photovoltaic panels or in extreme latitudes and therefore without sun during months. As a solution, the present Ph. D. dissertation proposes thermoelectric generators to supply the low power required by the stations by transforming the heat available at volcanic fumaroles directly into electricity, making them completely autonomous regardless of the environmental conditions.

The development of the former applications is encompassed in the research project ELECTROVOLCAN, founded by the Spanish Ministry of Science, Innovation, and Universities under the grant RTC–2017–6628–3, which focuses on the geothermal anomalies located in the Canary Islands (Spain). For this purpose, the project consortium, composed of the Institute of Technology and Renewable Energies (ITER), the Volcanological Institute of the Canary Islands (INVOLCAN), the Insular Agency of Energy of Tenerife (AIET), the Spanish Geological and Mining Institute (IGME), GAIA Geothermal Energy and Mineral Waters, Constante Group, and the Thermal and Fluids Engineering Research Group ITF from Public University of Navarre (UPNA), counts on a budget of 1 254 649 € during 3 years.

The Canary Islands are an archipelago of volcanic origin located in the Atlantic Ocean, in front of the African northwest coast, that presents the highest geothermal potential in Spain. Among the eight islands that compose the archipelago, Lanzarote and Tenerife are of interest for the project (Figure 1.5). Lanzarote is the eastern island in the archipelago and hosts Timanfaya National Park, one of the most significant HDR fields in the world, both in extension and intensity, with more than 11 700 m^2 of geothermal anomalies with temperatures of 100–400 °C at ground level and 210–550 °C at a depth of 5–10 m [Diez-Gil1987, IGME1992, Gomez-Ortiz2019].

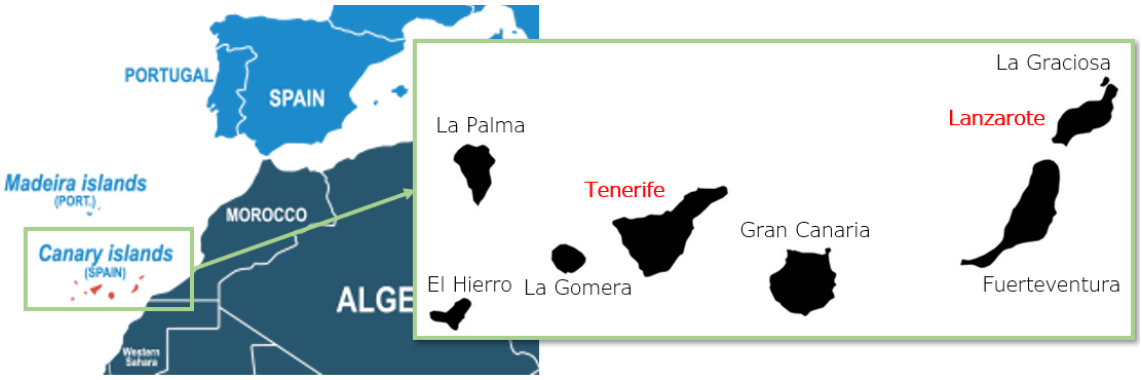

Figure 1.5: Location of the Canary Islands (Spain). Among the eight islands that compose the archipelago, Lanzarote and Tenerife are of interest for ELECTROVOLCAN project.

Due to the geographic isolation of the Canary archipelago, since the 1980s there have existed different projects oriented to the characterization of the geothermal anomalies located within the protected area of Timanfaya National Park due to their elevated temperatures [IGME1992]. Nevertheless, ELECTROVOLCAN is the first one focused on electricity generation, for which the results from the previous projects will be of great interest, especially those related to thermodynamic aspects, which are summarized below.

Firstly, it was demonstrated that the low thermal diffusivity of the superficial hot rock ($8 \cdot 10^{-4}$ cm^2/s) complicates the heat transfer by conduction and causes a slow recovery of the system after heat extraction. Figure 1.6 shows the temperature evolution of a borehole in which water was introduced 30 hours after commencing the experiment. As can be observed, in more than 60 hours the system was not able to return to the initial state. Consequently, it was concluded that conduction is not a viable heat transfer mechanism and convection needs to be used.

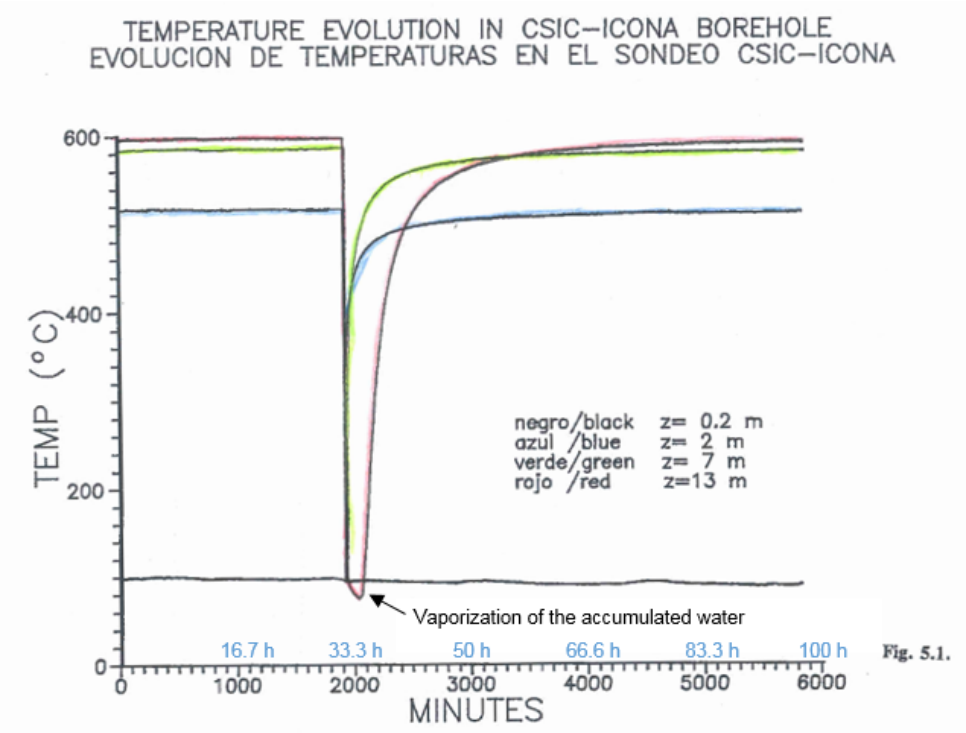

Figure 1.6: Temperature evolution of a borehole in the experiment to determine the conduction capability of the rocks. *Adapted with the permission from [IGME1992].*

Based on the previous statement, different experiments intended to evaluate the gas fluxes that naturally ascend from the boreholes were performed. Hence, two different locations within the park were characterized. *Islote Hilario*, with an extension of 3000 m^2, is the location with the highest temperatures. As depicted in Figure 1.7(a), at ground

level temperatures of 450 °C are measured, which increase with depth up to 580 °C. In *Casa de los Camelleros*, with an extension of 2000 m^2, the temperature range is lower, with maximum temperatures at ground level of 215 °C, and of less than 300 °C at higher depths. Apart from temperature measurements, the velocity of the upcoming gases was also measured in different boreholes. Thus, in *Islote Hilario*, the gases present a velocity of 11.15 m/s, while in *Casa de los Camelleros* is of 6.03 m/s.

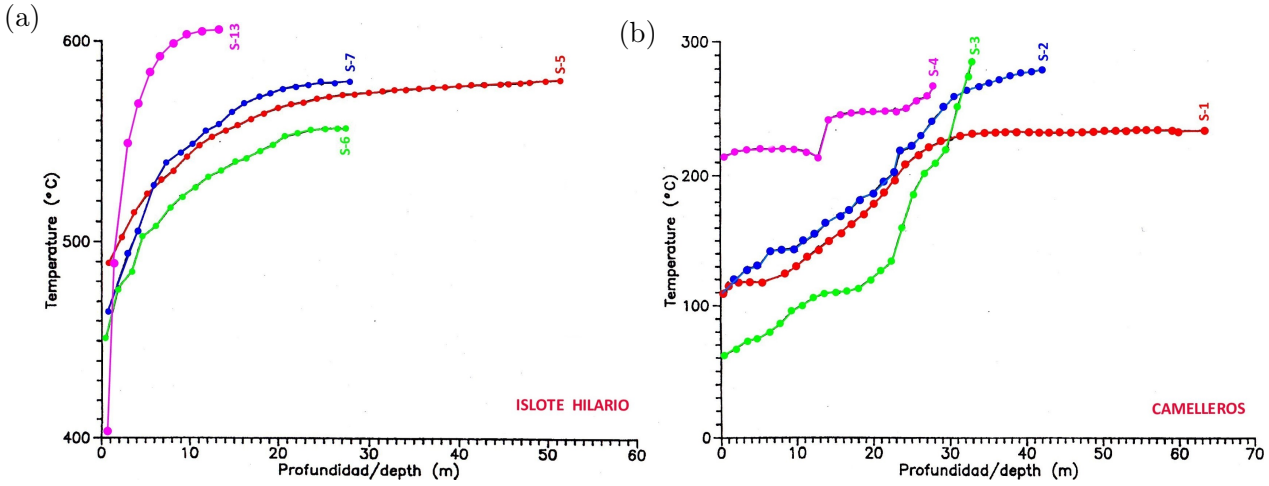

Figure 1.7: Temperature of the volcanic gases with respect the depth in **(a)** Islote Hilario and **(b)** Casa de los Camelleros.

On its behalf, Tenerife is the biggest island in the archipelago and presents a landscape molded by several volcanoes. Teide is not only the highest volcano on the island, with an altitude of 3718 m, but also the third highest volcano in the world from its base on the seafloor (Figure 1.8(a)). This volcano is one of the most evident manifestations of the active volcanism of the islands, which, among other phenomena, reveals in the form of fumaroles (Figure 1.8(b)). These fumaroles present a temperature of around 83 °C, which corresponds with water vaporization temperature at that height, and an average volumetric composition of 83 % water vapor and 17 % volcanic gases, mainly CO_2 (99.225 %), but also other gases in lower proportions: 0.375 % nitrogen N_2, 0.275 % hydrogen H_2, 0.1225 % hydrogen sulfide H_2S and 0.0025 % ammonia CH_4 [Alonso2019, Melian2012]. Figure 1.9 depicts one of the existing monitoring stations located at Teide volcano to monitor the activity of the volcano and predict future eruptions.

Once introduced the context of the present Ph. D. dissertation, Section 1.2 reviews the related state of the art. Afterwards, the motivation of the thesis is explained in Section 1.3, the objectives detailed in Section 1.4, and the structure of the following chapters covered in Section 1.5.

Figure 1.8: **(a)** Teide volcano, located in Tenerife, with an altitude of 3718 m. **(b)** Fumaroles, one of the most evident manifestations of the activity of the volcano.

Figure 1.9: Volcanic monitoring station located at Teide volcano.

1.2 State of the Art

Nowadays, the development of thermoelectric generation presents two parallel research lines. On the one hand, there is an important investigation branch focused on materials, which deals with both the search of new materials and the optimization of available ones so that the efficiency of the thermoelectric modules is improved. On the other hand, there exists another research line focused on the application of thermoelectric generators developed with the actual resources to different fields. This line includes the design and optimization of the thermoelectric generators taking into account not only the thermoelectric modules, but also the rest of the components that compose these generators, such as the heat exchangers, the assembly systems, or the inter–phase materials.

The present Ph. D. dissertation is encompassed in the second research line, developing thermoelectric generators able to transform shallow geothermal heat of volcanic origin into electricity for two different applications. For this purpose, an optimization of all the involved components would be necessary, especially the heat exchangers. Therefore, the state of the art exposed in this section is mainly focused on the applications of thermoelectric generators and on the study of the different heat exchangers that are typically employed in these devices. Nonetheless, due to the importance of thermoelectric materials, a brief review of the most relevant research in this topic is also performed.

Subsection 1.2.1 describes some of the existing applications, in which the viability of this technology has been proven. In this part, the applications that use geothermal energy as heat source are emphasized. Afterwards, Subsection 1.2.2 analyzes the main heat exchangers installed in geothermal thermoelectric generators in order to increase the temperature difference between the sides of the thermoelectric modules, and therefore, obtain a higher generation. The composition of these thermoelectric modules and the advances in thermoelectric materials is briefly analyzed in Subsection 1.2.3. Finally, Subsection 1.2.4 deals with the most common computational approaches for the modelization of thermoelectric generators.

1.2.1 Thermoelectric Applications

As exposed in the introduction, thermoelectric generators present several advantages: electricity generation regardless of the thermal level of the heat source; direct energy conversion, avoiding the intermediate transformation of thermal energy into mechanical one; no moving parts nor working fluids inside the thermoelectric modules, and therefore noiseless operation; possibility to work in any position or environment; and scalability, being able

to be used for micro–generation or to produce kilowatts, simply modifying the number of thermoelectric modules installed.

Nevertheless, despite their numerous advantages, the development of thermoelectric generators has been limited by their low efficiency and high cost. Hence, for many years they have just been restricted to space applications where their extreme reliability and lack of maintenance justified their use. Nonetheless, in the last years, different applications are emerging, taking advantage of their benefits. This section describes some of these applications, insisting on those that use geothermal energy as heat source.

Spatial applications

Electricity generation in aerospace represents the first and most important application of thermoelectric generation [Abelson2006]. Space exploration requires extremely reliable systems that guarantee the power supply of all the equipment during extended periods of time in which maintenance cannot be performed. Therefore, the space industry has been using thermoelectric generators since the beginning of the conquest of space in combination with thermal generators based on nuclear technology: the heat generated from the natural decay of radioactive isotopes such as uranium–235 or plutonium–238 serves as heat source for high power thermoelectric generators. These are the so–called Radioisotope Thermoelectric Generators (RTGs) that have been installed in more than twenty manned spacecrafts, spatial probes, and satellites.

Voyager probes are one of the best examples of durability and reliability. Initially launched in 1977 with the objective of studying the planetary systems of Jupiter and Saturn, these probes have exceeded the expectations and now, after more than 40 years, they are still in operation exploring the outer boundary of the heliosphere in interstellar space [JPL2020]. Nonetheless, due to the degradation of the nuclear fuel and the thermoelectric materials, the generated power has diminished from the initial 453 W to the current 250 W, forcing to disconnect some of the equipment [Champier2017].

Besides Voyager, thermoelectric generators have also been included in the navigation satellite Transit (1961), in the weather satellite Nimbus (1969), in the Apollo projects for lunar inspection (1969–1972), in the Viking plans for martial exploration (1975), as well as in the probes Pioneer (1972), Galileo (1989), Ulysses (1990), Mars–96 (1996), Cassini (1997) and New Horizons (2006) [NASA2020a]. More recently, a 250 W RTG was part of the vehicles of the MSL–Curiosity mission in Mars, launched in November 2011, which represents the first application of an RTG to a Martian rover. On 30^{th} July 2020, a new rover powered with RTGs, Perseverance, was launched with the objective of determining

the habitability of Mars, searching for signs of ancient Martian life, and assessing natural resources for future human explorers [NASA2020b]

The previous examples have proven that thermoelectric generators represent a compact, light, durable, and highly–reliable source of electrical energy to explore the space, especially for distant missions where sunlight is insufficient to supply solar panels. These characteristics make them also suitable for those terrestrial environments that require a reliable source over a very long period of time, bearing extreme operating conditions either weather–related (very hot or very cold, very wet or very dry) or mechanic related (high vibrations), and requiring maintenance as low as possible, as it is the case of supplying power to remote volcanic vigilance stations, subject of study of the present Ph. D. dissertation.

Waste heat recovery

Apart from spatial applications, the advantages of thermoelectric generators also make them suitable for many more applications. One of the categories that is undergoing more intense research is waste heat recovery, since it offers an opportunity for low–cost and emission–free energy [Johnson2008]. A heat is denoted as *waste* if it has been obtained as a sub–product of some processes and it is not used afterwards, but dissipated to the environment. These days, waste heat accounts for 40 % of the primary energy consumed in industrialized countries [Rattner2011, Lawrence2020]. Hence, in order to recover this heat and make the most of the primary energy, two main trends have emerged: waste heat recovery from transportation and waste heat harvesting from industry.

Transportation is the most researched sector for waste heat recovery by means of thermoelectric generators due to its permanent interest in obtaining more efficient vehicles that consume less fuel. For a typical gasoline–fueled internal combustion engine vehicle, only about 25 % of the fuel energy is utilized for vehicle mobility. The remainder breaks down into 30 % in coolant, 40 % in exhaust gas and 5 % of other parasitic losses [Yang2005]. Therefore, converting this lost energy into electricity can improve the overall efficiency of the vehicle and reduce its CO_2 emissions, which results of great importance taking into account the more and more restrictive normative about emissions from the European Commission as well as its penalties [DiBattista2015].

In the literature, both computational and experimental studies can be found, with a special focus on the optimization of the heat exchangers due to the requirements of being light and compact while presenting low thermal resistances. Hence, one of the most common alternatives consists in adding fins inside the exhaust pipe and taking advantage of the cooling system built into the vehicle to release the heat not converted into electric-

ity [Kempf2016]. In other cases, it is preferred to use passive heat exchangers, without auxiliary consumption, and heat pipes are commonly installed due to their low thermal resistance and better heat distribution [Pacheco2020]. These studies, which in most cases are supported by automotive companies, have demonstrated the technical feasibility of thermoelectric generators for the automobile industry if their introduction does not change the operating point of the engine (the acceptable pressure losses are limited to around a few tens of millibars) [Champier2017]. However, their cost is still too expensive and they have just been applied in laboratory tests.

Waste heat can also be recovered from industries, since heat is often a byproduct of the processes. Some examples of waste heat sources include waste water derived from washing, cooling, drying or refrigeration systems, and exhaust air emitted from furnaces or production halls [Elghool2017]. In some cases, this heat is used to preheat another process or for district heating, while on other occasions, electricity is generated. In the latter, organic Rankine cycles, Kalina cycles, or thermoelectric generators are generally used [Huang2017]. Nonetheless, due to the complexity of the cycles and the habitual low temperature of the waste heat, the studies about thermoelectric generators are widening and therefore, the optimization of heat exchangers becomes again crucial. These studies are mainly computational with small–scale laboratory setups to confirm the correctness of the model, such as the one performed by Mirhosseini et al., who optimized a thermoelectric generator for a rotary cement kiln at 500 °C, obtaining an average generation of 106 $\mathrm{W/m^2}$ with an average cost of 20.32 \$/W [Mirhosseini2019]; or the one carried out by Araiz et al., who focused on obtaining a completely passive thermoelectric generator with fin dissipators in the hot side and loop thermosyphons in the cold one, and estimated that with this system 240 $\mathrm{W/m^2}$ can be obtained, which applied to a real rockwool manufacturing plant entails an annual electricity generation of 363 MWh with an investment of 10 €/W [Araiz2018, Araiz2020].

Micro–generation for sensors

Another area with promising prospects for thermoelectric generators is micro–generation for sensors, whose research has intensified in the last years. Nowadays, the implementation of sensors is expanding at an impressive rate worldwide. For instance, industries are incorporating new sensors in order to have better control of the process and improve the quality. However, their implementation is not simply reduced to industries, sensors are everywhere: wearables, alarms, presence detectors, cars...

Current intelligent sensors require only a few hundred microwatts or a few milliwatts to

operate. Powering these devices from the electrical grid often requires very long cables to provide very little energy. Hence, the alternative up to date has been batteries. Nevertheless, in some applications, such as chemical and military facilities, power plants, or secure data centers, battery changes are often difficult and costly [Champier2017]. This has led to the search of micro–generators producing a few milliwatts to power these instruments and make them autonomous.

In this context, thermoelectric generators, with their low maintenance, good performance even in difficult environments, and capability of operating with any heat source, are an ideal candidate for the challenge. In the literature, all kinds of heat sources have been proposed: waste heat from industrial processes, solar energy, human body... Moreover, there even exist companies as Micropelt prepared for commercializing such devices. The thermoharvesting power module developed by this company is capable of operating with temperatures differentials of less than 10 °C, leading to a configurable voltage between 1.8 and 4.5 V provided that the heat source temperature does not exceed 105 °C [Micropelt2020].

Geothermal energy has also been considered as heat source for thermoelectric generators oriented to sensors. Thus, two tendencies can be found. On the one hand, some proposals combine traditional geothermal plants with thermoelectric generators. Hence, these devices are installed on existing pipes, either from district heating or from geothermal power plants, and supply power to all kind of sensors and actuators, such as an automated irrigation system [Foley2015], a quadruped robotic system [Dell2016], a security camera [Dell2018], or control systems [Liu2020].

On the other hand, there exist other examples of thermoelectric generators installed directly in the ground. Due to the difference in heat capacity and conduction rate between the air and the ground, there normally exists a temperature difference between them [Stevens2004]. Lawrence and Stevens demonstrated that this temperature difference can be transformed into electricity by means of thermoelectric generators, permitting obtaining a few milliwatts to supply power to remote sensors [Lawrence2002, Stevens2013]. As indicated by Stokes et al., this type of self–sufficient power sources could serve for unattended ground sensors (UGS) in defense and security [Stokes2010]. They experimented this proposal at the laboratory, developing a complete sensor consisting of a thermoelectric generator, a DC–DC boost converter, a wireless sensor transmitter, and supercapacitors, which presented good performance with temperature differences as low as 1 °C.

Forest monitoring is another possible application. Similarly to volcano surveillance, forests are also monitored in order to analyze the impact of droughts or fires, to uncover

their structure, and to study variations of their biota, for which wireless sensors are used [Yan2016, Norman2016, Cale2016]. Nevertheless, these sensors also present energy supply problems due to their remoteness. As a solution, Wang et al. proposed the utilization of thermoelectric generators to provide a stable power supply, taking advantage of the mentioned temperature difference between the ground and the air [Wang2017]. Huang et al. improved the previous micro–generator and performed field experiments under natural conditions in two different locations [Huang2019a]. The results obtained during 6 months revealed that the location influences the power generation that can be obtained. Hence, in Harbin an average of 0.335 mW were generated, while in Beijing, only 0.076 mW could be produced. In a later article, they concluded that in order to efficiently harvest micro–energy from shallow soil, the thermoelectric generator needs to be placed where the soil moisture is greater than 30 % [Huang2019b].

Roadway and bridge infrastructures also require energy harvesting in order to power a multitude of data collection and communication applications [Wang2018a]. For this purpose, it is considered that thermoelectric generators are one of the most readily available methods [Gholikhani2020], transforming the heat absorbed from the exposure to solar radiation into electricity. For instance, Tahami et al. fabricated a system to embed into asphalt pavements, so that with the temperature difference between the pavement surface and the soil below it, electricity could be generated. They optimized and tested a prototype on field, obtaining 29 mW [Tahami2019]. Another alternative consists in making use of the temperature difference between the road surface and ambient air, as proposed by Jiang et al., who obtained up to 45 mW [Jiang2017].

As can be observed, all the previous examples lead to a generation in the range of milliwatts. Nevertheless, for the unprecedented application of supplying power to volcanic vigilance stations to be developed in the present Ph. D. dissertation, a larger generation is expected, in the watts range. The only existing example in the literature with similar characteristics is the thermoelectric generator developed by Xie et al., which led to a maximum generation of 0.975 W per thermoelectric module from a 379 °C hydrothermal vent located at a depth of 2765 m in the Indian Ocean [Xie2016]. However, their device did not include the communications part, which is of great importance in the application under consideration in this thesis, since data emission over several kilometers is required.

Medium and large scale geothermal thermoelectric generation

Geothermal energy has recently started to be also used as heat source for medium and large scale geothermal power generation. In fact, due to their advantages, thermoelectric

generators have been identified as the key technology for clean geothermal power generation [Yu2020], and one of the proposals to speed up the installation of geothermal heat [Li2015]

Niu et al. [Niu2009] were the first ones building a geothermal thermoelectric generator (GTEG). They were able to generate 146.5 W with 56 thermoelectric modules and a temperature difference between the heat reservoirs of 120 °C (2.62 W per module). Based on a similar design, Suter et al. [Suter2012] optimized a 1 kW thermoelectric stack by simulating different operating parameters and stack geometries considering a 100 °C gradient. Liu et al. [Liu2013, Liu2014a, Liu2014b] were also convinced about this technology. Hence, they built a thermoelectric generator composed by 96 thermoelectric modules that generated 160 W with a temperature difference of 80 °C. They estimated that this prototype could reach 500 W with a temperature difference of 200 °C. With another prototype with 600 modules they predicted a generation of 1 kW with a temperature difference of 120 °C. More recently, Ahiska and Mamur [Ahiska2013, Ahiska2016] developed a prototype capable of producing 41.6 W with 20 modules and 67 °C temperature difference (2.08 W per module), while Trip et al. [Trip2017] developed a 0.4 W generator with a temperature difference of 72 °C, composed by 40 thermoelectric modules (9.7 mW per module). On their behalf, Wang et al. defended the combination of geothermal and hydrocarbons, integrating thermoelectric generators downhole in oil and gas wells. By means of a computational model, they estimated a maximum power output of 8538 W with a 100 °C temperature difference in a vertical well in China [Wang2018b], and 128 024 W in case of a horizontal one with a 156 °C gradient [Wang2019].

All the previous geothermal thermoelectric generators focus on medium–low temperature geothermal fields (<180 °C), hence competing with Organic Rankine Cycle (ORC) binary power generators, the frequently used technology to generate electricity from this low enthalpy geothermal heat. The evaluation of possibilities in high–temperature geothermal fields has just been analyzed for the extraction of this energy from oceanic crust in offshore wind turbine monopiles, which estimates a maximum power output of 242 kW [Banerjee2018]. Therefore, the application of thermoelectric generators to high temperature shallow Hot Dry Rock (HDR) fields is studied for the first time in the present Ph. D. dissertation. Furthermore, in contrast to the previous examples, the development of this application includes field testing, not limiting to laboratory experiments or computational studies, and will make an effort to reduce the moving parts and auxiliary consumption of the heat exchangers, as analyzed in the next section.

1.2.2 Heat Exchangers for Geothermal Thermoelectric Generators

In order to maximize power generation in the previous applications, a proper design and optimization of the heat exchangers become indispensable. The purpose of these systems is to approach the temperatures of the sides of the thermoelectric modules to the reservoirs' ones, since the higher the gradient in the thermoelectric modules, the greater the generation. In fact, a reduction of 10 % in the thermal resistance of the heat exchangers leads to an 8 % higher generation [Astrain2010].

The decision about which type of heat exchanger is better for a certain application will depend on the characteristics of the thermal reservoirs and the limitations of the considered application. In this subsection, the most common technologies used as heat exchangers for thermoelectric generators are addressed, concentrating on those that use geothermal energy as heat source.

Hot side heat exchangers

The hot side heat exchanger of a geothermal thermoelectric generator (GTEG) has to absorb geothermal heat and transfer it with a minimal temperature difference to the thermoelectric modules located overground. Therefore, its design is key, since heat may be transmitted over relatively long distances depending on the depth of the geothermal anomalies, as well as because it is necessary to ensure a good heat transfer between the ground and the heat exchanger.

As derived from Subsection 1.2.1, there exist two different applications of GTEGs, with a completely different scale. Therefore, the requirements of the heat exchangers will vary depending on each case. On the one hand, for high scale geothermal thermoelectric generators, heat needs to be absorbed from several meters deep into the ground. Hence, as an imitation to traditional geothermal cycles, all the existing proposals incorporate heat exchangers with a fluid as heat carrier. Thus, a fluid is pumped into the ground so that it absorbs geothermal heat, and then transfers it to the thermoelectric modules. These systems permit obtaining low thermal resistances due to the high heat transfer coefficients that can be achieved with forced convection. Nevertheless, they require an auxiliary consumption that reduces net generation. Apart from the extra consumption, these type of heat exchangers also presents the handicap of being composed of an elevated number of elements (the heat exchanger itself, the pump responsible for the circulation of the fluid, and several pipes) that include moving parts. Consequently, they normally require frequent maintenance.

In the application under consideration in the present Ph. D. dissertation that studies the possibilities of geothermal thermoelectric generation from shallow HDR fields, the use of heat exchangers with a fluid as heat carrier would require rock fracture. Therefore, it will be necessary to analyze other alternatives with minimal environmental impact, an aspect of great importance since the geothermal field under consideration is located at a natural reserve. The prerequisites of absence of moving parts and auxiliary equipment will have a great influence on the final decision.

On the other hand, in the case of supplying power to sensors, heat is absorbed close to the surface. In this application, the compactness of the device and the lack of maintenance are important aspects to take into consideration. Therefore, the existing proposals use passive heat exchangers to absorb geothermal heat, without moving parts nor auxiliary consumption. Hence, Stevens as well as Stokes et al. opted for the simplest heat exchanger: a solid metallic bar, similar to a stake [Stevens2013, Stokes2010]. Tahami et al. also used a solid heat exchanger, but since in their case they wanted to absorb heat from the asphalt, they installed a copper collector plate [Tahami2019].

The rest of the examples available in the literature preferred to install heat exchangers based on phase change. These devices take advantage of the latent heat of an internal working fluid that is cyclically vaporizing and condensing to transfer large amounts of heat, nearly isothermally [Shabgard2015]. Hence, Lawrence, Wang et al., Huang et al., and Xie et al. used the so–called heat pipes, in which the condensed liquid returns by capillary effect in the wick that covers the internal surface of the pipe [Lawrence2002, Wang2017, Huang2019a, Huang2019b, Xie2016]. On their behalf, Jiang et al. installed a vapor chamber because they needed a large and planar contact surface with the asphalt [Jiang2017].

The advantages of heat exchangers based on phase change are their low thermal resistance, their compactness, and that they do not need moving parts nor auxiliary consumption. Moreover, these devices can transfer heat regardless of the distance, which is of great utility with geothermal energy as heat source, since temperature normally increases with depth. The best example of this aspect is demonstrated in the 400 m long thermosyphon installed in Hannover for a geothermal heat pump [Ebeling2016], which reflects the viability of this type of phase change heat exchangers for geothermal applications. Thermosyphons differ from heat pipes because the former does not include the wick material of the latter, and the return of liquid occurs simply by gravity.

Cold side heat exchangers

The cold side heat exchanger of a GTEG is responsible for releasing the heat that has not been transformed into electricity by the thermoelectric modules, a common task in other thermoelectric applications as well. For this purpose, the most frequent heat exchangers are fin dissipators, heat exchangers with a fluid as heat carrier, heat pipes, and thermosyphons [Elghool2017]. Fin dissipators stand out due to their simplicity, robustness, and low price, achieving low thermal resistances when working as active cooling systems, i.e. aided by a fan so that forced convection conditions are obtained [Martinez2016, Tzeng2014]. Nonetheless, they can also operate under natural convection, which supposes an increase of their thermal resistance, but avoids auxiliary consumption. On their behalf, liquid–based heat exchangers present better convection coefficients, improving the performance of the system. However, the pumps necessary to propel the liquid through the circuit require a higher auxiliary consumption and therefore reduce net generation [Aranguren2014, Aranguren2018]. Finally, heat pipes and thermosyphons are gaining attention in the last years. As exposed previously, making use of the latent heat of an internal fluid that cyclically vaporizes and condenses, these heat exchangers obtain low thermal resistances without requiring auxiliary equipment [Shabgard2015, Remeli2015, Araiz2017].

Similarly to the hot side heat exchangers, depending on the specific application of GTEGs, the existing proposals in the literature present different types of heat exchangers. Thus, for medium and large scale geothermal thermoelectric generation, again heat exchangers with a liquid as heat carrier is the only chosen alternative. This is due to the resemblance to traditional geothermal power plants, dissipating the heat analogously to condensers. On the other hand, when supplying power to sensors with a GTEG, the unique criteria in this case opts for fin dissipators due to their simplicity, compactness, and low cost. The use of phase change heat exchangers in the cold side is not contemplated in any application of GTEGs, although they have been considered the most appropriate one for this purpose for temperatures under 300 °C [Elghool2020].

1.2.3 Thermoelectric Modules

As exposed in the introduction, thermoelectric modules are the most essential element of a thermoelectric generator since the direct transformation of heat into electricity is held in them. Moreover, these components are also responsible for the low efficiency and elevated cost of thermoelectric systems, which supposes a barrier for the broad implementation of this type of generators [Champier2017]. Consequently, many researchers are focused on the search and development of materials that permit obtaining a higher efficiency and working

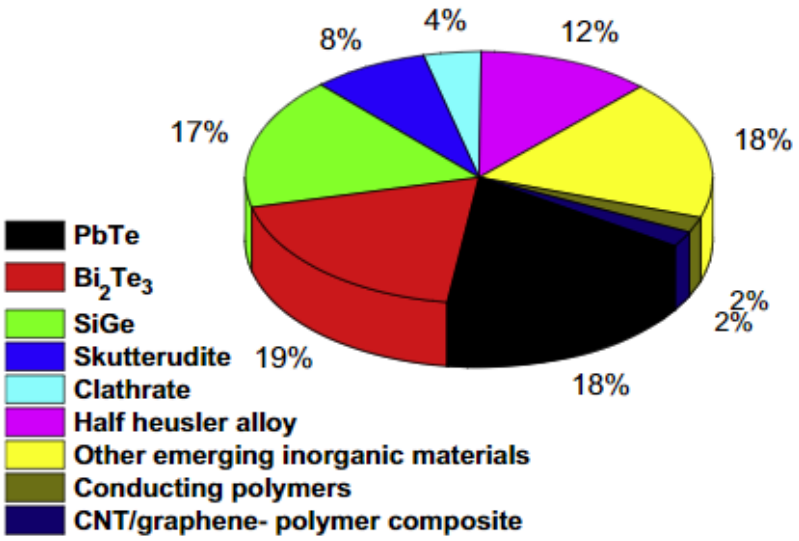

Figure 1.10: Contribution of various materials used in thermoelectric research. *Reprinted with the permission of [Gayner2016].*

under a wider range of temperatures, while presenting lower costs.

Figure 1.10 depicts the individual contribution of various materials used in thermoelectric research [Gayner2016]. As can be observed, the classic inorganic materials, such as telluride–based materials (e.g. Bi_2Te_3 and PbTe), silicon–germanium alloys SiGe, half–Heusler alloys, skutterudites, and clathrates, present the highest contribution. Nonetheless, in the last years, there has been an increase in the development of organic materials due to their cost–effectiveness, easy processing, low density, low thermal conductivity, and high flexibility [Yao2019]. However, to meet the requirements of practical applications, the performance of these materials still needs much improvement.

Figure 1.11 summarizes the ZT as a function of temperature for the former thermoelectric materials [Yang2018]. Hence, as can be observed, most of the existing materials present a value of ZT lower than 1.5, which is also highly dependent on temperature. According to the inset included at the top left of the figure, this value of ZT leads to an efficiency of less than 20 %. In the case of geothermal thermoelectric generators, it is expected that a value of ZT of 2 would be necessary in order to be applied on a large scale in low and medium temperature geothermal power fields [Yu2020].

In order to obtain high–performance materials, two complementary approaches can be distinguished: search for new materials with intrinsically high ZT or optimize the thermoelectric properties of existing materials [Yang2018]. Thus, in the former, machine–learning

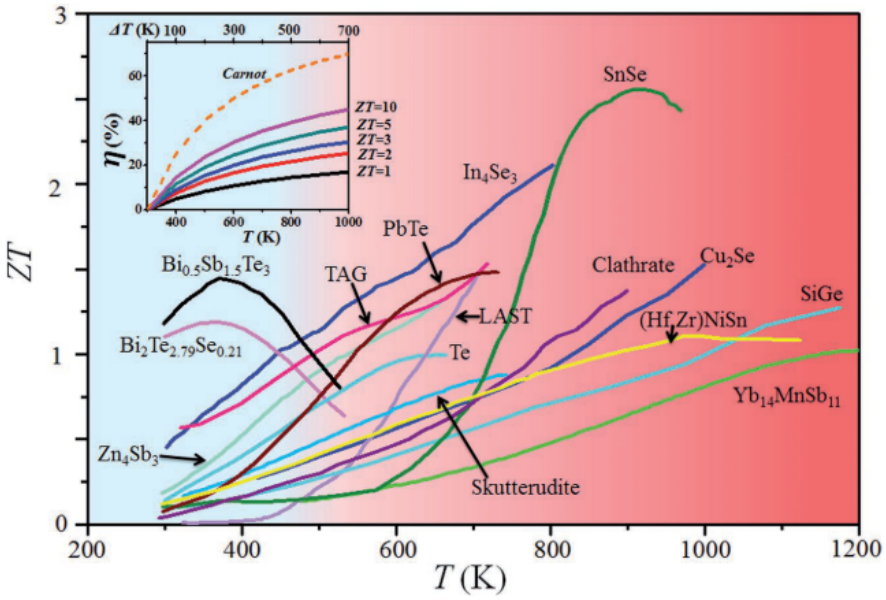

Figure 1.11: ZT as a function of temperature for typical high efficiency thermoelectric materials, inset is the relation between the efficiency η, temperature T, and temperature difference ΔT of materials with different ZT values. *Reprinted with the permission of [Yang2018].*

is spreading in the last years to discover new materials or new combinations of materials more rapidly [Recatala-Gomez2020, Iwasaki2019]. In the latter, several techniques to modify some properties such as their electrical resistivity, Seebeck coefficient or thermal conductivity have been developed: phonon glass electron crystal (PGEC), doping, energy filtering, resonant states, multiple–band conduction mechanism and convergence of electronic bands, scattering from nanoscale endotaxial precipitation and mesoscale grain boundaries, atomic–scale alloy scattering, nanostructuring, quantum confinement, superlattices, and nanocomposites [Gayner2016, Maier2018].

Besides obtaining promising thermoelectric materials with elevated ZT, it is also important to be able to implement them in thermoelectric modules, for which it is necessary to develop manufacturing techniques [Tan2019]. However, there is still a lack of technological transfer between research and commercialization. Thus, most of the commercially available thermoelectric modules are based on alloys of bismuth and tellurium, Bi_2Te_3, which present values of the dimensionless figure of merit, ZT, of 1 or less, and maximum operating temperatures in the range between 200 and 300 °C [Marlow2020, TECTEG2020, TEGMART2020]. Apart from Bi_2Te_3 thermoelectric modules, there also exist others made up of $PbTe$ that can operate efficiently at medium temperatures, between 327 and 527 °C, with a low thermal conductivity, 2.3 W/mK, and a high Seebeck coefficient, 500 µV/K.

For those applications with even higher temperatures, alloys of silicon and germanium, $SiGe$, are used because of the elevated melting point of these compounds ($\sim$ 1027 °C). However, due to their high thermal conductivity at ambient temperature, their use has been restricted to very specific applications or laboratory experiments [Wang2008]. Taking into account the temperature range and the heat transfer mechanisms involved in the applications under study in this Ph. D. dissertation and the commercial availability, the experimental prototypes to be developed in this thesis will include Bi_2Te_3 thermoelectric modules.

1.2.4 Computational Models for Thermoelectric Generators

In the previous subsections, several studies of geothermal thermoelectric generators (GTEGs) have been mentioned, both for micro–generation oriented to sensors and for medium to large scale generation. Although in some cases laboratory prototypes were developed, the general tendency is to employ computational models for the studies. The use of these models has widely spread in the last years, becoming an indispensable tool for the design, analysis, and optimization of real applications, since they reduce the necessity of building prototypes and limit the number of experimental tests necessary in order to obtain significant information, which translates into cost savings. In the case of medium to large scale GTEGs, these aspects gain even more importance.

Nevertheless, the modeling of thermoelectric generators (TEGs) is not an easy task since phenomena related to heat, electricity, and the interaction between them, are simultaneously involved. Hence, a system of equations that considers the fundamental laws of heat conduction, convection, and thermoelectric effects, needs to be solved, which has historically caused many problems due to its high complexity. Nowadays, in the modeling of TEGs, there exist four major kinds of models: standard simplified models, analytical models, models based on the electrical analogy between heat transfer and electricity, and numerical models based on finite elements [Fraisse2013].

The simplified models are the simplest approach to model a thermoelectric generator and are based on a global balance of heat transfer and thermoelectric effects (macro approach). These models assume a symmetrical distribution of the Joule effect between the hot and cold side of the thermoelements and, in general, consider constant thermoelectric properties (Seebeck coefficient, thermal conductivity, and electrical resistivity). In some cases, the Thomson effect is taken into account and assumed equitably distributed on both sides of the semiconductors, leading to the so–called improved simplified models.

The analytical models are based on a local energy balance, permitting a more precise

representation of the behavior of the thermoelectric modules. Nonetheless, like every analytical model proposed to solve a system of equations of a certain complexity, these models also require the simplifying hypothesis of the simplified models so that the difficulty is considerably reduced and an analytical expression is feasible. Another limitation of these models is that they only focus on the thermoelectric modules and require the hot and cold side temperatures as boundary conditions, which are indeed dependent on the thermal characteristics of the heat reservoirs, the heat exchangers, and even the thermoelectric modules themselves.

The models based on the electrical analogy between heat transfer and electricity have demonstrated to be a reliable and quick alternative to model complex phenomena. This thermal–electrical analogy is actually derived from the application of the implicit finite difference method to heat conduction equation, and its basic idea consists in discretizing the system in several nodes. The solution of the problem is obtained for those finite number of nodes. Thus, the thermal dependence of the thermal coefficients, the transient regime, or the variable section of the thermoelectric legs can be easily represented. Another advantage of this analogy is that it permits modeling the heat exchangers in detail, including all the involved phenomena.

Finally, numerical models based on finite elements permit the highest accuracy. Hence, these models take into account the non–linearity of the thermoelectric materials resulting from the temperature dependency of the material properties, allow the coupling of thermoelectric simulations to computational fluid dynamics models, and are suitable for 3D and complex geometries, both in steady and transient regimes. Nevertheless, they present the disadvantage of their complexity, the hardware requirements, and the increased computational time.

The models used for GTEGs are mainly simplified models, which neglect the Thomson effect and assume constant thermoelectric properties [Suter2012, Liu2014b, Wang2019]. Most of them, concentrate on a correct simulation of the heat exchangers, but simplify the modeling of the thermoelectric modules, leading to a slight deviation in the calculation of power generation [Fraisse2013]. The more precise thermo–electrical analogy has never been used for the modeling of GTEGs.

1.3 Motivation

Thermoelectricity has demonstrated to be a robust, reliable, and scalable technology that does not require moving parts, working fluids nor auxiliary equipment. Nevertheless, in civil applications, their development is mainly restricted to the academic field. Therefore, there is an interest to find new applications in which thermoelectric generators can finally be made a reality despite their low efficiency.

The development of such applications needs to be performed completely, with a proper design and optimization of the whole generators, and a posterior experimental demonstration on field, not limiting to computational or low–scale proposals. Hence, there is a necessity of an accurate computational model that considers all the involved elements, including the modeling of not only the thermoelectric modules with all their thermoelectric effects, but also the heat exchangers and the heat reservoirs taking into account all the heat transfer mechanisms. Such a model serves as basis for the design and optimization of real prototypes than can be subsequently built and installed on field.

In this process, it is of utmost importance to take into account that the robustness of thermoelectric generators is one of their main advantages. Therefore, there is a great interest in the development of high–efficiency heat exchangers without moving parts nor auxiliary equipment, so that the advantages of the thermoelectric modules are extended to the whole device.

In this scenario, the present Ph. D. dissertation studies the viability of two novel applications of thermoelectric generators based on shallow geothermal anomalies of volcanic origin. Thus, on the one hand, the prospects of this technology in hot dry rock fields will be analyzed for the first time, as a more environmentally friendly alternative to the actual enhanced geothermal systems, the only existing technique nowadays that causes induced seismicities. On the other hand, the feasibility of completely autonomous volcanic vigilance stations powered only by thermoelectricity will also be examined, taking a step forward with respect to the available state of the art, developing a complete system that generates in the watts range and communicates over several kilometers.

In order to accomplish these purposes, the present work contextualizes in an incomparable framework within the ELECTROVOLCAN project, counting on the experience in thermoelectrics of the Thermal and Fluids Engineering research group from the Public University of Navarre, with an extensive career in the development of thermoelectric devices for both cooling and generation that includes deep research on heat exchangers; the knowledge of expert geologists and volcanologists specialized in the geothermal anomalies

of the Canary Islands; as well as the counseling of a company that focuses on the real manufacturing of the developed devices and their commercialization.

1.4 Objectives

Considering the actual state of the art and once the motivation of the present Ph. D. dissertation has been explained, the following general objective is contemplated:

Development of thermoelectric generators for shallow geothermal anomalies of volcanic origin and their application to medium–scale renewable power generation and stand–alone power supply of volcanic vigilance stations.

The attainment of this main objective encompasses a series of specific objectives to be developed during the thesis. The specific objectives 1 and 2 lay the foundations of thermoelectric generators for shallow geothermal anomalies, focusing the rest on the two applications subject of study. Hence, medium–scale renewable generation is considered in the specific objectives 3 and 4, while the specific objectives 5 and 6 concern the stand–alone power supply of volcanic vigilance stations.

Specific Objective 1:

The first specific objective deals with the development of a computational model to simulate the behavior of geothermal thermoelectric generators. For the following objectives of design and optimization, it is necessary to take into account that several aspects have an influence: the type of heat exchangers, their geometry and materials, the nature of the heat source and sink, the number of thermoelectric modules, or the disposition and assembly of the different elements among others. Therefore, it is essential to have a versatile computational tool capable of predicting the behavior of a complete geothermal thermoelectric generator, including an exhaustive discretization of the heat exchangers that considers all the heat transfer mechanisms involved, and the singularities of the heat reservoirs.

The implementation of this computational model will be performed with the numerical computing environment MATLAB, based on the implicit finite difference method, also known as thermal–electrical analogy. Furthermore, in order to obtain a reliable tool, this specific objective also includes the experimental validation of the computational model, analyzing the capacity of both the individual parts and the complete model to resemble the behavior of a real prototype.

Specific Objective 2:

As exposed in previous sections, the heat exchangers are key elements of thermoelectric generators, since they determine the temperature difference across the thermoelectric modules. Therefore, the second specific objective considers the study of high–efficiency heat exchangers for geothermal thermoelectric generators.

In the two applications under consideration in the present Ph. D. dissertation, it will be of utmost importance to accomplish the requirements of robustness and absence of moving parts nor auxiliary equipment without jeopardizing efficiency. Hence, different types of heat exchangers will be studied both computational and experimentally. More specifically, purely conductive solid heat exchangers, fin dissipators, heat pipes, and thermosyphons will be characterized considering different geometries and configurations. This characterization will enable analyzing the influence of different factors in the operation of these devices, serving as basis for their optimization in the following specific objectives.

Specific Objective 3:

The third specific objective focuses on the application of medium–scale renewable power generation. Hence, based on the results obtained with the specific objectives 1 and 2, two prototypes will be designed and optimized for the hot dry rock field located at Timanfaya National Park (Canary Islands, Spain), one per each available temperature range. In this process, apart from the maximization of the power generated per thermoelectric generator for which different geometries and number of thermoelectric modules will be analyzed, it will be of great importance to consider constructional aspects, facilitating the assembly and installation of the devices while causing a minimal visual impact.

The final designs will be built at the laboratories of the Public University of Navarre, assessing their technical viability. Moreover, prior to their installation at Lanzarote, the behavior of the devices will be deeply studied at the laboratory, characterizing the behavior of the heat exchangers individually and determining the power generation capabilities of the complete generator under several operating conditions.

Specific Objective 4:

The second objective related to medium–scale renewable power generation, which is in turn the fourth specific objective of the thesis, concerns the estimation of the energetic potential of the high–scale implementation of the devices developed in the previous point,

thanks to their scalability. In comparison with other renewable sources, geothermal energy characterizes by its constancy, being always available independently of weather conditions, which permits obtaining a high capacity factor.

The study will be performed by means of the computational model developed in the first specific objective and will consider again Timanfaya National Park as reference. For this purpose, it will be necessary to determine the specifications of the geothermal field, including not only the temperature and mass flow of the gases, but also the capacity of the system for heat extraction without cooling down.

Specific Objective 5:

Regarding the attainment of autonomous volcanic monitoring stations, the fifth specific objective is related to the design and optimization of a thermoelectric generator to be installed in volcanic fumaroles, one of the most evident manifestations of geothermal energy in volcanoes. In this low–power application, the durability, and reliability of the developed device gain importance versus the maximization of power generation. Therefore, it will be necessary to develop a robust generator, without moving parts, capable of resisting in a harsh and remote environment without maintenance.

After a design and optimization process thanks to the tools obtained in the specific objectives 1 and 2, the designed generator will be built and characterized at the laboratories of the Public University of Navarre, studying the behavior of both the individual components and the complete generator under different operating conditions. Afterwards, the designed generator will be installed at Teide volcano (Canary Islands, Spain), where its real viability will be analyzed. The field installation will also permit gaining experience about the heat transfer mechanism with the fumaroles and the corrosive environment characteristic of volcanoes, providing essential information for future designs.

Specific Objective 6:

Finally, the last specific objective complements the previous one, concentrating on the development of the electronic part necessary to achieve completely autonomous volcanic vigilance stations. Hence, while the previous specific objective focuses on the generation part, this one deals with the processing of the generated power ensuring that the thermoelectric modules work at their optimal point, the storage of the excess energy, the control of different sensors, and the emission of the measured data to a center that can be located various kilometers away.

The development of such an electronic system will be designed and evaluated at the Public University of Navarre, previous to its field testing at Teide volcano. This field testing will be performed simultaneously with the generator conceived in the specific objective 5, so that the viability of a complete system that monitors different variables and emits them to a center located several kilometers away, powered only with a thermoelectric generator installed in a volcanic fumarole, can be confirmed.

1.5 Thesis Structure

In order to accomplish the previous objectives, the present Ph. D. dissertation is structured in seven chapters. Following this introduction, Chapter 2 represents the first approximation to geothermal thermoelectric generators. Hence, the use of different heat exchangers is experimentally studied. This chapter corresponds with the article "New opportunities for electricity generation in shallow hot dry rock fields: A study of thermoelectric generators with different heat exchangers" published in *Energy Conversion and Management* 200 (2019) 112061. Although the manuscript is oriented to medium–scale generation from shallow hot dry rock fields, the study of the different heat exchangers is also applicable to the stand–alone power supply of volcanic vigilance stations.

Afterwards, Chapter 3 presents the development and validation of the computational model that simulates the behavior of geothermal thermoelectric generators. This chapter coincides with the publication "Computational study of geothermal thermoelectric generators with phase change heat exchangers" published in *Energy Conversion and Management* 221 (2020) 113120. The manuscript not only makes a detailed description of the computational model including all the involved heat transfer phenomena, but also validates it thanks to the experimental tests of Chapter 2 and studies the potential at Timanfaya National park, analyzing the influence of different geometries, number of thermoelectric modules and heat exchangers. As a result, an optimized design is obtained.

Based on the previous optimization, Chapter 4 details the prototype that has been developed to be installed in a real HDR field located in Timanfaya National Park considering all the constructional aspects. Its experimental characterization at the laboratory is also included in this chapter.

On its behalf, Chapter 5 is applied to obtaining autonomous volcanic vigilance stations. Hence, as developed in the article "Prospects of Autonomous Volcanic Monitoring Stations: Experimental Investigation on Thermoelectric Generation on Fumaroles" published in *Sensors* 20 (2020) 3547, the viability of thermoelectric generation from volcanic fumaroles is studied by means of the installation of a prototype at Teide volcano.

Chapter 6 delves into the former application, with the objective of achieving a complete autonomous volcanic monitoring station, capable of generating the required energy from volcanic fumaroles with thermoelectric generators, ensuring that the modules work with the optimal load resistance, managing the storage system, monitoring different parameters, and sending them to a center located several kilometers away. This chapter corresponds with the manuscript "Experimental evidence of the viability of thermoelectric generators

to power volcanic monitoring stations" published in *Sensors* 20 (2020) 4839.

Finally, Chapter 7 highlights the main conclusions obtained in the thesis, exposes the contributions achieved during its development, and presents the future lines arisen.

1.6 Bibliography

[Abelson2006] R.D. Abelson. Space Missions and Applications. In *Thermoelectrics handbook: macro to nano*, pages 56.1–56.29. CRC Press, Boca Raton, 1st edition, 2006.

[Ahiska2013] R. Ahiska and H. Mamur. Design and implementation of a new portable thermoelectric generator for low geothermal temperatures. *IET Renewable Power Generation*, 7(6):700–706, 2013.

[Ahiska2016] R. Ahiska and H. Mamur. Development and application of a new power analysis system for testing of geothermal thermoelectric generators. *International Journal of Green Energy*, 13(7):672–681, 2016.

[Alonso2019] M. Alonso, E. Padrón, H. Sumino, P.A. Hernández, G.V. Melián, M. Asensio-Ramos, F. Rodríguez, G. Padilla, M. García-Merino, C. Amonte, and N.M. Pérez. Heat and Helium-3 Fluxes from Teide Volcano, Canary Islands, Spain. *Geofluids*, 2019, 2019.

[Araiz2017] M. Araiz, A. Martínez, D. Astrain, and P. Aranguren. Experimental and computational study on thermoelectric generators using thermosyphons with phase change as heat exchangers. *Energy Conversion and Management*, 137:155–164, 2017.

[Araiz2018] M. Araiz. *Modelización y desarrollo de un sistema de generación termoeléctrica basado en efecto Seebeck. Aplicación a gase de escape en calderas de combustión.* PhD thesis, Public University of Navarre, 2018.

[Araiz2020] Miguel Araiz, Álvaro Casi, Leyre Catalán, Álvaro Martínez, and David Astrain. Prospects of waste-heat recovery from a real industry using thermoelectric generators: Economic and power output analysis. *Energy Conversion and Management*, 205(112376), 2020.

[Aranguren2014] P. Aranguren, D. Astrain, and M.G. Pérez. Computational and experimental study of a complete heat dissipation system using water as heat carrier placed on a thermoelectric generator. *Energy*, 74:346–358, 2014.

[Aranguren2018] P. Aranguren, M. Araiz, and D. Astrain. Auxiliary consumption: A necessary energy that affects thermoelectric generation. *Applied Thermal Engineering*, 141:990–999, 2018.

[Astrain2010] D. Astrain, J. G. Vián, A. Martínez, and A. Rodríguez. Study of the influence of heat exchangers' thermal resistances on a thermoelectric generation system. *Energy*, 35(2):602–610, 2010.

[Banerjee2018] A. Banerjee, T. Chakraborty, and V. Matsagar. Evaluation of possibilities in geothermal energy extraction from oceanic crust using offshore wind turbine monopiles. *Renewable and Sustainable Energy Reviews*, 92:685–700, 2018.

[Cale2016] J.A. Cale, J.G. Klutsch, N. Erbilgin, J.F. Negrón, and J.D. Castello. Using structural sustainability for forest health monitoring and triage: Case study of a mountain pine beetle (Dendroctonus ponderosae)-impacted landscape. *Ecological Indicators*, 70:451–459, 2016.

[Champier2017] D. Champier. Thermoelectric generators: A review of applications. *Energy Conversion and Management*, 140:167–181, 2017.

[Dell2016] R. Dell, R. Unnthorsson, C.S. Wei, and N. Mitchell. A Thermoelectric Powered Quadruped Robotic System for Remote Monitoring of Geothermal Open Field Heated Gardens in Iceland. *GRC Transactions*, 40:173–180, 2016.

[Dell2018] R. Dell, C.S. Wei, M.T. Petralia, G. Gislason, and R. Unnthorsson. Thermoelectric Powered Security Systems in Iceland Using a Geothermal Steam Pipe as a Heat Source. *Proceedings*, 2(440), 2018.

[Dey2016] A. Dey, O.P. Bajpai, A.K. Sikder, S. Chattopadhyay, and M.A. Shafeeuulla Khan. Recent advances in CNT/graphene based thermoelectric polymer nanocomposite: A proficient move towards waste energy harvesting. *Renewable and Sustainable Energy Reviews*, 53:653–671, 2016.

[DiBattista2015] D. Di Battista, M. Muriello, and R. Cipollone. Waste heat recovery of an ORC-based power unit in a turbocharged diesel

engine propelling a light duty vehicle. *Applied Energy*, 152:109–120, 2015.

[Dickson2004] M.H. Dickson and M. Fanelli. *What is geothermal energy?* International Geothermal Association, 2004. `https://www.geothermal-energy.org/print/what_is_geothermal_energy.html`.

[Diez-Gil1987] J.L. Diez-Gil, V. Araña, R. Ortiz, and J. Yuguero. Stationary convection model for heat transfer by means of geothermal fluids in post eruptive systems. *Geothermics*, 16(1):77–89, 1987.

[Ebeling2016] J. Ebeling, S. Kabelac, S. Luckmann, and H. Kruse. Simulation and experimental validation of a 400 m vertical CO2 heat pipe for geothermal application. In *Joint 18th IHPC and 12th IHPS*, pages 218–225, 2016.

[Elghool2017] A. Elghool, F. Basrawi, T.K. Ibrahim, K. Habib, H. Ibrahim, and D. Idris. A review on heat sink for thermo-electric power generation: Classifications and parameters affecting performance. *Energy Conversion and Management*, 134:260–277, 2017.

[Elghool2020] A. Elghool, F. Basrawi, H. Ibrahim, T.K. Ibrahim, M. Ishak, T.M. Yusof, and S.A. Bagaber. Enhancing the performance of a thermo-electric generator through multi-objective optimisation of heat pipes-heat sink under natural convection. *Energy Conversion and Management*, 209(112626), 2020.

[Foley2015] W. Foley, R. Dell, C.S. Wei, and R. Unnthorsson. Point of use thermoelectric powered automated irrigation system for an intesive shallow bottom heat system using waste geothermal hot water and steam condensate in Iceland. *Transactions - Geothermal Resources Council*, 39:117–124, 2015.

[Fraisse2013] G. Fraisse, J. Ramousse, D. Sgorlon, and C. Goupil. Comparison of different modeling approaches for thermoelectric elements. *Energy Conversion and Management*, 65:351–356, 2013.

[Gayner2016] C. Gayner and K.K. Kar. Recent advances in thermoelectric materials. *Progress in Materials Science*, 83:330–382, 2016.

[Gholikhani2020] M. Gholikhani, H. Roshani, S. Dessouky, and A.T. Papagiannakis. A critical review of roadway energy harvesting technologies. *Applied Energy*, 261(114388), 2020.

[Gomez-Ortiz2019] D. Gomez-Ortiz, I. Blanco-Montenegro, J. Arnoso, T. Martin-Crespo, M. Solla, F.G. Montesinos, E. Vélez, and N. Sánchez. Imaging thermal anomalies in hot dry rock geothermal systems from near-surface geophysical modelling. *Remote Sensing*, 11(675), 2019.

[Huang2017] F. Huang, J. Zheng, J.M. Baleynaud, and J. Lu. Heat recovery potentials and technologies in industrial zones. *Journal of the Energy Institute*, 90:951–961, 2017.

[Huang2019a] Y. Huang, D. Xu, J. Kan, and W. Li. Study on field experiments of forest soil thermoelectric power generation devices. *PLoS ONE*, 14(8), 2019.

[Huang2019b] Y. Huang, W. Li, D. Xu, and Y. Wu. Spatiotemporal rule of heat transfer on a soil/finned tube interface. *Sensors*, 19(5), 2019.

[IEA2019] International Energy Agency (IEA). Energy Efficiency. Technical report, 2019. `https://www.iea.org/reports/energy-efficiency-2019`.

[IEA2020a] International Energy Agency (IEA). World Energy Balances. Technical report, 2020. `https://www.iea.org/reports/world-energy-balances-overview`.

[IEA2020b] International Energy Agency (IEA). Electricity information. Technical report, 2020. `https://www.iea.org/reports/electricity-information-overview`.

[IGME1992] Instituto Geológico Minero Español. Evaluación del potencial geotérmico superficial de Montañas de Fuego como Sistema de Roca Caliente Seca. Technical report, 1992.

[Iwasaki2019] Y. Iwasaki, I. Takeuchi, V. Stanev, A.G. Kusne, M. Ishida, A. Kirihara, K. Ihara, R. Sawada, K. Terashima, H. Someya, K. Ichi Uchida, E. Saitoh, and S. Yorozu. Machine-learning guided discovery of a new thermoelectric material. *Scientific Reports*, 9(2751), 2019.

[JPL2020] Jet Propulsion Laboratory. Voyager. Mission status, 2020. `https://voyager.jpl.nasa.gov/mission/status/`.

[Jiang2017] W. Jiang, D. Yuan, S. Xu, H. Hu, J. Xiao, A. Sha, and Y. Huang. Energy harvesting from asphalt pavement using thermoelectric technology. *Applied Energy*, 205:941–950, 2017.

[Johnson2008] I. Johnson, W.T. Choate, and A. Davidson. Waste Heat Recovery: Technology and Opportunities in U.S. Industry. Technical report, 2008.

[Kempf2016] N. Kempf and Y. Zhang. Design and optimization of automotive thermoelectric generators for maximum fuel efficiency improvement. *Energy Conversion and Management*, 121:224–231, 2016.

[Lawrence2002] E.E. Lawrence and G.J. Snyder. A study of heat sink performance in air and soil for use in a thermoelectric energy harvesting device. In *International Conference on Thermoelectrics, ICT, Proceedings*, pages 446–449, 2002.

[Lawrence2020] Lawrence Livermore National Laboratory. Estimated U.S. Energy Consumption in 2019, 2019. `https://flowcharts.llnl.gov/content/assets/images/energy/us/Energy_US_2019.png`.

[Li2015] K. Li, H. Bian, C. Liu, D. Zhang, and Y. Yang. Comparison of geothermal with solar and wind power generation systems. *Renewable and Sustainable Energy Reviews*, 42:1464–1474, 2015.

[Liu2013] C. Liu, P. Chen, and K. Li. Geothermal Power Generation Using Thermoelectric Effect. *GRC Transactions*, 37, 2013.

[Liu2014a] C. Liu, P. Chen, and K. Li. A 500 W low-temperature thermoelectric generator: Design and experimental study. *International Journal of Hydrogen Energy*, 39:15497–15505, 2014.

[Liu2014b] C. Liu, P. Chen, and K. Li. A 1 KW Thermoelectric Generator for Low-temperature Geothermal Resources. In *Thirty-Ninth Workshop on Geothermal Reservoir Engineering*, 2014.

[Liu2020] J. Liu, Z. Wang, K. Shi, Y. Li, L. Liu, and X. Wu. Analysis and modeling of thermoelectric power generation in oil wells: A potential power supply for downhole instruments using in-situ geothermal energy. *Renewable Energy*, 150:561–569, 2020.

[Maier2018] S. Maier, S. Ohno, G. Yu, S.D. Kang, T.C. Chasapis, V.A. Ha, S.A. Miller, D. Berthebaud, M.G. Kanatzidis, G.M. Rignanese, G. Hautier, G.J. Snyder, and F. Gascoin. Resonant Bonding, Multiband Thermoelectric Transport, and Native Defects in n-Type BaBiTe3-xSex (x = 0, 0.05, and 0.1). *Chemistry of Materials*, 30:174–184, 2018.

[Marlow2020] Marlow Industries Inc. Technical Data Sheet for TG12-8, 2020. `https://cdn2.hubspot.net/hubfs/547732/Data_Sheets/TG12-8.pdf`.

[Martinez2016] A. Martinez, D. Astrain, and P. Aranguren. Thermoelectric self-cooling for power electronics: Increasing the cooling power. *Energy*, 112:1–7, 2016.

[Melian2012] G. Melián, F. Tassi, N. Pérez, P. Hernández, F. Sortino, O. Vaselli, E. Padrón, D. Nolasco, J. Barrancos, G. Padilla, F. Rodríguez, S. Dionis, D. Calvo, K. Notsu, and H. Sumino. A magmatic source for fumaroles and diffuse degassing from the summit crater of Teide Volcano (Tenerife, Canary Islands): A geochemical evidence for the 2004-2005 seismic-volcanic crisis. *Bulletin of Volcanology*, 74:1465–1483, 2012.

[Micropelt2020] Micropelt. TE–CORE Thermoharvesting Power Module. Preliminary Datasheet, 2020. `http://www.micropelt.com/fileadmin/user_upload/_PDF_TE-CORE.pdf`.

[Mirhosseini2019] M. Mirhosseini, A. Rezania, and L. Rosendahl. Power optimization and economic evaluation of thermoelectric waste heat recovery system around a rotary cement kiln. *Journal of Cleaner Production*, 232:1321–1334, 2019.

[NASA2020a] NASA. Radioisotope power systems. Missions, 2020. `https://rps.nasa.gov/missions/`.

[NASA2020b] NASA. Radioisotope power systems. Mars 2020, 2020. `https://rps.nasa.gov/missions/14/mars-2020/`.

[Niu2009] X. Niu, J. Yu, and S. Wang. Experimental study on low-temperature waste heat thermoelectric generator. *Journal of Power Sources*, 188:621–626, 2009.

[Norman2016] S.P. Norman, F.H. Koch, and W.W. Hargrove. Review of broad-scale drought monitoring of forests: Toward an integrated data mining approach. *Forest Ecology and Management*, 380:346–358, 2016.

[Pacheco2020] N. Pacheco, F.P. Brito, R. Vieira, J. Martins, H. Barbosa, and L.M. Goncalves. Compact automotive thermoelectric generator with embedded heat pipes for thermal control. *Energy*, 197(117154), 2020.

[REN21-2020] REN21. Renewables 2020 Global Status Report. Technical report, Paris, 2020. `https://www.ren21.net/gsr-2020/`.

[Rattner2011] A.S. Rattner and S. Garimella. Energy harvesting, reuse and upgrade to reduce primary energy usage in the USA. *Energy*, 36:6172–83, 2011.

[Recatala-Gomez2020] J. Recatala-Gomez, A. Suwardi, I. Nandhakumar, A. Abutaha, and K. Hippalgaonkar. Toward Accelerated Thermoelectric Materials and Process Discovery. *ACS Applied Energy Materials*, 3:2240–2257, 2020.

[Remeli2015] M.F. Remeli, L. Tan, A. Date, B. Singh, and A. Akbarzadeh. Simultaneous power generation and heat recovery using a heat pipe assisted thermoelectric generator system. *Energy Conversion and Management*, 91:110–119, 2015.

[Rowe2006] D.M. Rowe. General Principles and Considerations. In *Thermoelectrics handbook: macro to nano*, pages 1.1–1.14. CRC Press, Boca Raton, 2006.

[Shabgard2015] H. Shabgard, M.J. Allen, N. Sharifi, S.P. Benn, A. Faghri, and T.L. Bergman. Heat pipe heat exchangers and heat sinks: Opportunities, challenges, applications, analysis, and state of the art. *International Journal of Heat and Mass Transfer*, 89:138–158, 2015.

[Snyder2008] G.J. Snyder and E.S. Toberer. Complex thermoelectric materials. *Nature Materials*, 7:105–114, 2008.

[Stevens2004] J.W. Stevens. Optimal placement depth for air-ground heat transfer systems. *Applied Thermal Engineering*, 24:149–157, 2004.

[Stevens2013] J.W. Stevens. Performance factors for ground-air thermoelectric power generators. *Energy Conversion and Management*, 68:114–123, 2013.

[Stokes2010] C.D. Stokes, E. Duff, M.J. Mantini, B. Grant, and R. Venkatasubramanian. Nanostructured thermoelectric material and device technology for energy harvesting applications. In *2010 IEEE Nanotechnology Materials and Devices Conference*, pages 154–159, 2010.

[Suter2012] C. Suter, Z.R. Jovanovic, and A. Steinfeld. A 1kWe thermoelectric stack for geothermal power generation - Modeling and geometrical optimization. *Applied Energy*, 99:379–385, 2012.

[TECTEG2020] TEGMART. TEG Modules, 2020. `https://www.tegmart.com/thermoelectric-modules/`.

[TEGMART2020] Thermoelectric Gencell Technology. Thermoelectric power modules, 2020. `https://tecteg.com/`.

[Tahami2019] S.A. Tahami, M. Gholikhani, R. Nasouri, S. Dessouky, and A.T. Papagiannakis. Developing a new thermoelectric approach for energy harvesting from asphalt pavements. *Applied Energy*, 238:786–795, 2019.

[Tan2019] G. Tan, M. Ohta, and M.G. Kanatzidis. Thermoelectric power generation: From new materials to devices. *Philosophical Transactions of the Royal Society A: Mathematical, Physical and Engineering Sciences*, 377(20180450), 2019.

[Trip2017] N.D. Trip, A. Burca, and L. Morgos. Considerations on the use of thermoelectric generators at low temperatures to recover waste geothermal energy. In *14th International Conference on Engineering of Modern Electric Systems, EMES*, pages 248–251, 2017.

[Tzeng2014] S.C. Tzeng, T.M. Jeng, and Y.L. Lin. Parametric study of heat-transfer design on the thermoelectric generator system. *International Communications in Heat and Mass Transfer*, 52:97–105, 2014.

[UN2000] United Nations Development Programme, United Nations Department of Economic and Social Affairs, World Energy Council.

World Energy Assessment. Energy and the challenge of Sustainability. United Nations Development Programme, New York, 2000.

[Wang2008] X.W. Wang, H. Lee, Y.C. Lan, G.H. Zhu, G. Joshi, D.Z. Wang, J. Yang, A.J. Muto, M.Y. Tang, J. Klatsky, S. Song, M.S. Dresselhaus, G. Chen, and Z.F. Ren. Enhanced thermoelectric figure of merit in nanostructured n -type silicon germanium bulk alloy. *Applied Physics Letters*, 93(193121), 2008.

[Wang2017] N. Wang, D. Xu, W. Li, C. Chen, and Y. Huang. Feasibility study of a new thermoelectric conversion device utilizing the temperature differences in forest soil. *Acta Technica CSAV (Ceskoslovensk Akademie Ved)*, 62(1B):1–12, 2017.

[Wang2018a] H. Wang, A. Jasim, and X. Chen. Energy harvesting technologies in roadway and bridge for different applications – A comprehensive review. *Applied Energy*, 212:1083–1094, 2018.

[Wang2018b] K. Wang, J. Liu, and X. Wu. Downhole geothermal power generation in oil and gas wells. *Geothermics*, 76:141–148, 2018.

[Wang2019] K. Wang and X. Wu. Downhole thermoelectric generation in unconventional horizontal wells. *Fuel*, 254(115530), 2019.

[Xie2016] Y. Xie, S.J. Wu, and C.J. Yang. Generation of electricity from deep-sea hydrothermal vents with a thermoelectric converter. *Applied Energy*, 164:620–627, 2016.

[Yan2016] X. Yan, H. Cheng, Y. Zhao, W. Yu, H. Huang, and X. Zheng. Real-time identification of smoldering and flaming combustion phases in forest using a wireless sensor network-based multi-sensor system and artificial neural network. *Sensors*, 16(1228), 2016.

[Yang2005] J. Yang. Potential applications of thermoelectric waste heat recovery in the automotive industry. In *24th International Conference on Thermoelectrics*, pages 155–159, 2005.

[Yang2018] L. Yang, Z.G. Chen, M.S. Dargusch, and J. Zou. High Performance Thermoelectric Materials: Progress and Their Applications. *Advanced Energy Materials*, 8(1701797), 2018.

[Yao2019] C.J. Yao, H.L. Zhang, and Q. Zhang. Recent progress in thermoelectric materials based on conjugated polymers. *Polymers*, 11(107), 2019.

[Yu2020] K. Yu, Y. Zhou, Y. Liu, F. Liu, L. Hu, W. Ao, C. Zhang, Y. Li, J. Li, and H. Xie. Near-room-temperature thermoelectric materials and their application prospects in geothermal power generation. *Geomechanics and Geophysics for Geo-Energy and Geo-Resources*, 6(12), 2020.

[Zhou2018] X. Zhou, Y. Yan, X. Lu, H. Zhu, X. Han, G. Chen, and Z. Ren. Routes for high-performance thermoelectric materials. *Materials Today*, 21(9):974–988, 2018.

Chapter 2

First Approximation to Geothermal Thermoelectric Generators

This chapter supposes the first approximation to geothermal thermoelectric generators (GTEGs), which need to absorb heat contained within the Earth and transport it overground to the thermoelectric modules, that will transform part of it directly into electricity, releasing the rest to the environment. For this purpose, this chapter performs a conceptual design of the heat exchangers more appropriate for this task, taking into account the importance of devices without moving parts nor auxiliary equipment mentioned in the introduction. This study is carried out experimentally, considering different types of heat exchangers.

The obtained results are gathered in the publication "New opportunities for electricity generation in shallow hot dry rock fields: A study of thermoelectric generators with different heat exchangers" published in the journal *Energy Conversion and Management* 200 (2019) 112061. Hence, after contextualizing traditional and thermoelectric geothermal generation, the operation of a geothermal thermoelectric generator is described, analyzing different possibilities of hot side heat exchangers. Afterwards, it is experimentally studied the performance of fin dissipators and loop thermosyphons as cold side heat exchangers, for which the conditions available at Timanfaya National Park (Canary Islands, Spain) are taken as reference. Although the study is focused on the application of medium–scale generation from hot dry rock fields, the obtained results can also be extrapolated to the stand–alone power supply of volcanic vigilance stations.

In the published article, there is a typographic error from the journal edition process and **Table 2** has some columns displaced to the left. The correct table is depicted below:

Table 2.1: Useful heat flux, percentage of heat losses, thermal resistance of the hot side two-phase closed thermosyphon (TPCT), total and net power generated by the two thermoelectric modules, and total and net efficiencies for each experiment.

Cold side heat exchanger	T (°C)	Fan voltage (V)	Load Resistance (Ω)	$\dot{Q}$ (W)	%losses (W)	R_{TPCT} (K/W)	$\sum P_{total}$ (W)	$\sum P_{net}$ (W)	η_{total} (%)	η_{net} (%)
Loop thermosyphons	200	-	inf	201.23	8.11%	0.29	-0.01	-0.01	0.00%	0.00%
			1	241.81	6.95%	0.30	4.32	4.32	1.79%	1.79%
			2.2	228.81	7.42%	0.30	5.50	5.50	2.41%	2.41%
			3.2	223.34	8.46%	0.30	5.67	5.67	2.54%	2.54%
			4.7	217.73	8.68%	0.30	5.36	5.36	2.46%	2.46%
	180	-	inf	172.94	8.53%	0.30	0.01	0.01	0.00%	0.00%
			1	204.84	7.52%	0.32	3.29	3.29	1.61%	1.61%
			2.2	199.39	7.64%	0.31	4.29	4.29	2.15%	2.15%
			3.2	194.28	7.57%	0.31	4.37	4.37	2.25%	2.25%
			4.7	190.71	8.20%	0.31	4.21	4.21	2.21%	2.21%
	160	-	inf	146.20	8.49%	0.32	0.00	0.00	0.00%	0.00%
			1	173.87	7.41%	0.34	2.41	2.41	1.38%	1.38%
			2.2	167.78	7.63%	0.34	3.22	3.22	1.92%	1.92%
			3.2	163.74	7.77%	0.33	3.30	3.30	2.02%	2.02%
			4.7	160.38	8.08%	0.33	3.14	3.14	1.96%	1.96%
Fin dissipators	200	12	inf	180.11	8.57%	0.31	0.00	-3.84	0.00%	-2.13%
			1	202.82	7.72%	0.32	3.85	0.01	1.90%	0.01%
			2.2	197.65	8.07%	0.32	4.92	1.08	0.00%	0.00%
			3.2	194.13	8.39%	0.32	5.15	1.31	2.65%	0.67%
			4.7	191.39	8.49%	0.32	4.96	1.12	2.59%	0.59%
		10	inf	177.04	8.90%	0.31	0.00	-2.90	0.00%	-1.64%
			1	202.79	7.73%	0.32	3.51	0.61	1.73%	0.30%
			2.2	196.91	8.07%	0.32	4.78	1.88	0.00%	0.00%
			3.2	193.40	8.33%	0.32	4.93	2.03	2.55%	1.05%
			4.7	191.23	8.57%	0.32	4.69	1.79	2.45%	0.94%
		8	inf	177.16	8.84%	0.31	0.00	-2.00	0.00%	-1.13%
			1	201.76	7.81%	0.32	3.45	1.45	1.71%	0.72%
			2.2	195.85	8.17%	0.32	4.52	2.52	0.00%	0.00%
			3.2	191.94	8.63%	0.32	4.71	2.71	2.45%	1.41%
			4.7	190.07	8.72%	0.32	4.60	2.60	2.42%	1.37%
		6	inf	173.60	9.03%	0.32	0.00	-1.26	0.00%	-0.73%
			1	196.77	8.14%	0.32	3.12	1.86	1.59%	0.95%
			2.2	191.38	8.49%	0.32	4.08	2.82	0.00%	0.00%
			3.2	188.72	8.57%	0.32	4.29	3.03	2.27%	1.60%
			4.7	185.35	9.01%	0.32	4.13	2.87	2.23%	1.55%
		4	inf	165.93	9.34%	0.31	0.00	-0.68	0.00%	-0.41%
			1	185.61	8.47%	0.32	2.39	1.71	1.29%	0.92%
			2.2	181.52	8.88%	0.32	3.31	2.63	0.00%	0.00%
			3.2	179.45	9.11%	0.32	3.49	2.81	1.95%	1.57%
			4.7	177.61	9.33%	0.32	3.38	2.70	1.90%	1.52%
		0	3.2	158.38	9.50%	0.31	2.24	2.24	1.42%	1.42%

Energy Conversion and Management 200 (2019) 112061

Contents lists available at ScienceDirect

Energy Conversion and Management

journal homepage: www.elsevier.com/locate/enconman

New opportunities for electricity generation in shallow hot dry rock fields: A study of thermoelectric generators with different heat exchangers

Leyre Catalan, Patricia Aranguren, Miguel Araiz, Gurutze Perez, David Astrain*

Institute of Smart Cities, Public University of Navarre, Pamplona, Spain

ARTICLE INFO

Keywords:
Thermoelectric generator
Geothermal
Hot dry rock
Thermosyphon
Fin dissipator

ABSTRACT

Despite being one of the largest renewable sources, geothermal energy is not widely utilized for electricity generation. In order to leverage shallow hot dry rock (HDR) fields, the present paper proposes an alternative to enhanced geothermal systems (EGS): thermoelectric generators. Based on the conditions of Timanfaya National Park, a prototype has been built to experimentally analyze the feasibility of the proposed solution. The prototype is composed by a two phase closed thermosyphon (TPCT) as hot side heat exchanger, two thermoelectric modules, and it considers different cold side heat exchangers: fin dissipators assisted by a fan and loop thermosyphons, both with various geometries. Experiments have demonstrated that loop thermosyphons represent the best alternative due to their low thermal resistance and, especially, due to their lack of auxiliary consumption, leading to a maximum net power generation of 3.29 W per module with a temperature difference of 180 °C (200 °C in the hot side and 20 °C as ambient temperature), 54% more than with fin dissipators. Hence, there exists a new opportunity for electricity generation in shallow hot dry rock fields: thermoelectric generators with biphasic thermosyphons as heat exchangers, a patented and robust solution.

1. Introduction

Geothermal energy is considered one of the largest renewable sources and lacks one of the main disadvantages of other renewable energies: it is not weather affected [1]. Nevertheless, electricity generation based on geothermal energy represents less than 0.4% of the global electricity generation thanks to the installed capacity of 13.5 GW, which seems insignificant compared to hydro-power (1096 GW), wind power (487 GW), or photovoltaics (303 GW) [2].

Li et al. [3] identified that the reasons causing the low growth rate of geothermal power are the high initial investment, the long payback and construction time, as well as the difficulties assessing the resource and modularizing. In order to speed up its growth, they pointed out three possible directions: co-produced geothermal power from oil/gas fields, enhanced geothermal systems, and development and utilization of new technologies such as thermoelectric generators. The present paper focuses on the latter, trying to analyze the possibilities of thermoelectric generators to directly convert geothermal heat into electricity.

Traditionally, in order to generate electricity from the heat contained within the Earth, a geothermal system is required. Geothermal systems are characterized by three elements: a heat source, a fluid that acts as heat carrier, and a reservoir. However, geothermal systems are not always available, as it occurs in one of the most extended geothermal fields: Hot Dry Rock (HDR) fields, which in the United States represent 99% of the available resources [4]. These fields, as indicated by their name, are characterized by high temperature compact rock. Thus, their lack of both reservoir and natural working fluid difficults electricity generation.

Nowadays, there only exists one process capable of generating electricity based on HDR fields: enhanced geothermal systems (EGS), which consist in the artificial creation of a geothermal system. For this purpose, a fluid is pumped at high pressure causing hydraulic fractures in the rock and leading to an artificial reservoir. Once created, a working fluid is cyclically introduced at certain pressure so that part of the heat of the rocks is absorbed. The expansion of the vaporized fluid generates electricity in an alternator similarly to natural geothermal systems.

The most critical issue of the hydraulic fracturing method are the induced seismicities, which can cause a considerable impact in the environment and can become critical in those fields bounded to recent vulcanism. To the previous issue, it is necessary to add the required equipment in the cycles (turbines, pumps, cooling towers…), which are complex, expensive, require recurrent maintenance, and present elevated operating costs. This series of technical problems cause the existence of numerous HDR fields which, despite having elevated

* Corresponding author.

https://doi.org/10.1016/j.enconman.2019.112061
Received 2 August 2019; Received in revised form 9 September 2019; Accepted 10 September 2019

Nomenclature

Variables

$\dot{Q}$	heat flux. If not specified, useful heat flux (substracting thermal losses) (W)
η	efficiency
A	area (m^2)
h	convection coefficient ($W/m^2 K$)
I	electrical current (A)
k	thermal conductivity (W/mK)
L	thickness (m)
Nu	Nusselt number
P	electric power (W)
p_{int}	internal pressure (bar)
Pr	Prandtl number
R	thermal Resistance (W/mK)
Re	Reynolds number
T	temperature (°C)
V	voltage (V)
M	number of thermoelectric modules

Subscripts

amb	ambient
fan	auxiliary fan
he	base of the heat exchanger
ins	insulation
mod	thermoelectric module
net	net, removing auxiliary consumption
p	heating plate
tl	thermal losses
total	total, including thermal losses or auxiliary consumption
1	upper part of the TPCT
2	hot side of the thermoelectric module
3	cold side of the thermoelectric module
4	cold side heat exhanger
R	heating resistances

Abbreviations

EGS	enhanced geothermal system
FD	fin dissipator
GTEG	geothermal thermoelectric generator
HDR	hot dry rock
LT	loop thermosyphon
ORC	organic rankine cycle
TEG	thermoelectric generator
TPCT	two phase closed thermosyphon

temperatures, are not currently under exploitation. Nowadays, the Geodynamics plant in Habanero (Australia) is the only commercial EGS plant in the world [5].

Faced with this situation, for those shallow HDR fields, thermoelectric generators (TEGs) can represent an alternative with reduced environmental impact and a greater ability to modularize. TEGs are devices based on solid-state physics whereby heat is directly converted into electricity due to Seebeck effect. This transformation is held on the so-called thermoelectric modules. Since the efficiency of the thermoelectric modules increases as their sides approach the temperature of the heat source and sink, the introduction of heat exchangers with low thermal resistance between the modules and each of the thermal reservoirs becomes necessary in order to maximize the temperature difference of the modules and therefore, their generation [6]. Thus, a thermoelectric generator is composed by thermoelectric modules and heat exchangers.

The most typical heat exchangers used in TEGs are fin dissipators and liquid based heat exchangers [7]. Fin dissipators are simple, robust, as well as easy and cheap to manufacture. These dissipators lead to relatively low thermal resistances when working as active systems, this is, assisted by a fan [8–10]. Since liquids normally present higher convective coefficients than air, heat exchangers based on a liquid are also very common [11]. They present lower values of thermal resistance, with the drawback of being more complex and requiring a higher number of elements (pump, pipes, secondary heat exchanger…) [12]. In both cases, the most important limitation is their auxiliary consumption due to the electric power necessary to operate the fans responsible of the forced convection, and the pumps that provoke the recirculation of the working fluid, which can drastically reduce power generation of TEGs [13].

In the last years, heat exchangers based on phase change (heat pipes and biphasic thermosyphons) have received a lot of attention [11]. These devices take advantage of the latent heat of an internal working fluid to transfer a large amount of heat, nearly isothermally, with a minimal driving temperature difference through a small cross sectional area [14]. Their operation is similar: the absorption of heat causes the evaporation of the working fluid, which will naturally ascend until it reaches the lower temperature condenser section, within which condensation of the fluid occurs. Heat pipes and thermosyphons differ only in the inclusion of an internal wick in the former, which acts as a capilary pump that moves the condensed liquid from the condenser to the evaporation section, a process driven by gravity in thermosyphons [15]. As a consequence, heat pipes are able to work in any orientation and even in zero-gravity environments. However, this gives rise to some negative aspects such as the introduction of an extra thermal resistance, lower heat fluxes, and a higher complexity for design and construction that makes them more expensive [16].

There already exist different proposals to transform geothermal heat directly into electricity by means of TEGs. Niu et al. [17] were the first ones building a geothermal thermoelectric generator (GTEG). They were able to generate 146.5 W with 56 thermoelectric modules and a temperature difference between sources of 120 °C (2.62 W per module). Based on a similar design, Suter et al. [18,19] optimized a 1 kW thermoelectric stack by simulating different operating parameters and stack geometries considering a 100 °C gradient. Liu et al. [20–22] were also convinced about this technology. Hence, they built a thermoelectric generator composed by 96 thermoelectric modules that generated 160 W with a temperature difference of 80 °C. They estimated that this prototype could reach 500 W with a temperature difference of 200 °C. With another prototype with 600 modules they predicted a generation of 1 kW with a temperature difference of 120 °C. More recently, Ahiska and Mamur [23,24] developed a prototype capable of producing 41.6 W with 20 modules and 67 °C temperature difference (2.08 W per module), while Trip et al. [25] developed a 0.4 W generator with a temperature difference of 72 °C, composed by 40 thermoelectric modules (9.7 mW per module). On their behalf, Wang et al. defended the combination of geothermal and hydrocarbons, integrating thermoelectric generators downhole in oil and gas wells. By means of a computational model, they estimated a maximum power output of 8538 W with a 100 °C temperature difference in a vertical well in China [26], and 128024 W in case of a horizontal one with a 156 °C gradient [27].

All the previous geothermal thermoelectric generators (GTEGs) have two aspects in common. On the one hand, they focus on medium-low temperature geothermal fields (< 180 °C), hence competing with Organic Rankine Cycle (ORC) binary power generators, the frequently used technology to generate electricity from this low enthalpy

geothermal heat. The evaluation of possibilities in high-temperature geothermal fields has just been analyzed for the extraction of this energy from oceanic crust in offshore wind turbine monopiles, which estimates a maximum power output of 242 kW [28]. On the other hand, all these generators use liquid based heat exchangers, normally with water, achieving low values of thermal resistances but presenting an extra consumption that reduces net generation.

The application of thermoelectric generators in HDR fields nor the utilization of heat exchangers other than those based on liquidshas never been studied. Hence, the objective of the present paper is to, for the first time, experimentally analyze the possibilities of thermoelectric generators in shallow HDR fields, studying different heat exchangers. For this purpose, the conditions available at Timanfaya National Park (Spain) will be taken as reference. Due to the last eruptions in 1730–36 and 1824, this National Park hosts one of the greatest shallow HDR geothermal system in the world, both in extension, with more than 11,700 m^2 of geothermal anomalies, and intensity, with temperatures of 100–400 °C at ground level and 210–550 °C at a depth of 5–10 m [29].

Section 2 describes the geothermal thermoelectric generator (GTEG) developed in order to experimentally analyze the feasibility of a GTEG with different heat exchangers for shallow HDR fields. Section 3 details the methodology followed in all the experimental tests while Section 4 shows and discusses the obtained results. Finally, Section 5 collects the main conclusions of the present paper.

2. Description of the GTEG

Fig. 1 depicts the operation principle of a geothermal thermoelectric generator (GTEG) for shallow HDR fields. A heat exchanger introduced in the superficial geothermal anomalies will transfer heat to the thermoelectric modules, which will transform part of this heat into electricity, releasing the rest to the environment by means of the cold side heat exchangers.

The present section details all the elements that constitute the prototype used in order to experimentally analyze the possibilities of GTEGs in HDR fields: hot side heat exchanger, thermoelectric modules and cold side heat exchangers.

2.1. Hot side heat exchanger

The purpose of the heat exchanger located at the hot side of the thermoelectric generator is to transmit the necessary geothermal heat flux to the hot face of the modules, trying to approximate the temperature of the modules to the temperature of the heat source. In order to carry this heat without fracturing the rock, the simplest device consists in a solid bar of a highly conductive material such as aluminum. However, the temperature loss is considerable. According to Fourier's law of heat conduction, the rate of heat transfer through any material is proportional to the temperature gradient ΔT, the area A and the inverse of the thickness L. For a unidirectional flux and focusing on the magnitude rather than in the heat flow direction, Eq. (1) is obtained, where k represents the proportionality constant, which is known as *thermal conductivity* [W/mK].

$$\frac{\Delta T}{L} = \frac{\dot{Q}}{A \cdot k} \tag{1}$$

Based on this equation, Fig. 2 represents the temperature drop per unit of length for different highly conductive materials (aluminum, copper, and silver) with respect the transmitted heat flux. As it can be observed, in order to obtain a minimum temperature loss, low heat fluxes and big sections are required, which increment the weight and cost of the solution. In the case of a GTEG that needs to extract heat located several meters deep in the ground, and whose generation is proportional to its temperature difference and heat flux, this solution is considered unacceptable.

The temperature drop can be reduced by means of a heat exchanger based on phase change, as it is the case of two-phase closed thermosyphons (TPCTs), a type of biphasic thermosyphon. The use of this type of heat exchangers in order to absorb geothermal heat with a minimum temperature loss has already been proven for distances as high as 400 m [30] in their application for a heat pump. Chet et al. [31] also proposed it for a geothermal thermoelectric generator (GTEG) due to its passive character and good heat transfer capacity, but they did not experimentally tested it. Hence, the thermoelectric generator experimented in this paper incorporates a TPCT as hot side heat exchanger.

The hot side TPCT consists in a one meter long stainless steel AISI 304 ACX 120 squared tube with a section of 60 × 60 mm^2 and a thickness of 5 mm (Fig. 3). This heat exchanger is designed to hold water as working fluid up to pressures of 20 bar and its squared shape facilitates thermal contact with the thermoelectric modules. The design is completed with two valves (one in each end), which permit filling up the thermosyphon with the working fluid; as well as two metallic plates in the middle, with the only objective of holding the prototype during the experiments.

2.2. Thermoelectric modules

Thermoelectric modules represent the most important element of the generator, since the transformation of heat into electricity is held on them. For the considered prototype, two Marlow TG12-8L modules [32] have been used, each of them releasing heat to one of the heat exchangers detailed in next subsection. These thermoelectric modules are composed by 127 Bismuth-Telluride thermocouples and are able to operate with temperatures up to 230 °C.

2.3. Cold side heat exchangers

The purpose of the heat exchangers located at the cold side of the thermoelectric generator is to approximate the temperature of the cold side of the thermoelectric modules to the temperature of the heat sink, the environment. In order to determine the best configuration for a GTEG, two different alternatives of cold side heat exchangers have been analyzed: fin dissipators and loop thermosyphons.

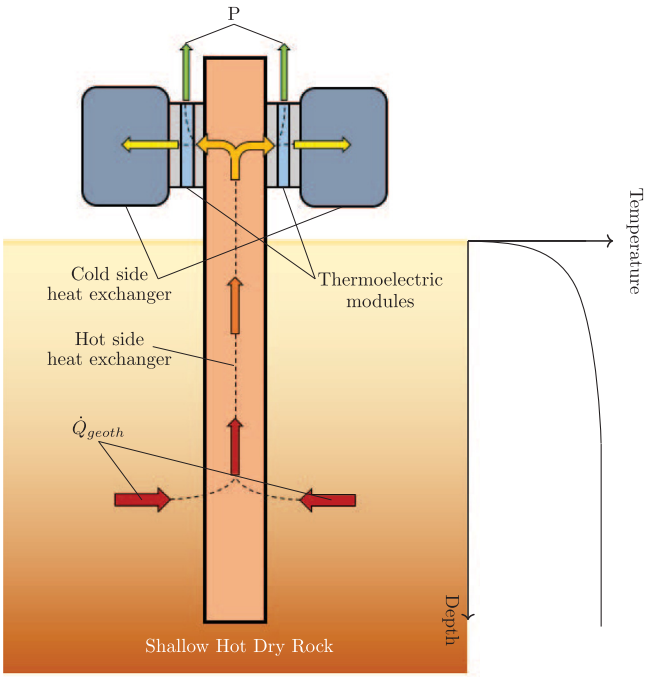

Fig. 1. Schematics of the operation of a geothermal thermoelectric generator (GTEG).

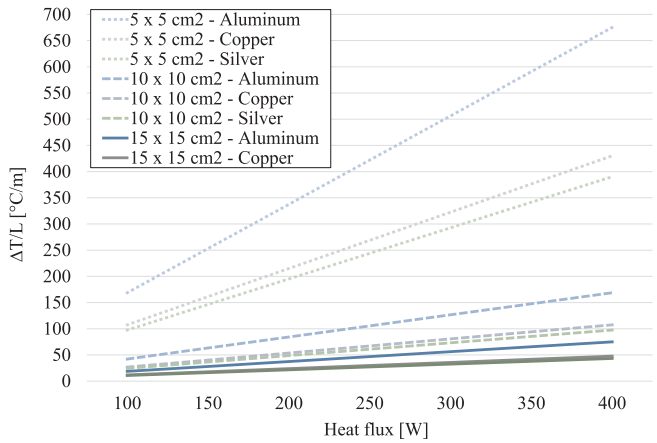

Fig. 2. Temperature drop per unit of length for aluminum, copper, and silver with respect the transmitted heat flux, considering different cross-sectional areas.

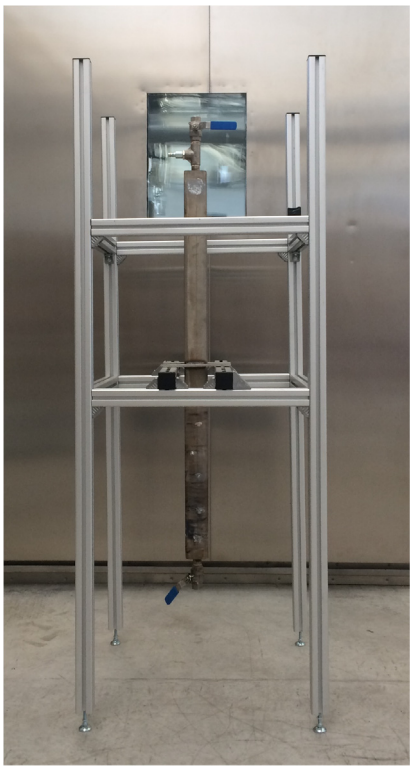

Fig. 3. Designed two phase closed thermosyphon (TPCT) for the hot side of the geothermal thermoelectric generator (GTEG).

2.3.1. Fin dissipators

As a consequence of heat transfer laws, the easiest way for reducing the thermal resistance of a heat exchanger is to increase its area. This is the essence of fin dissipators, which increment the surface of a highly conductive plate by means of a metallic fin array, normally presenting a rectangular profile. A further reduction of the thermal resistance can be obtained thanks to a fan since it improves the convection coefficient, with the disadvantage of presenting an extra consumption.

Thermoelectric modules are characterized by elevated heat fluxes across a relatively small surface (typically $40 \times 40\ mm^2$). Hence, the spreading component gains importance in the total thermal resistance of a fin dissipator [33]. In order to study the real influence of this phenomenon, in the present paper, the two different geometries of aluminum fin dissipators shown in Fig. 4(a) have been analyzed. Both dissipators are 90 mm wide, have a base 14.5 mm high and present a pattern of 1.5 mm wide and 39.5 mm high fins spaced 4.8 mm apart. Each dissipator is also assisted by an $80 \times 80\ mm^2$ ventilator in its lowest part, perpendicular to the fins and aligned with the thermoelectric module. The only difference between both dissipators is their length: one is 150 mm long and the other 250 mm. Thus, it will be experimentally analyzed the importance of increasing the area (which theoretically leads to lower thermal resistance) versus the spreading phenomenon (which can curb the previous increase).

2.3.2. Loop thermosyphons

The second type of heat exchangers studied for the cold side of the geothermal thermoelectric generator is similar to the one used for the hot side: biphasic thermosyphons. As it has been stated, these heat exchangers present low thermal resistances, being able to transmit a large amount of heat with a minimal temperature loss thanks to phase change.

In the present paper, the two different geometries of loop thermosyphons shown in Fig. 4(b) have been analyzed. Both loop thermosyphons have a $50 \times 50\ mm^2$ boiling area, 35 mm wide, and a mixture of water/ammonia as working fluid. The only difference between them is the condensation/convection zone: one presents 8 levels of 420 mm long tubes with a diameter of 6 mm, and the other one only 6. In both cases, there are two sets of tubes. The loop thermosyphons will work passively, without any external fan. Hence, convection is expected to be important in the total thermal resistance of the loop thermosyphons, and presumably, the difference of size will lead to different values of thermal resistance, being lower with higher convection areas.

3. Methodology

Based on the prototype described in the last section, different experiments have been carried out. The methodology followed in each of them is explained in this section, differentiating, on the one hand, the characterization of the cold side heat exchangers and, on the other hand, the study of the geothermal thermoelectric generator (GTEG) for

Fig. 4. Experimented heat exchangers: (a) 150 mm and 250 mm long fin dissipators (b) 8 level and 6 level loop thermosyphon.

Timanfaya National Park. In both cases, each experiment has been repeated three times and the uncertainties have been calculated according to [34].

3.1. Characterization of the cold side heat exchangers

The characterization of the cold heat exchangers refers to the experimental determination of the thermal resistances of the heat exchangers for different heat fluxes and air velocities (in the case of fin dissipators).

In order to experimentally determine the thermal resistance of the fin dissipators described in Section 2.3.1, a $40 \times 40\ mm^2$ electric heating plate provided a heat flux $\dot{Q}_{total}$, which was in turn divided into useful heat flux $\dot{Q}$ and thermal losses $\dot{Q}_{tl}$. The heat flux corresponding to these thermal losses was minimized with an 8 cm rock-wool insulation and an additional 2 cm neoprene-sheet layer, so that thermal losses were lower than 1%.

The thermal resistance R of each fin dissipator was calculated according to Eq. (2), where T_{he} is the temperature measured at the base of the dissipator thanks to a groove that reaches the center of the heating plate, T_{amb} is the ambient temperature, and $\dot{Q}$ is the useful heat flux obtained subtracting the thermal losses $\dot{Q}_{tl}$ to the power supplied to the electric heating plate $\dot{Q}_{total}$ (Eq. (3)). The thermal losses $\dot{Q}_{tl}$ were calculated thanks to the temperature difference between the external part of the insulation (T_{ins}) and the ambient (T_{amb}), the insulation area A_{ins} and a convection coefficient h derived from Eq. (4) [35].

$$R = \frac{T_{he} - T_{amb}}{\dot{Q}} \tag{2}$$

$$\dot{Q} = \dot{Q}_{total} - \dot{Q}_{tl} = V_p \cdot I_p - h \cdot A_{ins} \cdot (T_{ins} - T_{amb}) \tag{3}$$

$$Nu_L = 0.664 \cdot Pr^{1/3} \cdot Re_L^{1/2} \quad \begin{bmatrix} 0.6 \leqslant Pr \leqslant 50 \\ Re < Re_{x,c} \approx 5 \cdot 10^5 \end{bmatrix} \tag{4}$$

For each fin dissipator, its thermal resistance was calculated for the heat fluxes and air velocities summarized in Table 1.

The methodology followed for determining the thermal resistance of the loop thermosyphons described in Section 2.3.2 was similar to the one described for the fin dissipators. The only difference is that in this case, the study was just referred to different heat fluxes since the considered loop thermosyphons work passively and therefore, do not include auxiliary fans. The studied values are summarized again in Table 1.

3.2. Study of the GTEG for Timanfaya National Park

Aligned with the objective of the present paper, this section deals with the study of the geothermal thermoelectric generator described in Section 2 for the two characterized cold side heat exchangers and for different conditions. The study includes an analysis of the temperature distribution, an evaluation of the generation possibilities, the characterization of the thermal resistance of the hot side TPCT as well as the determination of the prototype efficiencies (total and net efficiencies).

Boreholes located at Timanfaya National Park present temperatures ranging from 200 to 500 °C in their first meters [29]. In order to simulate these extraordinary conditions in the laboratory, some heat was directly applied to the lower part of the hot side TPCT by means of rope heaters tighten thanks to several clamps (Fig. 5). Rope heaters covered exactly the same height as the working fluid: 0.36 m, approximately one third of the total height of the TPCT. A 115 mm layer of rockwool followed by 59 mm of neoprene prevented heat losses to the environment along the total height of the heat exchanger (Fig. 6). Rockwool and neoprene were also added in order to minimize heat losses in the valves and the supporting plates.

Experiments purposed to determine the best configuration for a GTEG: with loop thermosyphons or with fin dissipators in the cold side. On the one hand, for the analysis of loop thermosyphons, the two sizes described in Section 2.3.2 were studied simultaneously, opposite to each other as depicted in Fig. 7(a). The power generation of each thermoelectric module was studied separately for different temperatures of the hot source (160 °C, 180 °C, and 200 °C), and load resistances (1, 2.2, 3.2, and 4.7Ω, as well as open circuit). This generation was monitored by means of ALMEMO voltmeters and ammeters ZA9900 AB and ZA9901 AB respectively, so that:

$$P_{total} = V_{mod} \cdot I_{mod} \tag{5}$$

On the other hand, in the case of fin dissipators, the two considered sizes were independently analyzed (Fig. 7(b)). In this case, it was also necessary to consider another variable of study: voltage supplied to the fans. In particular, 0 (natural convection), 4, 6, 8, 10, and 12 V were studied. This extra consumption needs to be subtracted from the total generation of the modules P_{total} (Eq. (5)), leading to a net generation of:

$$P_{net} = P_{total} - P_{fan} = V_{mod} \cdot I_{mod} - V_{fan} \cdot I_{fan} \tag{6}$$

Besides power generation, temperatures were also monitored. A total of 21 K-type thermocouples were distributed as depicted in Fig. 8: 5 in the heating resistances (T_{R1-A}, T_{R1-B}, T_{R2-D}, T_{R3-A} *and* T_{R3-B}), 6 in the exterior part of the insulation in order to measure heat losses (T_{E1}, T_{E2}, T_{E3}, T_{E4}, T_{E5} *and* T_{E6}), one in the adiabatic part of the hot side thermosyphon T_{AD}, one to measure the ambient temperature T_{amb}, and 8 to determine the temperature of the hot and the cold side of the modules (T_{B1}, T_{B2}, T_{B3}, T_{B4}, T_{S1}, T_{S2}, T_{S3}, T_{S4}), 4 per each module (it was necessary to add a $40 \times 40\ mm^2$ aluminum heat extender with grooves to measure these temperatures without affecting thermal contact). Moreover, a pressure sensor determined the internal pressure of the hot side thermosyphon (p_{int}). As before, an ALMEMO data-logger collected the information of all these sensors.

Based on these temperature measurements, an analysis of the temperature distribution was performed, paying special attention to the effect of the values of thermal resistances studied in the last section. Furthermore, these temperatures allowed the calculation of the thermal resistance per module of the hot side TPCT according to:

$$R_{TPCT} = M \cdot \frac{T_R - T_1}{\dot{Q}} \tag{7}$$

where T_R is the mean temperature of the heating resistances, T_1 is the average temperature in the upper part of the TPCT and $\dot{Q}$ is the useful heat, which is in turn calculated by subtracting the thermal losses $\dot{Q}_{tl}$ to the total heat provided by the heating resistances $\dot{Q}_R$ (Eq. (8)). Since the parameter of interest is the thermal resistance per thermoelectric module, the previous expression was multiplied by the number of modules $M = 2$.

$$\dot{Q} = \dot{Q}_R - \dot{Q}_{tl} = V_R \cdot I_R - \sum h \cdot A_{ins} \cdot (T_{ins} - T_{amb}) \tag{8}$$

Thermal losses $\dot{Q}_{tl}$ were calculated by adding the thermal losses of the lower cap, the inferior part (under the supporting plates), the adiabatic part over the supporting plates and the upper cap that insulates the filling valve (Fig. 8).

Table 1
Heat fluxes and air velocities (function of the supply voltage) analyzed for the characterization of each fin dissipator and loop thermosyphon.

150 mm long Fin dissipators		250 mm long Fin Dissipator		Loop Thermosyphons
Heat flux	Air velocity (Fan voltage)	Heat flux	Air velocity (Fan voltage)	Heat flux
20 W	0.62 m/s (6 V)	20 W	0.53 m/s (6 V)	20 W
60 W	0.78 m/s (8 V)	60 W	0.70 m/s (8 V)	40 W
100 W	0.89 m/s (10 V)	100 W	0.81 m/s (10 V)	60 W
140 W	0.97 m/s (12 V)	140 W	0.89 m/s (12 V)	100 W
				140 W

Fig. 5. Rope heaters used as heat source: (a) detail of the rope heaters (b) clamps used to ensure good contact between the heaters and the hot side TPCT.

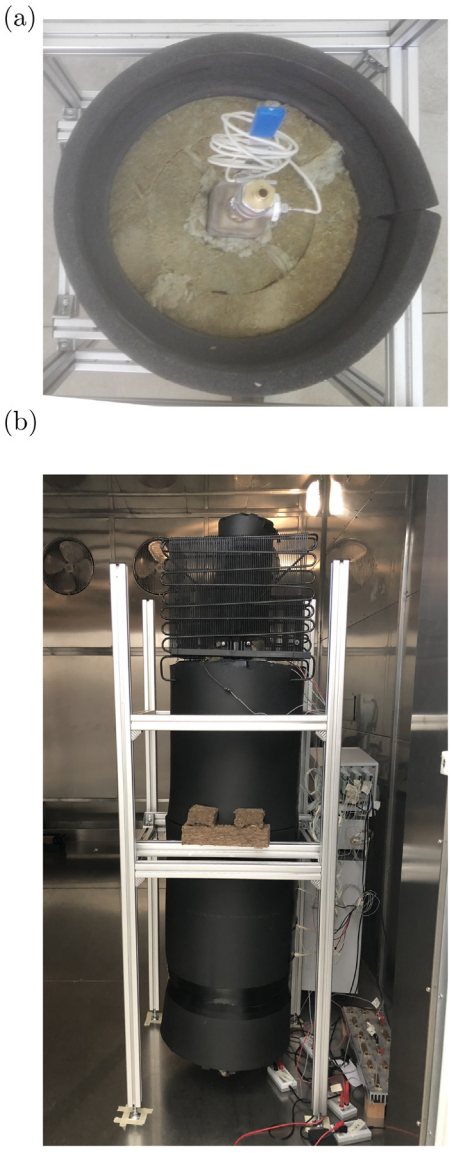

Fig. 6. Insulation to prevent heat losses: (a) Bottom view of the insulation layers (b) global view of the insulation of the hot side TPCT.

Finally, the efficiencies of the GTEG were estimated with Eq. (9), dividing the sum of the electric power generated by the two modules installed in the prototype by the useful heat $\dot{Q}$ calculated with Eq. (8). The sum of P_{total} gives rise to the total efficiency η_{total}, while the sum of P_{net} leads to the net efficiency η_{net}.

$$\eta = \frac{\sum_{M=1}^{2} P}{\dot{Q}} \tag{9}$$

4. Results and discussion

Based on the previous methodology, this section presents and explains the obtained results. First, Section 4.1 details the characterization of the cold side heat exchangers. Afterwards, Section 4.2 studies the whole geothermal thermoelectric generator based on the conditions of Timanfaya National Park.

4.1. Characterization of the cold side heat exchangers

As it has been stated before, in thermoelectric generators it is of utmost importance to include heat exchangers with low thermal resistances so that the temperature of the sides of the thermoelectric modules approximates, as much as possible, to the temperature of the heat source and sink. Nevertheless, this is not always an easy task and it often requires an extra consumption of energy.

Fig. 9(a) shows the thermal resistance of the fin dissipators with respect to the useful heat flux $\dot{Q}$ for different supply voltages and sizes. As it was expected, thermal resistance does not vary with heat flux due to the fact that the properties barely change with temperature. For the considered range, the thermal conductivity of aluminum remains almost constant and the variations on air properties blur due to forced convection.

Nonetheless, the thermal resistance of fin dissipators does vary with air velocity, this is, with the voltage supplied to the fans responsible of forced convection (Fig. 9(b)). Thus, thermal resistance follows a similar trend regardless the length: due to the improvement in the convection coefficient, thermal resistance decreases as voltage increases, showing values ranging from 0.27 to 0.37 K/W in case of the 250 mm long fin dissipator and from 0.28 to 0.38 K/W in case of the 150 mm one. However, values do not differ much with respect to the length due to two aspects. On the one hand, the importance of spreading: not all the area is effective for heat dissipation. On the other hand, the higher pressure losses in the 250 mm fin dissipator, which cause a reduction in the air velocity for the same fan voltage (Table 1), and therefore, a deterioration of the convection coefficient.

Passive loop thermosyphons are the other type of heat exchangers that have been studied. Since these heat exchangers are based on the phase change of an internal fluid and the properties of this fluid improve with temperature, heat flux does influence on their thermal resistance (Fig. 10). Hence, as heat flux increases, thermal resistance decreases. In this case, the difference on size has a greater influence than in fin dissipators, with values that vary from 0.16 to 0.29 K/W in case of the 8 levels loop thermosyphon, and from 0.24 to 0.4 K/W in case of the 6 levels one. One of the main advantages of loop thermosyphons is that all the convective area is effective for heat dissipation since heat flux is uniformly distributed among it, leading to lower thermal resistances with bigger convective areas. Due to this aspect, it is possible to obtain low values of thermal resistance without the need for forced convection.

In comparison with fin dissipators, the 8 levels loop thermosyphon presents lower values of thermal resistances, while the 6 levels one present similar ones. Nonetheless, it is necessary to take into account that fin dissipators are active heat exchangers that require a fan, with its corresponding energy demand, in order to achieve those values of

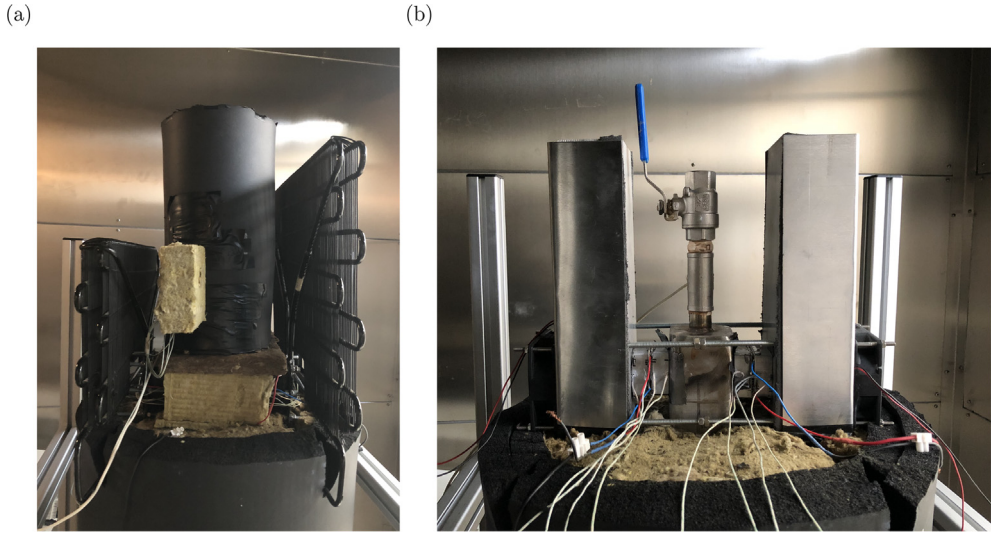

Fig. 7. Studied configurations in the cold side: (a) loop thermosyphons (b) 250 mm fin dissipator.

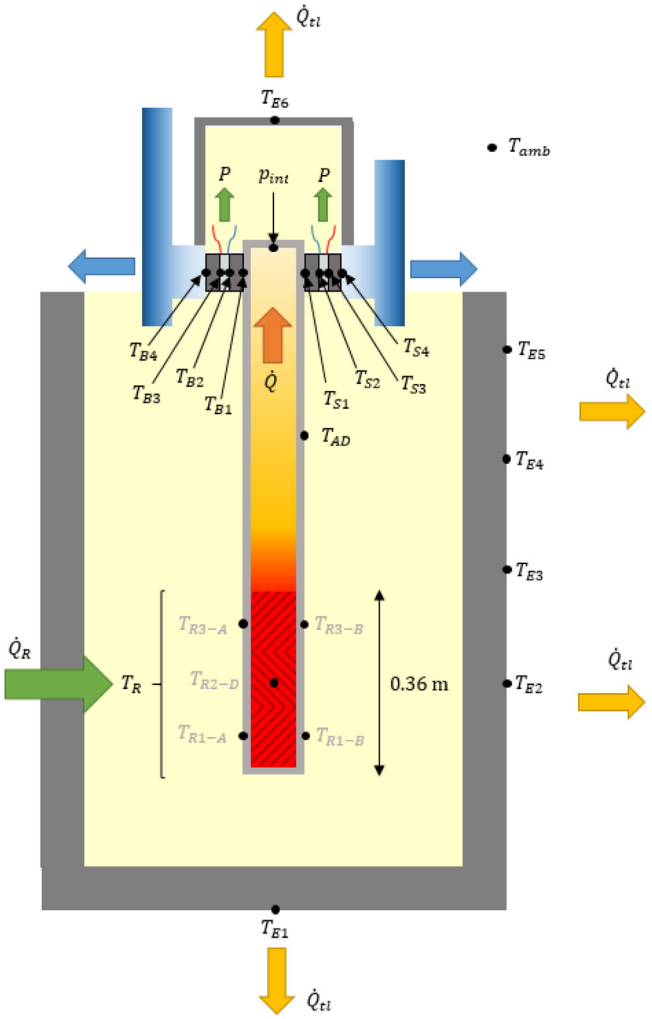

Fig. 8. Distribution of the K-type thermocouples installed in order to monitorize the prototype and detail of the heat fluxes.

thermal resistances. Therefore, it will be necessary to consider this consumption of energy when determining the net generation of the thermoelectric generators presented in the next section.

4.2. Study of the GTEG for Timanfaya National Park

The previous cold side thermal resistances influence the temperature distribution in the geothermal thermoelectric generator (GTEG). Fig. 11 shows the temperature of the heat source (T_R), the upper part of the hot side thermosyphon (T_1), the hot and the cold side of the thermoelectric modules (T_2 and T_3 respectively), the cold side heat exchanger (T_4), as well as the ambient temperature (T_{amb}). For all the studied cases, as desired, the maximum temperature difference occurs between the hot and the cold side of the modules. Nonetheless, this difference depends on the temperature of the heat source and the thermal resistance of the cold side heat exchangers. The introduced heat extenders cause a reduction of the temperature difference between the sides of the modules ($T2 - T3$), which will lead to a lower generation. However, they are necessary in order to measure the temperature of the hot and the cold side of the modules without affecting the thermal contact.

Since loop thermosyphons present lower values of thermal resistances, the present section emphasizes their analysis. Fig. 11(a) depicts the temperature distribution for the loop thermosyphons configuration taking into account different temperatures of the heat source. As it can be observed, the variation on the heat source temperature principally affects those points located close to the source. Thus, since the hot side temperature of the thermoelectric modules approaches the temperature of the heat source, there exists a greater difference between the sides of the module with higher source temperatures. This temperature difference is slightly higher for the 8 levels loop thermosyphon since its lower value of thermal resistance causes the temperature of this heat exchanger to resemble the ambient one more. Furthermore, it can also be observed that the temperature difference in the hot side TPCT remains practically constant regardless the heat source temperature, so it appears that its thermal resistance does not vary. This fact will be studied later in this section.

For the configuration with fin dissipators, only the temperature distribution for a heat source of 200 °C and 250 mm long fin dissipators is shown for different supply voltages of the auxiliary fans. In this case, the higher the voltage (and consequently the velocity of the forced air), the higher the temperature difference between the sides of the module, since the lower values of the thermal resistance lead again to an approximation of the temperature of the cold side of the module to the ambient one. Regarding the temperature difference in the hot side TPCT, in this case all the experiments also present similar values. This temperature difference practically coincides with the one obtained with loop thermosyphons.

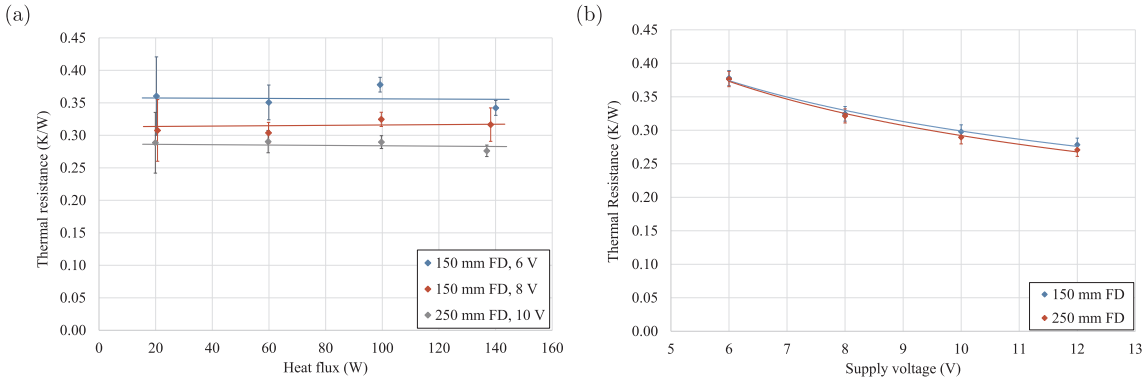

Fig. 9. Experimental thermal resistances of the fin dissipators (a) with respect to the useful heat flux and (b) with respect to the fan supply voltage.

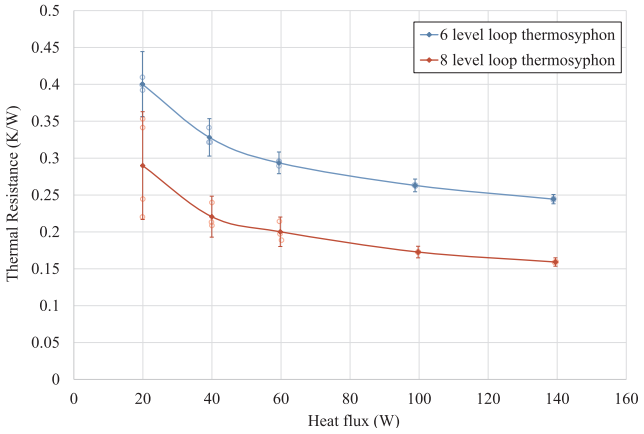

Fig. 10. Experimental thermal resistances of the 8 levels (red) and 6 levels (blue) loop thermosyphons with respect to the useful heat flux. (For interpretation of the references to colour in this figure legend, the reader is referred to the web version of this article.)

Continuing with the comparison between Fig. 11(a) and (b), the importance of having cold side heat exchangers with a low thermal resistance becomes definitely evident. The lower thermal resistance of loop thermosyphons leads to a lower temperature difference on those heat exchangers so that the cold face of the thermoelectric modules is closer to the ambient temperature and the temperature difference of the modules is higher. Hence, the lower the value of the thermal resistance, the higher the temperature difference in the thermoelectric modules, leading to a greater generation.

Fig. 12 represents the power generation per thermoelectric module for different load resistances and temperatures of the heat source, in the case of the loop thermosyphons configuration. Regardless the size of the thermosyphon, maximum generation is obtained with a load resistance of 3.2 Ω, which corresponds with the electrical resistance of Marlow TG12-8L modules. This generation is proportional to the temperature of the heat source due to the higher temperature difference between the sides of the modules with higher heat source temperatures. Nonetheless, its value depends on the size of the loop thermosyphon used as cold side heat exchanger. Thus, for the 8 levels thermosyphon, which presents a lower value of thermal resistance, a power generation of 3.3 W is achieved for a temperature of 200 °C, while in the case of the 6 levels one only 2.4 W are obtained. Fig. 13 summarizes the influence of both the heat source temperature and the value of the thermal resistance, representing the maximum generated power per module (corresponding to a load resistance of 3.2 Ω) with respect to the temperature of the heat source. Hence, for a GTEG, it is interesting to have high temperature heat sources and heat exchangers with thermal resistances as low as possible.

In the case of fin dissipators, the maximum total power generation per thermoelectric module is 2.3 W, which is obtained for the 250 mm long dissipator when its auxiliary fan was working at its maximum voltage: 12 V (Fig. 14), and the load resistance connected was 3.2 Ω. Nevertheless, it is necessary to subtract the consumption of the fan in order to obtain the net generation per thermoelectric module, which can even be negative for small load resistances. Considering only net generation, the maximum power generated per thermoelectric module with fin dissipators is 1.5 W for the case of a fan supply voltage of 6 V (and again for a load resistance of 3.2 Ω). As it can be observed in Fig. 14(b), total power generation increases with the fan supply voltage, since the increased air velocity leads to a better forced convection and therefore a lower thermal resistance. However, net generation presents a maximum for a supply voltage of 6 V when there is an equilibrium between thermal resistance and fan consumption.

If generation with loop thermosyphons and fin dissipators is compared, it is demonstrated that loop thermosyphons are a better

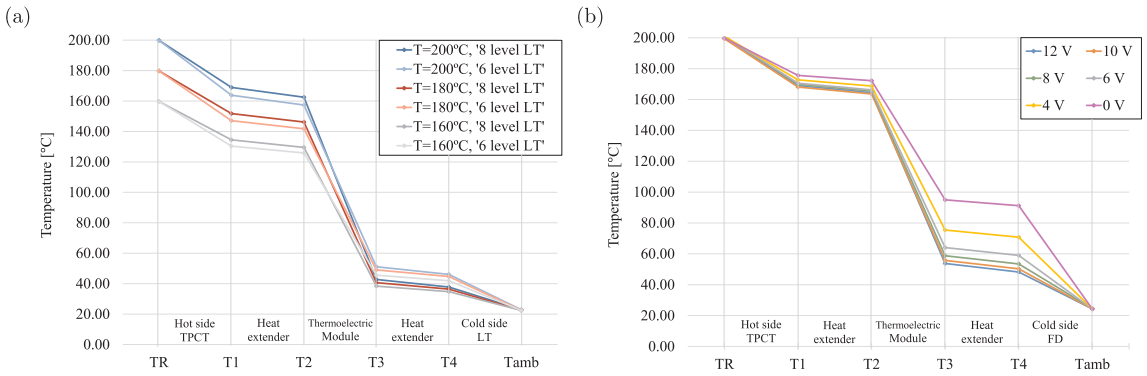

Fig. 11. Temperature distribution at relevant points: (a) for the loop thermosyphons configuration and different temperatures (b) for the fin dissipator configuration, T = 200 °C and different fan voltages.

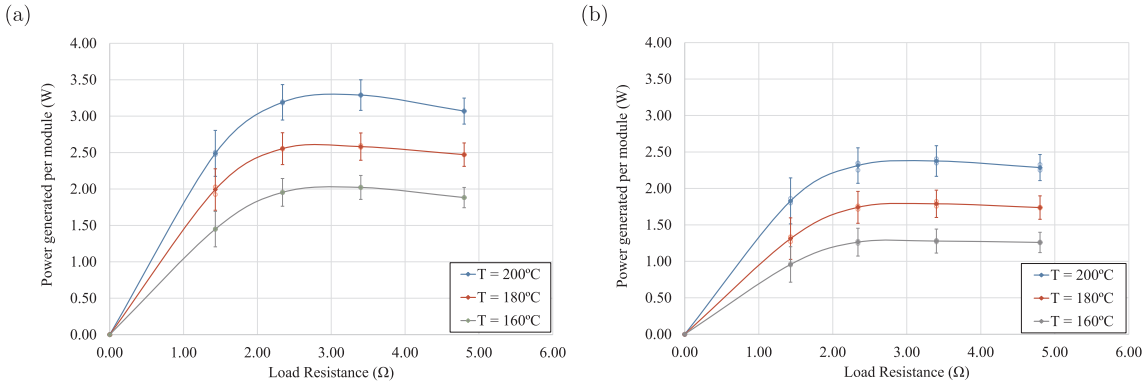

Fig. 12. Power generation per module for different temperatures and load resistances: (a) with the 8 levels thermosyphon (b) with the 6 levels thermosyphon.

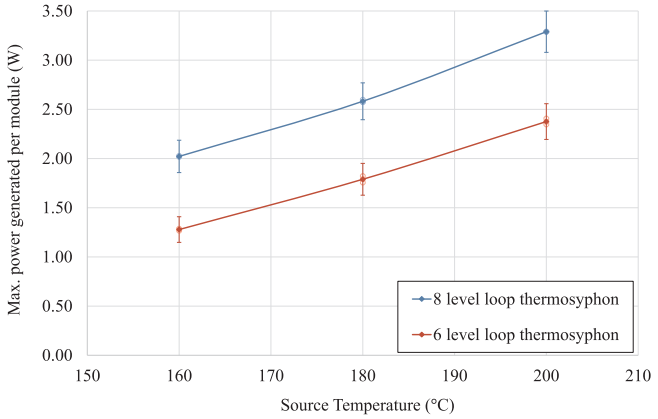

Fig. 13. Maximum power generated per module (corresponding to a load resistance of 3.2 Ω) with respect to the temperature of the heat source, for the two considered loop thermosyphons.

alternative for a geothermal thermoelectric generator. Although the thermal resistance of the 6 level loop thermosyphon and the fin dissipators are similar, the auxiliary consumption of the fans harms the net generation for the fin dissipator configuration, leading to a 37.5% lower generation if compared with the 6 levels loop thermosyphon configuration, and to a 54.5% less if compared with the 8 levels one. This fact justifies why the study of the influence of the temperature of the heat source has just been performed for loop thermosyphons (Fig. 13).

Finally, Table 2 shows for each experiment, the useful heat fluxes, the magnitude of the thermal losses, the thermal resistance of the TPCT located at the hot size, the total and net power generated by the two thermoelectric modules installed, and the total and net efficiencies.

As it can be observed, for all cases, the magnitude of the thermal losses is similar: around 8%. For small load resistances, such as 1 and 2.2 Ω, the thermal losses are in general slightly lower than 8%, while for bigger load resistances, the percentage of heat losses faintly increases. These losses are mainly located at the supporting plates and the upper cap, as shown in the thermography of Fig. 15. Nonetheless, the notorious insulation has achieved its purpose, leading to minimal heat losses.

Thanks to the useful heat flux and the temperature distribution, the thermal resistance of the TPCT per module has been calculated. Temperature difference in the TPCT remained practically constant regardless the cold side heat exchanger, and this fact causes an almost constant value of thermal resistance of around 0.31 K/W. This value slightly increments with lower temperatures of the heat source, presenting values of up to 0.34 K/W for 160 °C. The obtained value of thermal resistance is considered very good and it is on concordance with the thermal resistances of the cold side heat exchangers. In this sense, it has been experimentally demonstrated the feasibility of a two-phase closed thermosyphon (TPCT) as hot side heat exchanger. It presents a suitable thermal resistance (considerably lower than the solid bar alternative), it does not require any auxiliary consumption nor moving parts (as it was the case of the traditional liquid based heat exchangers), and it is noiseless, modular and robust.

Lastly, considering also the total and the net power generated by the two thermoelectric modules installed in the prototype, the total and the net efficiencies have been respectively calculated. The efficiencies follow the same trend as the power generated values. Thus, with the 3.2 Ω load resistance, the higher efficiencies are obtained.

On the one hand, in the case of the loop thermosyphons configuration, the higher the temperature of the heat source, the higher the efficiency. In this case, the total and the net efficiencies coincide due to the passive nature of the loop thermosyphons used, reaching a maximum of 2.54% in the optimum case, with a heat source temperature of

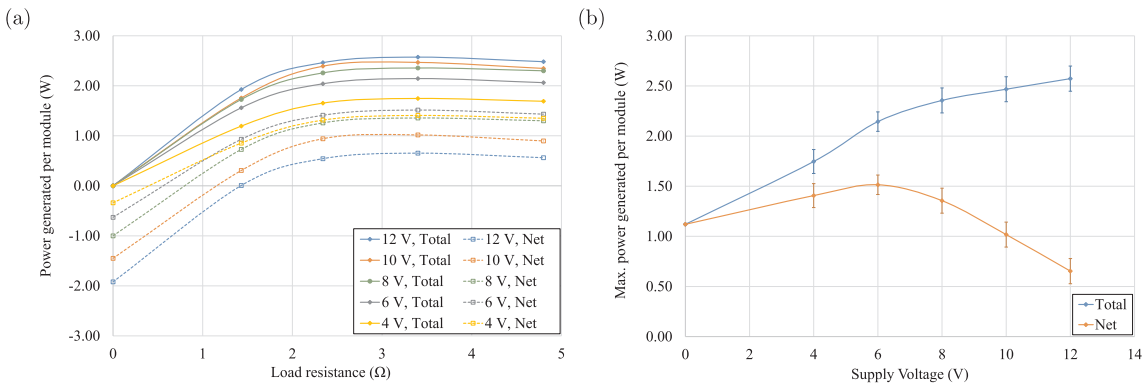

Fig. 14. Power generation per module for the case of 250 mm fin dissipator and T = 200 °C: (a) Total and net generation for different load resistances and fan voltages (b) Maximum total and net generation for each fan voltage.

Table 2
Useful heat flux, percentage of heat losses, thermal resistance of the hot side two-phase closed thermosyphon (TPCT), total and net power generated by the two thermoelectric modules, and total and net efficiencies for each experiment.

Cold side heat exchanger	T °C	Fan voltage (V)	Load Resistance (Ω)	$\dot{Q}$ (W)	%losses (W)	R_{TPCT} (K/W)	$\sum P_{total}$ (W)	$\sum P_{net}$ (W)	η_{total} (%)	η_{net} (%)
Loop thermosyphons	200	–	inf	201.23	8.11%	0.29	−0.01	−0.01	0.00%	0.00%
			241.81	6.95%	0.30	4.32	4.32	1.79%	1.79%	
			228.81	7.42%	0.30	5.50	5.50	2.41%	2.41%	
			223.34	8.46%	0.30	5.67	5.67	2.54%	2.54%	
			217.73	8.68%	0.30	5.36	5.36	2.46%	2.46%	
	180	–	inf	172.94	8.53%	0.30	0.01	0.01	0.00%	0.00%
			204.84	7.52%	0.32	3.29	3.29	1.61%	1.61%	
			199.39	7.64%	0.31	4.29	4.29	2.15%	2.15%	
			194.28	7.57%	0.31	4.37	4.37	2.25%	2.25%	
			190.71	8.20%	0.31	4.21	4.21	2.21%	2.21%	
	160	–	inf	146.20	8.49%	0.32	0.00	0.00	0.00%	0.00%
			173.87	7.41%	0.34	2.41	2.41	1.38%	1.38%	
			167.78	7.63%	0.34	3.22	3.22	1.92%	1.92%	
			163.74	7.77%	0.33	3.30	3.30	2.02%	2.02%	
			160.38	8.08%	0.33	3.14	3.14	1.96%	1.96%	
Fin dissipators	200	12	inf	180.11	8.57%	0.31	0.00	−3.84	0.00%	−2.13%
			202.82	7.72%	0.32	3.85	0.01	1.90%	0.01%	
			197.65	8.07%	0.32	4.92	1.08	0.00%	0.00%	
			194.13	8.39%	0.32	5.15	1.31	2.65%	0.67%	
			191.39	8.49%	0.32	4.96	1.12	2.59%	0.59%	
		inf	177.04	8.90%	0.31	0.00	−2.90	0.00%	−1.64%	
		1	202.79	7.73%	0.32	3.51	0.61	1.73%	0.30%	
		2.2	196.91	8.07%	0.32	4.78	1.88	0.00%	0.00%	
		3.2	193.40	8.33%	0.32	4.93	2.03	2.55%	1.05%	
		4.7	191.23	8.57%	0.32	4.69	1.79	2.45%	0.94%	
		inf	177.16	8.84%	0.31	0.00	−2.00	0.00%	−1.13%	
		1	201.76	7.81%	0.32	3.45	1.45	1.71%	0.72%	
		2.2	195.85	8.17%	0.32	4.52	2.52	0.00%	0.00%	
		3.2	191.94	8.63%	0.32	4.71	2.71	2.45%	1.41%	
		4.7	190.07	8.72%	0.32	4.60	2.60	2.42%	1.37%	
		inf	173.60	9.03%	0.32	0.00	−1.26	0.00%	−0.73%	
		1	196.77	8.14%	0.32	3.12	1.86	1.59%	0.95%	
		2.2	191.38	8.49%	0.32	4.08	2.82	0.00%	0.00%	
		3.2	188.72	8.57%	0.32	4.29	3.03	2.27%	1.60%	
		4.7	185.35	9.01%	0.32	4.13	2.87	2.23%	1.55%	
		inf	165.93	9.34%	0.31	0.00	−0.68	0.00%	−0.41%	
		1	185.61	8.47%	0.32	2.39	1.71	1.29%	0.92%	
		2.2	181.52	8.88%	0.32	3.31	2.63	0.00%	0.00%	
		3.2	179.45	9.11%	0.32	3.49	2.81	1.95%	1.57%	
		4.7	177.61	9.33%	0.32	3.38	2.70	1.90%	1.52%	
		3.2	158.38	9.50%	0.31	2.24	2.24	1.42%	1.42%	

200 °C and a load resistance of 3.2 Ω.

On the other hand, for the fin dissipators configuration, due to the auxiliary fans, net efficiency is lower than the total one. Total efficiency increases with the supply voltage of the auxiliary fans since convection improves and their thermal resistance decreases, leading to more generation. Thus, for the case of 12 V, the total efficiency reaches a maximum of 2.65%, which is even a bit greater than for the loop thermosyphons configuration due to a lower heat flux. If the consumption of the auxiliary fans is taken into account, efficiencies greatly decrease, with even negative or zero values. As it occurred with net generation, the highest efficiency is obtained for a supply voltage of 6 V, when there is an equilibrium between thermal resistance and auxiliary consumption.

5. Conclusions

The present paper has experimentally demonstrated the feasibility of thermoelectric generators for shallow hot dry rock (HDR) fields, leading to an alternative with minimal environmental impact and elevated modularizing capacity in comparison with enhanced geothermal systems (EGS). The experimented prototype includes an innovative heat exchanger to extract geothermal heat: a two-phase closed thermosyphon (TPCT), which presents a low thermal resistance ($R \approx 0.31$ per module), allowing elevated a elevated heat tranfer with minimum temperature loss. Furthermore, it does not include any moving part, removing maintenance requirements, and it is completely noiseless.

For the cold side, two different types of heat exchangers have been studied: fin dissipators assisted by a fan and loop thermosyphons. Loop thermosyphons have demonstrated to be a better option in the two studied geometries: 6 and 8 condensation levels. Due to the lower thermal resistance of the 8 levels loop thermosyphon, its associated thermoelectric module generates 3.3 W for a heat source temperature of 200 °C, while the 6 levels one only generated 2.4 W. The latter value is comparable to the fin dissipators configuration. However, the auxiliary consumption of the fans harms the net generation for the fin dissipator configuration, leading to a 37.5% lower generation if compared with the 6 levels loop thermosyphon configuration, and to a 54.5% less if compared with the 8 levels one.

Thus, the importance of using passive heat exchangers, with no auxiliary consumption, and presenting low thermal resistances has become evident. The best configuration for a GTEG is therefore composed by biphasic thermosyphons in both sides of the thermoelectric modules. This solution is under the process of international patenting due to its numerous advantages: robustness, modularizing capacity, no moving parts, no maintenance requirements, noiseless operation, and no auxiliary consumption, so that generation is maximized. This

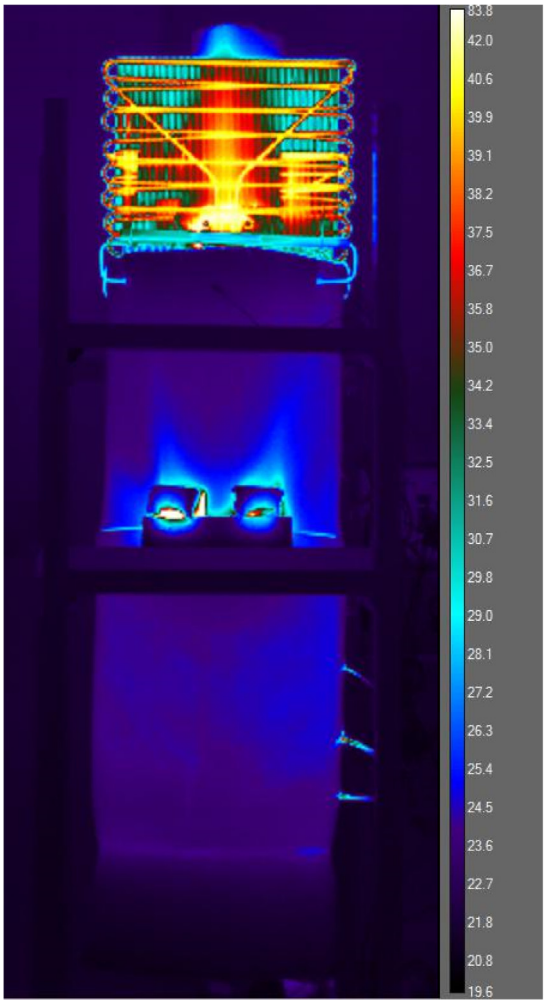

Fig. 15. Thermal distribution captured by a FLIR camera for the configuration of loop thermosyphons.

generation will also be increased with higher temperatures of the heat source as well as with heat exchangers with lower thermal resistances.

Acknowledgements

We would like to acknowledge the support of the Spanish State Research Agency and FEDER-UE under the grants DPI2014-53158-R and RTC-2017-6628-3; as well as the FPU Program of the Spanish Ministry of Science, Innovation and Universities (FPU16/05203).

References

[1] World Energy Assessment. Energy and the challenge of sustainability; 2000.
[2] REN21. Renewables 2017 Global Status Report [Tech. rep.], Paris; 2017.
[3] Li K, Bian H, Liu C, Zhang D, Yang Y. Comparison of geothermal with solar and wind power generation systems. Renew Sustain Energy Rev 2015;42:1464–74. https://doi.org/10.1016/j.rser.2014.10.049.
[4] Brown D. The enormous potential for hot dry rock geothermal energy. Mining the Earth's heat: hot dry rock geothermal energy Berlin Heidelberg: Springer-Verlag; 2012. https://doi.org/10.1007/978-3. Ch. 2. arXiv:1107.2286.
[5] Olasolo P, Juárez MC, Morales MP, Damico S, Liarte IA. Enhanced geothermal systems (EGS): a review. Renew Sustain Energy Rev 2016;56:133–44. https://doi.org/10.1016/j.rser.2015.11.031.
[6] Astrain D, Vián JG, Martínez A, Rodríguez A. Study of the influence of heat exchangers' thermal resistances on a thermoelectric generation system. Energy 2010;35(2):602–10. https://doi.org/10.1016/j.energy.2009.10.031.
[7] Elghool A, Basrawi F, Ibrahim TK, Habib K, Ibrahim H, Idris DMND. A review on heat sink for thermo-electric power generation: Classifications and parameters affecting performance. Energy Conversion and Management 2017;134:260–77. https://doi.org/10.1016/j.enconman.2016.12.046.
[8] Martinez A, Astrain D, Aranguren P. Thermoelectric self-cooling for power electronics: increasing the cooling power. Energy 2016;112:1–7. https://doi.org/10.1016/j.energy.2016.06.007.
[9] Gou X, Xiao H, Yang S. Modeling, experimental study and optimization on low-temperature waste heat thermoelectric generator system. Appl Energy 2010;87(10):3131–6. https://doi.org/10.1016/j.apenergy.2010.02.013.
[10] Tzeng SC, Jeng TM, Lin YL. Parametric study of heat-transfer design on the thermoelectric generator system. Int Commun Heat Mass Transfer 2014;52:97–105. https://doi.org/10.1016/j.icheatmasstransfer.2014.01.021.
[11] Araiz M, Martínez A, Astrain D, Aranguren P. Experimental and computational study on thermoelectric generators using thermosyphons with phase change as heat exchangers. Energy Convers Manage 2017;137:155–64. https://doi.org/10.1016/j.enconman.2017.01.046.
[12] Aranguren P, Astrain D, Martínez A. Study of complete thermoelectric generator behavior including water-to-ambient heat dissipation on the cold side. J Electron Mater 2014;43(6):2320–30.
[13] Aranguren P, Araiz M, Astrain D. Auxiliary consumption: a necessary energy that affects thermoelectric generation. Appl Therm Eng.https://doi.org/10.1016/j.applthermaleng.2018.06.042.
[14] Shabgard H, Allen MJ, Sharifi N, Benn SP, Faghri A, Bergman TL. Heat pipe heat exchangers and heat sinks: opportunities, challenges, applications, analysis, and state of the art. Int J Heat Mass Transfer 2015;89:138–58. https://doi.org/10.1016/j.ijheatmasstransfer.2015.05.020.
[15] Reay D, Kew P, McGlen R. Heat pipes. Theory, design and applications. Waltham, USA: Butterworth-Heinemann; 2014.
[16] Imura H, Sasaguchi K, Kozai H, Numata S. Critical heat flux in a closed two-phase thermosyphon. Int J Heat Mass Transfer 1983;26(8):1181–8. https://doi.org/10.1016/S0017-9310(83)80172-0.
[17] Niu X, Yu J, Wang S. Experimental study on low-temperature waste heat thermoelectric generator. J Power Sour 2009;188(2):621–6. https://doi.org/10.1016/j.jpowsour.2008.12.067.
[18] Suter C, Jovanovic ZR, Steinfeld A. A 1kWe thermoelectric stack for geothermal power generation – modeling and geometrical optimization. Appl Energy 2012;99:379–85. https://doi.org/10.1016/j.apenergy.2012.05.033.
[19] Suter C, Jovanovic Z, Steinfeld A. A 1 kWel thermoelectric stack for geothermal power generation – modeling and geometrical optimization. AIP Conf Proc 2012;1449:540–3. https://doi.org/10.1063/1.4731613.
[20] Liu C, Chen P, Li K. Geothermal power generation using thermoelectric effect. GRC Trans 37.
[21] Liu C, Chen P, Li K. A 500 W low-temperature thermoelectric generator: design and experimental study. Int J Hydrogen Energy 2014;39(28):15497–505. https://doi.org/10.1016/j.ijhydene.2014.07.163.
[22] Liu C, Chen P, Li K. A 1 KW thermoelectric generator for low-temperature geothermal resources. Thirty-ninth workshop on geothermal reservoir engineering, no. 2001. 2014. p. 1–12.
[23] Ahiska R, Mamur H. Design and implementation of a new portable thermoelectric generator for low geothermal temperatures. IET Renew Power Gener 2013;7(6):700–6. https://doi.org/10.1049/iet-rpg.2012.0320.
[24] Ahiska R, Mamur H. Development and application of a new power analysis system for testing of geothermal thermoelectric generators. Int J Green Energy 2016;13(7):672–81. https://doi.org/10.1080/15435075.2015.1017102.
[25] Trip ND, Burca A, Morgos L. Considerations on the use of thermoelectric generators at low temperatures to recover waste geothermal energy. 2017 14th international conference on engineering of modern electric systems, EMES 2017 2017. p. 248–51. https://doi.org/10.1109/EMES.2017.7980426.
[26] Wang K, Liu J, Wu X. Downhole geothermal power generation in oil and gas wells. Geothermics 2018;76(October):141–8. https://doi.org/10.1016/j.geothermics.2018.07.005.
[27] Wang K, Wu X. Downhole thermoelectric generation in unconventional horizontal wells. Fuel 2019;254(March):115530https://doi.org/10.1016/j.fuel.2019.05.113.
[28] Banerjee A, Chakraborty T, Matsagar V. Evaluation of possibilities in geothermal energy extraction from oceanic crust using offshore wind turbine monopiles. Renew Sustain Energy Rev 2018;92(May):685–700. https://doi.org/10.1016/j.rser.2018.04.114.
[29] Instituto Geológico Minero Español. Evaluación del potencial geotérmico superficial de Montañas de Fuego como Sistema de Roca Caliente Seca [Tech. rep.]; 1992.
[30] Ebeling J-C, Kabelac S, Luckmann S, Kruse H. Simulation and experimental validation of a 400 m vertical CO_2 heat pipe for geothermal application. Heat Mass Transfer 2016:218–25.
[31] Chet DL, Singh B, Remeli MF, Date A, Singh R, Akbarzadeh A. Prospects of power generation from geothermal energy using thermoelectric modules. Proc World Geotherm Congress 2015;2015(April):8.
[32] II-VI Marlow. Technical Data Sheet for TG12-8. URL:https://cdn2.hubspot.net/hubfs/547732/Data_Sheets/TG12-8.pdf.
[33] Lee S, Song S, Au V, Moran KP. Constriction/spreading resistance model for electronics packaging. 4th ASME/JSME thermal engineering conference, 4. 1995. p. 199–206. URL:http://www.digikey.it/WebExport/SupplierContent/Aavid_59/PDF/Aavid_ConstrictionModel.pdf.
[34] Coleman H, Steele W. Experimentation, validation and uncertainty. Analysis for engineers. 3rd ed., Wiley.
[35] Parmelee G, Huebscher R. Heat transfer by forced convection along a smooth flat surface. Heat Piping Air Condition 1947;19(8):115.

Chapter 3

Development of a Computational Model to Design and Optimize Geothermal Thermoelectric Generators

In the previous publication, it has been derived that heat exchangers based on phase change are the most adequate ones for geothermal thermoelectric generators. Hence, this chapter delves into their study, developing a computational model that serves as a true design and optimization tool for the development of the two applications subject of study in the present Ph. D. dissertation.

Due to the complexity of the phenomena that take place inside thermoelectric generators, in the last years, computational models have emerged as indispensable tools for the design and optimization of real applications, predicting the behavior of such systems. These models reduce the necessity of building prototypes and limit the number of experimental tests necessary in order to obtain significant information, which translates into cost savings. Nonetheless, in order to obtain a reliable tool, it is necessary to validate the developed model, determining its capacity of resembling a real system.

This chapter corresponds with the article "Computational study of geothermal thermoelectric generators with phase change heat exchangers" published in the journal *Energy Conversion and Management* 221 (2020) 113120. This paper thoroughly describes the development of a computational model based on the finite difference method, also known as thermal–electrical analogy, taking into account the discretization of the heat exchangers,

the thermoelectric modules, and the heat reservoirs, and considering all the thermoelectric effects, the thermal and electrical contacts, and the influence of temperature on the properties. In order to obtain a model that accurately resembles reality, the model has been validated with the experimental results obtained in the previous publication.

Although the model is valid for any thermoelectric application, the paper focuses on medium–scale geothermal generation in Hot Dry Rock (HDR) fields, analyzing the influence of different heat exchangers, geometries, and dimensions for the specific case of the HDR field located at Timanfaya National Park. Based on this analysis, an optimization of the thermoelectric generators is performed for the different anomalies available within the Park. Finally, the potential of the large–scale installation of such devices in the whole Park is also studied.

Energy Conversion and Management 221 (2020) 113120

Contents lists available at ScienceDirect

Energy Conversion and Management

journal homepage: www.elsevier.com/locate/enconman

Computational study of geothermal thermoelectric generators with phase change heat exchangers

Leyre Catalan*, Miguel Araiz, Patricia Aranguren, David Astrain

Department of Engineering, Institute of Smart Cities, Public University of Navarre, Pamplona, Spain

ARTICLE INFO

Keywords:
Computational model
Thermoelectric generator
Geothermal
Hot dry rock
Phase change
Timanfaya

ABSTRACT

The use of thermoelectric generators with phase change heat exchangers has demonstrated to be an interesting and environmentally friendly alternative to enhanced geothermal systems (EGS) in shallow hot dry rock fields (HDR), since rock fracture is avoided. The present paper studies the possibilities of the former proposal in a real location: Timanfaya National Park (Canary Islands, Spain), one of the greatest shallow HDR fields in the world, with 5000 m^2 of characterized geothermal anomalies presenting temperatures up to 500 °C at only 2 m deep. For this purpose, a computational model based on the thermal-electrical analogy has been developed and validated thanks to a real prototype, leading to a relative error of less than 8%. Based on this model, two prototypes have been designed and studied for two different areas within the park, varying the size of the heat exchangers and the number of thermoelectric modules installed. As a result, the potential of the solution is demonstrated, leading to an annual electricity generation of 681.53 MWh thanks to the scalability of thermoelectric generators. This generation is obtained without moving parts nor auxiliary consumption, thus increasing the robustness of the device and removing maintenance requirements.

1. Introduction

In the last decade, there has been much progress in the use of renewable energies and energy efficiency measures [1–3]. Nevertheless, the international climate goals established under the Paris Agreement are not on track to be met [4]. Therefore, there still exists a necessity for further development of renewable energies.

Among all the renewable sources, geothermal energy stands out because it is not affected by weather, it is stable, it can provide both heat and electricity, it has a high capacity factor, it can be used as base-load power, and it has a high thermal efficiency. However, despite these advantages, geothermal energy is positioned behind other renewable energies, especially in electricity generation, with only 13.3 GW installed accounting for less than 0.4% of global electricity production [5].

Recently, in order to increase the growth rate of geothermal power, thermoelectric generators (TEGs) have been proposed as an alternative to traditional cycles [6]. TEGs are devices formed by the interconnection of one or multiple thermoelectric modules (TEMs) that, due to Seebeck effect, generate electricity based on the heat received from a hot source, emitting the rest to a cold sink, which is normally the environment. Carnot theorem applied to a TEG concludes that the efficiency of the system increases as the sides of the TEMs approach the temperature of the heat source and sink. Therefore, the introduction of heat exchangers between the modules and each of the thermal reservoirs becomes necessary in order to maximize the temperature difference. In fact, Astrain et al. demonstrated that an improvement of 10% in the thermal resistance of the heat exchangers leads to an 8% higher generation [7]. Fin dissipators, heat exchangers with a fluid as heat carrier, and heat exchangers based on phase change are the most common alternatives found in TEGs [8].

Most of the proposed geothermal thermoelectric generators (GTEGs) use heat exchangers with a fluid as heat carrier, similarly to conventional geothermal cycles. Thus, a fluid is pumped into the ground so that it absorbs geothermal heat. The heat is then released to the thermoelectric modules, which transform part of it into electricity, releasing the rest into the environment by means of another heat exchanger based on a fluid, analogously to condensers. Since one of the main drawbacks of thermoelectricity is its low efficiency, these GTEGs are designed for low temperature geothermal fields ($T < 150\,°C$), where they can become competitive in comparison to binary cycles (ORC and Kalina), the most commonly used technology in the low temperature range.

Among low temperature GTEGs with heat exchangers with a fluid as heat carrier, their integration downhole in oil and gas wells seems to have the highest potential. Thanks to this synergy, Wang et al.

* Corresponding author.

https://doi.org/10.1016/j.enconman.2020.113120
Received 16 April 2020; Received in revised form 13 June 2020; Accepted 15 June 2020

Nomenclature

α	Seebeck coefficient (K/W)
ΔP_{sat}	Difference in saturation pressure corresponding to ΔT_{sat} (Pa)
ΔT_{sat}	Difference between wall and saturation temperature (°C)
$\dot{Q}$	Heat flux (W)
ϵ	Ratio between equivalent radius, e.g. for the hot side $\epsilon = \sqrt{A_{TEM}/\pi}/\sqrt{A_c/\pi}$
η	Efficiency
γ	Surface tension (N/m)
λ_c	$\lambda_c = \pi + 1/(\sqrt{\pi}\cdot\epsilon)$
μ	Dynamic viscosity (Pa·s)
ν	Kinematic viscosity (m^2/s)
ϕ_c	Parameter given by Eq. (13)
ψ	Dimensionless constriction resistance
ρ	Electrical resistivity (Ω·m)
σ	Thomson coefficient (V/K)
τ	$\tau = e_c/\sqrt{A_c/\pi}$
A	Area (m^2)
Bi	Biot number $Bi = h_b\cdot(\sqrt{A_c}/\pi)/k$
cp	Specific heat (J/kg·K)
D	Diameter (m)
d	Density (kg/m^3)
e	Thickness (m)
Et	Electromotive force (V)
G	Total mass flux (liquid + gas) per unit of area
g	Gravity acceleration (m/s^2)
h	Heat transfer coefficient ($W/m^2\cdot K$)
I	Intensity (A)
i_{lg}	Latent heat of vaporization (J/kg)
J_g	Dimensionless vapour velocity
k	Thermal conductivity (W/m·K)
L	Length (m)
L_{ch}	Characteristic length (m)
L_{ch-fin}	Characteristic length of a fin $L_{ch-fin} = L_{fin} + (t/2)$
m_w	$m_w = \sqrt{h_w\cdot S_w^2/(k_w\cdot D_w)}$
m_{fin}	$m_{fin} = \sqrt{2\cdot h_{conv}^H/k\cdot t}$
N	Number
Nu	Nusselt number $Nu = h\cdot L_{ch}/k$
P	Electric power (W)
p_r	Reduced pressure
Pr	Prandtl number $Pr = cp\cdot\mu/k$
R	Thermal resistance (K/W)
R_0	Internal electrical resistance (Ω)
R_{load}	Load electrical resistance (Ω)
Re	Reynolds number $Re = v\cdot L_{ch}/\nu$
S	Space between (m)
t	Fin thickness (m)
V	Voltage (V)
v	Velocity (m/s)
x	Vapor quality
y	Mass fraction
Z	Shah's correlating parameter: $Z = (1/x - 1)^{0.8} p_r^{0.4}$

Subscripts and Superscripts

air	Air/ Wind
amb	Ambient
b	Boiling
C	Cold side
c	Condensation/Condenser
co	Contact
cond	Pure conduction
const	Constriction
conv	Convective
e	External
ev	Evaporator
exp	Experimental
fin	Fin
G	Geothermal gases
g	Gas
H	Hot side
i	Internal
ins	Insulator
	Conductive
l	Liquid
n	Semiconductor n
p	Semiconductor p
R	Rope heaters
s	Surface
sat	Saturation
sim	Simulated
sup	Per unit of area
T	Temperature (°C)
t	Tubes
tc	Thermocouple
u	Union material
w	Wired fins
i	Node number

Abbreviations

CHE	Cold side Heat Exchanger
EGS	Enhanced Geothermal System
FD	Fin dissipator
GTEG	Geothermal Thermoelectric Generator
HDR	Hot Dry Rock
HHE	Hot side Heat Exchanger
LT	Loop Thermosyphon
ORC	Organic Rankine Cycle
TEG	Thermoelectric Generator
TEM	Thermoelectric Module
TPCT	Two Phase Closed Thermosyphon

estimated that 8538 W can be produced in a vertical well located in China, where there exists a 100 °C temperature difference [9], and 128024 W in a horizontal one, also in China, with a 156 °C gradient [10]. Apart from the combination of geothermal energy and hydrocarbons, there also exist some proposals of GTEGs for traditional low temperature geothermal systems with again heat exchangers with a fluid as heat carrier. Suter et al. modeled and optimized a 1 kW GTEG working with a 100 °C gradient by modifying different operating parameters and geometries [11,12]. Liu et al. also designed a 1 kW GTEG consisting of 600 TEMs and working with a temperature difference of 120 °C [13]. In order to obtain this design, they had previously built a real prototype with 96 TEMs that generated 160 W under a 120 °C gradient, and by extrapolation, 500 W with a temperature difference of 200 °C [14,15]. Niu et al. as well as Ahiska and Mamur also built a prototype in order to demonstrate the viability of the technology. Thus, Niu et al. generated 146.5 W with 56 TEMs and 120 °C gradient [16], and Ahiska and Mamur, on their behalf, produced 41.6 W with 20 TEMs and a temperature difference of 67 °C [17,18].

Only a couple of examples of GTEGs for high temperature geothermal fields can be found in the literature. On the one hand, Banerjee studied the installation of TEGs in offshore wind turbine monopiles to extract geothermal energy and produce up to 242 kW using again heat

exchangers with a fluid as heat carrier [19]. On the other hand, Catalan et al. proposed the use of GTEGs in shallow hot dry rock (HDR) fields [20], one of the most extended and potential geothermal fields [21], leading to a generation of up to 3.2 W per module with a temperature difference between sources of 180 °C. The novelty of this proposal was not only the application itself, but also their conclusion, experimentally demonstrating that passive heat exchangers based on phase change are the most suitable ones for both sides of GTEGs, with a 54% higher generation than fin dissipators.

Heat exchangers based on phase change take advantage of the latent heat of an internal fluid, which is cyclically vaporizing and condensing, to transfer a large quantity of heat over relatively long distances, thus leading to a low thermal resistance. In combination with thermoelectric generators, their use has generalized in the last years and these heat exchangers can be found in several applications: waste heat recovery from industries [22,23], automotive thermoelectric generators [24–26], or concentrated solar thermoelectric generators [27] among others. Some of them include an auxiliary consumption to reduce even more the thermal resistance of the heat exchangers, especially improving convection with the environment with the aid of a ventilator, while others do not include any auxiliary component, obtaining a completely passive heat exchanger.

In GTEGs, there do not exist many examples with phase change heat exchangers. Huang et al. developed a thermoelectric micro-generator with a heat pipe as hot side heat exchanger and fin dissipators as cold side ones, to power forest wireless sensors in remote areas using the temperature difference between the soil and the air [28,29]. On their behalf, Dell et al. combined conventional geothermal steam pipes with a thermoelectric generator with heat pipes as cold side heat exchangers, so that different electronics systems were powered [30,31]. Catalan et al. were the first ones proposing a GTEG with passive phase change heat exchangers at both sides of the thermoelectric modules for high scale generation, leading to a robust generator with minimal maintenance requirements. In their application to HDR fields, their use also prevents rock fracture and induced seismicities, one of the most critical issues of enhanced geothermal systems (EGS), the only existing technique nowadays.

The present paper delves into the study of these GTEGs with passive phase change heat exchangers for high temperature HDR fields. More specifically, its objective is to analyze the influence of different parameters taking as reference a real HDR field, Timanfaya National Park (Canary Islands, Spain), whose potential will be also estimated. In order to achieve this objective, it will be necessary to develop and experimentally validate a computational model.

Section 2 details the operation of a GTEG with phase change heat exchangers, Section 3 describes the computational model that has been developed. This computational model has been validated with experimental results, as described in Section 4. Based on it, Section 5 describes the analysis of different parameters and the potential of the proposed solution considering as reference the HDR field located at Timanfaya National Park (Canary Islands, Spain). Finally, Section 6 summarizes the main conclusions obtained in the present paper.

2. GTEG with phase change heat exchangers

In order to leverage shallow hot dry rock (HDR) fields, Catalan et al. demonstrated the feasibility of thermoelectric generators as a greener alternative to enhanced geothermal systems (EGS) [20]. In their study of different heat exchangers, they concluded that those based on phase change are the most adequate ones for GTEGs. Hence, since the present paper delves into their development, analyzing the influence of different parameters and the potential of their large scale implementation in a real location by means of a computational model, this section details the operation of the GTEG that will be modeled, including not only the generator itself but also the heat source.

HDR fields represent the heat source of the generator. These fields

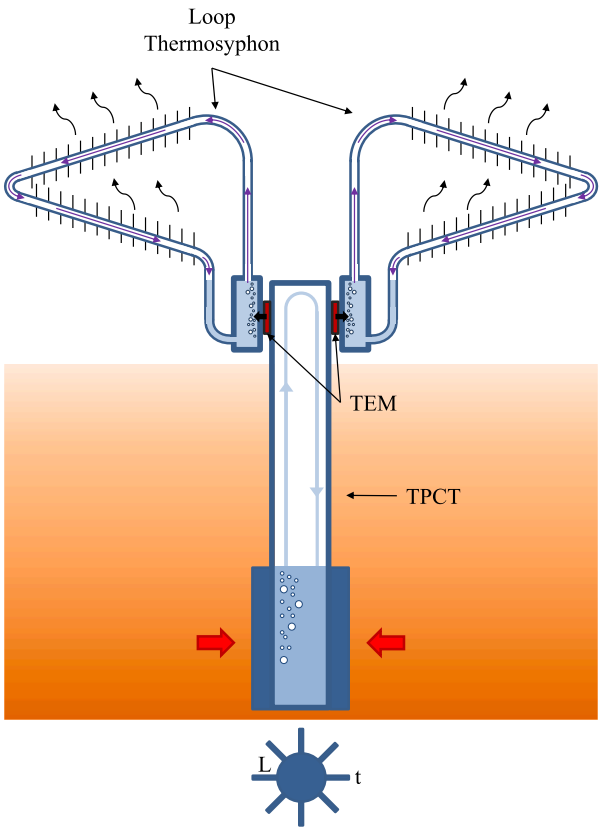

Fig. 1. Schematics of the operation of a cylindrical geothermal thermoelectric generator (GTEG) with phase change heat exchangers.

can be defined as geothermal fields characterized by high temperature compact rocks, where the absence of both reservoir and fluid that acts as a heat carrier prevents the existence of a geothermal system, which is necessary for traditional geothermal power generation. The present paper focuses on shallow HDR fields, where it would be easy to drill a borehole to insert the generator. Due to the absence of a fluid as heat carrier and the low diffusivity of the rocks, the transmission of heat to the GTEG occurs by convection with the air that is naturally heated up by the rocks [32]. Although this may seem an insufficient heat source, in the HDR taken as reference in this paper and that is more deeply described in Section 5, natural gas flows ascending at velocities of up to 11.15 m/s have been measured at temperatures higher than 200 °C, so it definitely is a heat source to consider.

Fig. 1 depicts the schematics of the operation of a cylindrical GTEG with phase change heat exchangers installed in a HDR field. The hot side heat exchanger is a two phase closed thermosyphon (TPCT), i.e. a hermetically sealed container filled with a small amount of working fluid [33]. In contact with the hot air, the internal fluid vaporizes and, due to natural convection, ascends to the upper part of the container, where it condensates releasing heat to the TEMs. Since this process is driven by phase change, heat is absorbed and transported with a minimal temperature difference regardless of the distance, as it has been previously demonstrated with a 400 m long TPCT [34]. In order to improve the convection between the hot air and the TPCT, the present paper will consider the addition of vertical fins to the external part of this hot side heat exchanger.

The heat released in the condensation of the TPCT is transmitted to the thermoelectric modules (TEMs), located overground in the upper part of that heat exchanger. These TEMs transform part of the received heat into electricity, releasing the rest to the cold side heat exchangers. In this paper, commercial bismuth telluride TEMs will be considered.

The heat released by the TEMs needs to be dissipated into the

environment. Heat exchangers based on phase change have been demonstrated to be the most appropriate ones for this purpose for medium temperature range under 300 °C [35] and the considered application of GTEGs [20]. Thus, loop thermosyphons will be considered in this paper due to their compactness. An individual loop thermosyphon will be used per each TEM.

Thanks to the use of heat exchangers based on phase change at both side of the TEMs, the proposed solution of GTEG presents several advantages: it is robust, modular, noiseless, independent of the depth of the borehole, has a minimal environmental impact, and does not present moving parts, removing maintenance requirements, nor auxiliary equipment, thus maximizing power generation.

3. Computational model

In order to study the feasibility of GTEGs, most of the existing proposals use computational models. The use of these models has spread in the last years becoming an indispensable tool for the design, analysis, and optimization of real applications, reducing the necessity of building prototypes and limiting the number of experimental tests necessary in order to obtain significant information, which translates in cost savings. In the case of GTEGs, these aspects gain even more importance due to the high scale implied. Aligned with the objective of the present paper, this section describes the computational model developed for the analysis of GTEGs with phase change heat exchangers at both sides of the TEMs.

In the modeling of TEGs, there exist four major kinds of models: standard simplified models, analytical models, models based on the electrical analogy between heat transfer and electricity, and numerical models based on finite elements [36]. The models used for GTEGs are mainly simplified models, which neglect Thomson effect and assume constant thermoelectric properties. Most of them, concentrate on a correct simulation of the heat exchangers, but simplify the modeling of the TEMs, leading to a slight deviation in the calculation of power generation [36].

Models based on the electrical analogy between heat transfer and electricity have demonstrated to be accurate alternatives with an assumable computational cost in different applications [23,36–38]. This thermal-electrical analogy also permits modeling heat exchangers based on phase change, as Araiz et al. demonstrated for a loop thermosyphon with errors lower than 9% [39]. Based on this characterization, they subsequently developed a computational model of a complete TEG with loop thermosyphons as cold side heat exchangers, and fin dissipators as hot side ones [40]. Other authors, such as Brito et al. and Pacheco et al. also use the electrical analogy in order to model heat exchangers based on phase change [25,41,42]. In particular, they model TEGs with heat pipes in the hot side and heat exchangers based on a fluid in the cold one in order to generate electricity from the exhaust gases of vehicles, although the resolution of the TEMs is simplified, neglecting Thomson effect and variable thermoelectric properties.

The computational model developed in this paper also follows the electrical analogy between heat transfer and electricity, and it considers, for the first time, heat exchangers based on phase change at both sides of the TEMs. The thermal-electrical analogy is actually derived from the application of the implicit finite difference method to heat conduction equation. Its basic idea consists in discretizing the system in several nodes. The solution of the original problem is obtained for those finite number of nodes.

Fig. 2 depicts the discretization of a general GTEG, such as the one described in Section 2. For simplicity, the explanation of the system will be performed according to the three different blocks that compose it: hot side heat exchanger (red block), TEMs (green block) and cold side heat exchanger (blue block). Afterwards, it will be described the union between these several blocks, which considers contact thermal resistances, as well as other phenomena such as thermal bridges. In their modeling, some simplification hypothesis have been considered: (i) all materials are homogeneous, with uniform composition and structure; (ii) the insulation of the electric circuit is perfect and the electric current is unidimensional; (iii) the heat flux is also unidimensional, thus lateral heat losses are neglected; (iv) only the stationary regime is considered; and (v) no subcooling nor reheating occur in the heat exchangers. Finally, once all the thermal resistances have been described, the resolution methodology to solve the system and obtain the temperature of each node is detailed.

3.1. Hot side heat exchanger

The hot side heat exchanger is a two phase closed thermosyphon

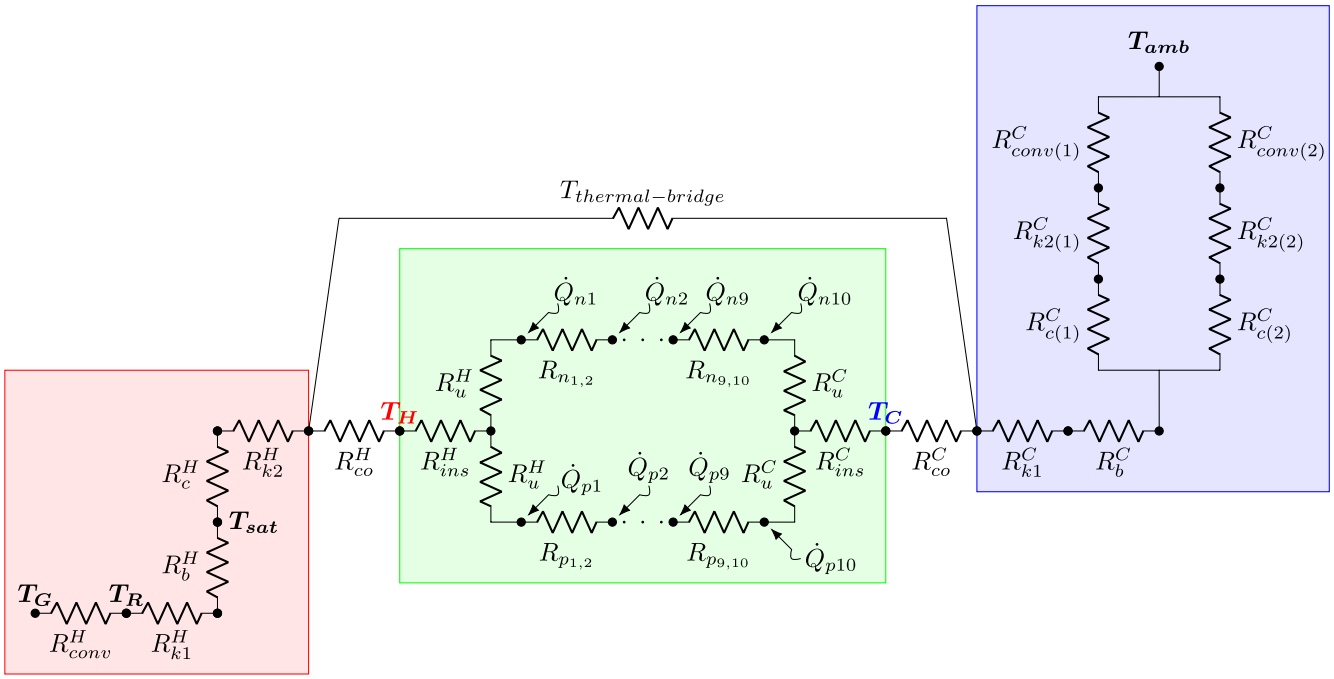

Fig. 2. Thermal-electrical analogy of a GTEG with phase change heat exchangers.

(TPCT). As a result of its discretization, the red block of Fig. 2 shows the thermal-electrical analogy taking into account all the phenomena occurring in this phase change heat exchanger. Superscript H refers to the hot side heat exchanger.

Following the heat flux from the air heated up by the geothermal HDR field, the first thermal resistance represents the convection between the hot air and the TPCT, which have fins in order to improve the heat transfer. This resistance can be estimated as follows:

$$R_{conv}^{H} = \frac{1}{h_{conv}^{H} \cdot A_{conv}^{H} \cdot \eta_{fin}^{H}} \tag{1}$$

where h_{conv}^{H} is the convective heat transfer coefficient derived from the Nusselt expression deduced by Sieder and Tate's correlation for forced convection in pipes (Eq. (2)) that is valid for Prandtl and Reynolds numbers in the ranges [0.7, 160] and [10^4, 10^6] respectively [43], A_{conv}^{H} is the area in contact with the hot air (taking into account the fins and up to the interior fluid's height), and η_{fin} is the efficiency of the fins, which is estimated with Eq. (3) [44].

$$Nu = 0.027 \cdot Re^{0.8} \cdot Pr^{1/3} \cdot \left(\frac{\mu}{\mu_s}\right)^{0.14} \tag{2}$$

$$\eta_{fin} = 1 - \frac{N_{fin} \cdot A_{fin}}{A_{conv}^{H}} \left(1 - \frac{\tanh(m_{fin} \cdot L_{ch-fin})}{m_{fin} \cdot L_{ch-fin}}\right) \tag{3}$$

The next thermal resistance R_{k1}^{H} represents the heat conduction through the wall of the evaporator, which is considered to take up to the internal fluid's height. In case of having a cylindrical TPCT, this resistance is estimated according to Eq. (4), while for a TPCT with planar surfaces, Eq. (5) applies [43].

$$R_{k1}^{H} = \frac{\ln(D_e^{H}/D_i^{H})}{2 \cdot \pi \cdot L \cdot k} \tag{4}$$

$$R_{k1}^{H} = \frac{e^{H}}{k^{H} \cdot A_{k1}^{H}} \tag{5}$$

The heat conducted through the wall causes the vaporization of part of the internal working fluid contained inside the TPCT. This process is modeled by the boiling thermal resistance R_b^{H}, for which a boiling coefficient is necessary (Eq. (6)). Assuming that nucleate pool boiling is taking place, the correlation proposed by Forster and Zuber in 1955 is used (Eq. (7)) [45]. This expression is commonly used due to its simplicity, although it does not take into account the combination between the surface and the boiling fluid [46].

$$R_b^{H} = \frac{1}{h_b^{H} \cdot A_b^{H}} \tag{6}$$

$$h_b^{H} = \frac{0.00122 \ \Delta T_{sat}^{0.24} \ \Delta P_{sat}^{0.75} \ cp_l^{0.45} \ d_l^{0.49} \ k_l^{0.79}}{\gamma^{0.5} \ i_{lg}^{0.24} \ \mu_l^{0.29} \ d_g^{0.24}} \tag{7}$$

Next, the vapor ascends, due to its lower density, to the upper part of the TPCT, where it condensates. In order to calculate the condensation thermal resistance, it is necessary to consider the area of condensation of all the TEMs, and a condensation coefficient (Eq. (8)). The phenomenon that takes place in this case is film condensation on a vertical plate. Therefore, the heat transfer coefficient is determined by Eq. (9) [46], which neglects convection effects in the film and assumes a constant wall temperature.

$$R_c^{H} = \frac{1}{h_c^{H} \cdot A_c^{H}} \tag{8}$$

$$h_c^{H} = 0.943 \left[\frac{k_l^3 \ d_l \ (d_l - d_g) \ g \ i_{lg}}{\mu_l \ \Delta T_{sat} \ L_c}\right]^{\frac{1}{4}} \tag{9}$$

Lastly, the thermal resistance R_{k2}^{H} represents the last element of the electrical analogy of a TPCT and deals with two different phenomena. On the one hand, it considers the conduction that takes place in the condenser. In this case, and since the TEMs need to be in contact with the upper part of the TPCT, only the expression of heat conduction for planar surfaces is considered (Eq. (10)) [43]. In this equation, subscript c has been added to differentiate that it refers to the condenser part of the TPCT.

$$R_{k2,cond}^{H} = \frac{e_c^{H}}{k^{H} \cdot A_c^{H}} \tag{10}$$

On the other hand, due to the fact that condensation occurs in an area a bit bigger than that of the module, constriction effect appears causing an increase in the thermal resistance. Lee et al. [47] estimated that constriction resistance can be calculated as:

$$R_{k2,const}^{H} = \frac{\Psi^{H}}{N_{TEM} \cdot k^{H} \cdot \sqrt{A_{TEM}}} \tag{11}$$

where N_{TEM} is the number of TEMs, k^{H} is the thermal conductivity of the material, A_{TEM} the area of a thermoelectric module, and Ψ^{H} is the dimensionless constriction resistance expressed by Eq. (12).

$$\Psi^{H} = \frac{1}{2} \cdot (1 - \epsilon^{H})^{3/2} \cdot \Phi_c^{H} \tag{12}$$

in which ϵ^{H} is the ratio between the equivalent radius of a module and the equivalent radius of the region in which condensation occurs per each module and Φ_c^{H} follows Eq. (13).

$$\Phi_c^{H} = \frac{\tanh(\lambda_c^{H} \cdot \tau^{H}) + \frac{\lambda_c^{H}}{Bi^{H}}}{1 + \frac{\lambda_c^{H}}{Bi^{H}} \cdot \tanh(\lambda_c^{H} \cdot \tau^{H})} \tag{13}$$

Thus, the thermal resistance R_{k2}^{H} is finally calculated by simply adding the conduction and constriction resistances:

$$R_{k2}^{H} = R_{k2,cond}^{H} + R_{k2,const}^{H} \tag{14}$$

3.2. Thermoelectric modules

The second block, corresponding to the TEMs and depicted in green color in Fig. 2, is the element most difficult to model since phenomena related to heat transmission and thermoelectricity take part at the same time. A TEM is made up of several thermocouples connected electrically in series and thermally in parallel. Each thermocouple itself is composed of an n-type semiconductor united by means of a conductive material to a p-type semiconductor.

In order to capture all the phenomena that occur simultaneously in a TEM, in each thermocouple, each semiconductor has been discretized into 10 nodes since this leads to accurate results without increasing the computational cost [23,37,38], and temperature dependent properties have been considered. Since the dominant heat transfer mechanism is conduction, all the thermal resistances of semiconductors n and p are calculated by means of Eqs. (15) and (16) respectively, in which it has been considered that the N_{tc} thermocouples that make up a TEM are connected thermally in parallel, similarly to the N_{TEM} thermoelectric modules.

$$R_{n(i,i+1)} = \frac{L_n/9}{N_{TEM} \cdot N_{tc} \cdot k_{n(i,i+1)} \cdot A_n} \qquad i = 1 - 9 \tag{15}$$

$$R_{p(i,i+1)} = \frac{L_p/9}{N_{TEM} \cdot N_{tc} \cdot k_{p(i,i+1)} \cdot A_p} \qquad i = 1 - 9 \tag{16}$$

In these equations, L_n and L_p are the lengths of the semiconductors, $k_{n(i,i+1)}$ and $k_{p(i,i+1)}$ are their thermal conductivities calculated at the mean temperature of their delimiting nodes i and $i + 1$, and A_n and A_p are their cross-sectional areas.

Both semiconductors are united by a conductive material. Many times, the thermal resistance of this union material is neglected due to its high thermal conductivity in comparison to the semiconductors.

However, in order to duly resemble the model to reality, the present paper considers it. As shown in Eq. (17), half of this material is considered in the n branch and the other half in the p one.

$$R_u^H = R_u^C = \frac{L_u}{N_{TEM}\cdot N_{tc}\cdot k_u\cdot A_u/2} \tag{17}$$

The last thermal resistances that need to be considered in the model are those corresponding to the electrical insulating material that protects the internal circuit and provides firmness to each TEM.

$$R_{ins}^H = R_{ins}^C = \frac{L_{ins}}{N_{TEM}\cdot k_{ins}\cdot A_{ins}} \tag{18}$$

Apart from the former thermal resistances, it is necessary to consider heat fluxes in the semiconductor nodes in order to model the thermoelectric effects that take place. All nodes generate heat due to Joule and Thomson effect. Furthermore, in extreme nodes, heat is also produced by Peltier effect in the semiconductors and Joule effect in the electrical contacts. For simplicity, only the expressions corresponding to n semiconductor are shown.

$$\dot{Q}_{n1} = N_{TEM}\cdot N_{tc}\cdot\left[\frac{-(\alpha_{p1}-\alpha_{n1})T_{n1}}{2}\cdot I + \frac{\rho_{u,n}^{sup}}{A_n}\cdot I^2 + \rho_{n1}\cdot I^2\cdot\frac{L_n/18}{A_n} - \sigma_{n1}\cdot I\cdot\frac{T_{n1}-T_{n2}}{2}\right] \tag{19}$$

$$\dot{Q}_{n(i)} = N_{TEM}\cdot N_{tc}\cdot\left(\rho_{n(i)}\cdot I^2\cdot\frac{L_n/9}{A_n} - \sigma_{n(i)}\cdot I\cdot\frac{T_{n(i-1)}-T_{n(i+1)}}{2}\right) \quad i = 2-9 \tag{20}$$

$$\dot{Q}_{n,10} = N_{TEM}\cdot N_{tc}\cdot\left[\frac{-(\alpha_{p10}-\alpha_{n10})T_{n10}}{2}\cdot I + \frac{\rho_{u,n}^{sup}}{A_n}\cdot I^2 + \rho_{n10}\cdot I^2\cdot\frac{L_n/18}{A_n} - \sigma_{n10}\cdot I\cdot\frac{T_{n9}-T_{n10}}{2}\right] \tag{21}$$

Seebeck effect is considered in the calculation of the power generated. Considering an electrical resistance R_{load} connected to the system, the power generated in this resistance can be calculated according to Eq. (22).

$$P = N_{TEM}\cdot Et^2\frac{m}{R_0\cdot(m+1)^2} \tag{22}$$

where Et is the electromotive force generated per TEM (Eq. (23)), R_0 is the internal resistance of each TEM (Eq. 24), and m is a parameter calculated with Eq. (25) in case that the TEMs are connected in series or with Eq. (26) in case of a parallel connection.

$$\begin{aligned} Et = N_{tc}\cdot\Bigg[&\alpha_{p1}T_{p1} - \alpha_{n1}T_{n1} - \alpha_{p10}T_{p10} + \alpha_{n10}T_{n10} - \sigma_{p1}\frac{T_{p1}-T_{p2}}{2} + \sigma_{n1}\frac{T_{n1}-T_{n2}}{2} \\ &- \sigma_{p10}\frac{T_{p9}-T_{p10}}{2} + \sigma_{n10}\frac{T_{n9}-T_{n10}}{2} - \sum_{i=2}^{9}\left(\sigma_{p(i)}\frac{T_{p(i-1)}-T_p(i+1)}{2}\right) \\ &+ \sum_{i=2}^{9}\left(\sigma_{n(i)}\frac{T_{n(i-1)}-T_{n(i+1)}}{2}\right)\Bigg] \end{aligned} \tag{23}$$

$$\begin{aligned} R_0 = N_{tc}\cdot\Bigg[&\frac{L_p/9}{A_p}\left(\frac{\rho_{p1}}{2} + \frac{\rho_{p,np}}{2} + \sum_{i=2}^{np}\rho_{p(i)}\right) \\ &+ 2\frac{\rho_{u,p}^{sup}}{A_p} + \frac{L_n/9}{A_n}\left(\frac{\rho_{n1}}{2} + \frac{\rho_{p,nn}}{2} + \sum_{i=2}^{nn}\rho_{n(i)}\right) + 2\frac{\rho_{u,n}^{sup}}{A_n}\Bigg] \end{aligned} \tag{24}$$

$$m^{series} = \frac{R_{load}}{N_{TEM}\cdot R_0} \tag{25}$$

$$m^{parallel} = \frac{N_{TEM}\cdot R_{load}}{R_0} \tag{26}$$

3.3. Cold side heat exchanger

Similarly to the hot side heat exchanger, the cold side one is also a biphasic thermosyphon. Nonetheless, its geometry changes, being a loop thermosyphon in this case, with a common evaporator and two sets of tubes for releasing the heat to the environment. As a consequence, some of the expressions change and two branches need to be considered.

Blue block in Fig. 2 depicts the discretization of this cold side heat exchanger, composed of five different thermal resistances, and where superscript C refers to the cold side. Following again the direction of the heat flux, the first thermal resistance that characterizes the cold loop thermosyphon $R_{k,1}^C$ represents the addition of two phenomena: conduction through the wall of the evaporator and spreading. Hence, the former resistance is modeled again according to Fourier law (Eq. (5)). Apart from pure conduction, $R_{k,1}$ also takes into account the spreading phenomenon, which occurs because heat flows from a small surface of the size of a TEM to a larger one, the evaporator's base. This thermal resistance is calculated as the constriction one (Eq. (11)), but considering the evaporator's area instead of the condenser one.

After conduction and spreading, heat causes the vaporization of the internal working fluid. In order to calculate this boiling resistance, Forster and Zuber's correlation is again used (Eq. (6)). Nonetheless, in this case, it has been considered a mixture of two substances as working fluid. The properties of the mixture are obtained with REFPROP [48], except the thermal conductivity, kinematic and dynamic viscosities, which have been calculated with Filippov and Novoselova [49], Gambill [50] and Graham's [51] models respectively (Eqs. (27)–(29)) using the REFPROP properties of each substance.

$$k = k_1\cdot y_1 + k_2\cdot y_2 - 0.72|k_1 - k_2|y_1\cdot y_2 \tag{27}$$

$$\nu^{1/3} = y_1\cdot\nu_1^{1/3} + y_2\cdot\nu_2^{1/3} \tag{28}$$

$$\mu = y_1\cdot\mu_1 + y_2\cdot\mu_2 \tag{29}$$

Next, the vaporized fluid condensates. Nevertheless, in the case of a loop thermosyphon, this process occurs along the loop tubes rather than on a vertical plate as it happens in the hot TPCT. Hence, the heat transfer coefficient of Eq. (8) varies. According to Shah's correlation [52], this coefficient depends on the regime of vapor calculated with the dimensionless vapor velocity J_g (Eq. (30)).

$$J_g = \frac{x\cdot G}{(g\cdot D_{in}\cdot d_g\cdot(d_l - d_g))^{0.5}} \tag{30}$$

If $J_g \geqslant 1/(2.4\cdot Z + 0.73)$ (with $Z = (1/x - 1^{0.8}p_r^{0.4})$), $h_c = h_I$, else if $J_g \leqslant 0.89 - 0.93\cdot exp(-0.087\cdot Z^{-1.17})$, $h_c = h_{Nu}$, else $h_c = h_I + h_{Nu}$, where

$$h_I = 0.023\cdot Re^{0.8}\cdot Pr^{0.4}\cdot\left(\frac{\mu_l}{14\cdot\mu_g}\right)^{0.0058+0.557p_r}\cdot\left[(1-x)^{0.8} + \frac{3.8\cdot x^{0.76}(1-x)^{0.04}}{p_r^{0.38}}\right] \tag{31}$$

$$h_{Nu} = 1.32\cdot Re^{-1/3}\left[\frac{d_l\cdot(d_l - d_g)\cdot g\cdot k_l^3}{\mu_l^2}\right]^{1/3} \tag{32}$$

The former correlation has shown to be in good agreement with 22 different fluids; horizontal, vertical, and downward-inclined tubes; tube diameters from 2 to 49 mm; reduced pressures from 0.0008 to 0.9; flow rates from 4 to 820 kg/m^2·s; all liquid Reynolds numbers from 68 to 85000; and all liquid Prandtl numbers from 1 to 18 [52].

After condensation, conduction needs to be considered. Due to the circular shape of the tubes, in this case, according to Fourier law, Eq. (4) applies again. Nonetheless, it is important to note that the length of all the loops must be considered.

Finally, convection with the environment needs to be taken into account. Hoke et al. experimentally determined the convective heat transfer from a loop tubular geometry with wire fins [53], the typical ones of loop thermosyphons. Hence,

$$R_{conv}^C = \frac{1}{h_t\cdot A_t + \eta_w\cdot h_w\cdot A_w} \tag{33}$$

where h_t is the convective coefficient of the tubes, which is indeed derived from the wires' one according to Eq. (34), A_t is the transmission area of the tubes, η_w is the fins efficiency (Eq. (35)), h_w is the convective

Fig. 3. GTEG with phase change heat exchangers developed and studied by Catalan et al. [20].

coefficient of the wires derived from the Nusselt coefficient calculated with Eq. (36) and A_w is the transmission area of the wires.

$$h_t = h_w \cdot \left(\frac{D_t}{D_w}\right)^{-0.5} \tag{34}$$

$$\eta_w = \frac{\tanh(m_w)}{m_w} \tag{35}$$

$$Nu = 0.027 \cdot Re^{0.819} \cdot [1 - 100 \cdot exp^{(-2.32 \cdot S_w/D_w)}] \tag{36}$$

3.4. Interconnection of blocks

Next, it is necessary to consider different phenomena consequence of the interconnection between the different parts: thermal contacts and thermal bridge [54]. On the one hand, the former deals with the fact that when two surfaces are confronted, due to their roughness, the contact is not perfect, introducing air gaps that reduce heat transmission. Different materials such as thermal grease, graphite sheets, or even phase change materials are normally introduced in order to improve this contact. The value of the thermal resistance depends on the interface material and the pressure distribution, but it is estimated to be between 0.01 and 0.1 K/W per module [54,55].

On the other hand, the latter can be defined as an area or component of an object which has higher thermal conductivity than the surrounding material, creating a path of least resistance for heat transfer [56]. In TEGs, the main sources for thermal bridges are the screws used to ensure a good contact and pressure distribution, and the direct heat transfer between the hot and cold heat exchanger, skipping the slim TEMs. Again, the value of this thermal resistance depends on the assembly, but as reference, it can be considered a value between 30 and 60 K/W [40].

3.5. Numerical resolution

Once all the thermal resistances have been detailed, it is necessary to address the numerical resolution of the system, so that the temperature of each of the nodes can be obtained. As has been stated before, the thermal-electrical analogy is actually derived from the application of the implicit finite difference method to heat conduction equation. As a consequence, for each node *i*, considering a permanent regime, Eq. (37) applies.

$$\sum_j \frac{T_j - T_i}{R_{ij}} + \dot{Q}_i = 0 \tag{37}$$

In this equation, *i* refers to the node under consideration, *j* to each adjacent node, *T* is their temperature, R_{ij} is the thermal resistance between nodes *i* and *j*, and $\dot{Q}_i$ is the heat flux generated or absorbed by node *i*. For an analogy with N nodes, a system of N equations with N unknowns is obtained.

In the present paper, the resolution of the former system of equations has been iterative. Thus, an initial temperature has been supposed for each node. Afterwards, new temperatures have been calculated with Eq. (37). The process has been iteratively repeated until the difference between the new and the last temperatures was lower than a tolerance. This tolerance has been defined to be 0.01.

4. Experimental validation

In order to validate the computational model, the experiments performed by Catalan et al. have been used [20]. The present section first describes the prototype employed. Next, the results and analysis of the validation are presented.

4.1. Prototype description

Fig. 3 depicts the GTEG with phase change heat exchangers developed and studied by Catalan et al. [20], based on which they concluded that this type of heat exchangers are the most suitable ones for GTEGs.

The hot side heat exchanger was a 1 m long stainless steel TPCT with a section of 60x 60 mm^2 and a thickness of 5 mm. The used working fluid was water up to a height of 0.36 m. The squared section of this TPCT facilitated the installation of the TEMs. More specifically, two Marlow TG12-8-01L bismuth telluride modules were used [57].

Each TEM dissipated heat to an individual loop thermosyphon. In the considered experiments, two different geometries of loop thermosyphons were studied simultaneously, leading to a non-symmetrical generator. Hence, one of the TEMs dissipated heat to a loop thermosyphon with a condensation/convection area consisting of 8 levels of tubes, while the other one did it to a 6 levels loop thermosyphon. Otherwise, the thermosyphons were similar: the evaporator had an area of 50 × 50 mm^2, a width of 35 mm and a thickness of 2 mm; the internal working fluid was a mixture of water and ammonia; and the condensation/convection section was composed of two sets of 6 mm tubes with a length of 420 mm per level, with 1.5 mm wire fins separated 5 mm.

4.2. Results and analysis

The experimental validation of the computational model has been performed on two steps. Firstly, only the cold side heat exchangers have been considered, measuring the capability of the model (blue block) to determine their thermal resistance for different heat fluxes. Secondly, the whole GTEG has been taken into consideration, leading to the validation of the whole computational model.

On the one hand, Fig. 4 shows the results corresponding to the estimation of the thermal resistance of the cold side heat exchangers. The two different sizes of loop thermosyphons (8 and 6 levels) have been

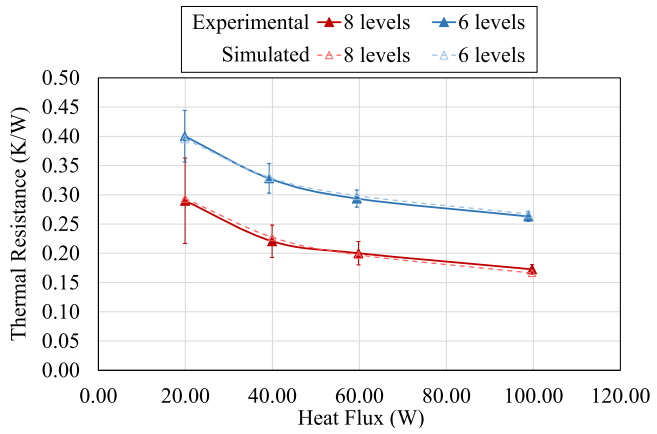

Fig. 4. Experimental and simulated thermal resistance of the loop thermosyphons for different heat fluxes.

characterized for four heat fluxes. In the experiments, a heating plate was responsible for providing the desired heat flux $\dot{Q}$, and temperature at the base of the evaporator T_{ev} and in the climatic chamber T_{amb} were measured. Thus, thermal resistance was calculated as:

$$R = \frac{T_{ev} - T_{amb}}{\dot{Q}} = \frac{T_{ev} - T_{amb}}{V \cdot I} \tag{38}$$

The experiments were repeated three times and the uncertainties calculated with [58], considering thermocouples with precision $\pm 0.5\ ^{\circ}C$. The model is deterministic, so no variation of the results is expected. As it can be observed, as heat flux increases, the thermal resistance decreases. This is due to the fact that these heat exchangers are based on the phase change of an internal fluid, and the properties of this fluid improve with temperature. Besides, it can also be observed a lower thermal resistance with more number of levels. Since in loop thermosyphons all the convective area is effective for heat dissipation, heat flux is uniformly distributed among it, leading to lower thermal resistances with bigger convective areas. Due to this aspect, with this type of heat exchangers, it is possible to obtain low values of thermal resistance without the need for forced convection.

The discrepancy between the model and the experimental results has been estimated by means of the relative error (Eq. (39)).

$$Relative\ error = \frac{Value_{exp} - Value_{sim}}{Value_{exp}} \cdot 100 \tag{39}$$

A statistical analysis of this relative error states that this sample can be described as a normal distribution with mean 0.26 and standard deviation 7.27. Therefore, the model predicts the thermal resistance of the loop thermosyphons with a relative error in the interval [−14.27%; 14.81%] in the 95% of the cases. The wideness of this interval is mainly due to the big experimental uncertainties with low heat fluxes. If only the operating range between 40 and 100 W is considered, in which the GTEG will work, the relative error presents a normal distribution with mean −0.43 and standard deviation 4.32, leading to a relative error in the [−9.08%; 8.21%] interval in the 95% of the cases.

On the other hand, once the cold side block had been validated, it was the turn of the whole GTEG. Since the prototype is non-symmetrical, being composed of two loop thermosyphons with different geometries, their thermal resistance is different, and so is the heat flux that goes through them. Therefore, it was necessary to adapt the developed computational model in order to correctly represent this behavior. Fig. 5 depicts the thermal-electrical analogy, differentiating the two branches that represent each loop thermosyphon. The split point between them is located between the boiling and the condensation resistances of the hot side TPCT, which corresponds with the node at the internal saturation temperature T_{sat}. Due to the difficulties of simulating the real conditions of an HDR field at the laboratory, rope heaters directly in contact with the TPCT's evaporator were used as heat source. As a consequence, the model does not include the convective resistance R^H_{conv}.

The validation of the model has been performed by comparing two different parameters: power generation and temperature. Fig. 6 shows the results corresponding to the estimation of power generation. More specifically, Fig. 6(a) depicts the power generated by a TEM with a loop thermosyphon composed of 8 levels for heat dissipation, while Fig. 6(b) does the same for a loop thermosyphon with 6 levels. In both cases, the values of power generation are shown for five different load resistances, and three temperatures of the heat source, maintaining the ambient temperature at 20 °C in all cases. As before, the experiments have been repeated three times and their uncertainties calculated, while the model is considered deterministic.

The maximum power generation is obtained with a load resistance of 3.2 Ω, whose value is similar to that of the internal electrical

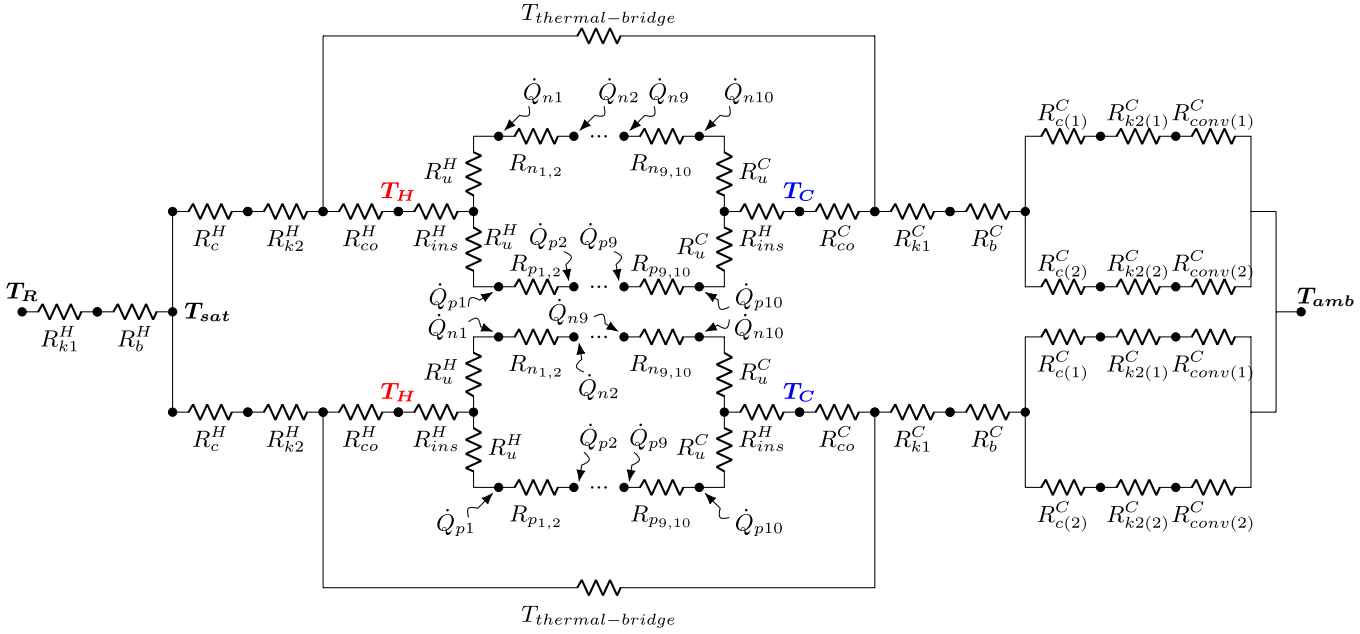

Fig. 5. Thermal-electrical analogy used in the experimental validation.

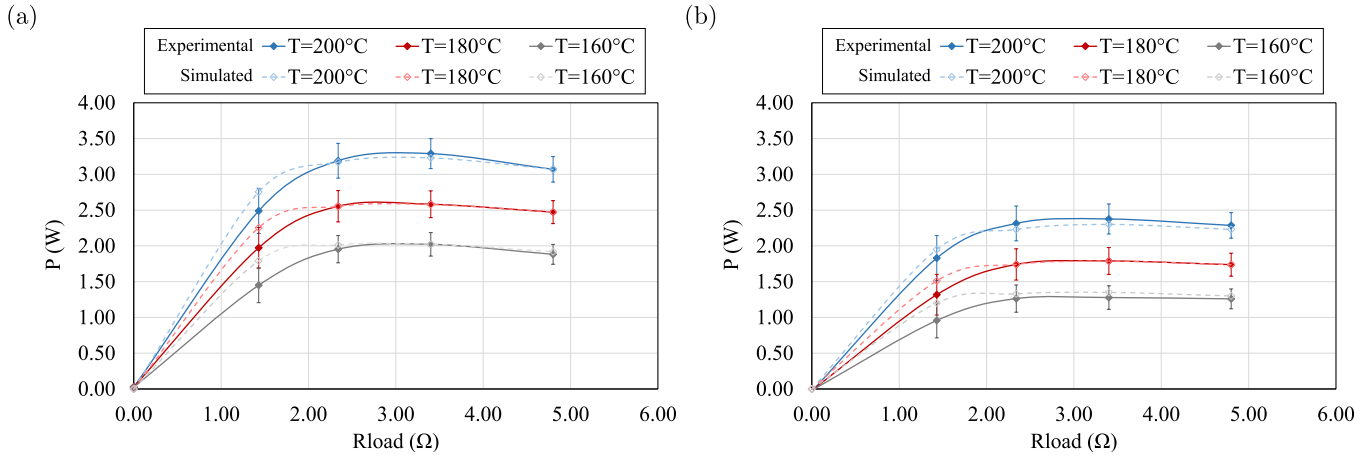

Fig. 6. Experimental and simulated power generated per module for different load resistances and heat source temperatures (a) considering an 8 levels loop thermosyphon as cold side heat exchanger and (b) considering a 6 levels one.

resistance of the TEM [57]. Moreover, this generation increases with higher heat source temperatures and lower thermal resistances of the cold side heat exchangers. Power generation depends on the temperature difference between the sides of the TEMs, and in order to increase this temperature difference, high temperature heat sources and heat exchangers with low thermal resistances are needed. Since the 8 levels loop thermosyphon had a lower thermal resistance in comparison with the 6 levels one, the generation obtained in the left graph is higher than in the right one.

The comparison between the experimental results and the model predictions reveals a good concordance except for the values for 1.43 Ω, for which the model estimates a generation higher than in reality, but still encompassed in the uncertainty ranges. Fig. 7(a) graphs the power estimated by the model versus the experimentally measured one. All the values are encompassed in a ± 6% range, except those for 1.43 Ω that enlarge the positive range to + 25%. The problem with relative deviations is that they soar for small values. The maximum absolute error is actually 0.34. If, as before, the discrepancy between the model and the experimental results is estimated by means of the relative error (Eq. (39)) and a statistical analysis is made, the total mean error is −3.4 considering all values. When neglecting those corresponding to 1.43 Ω, the errors follow a normal distribution with mean −0.28 and standard deviation 1.42. In the study of the next section, which serves to achieve the objective of this paper, generation will be always calculated with the load resistance that maximizes generation, for which the model is considered accurate enough.

A similar study has been performed for the temperature distribution. Hence, since the comparison of temperatures cannot be done in absolute values, the temperature difference of the hot and the cold side heat exchanger has been compared (HHE and CHE respectively). Fig. 7(b) graphs the estimated temperature differences versus the experimental ones. As it can be observed, there is a good concordance in the data, which is encompassed, in all cases, in the ± 8% range. A statistical analysis of the relative errors (Eq. (39)) reveals that they follow a normal distribution with a mean of 0.18 and a standard deviation of 3.06. Thus, it is demonstrated that the model has been validated both for optimal generation and temperature distribution, leading to a competent tool for the analysis of the operation of GTEGs, as it is developed in the next section.

5. Computational study of a GTEG at Timanfaya National Park

Based on the developed and validated model, the present section focuses on the analysis of the influence of different parameters on a GTEG considering a real location: Timanfaya National Park (Canary Islands, Spain), whose potential will also be estimated. Taking into account that it is a nature reserve, it will be important to maximize the power produced per thermoelectric generator, minimizing the number of boreholes required, as well as using water as the internal working fluid, so that the environmental impact is minimal.

Timanfaya National Park hosts one of the world's greatest shallow HDR field, both in intensity and extension. There are 11700 m^2 of geothermal anomalies presenting temperatures of more than 200 °C at ground level and 615 °C at a depth of 5–15 m [32,59,60]. The origin of these anomalies is believed to be a body of lava from the last eruptions in 1730-36 and 1824, which has not reached the surface and is slowly cooling down.

Due to the low thermal diffusivity of the superficial hot rocks ($8{\cdot}10^{-4}$ cm^2/s), which complicates the heat transfer by conduction and causes a slow recovery of the system, heat extraction mechanism needs to be convection [32]. Based on this statement, different experiments intended to evaluate the gas fluxes that ascend from the geothermal anomalies were performed, for which eight 60 m long boreholes were drilled in 1991 and 1992 [59]. Within the park, two different areas were studied: *Islote Hilario*, with 3000 m^2, is the area with the highest temperatures and air velocities, while *Casa de los Camelleros*, with 2000 m^2, although presents lower temperatures, it is still considered a high temperature geothermal field. Table 1 details the air velocity and ground temperatures at different depths characteristics of each site. These values were measured again in January 2019, so that it was verified that the system had not cooled down since the last measurements in the 1990s.

For each of the considered locations, the computational model depicted in Fig. 2 has been used to perform the computational study. The geometries taken as reference derive from constructional aspects. Hence, for *Islote Hilario*, due to its high temperatures and due to the limitations of both the critical temperature of water, the used working fluid, and the maximum temperature supported by Bi-Te TEMs (250 °C), the hot side TPCT is a stainless steel finless tube with a diameter of 48 mm and a thickness of 5 mm. In the case of *Casa de los Camelleros*, the TPCT is a 46 mm aluminum tube, 3.25 mm thick, with 31 vertical fins with a length of 17 mm and a thickness of 2 mm. In both cases, it is considered that water fills half of the inserted length of the TPCT. The variables of study, apart from the location, are: the inserted length of the TPCT (that determines the input temperature of the gases T_G), the size of the cold side thermosyphon (considering the two studied geometries of 8 and 6 levels loop thermosyphons), and the number of thermoelectric modules (TEMs). As before, each TEM incorporates an individual cold side loop thermosyphon.

The temperature of the gases T_G, which is one of the inputs of the model, is considered constant and with a value equal to the average temperature of the evaporator. Thus, for a TPCT inserted 3 m, whose

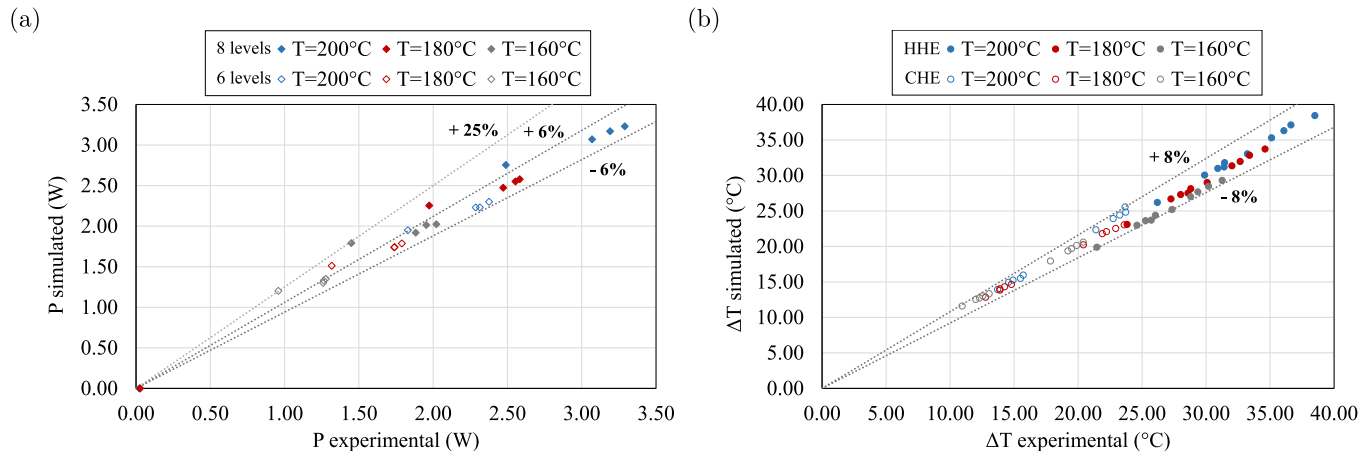

Fig. 7. (a) Simulated power generation versus real one, for different temperatures of the heat source and the two different geometries of loop thermosyphons studied, and (b) Simulated versus real temperature difference of the hot and cold side heat exchangers (HHE and CHE respectively) for different temperatures of the heat source.

Table 1
Air velocity and ground temperatures at different depths characteristics of the two areas of study within Timanfaya National Park.

	Casa de los Camelleros	Islote Hilario
v_{air} (m/s)	6.03	11.15
T at surface (°C)	200	480
T at 0.75 m (°C)	205	490
T at 1.125 m (°C)	207	495
T at 2.25 m (°C)	210	510

evaporator measures 1.5 m, the input temperature is the value at a depth of 2.25 m. On the ambient side, the average temperature and wind velocity of the park, 20.8 °C and 5.43 m/s, have been taken as reference [61]. Regarding the contact between the different parts, per each module, a thermal contact resistance of 0.05 K/W and a thermal bridge resistance of 41.6 K/W have been considered [54,55].

Fig. 8 depicts the power generated (left axis) and the efficiency (right axis) of GTEGs working with the optimal load resistance in *Islote Hilario*, considering a different number of TEMs, three inserted lengths of the hot side TPCT, and two sizes of cold side loop thermosyphons, with an 8 levels loop thermosyphon in Fig. 8 and a 6 levels one in Fig. 8(b). As can be observed, in all cases the efficiency of the generator decreases as the number of modules increases. This efficiency is higher with longer TPCTs, since the evaporator is larger and therefore convective R^H_{conv}, conductive R^H_{k1} and boiling R^H_b thermal resistances decrease (Eqs. (1), (4)–(6)) increasing the heat flux, as well as because of slightly higher air temperatures deeper in the boreholes. Thus, the temperature between the sides of the TEMs is higher, and so is their efficiency. This also occurs with lower thermal resistances of the cold side heat exchanger, leading to higher efficiencies in the case of the 8 levels loop thermosyphon.

Regarding total power generation, similarly to efficiency, with longer TPCTs and bigger loop thermosyphons, i.e. lower thermal resistances, more power is generated. Nonetheless, in this case, the variation with respect to the number of TEMs is different. Despite the continuous reduction of efficiency, in the beginning, when more TEMs are added, total generation of the GTEGs increases until an optimum point is reached, from which generation starts to decrease. This is due to the fact that the TEMs share a unique TPCT. Hence, the thermal resistances of convection with the hot geothermal gases, conduction in the evaporator, and boiling remain constant regardless of the number of TEMs. The rest of the thermal resistances of the thermal-electrical analogy of Fig. 2 decrease with more TEMs. Since each added TEM has its own cold side heat exchanger, the value of these resistances divides by the number of TEMs due to their parallel connection, leading to a lower global thermal resistance. As a consequence, more heat flux is absorbed by the GTEG and the temperature of the hot side of the TEMs decreases.

This reduction can be observed in Fig. 9(a), which shows the

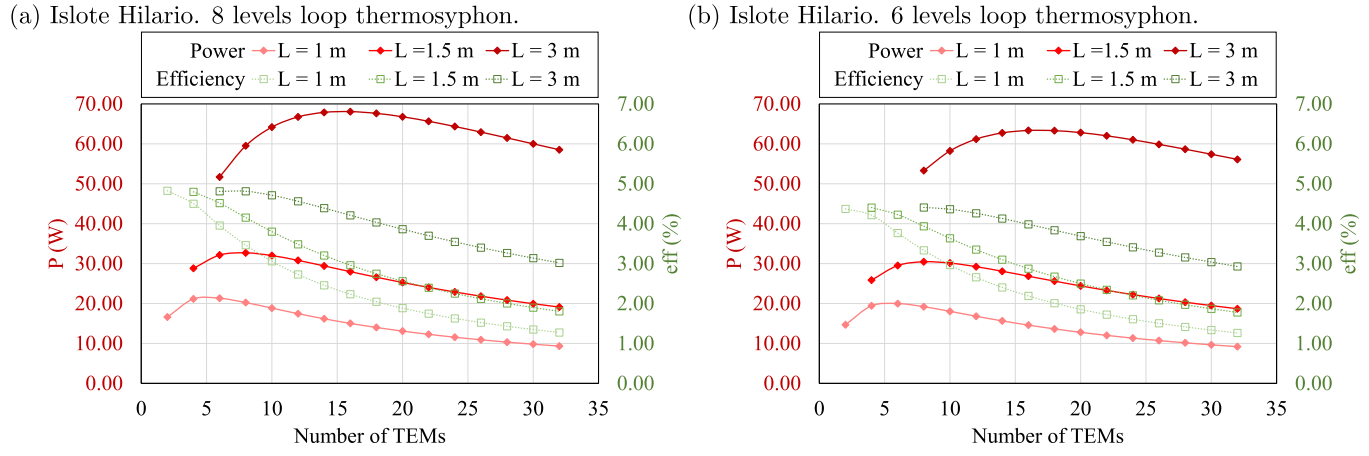

Fig. 8. Power generated (left axis) and efficiency (right axis) of GTEGs in *Islote Hilario*, considering a different number of TEMs, three inserted lengths of the hot side TPCT, and two sizes of loop thermosyphons: (a) with 8 levels and (b) with 6 levels.

temperatures of the gases T_G, the saturation of the internal working fluid T_{sat} (which never exceeds the critical value for water), the hot and the cold side of the modules T_H and T_C, and the ambient temperature T_{amb} for the case of a TPCT inserted 3 m in the ground and with 8 levels loop thermosyphons as cold side heat exchangers. As the number of TEMs increases, the temperature difference between the sides of the TEMs decreases, mainly due to the reduction of the hot side temperature. As a consequence, the efficiency decreases. Nonetheless, there is an optimum point where there exists an equilibrium between the number of TEMs and the decreased efficiency. Given a fixed size of the cold side loop thermosyphon, this optimum point occurs with more TEMs as the thermal resistances R^H_{conv}, R^H_{k1} and R^H_b decrease with longer inserted lengths of the TPCT. This is due to the fact that the power generated per module decreases at a slower rate with the addition of TEMs for lower resistances, as can be observed in the decrease of efficiency, moving the optimum point from 6 TEMs in the case of 1 m inserted, to 8 TEM for 1.5 m and to 16 TEMs for 3 m. The same optimum points are obtained for GTEGs with 6 levels loop thermosyphons. Considering all the studied cases, the optimal GTEG for *Islote Hilario* generates 68.07 W with 16 TEMs, when the inserted length of the hot side TPCT is 3 m and 8 levels loop thermosyphons are used as cold side heat exchangers.

In *Casa de los Camelleros* (from now on, Camelleros), due to the lower temperature of the gases, which made it impossible to exceed neither the critical point of water nor the maximum temperature stood by the modules, vertical fins were added in the external part of the evaporator. As it can be seen in Fig. 9(b), the addition of fins considerably improves the heat transfer between the gases and the TPCT, reducing its thermal resistance and leading to a smaller temperature difference between the gases and the hot side of the modules, a difference which also increases with more TEMs.

Fig. 10 depicts the power (with an optimal load resistance) and the efficiency with respect to the number of TEMs for all the studied geometries, which follow a similar trend that in *Islote Hilario*. The main difference between the two locations is that, for each geometry, the optimal generator of *Camelleros* is composed of a higher number of TEMs than in *Islote Hilario*. Due to the addition of fins, the thermal resistance of the hot side has diminished, causing a slower decreasing rate in the power generated per module with the addition of TEMs and shifting the optimum point to the right of the graph. Hence, for the case of having 8 levels loop thermosyphons in the cold side, the optimal GTEG is composed of 10 TEMs for 1 m inserted, 14 TEMs for 1.5 m and 28 for 3 m. Furthermore, in contrast to *Islote Hilario*, in this case there does exist a difference with the size of the cold side heat exchanger, since the thermal resistance of the hot side has less weight in the global thermal resistance. Thus, when having 6 levels loop thermosyphons at the cold side, the optimal GTEG is achieved with 30 TEMs for 3 m. The higher thermal resistance of the 6 levels loop thermosyphons causes a more noticeable decrease of the global cold side thermal resistance with the increase of TEMs, leading to a slower decrease of efficiency that, due to a smaller decrease in the power generated per TEM, provokes that the optimum point is achieved with more TEMs. Among all the studied cases, in *Camelleros* the optimal GTEG is again inserted 3 m in the ground and incorporates 8 levels loop thermosyphons as cold side heat exchangers. The maximum generation of this device is 43.23 W, achieved with 28 TEMs.

Instead of using phase change heat exchangers, an alternative configuration that also fulfills the requirements of robustness and absence of both moving parts and auxiliary consumption, but it is simpler, would have been solid heat exchangers. Hence, for the hot side heat exchanger the easiest option would consist of a solid bar of a metallic material, with suitable conductive properties; and for the cold side ones, fin dissipators (FD). Fig. 11(a) shows, in yellow, the generation obtained with a thermoelectric generator with the former configuration for the two considered locations: *Islote Hilario* with filled lines, and *Camelleros* with dashed ones. More specifically, the hot side heat exchangers present the same geometry and material than their equivalent TPCT, considering an inserted length of 3 m since it led to the best results. Each cold side heat exchanger is the fin dissipator characterized by Catalan et al., which presents a thermal resistance of 0.745 K/W under breeze conditions [20]. In order to simulate these results with the computational model, at the hot side heat exchanger only convective and conductive resistances have been taken into account, and in the cold side two fin dissipators per level with a separation of 25 cm between levels have been considered.

As it can be observed, as more TEMs are added, generation continuously increases. In this case, generation per level is practically constant, with a value that is higher for lower levels since its conductive thermal resistance is smaller. Hence, when more levels are added, more generation is obtained, although the increase in the total power generated gradually slows down with the addition of TEMs, stabilizing at a certain value when adding more TEMs barely increases generation. Nevertheless, in comparison with GTEGs with only phase change heat exchangers, there exists a huge detriment in the generation. In *Islote Hilario*, generation stabilizes at around 2 W, while in *Camelleros* at 8.2 W, 97% and 81% lower than the maximum values obtained previously. This reduction is caused by the enormous thermal resistance of the solid hot side heat exchanger. In Fig. 11(a) the generation obtained with 8 levels loop thermosyphons (LT) has also been depicted in addition to the values with fin dissipators (FD). Thus, although there exists a slight increase, the generation still shows a considerable reduction: 2 and 8.5 W respectively, confirming that the hot side heat exchanger is responsible for the detriment. The greater reduction in

(a) Islote Hilario. 8 levels LT. TPCT inserted 3 m.

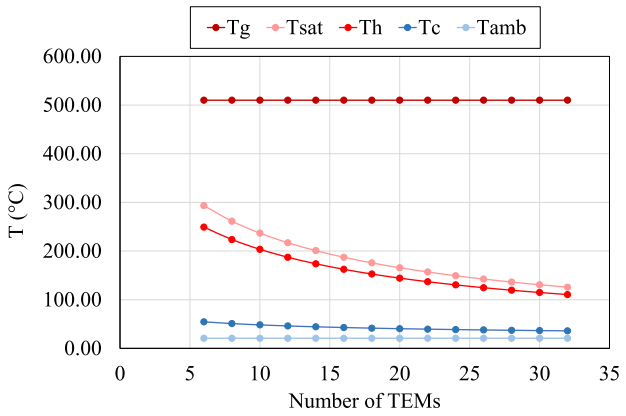

(b) Camelleros. 8 levels LT. TPCT inserted 3 m.

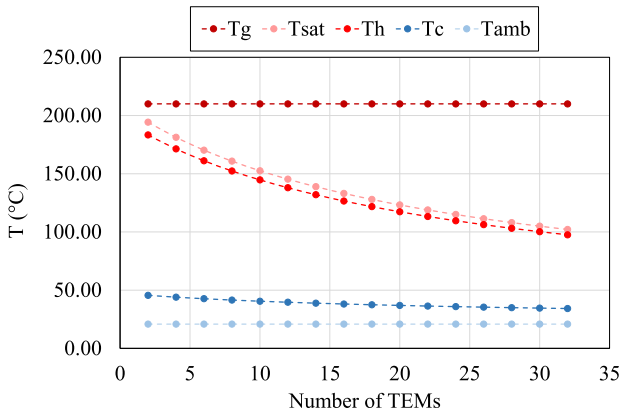

Fig. 9. Temperature distribution of the gases T_G, saturation of the internal working fluid T_{sat}, the hot and cold side of the modules T_H and T_C, and the ambient T_{amb} for a GTEG composed of a TPCT inserted 3 m and an 8 levels loop thermosyphons, located at (a) *Islote Hilario* or (b) *Casa de los Camelleros*.

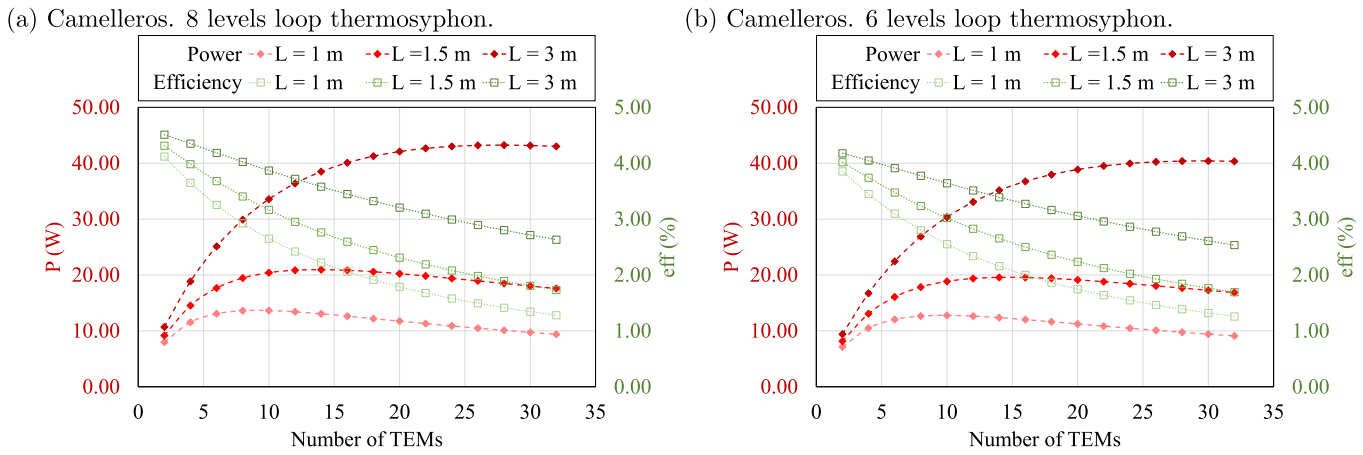

Fig. 10. Power generated (left axis) and efficiency (right axis) of GTEGs in *Casa de los Camelleros*, considering a different number of TEMs, three inserted lengths of the hot side TPCT, and two sizes of loop thermosyphons: (a) with 8 levels and (b) with 6 levels.

Islote Hilario is due to the low thermal conductivity of stainless steel, which is used because of the really high temperatures that exist in this location, and that other more conductor metals such as aluminum or copper would not resist.

The main component of the thermal resistance of the solid hot side heat exchanger is due to the conductive part. Fig. 11(b) depicts, for *Camelleros*, the temperatures of the geothermal gases T_G, the superficial temperature of the hot side heat exchanger T_{sup}, the hot and cold sides of the thermoelectric modules T_H and T_C of the highest level, and the ambient temperature T_{amb}. Hence, while the superficial temperature is very close to the gases' one, it can be seen that the principal temperature drop occurs in the conductive part. This drop increases with a higher number of TEMs, since apart from the effect of adding more modules to a unique hot side heat exchanger, the length of the bar outside the ground increases maintaining the same area and thermal conductivity. Hence, the decrease in the temperatures with the number of TEMs is more drastic than when having a TPCT. In *Islote Hilario*, although not represented, due to the lower thermal conductivity of stainless steel, the temperature difference is even higher and the reduction with the addition of TEMs is more severe.

Due to the high thermal resistance of the solid hot side heat exchanger, there was only a slight difference in the generation obtained using fin dissipators or loop thermosyphons as cold side heat exchangers. Hence, in order to determine which one entails a better alternative, Fig. 12 depics the generation results of a GTEG with again a TPCT as hot side heat exchanger, and fin dissipators (FD) and loop thermosyphons (LT) as cold side ones, both for *Islote Hilario* and *Camelleros*. As can be observed, the influence of the thermal resistance of the cold side heat exchanger is now more appreciable. Thus, with fin dissipators the maximum generation in *Islote Hilario* is of 46.34 W, obtained with 26 thermoelectric modules, while in *Camelleros*, the best value is 31.52 W with 42 modules, which supposes a reduction of 31.9% and 27.1% respectively in comparison with loop thermosyphons in the cold side. Apart from the decrease in the net power generation, the utilization of fin dissipators at the cold side also requires a higher number of thermoelectric modules to reach the optimal value, 10 and 14 more modules than with loop thermosyphons respectively, which would increase the size of the whole generator.

Consequently, it becomes patent that in order to have a robust GTEG without moving parts nor auxiliary consumption, the best configuration is composed of phase change heat exchangers, reaffirming the novelty proposed in the present paper.

Considering the optimal GTEG with phase change heat exchangers of each location and taking into account the monthly average temperature and wind velocity of Timanfaya National Park [61,62], Table 2 analyzes the energy that can be produced per year with each GTEG. For more information, the most significant temperatures, the thermal resistances of the hot and cold side heat exchangers (R_{HHE} and R_{CHE}), the power generated and its efficiency are also depicted. As it can be observed, the weather at Timanfaya National Park is quite stable all year

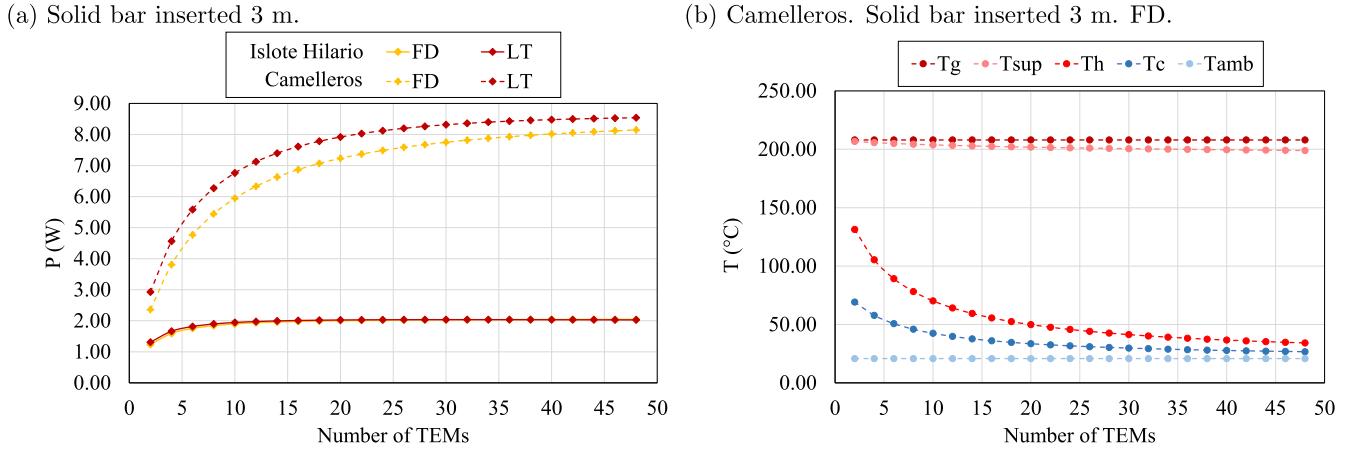

Fig. 11. (a) Power generated by GTEGs composed of a solid bar inserted 3 m in the ground as hot side heat exchanger, and fin dissipators (FD) or 8 levels loop thermosyphons (LT) as cold side ones. (b) Temperature distribution of the gases T_G, superficial temperature T_{sup}, the hot and cold side of the modules T_H and T_C of the top level, and the ambient T_{amb} for a GTEG composed of a solid bar inserted 3 m and fin dissipators, located at *Casa de los Camelleros*.

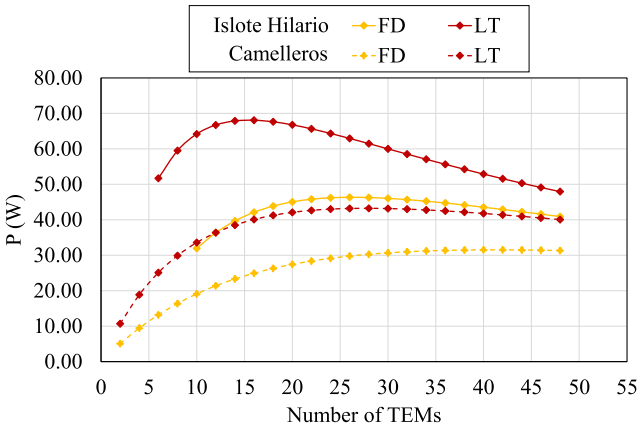

Fig. 12. Power generated by GTEGs composed of a TPCT inserted 3 m in the ground as hot side heat exchanger, and fin dissipators (FD) or 8 levels loop thermosyphons (LT) as cold side ones.

long, with average temperatures between 17.3 and 24.6 °C and wind velocities in the range from 4.6 to 6.4 m/s. As a consequence, the operation parameters of the GTEG remain practically constant during all months, and there is only 3.5 W of difference between the month with the highest generation (January) and the one with the lowest (September in *Islote Hilario* and August in *Camelleros*).

The GTEG of *Islote Hilario* operates with an average temperature difference in the TEMs of 120 °C, with approximately 162 °C in the hot side and 42 °C in the cold one, leading to an average power of 68.66 W. Given that the temperature of the geothermal gases is 510 °C, it is remarkable to note the big temperature loss that occurs in the hot side heat exchanger, which presents a value of 3.29 K/W per module, much higher than the cold side one of 0.16 K/W. In the case of *Camelleros*, the hot side heat exchanger has a considerably lower thermal resistance due to the addition of fins. As a consequence, the temperature difference in this heat exchanger is of just 101 °C approximately. In this case, the TEMs operate with an average temperature difference of 71 °C, leading to an average generated power of 43.5 W. Since geothermal energy is always available, GTEGs can generate energy permanently, during the 8760 h of a year. Hence, in *Islote Hilario* each GTEG annually generates 601.36 kWh and in *Camelleros*, 380.95 kWh are generated per device.

Finally, taking into account the extension of each area (3000 m^2 in *Islote Hilario* and 2000 m^2 in *Camelleros*), an extrapolation of total energy generation can be performed. It was estimated that 438.51 and 427.55 W/m^2 can be respectively extracted in these areas without affecting the geothermal field [59]. Therefore, up to 470.87 MWh can be generated in *Islote Hilario*, and 210.66 MWh in *Casa de los Camelleros*, leading to a total annual electricity generation of 681.53 MWh.

6. Conclusions

In conclusion, the present paper has delved into the study of geothermal thermoelectric generators (GTEGs) with phase change heat exchangers, demonstrating the potential of the solution for hot dry rock (HDR) fields with a minimal environmental impact. For this purpose, a computational model based on the thermal-electrical analogy between electricity and heat transfer has been developed and validated thanks to an experimental prototype, leading to an error estimating the generation in the maximum point of less than 6%, and of 8% in case of the prediction of the temperature differences in the heat exchangers.

Based on the model, a computational study of GTEGs has been performed for two areas within Timanfaya National Park (Canary Islands, Spain): *Islote Hilario*, where gases emerge at around 500 °C and more than 11 m/s; and *Casa de los Camelleros*, with 200 °C and 6 m/s respectively. The designed GTEGs are composed of a two phase closed thermosyphon (TPCT) with water as working fluid as hot side heat exchanger, and loop thermosyphons (one per thermoelectric module) as cold side ones. This configuration leads to a device without moving parts nor auxiliary consumption, resulting in a robust generator that maximizes net generation. In the study, the size of the heat exchangers, the number of thermoelectric modules (TEMs), and the addition or not of fins have been considered.

As a result, it has arisen the importance of using heat exchangers with low thermal resistance in order to maximize power generation. The lower the thermal resistance of the heat exchangers, the higher the

Table 2
Monthly analysis of the energy generated by the optimized GTEGs in each of the studied locations, showing also relevant operating information.

Location	Month	T_{amb} (°C)	v_{air} (m/s)	T_G (°C)	T_H (°C)	T_C (°C)	R_{HHE} (K/W)	R_{CHE} (K/W)	P (W)	η (%)	Energy (kWh)	Energy (kWh/year)
ISLOTE HILARIO	January	17.3	5.4	510.00	159.75	38.77	3.29	0.17	70.35	4.32	52.34	601.36
	February	17.7	5.5	510.00	159.94	39.05	3.29	0.16	70.20	4.31	47.17	
	March	18.8	5.4	510.00	160.60	40.03	3.29	0.16	69.64	4.28	51.81	
	April	19.2	5.7	510.00	160.77	40.28	3.29	0.16	69.50	4.28	50.04	
	May	20.4	5.4	510.00	161.55	41.44	3.29	0.16	68.85	4.25	51.22	
	June	22.1	5.5	510.00	162.50	42.85	3.29	0.16	68.05	4.21	49.00	
	July	23.4	6.4	510.00	163.08	43.71	3.29	0.16	67.57	4.19	50.27	
	August	24.6	6.1	510.00	163.83	44.83	3.29	0.15	66.94	4.16	49.81	
	September	24.3	4.9	510.00	163.95	45.00	3.29	0.16	66.85	4.15	48.13	
	October	22.9	4.6	510.00	163.23	43.94	3.29	0.16	67.45	4.18	50.18	
	November	20.6	5.1	510.00	161.73	41.71	3.29	0.16	68.69	4.24	49.46	
	December	18.4	5.2	510.00	160.43	39.78	3.29	0.16	69.78	4.29	51.92	
CAMELLEROS	January	17.3	5.4	210.00	104.21	31.87	1.70	0.20	45.27	2.98	33.68	380.95
	February	17.7	5.5	210.00	104.39	32.18	1.70	0.20	45.09	2.97	30.30	
	March	18.8	5.4	210.00	104.95	33.14	1.70	0.20	44.52	2.95	33.12	
	April	19.2	5.7	210.00	105.12	33.43	1.70	0.20	44.35	2.94	31.93	
	May	20.4	5.4	210.00	105.75	34.54	1.70	0.20	43.69	2.91	32.51	
	June	22.1	5.5	210.00	106.58	35.97	1.70	0.19	42.85	2.88	30.85	
	July	23.4	6.4	210.00	107.15	36.94	1.70	0.19	42.29	2.86	31.46	
	August	24.6	6.1	210.00	107.78	38.03	1.70	0.19	41.66	2.83	30.99	
	September	24.3	4.9	210.00	107.77	38.01	1.70	0.19	41.67	2.83	30.00	
	October	22.9	4.6	210.00	107.12	36.89	1.70	0.20	42.32	2.86	31.48	
	November	20.6	5.1	210.00	105.89	34.77	1.70	0.20	43.56	2.91	31.36	
	December	18.4	5.2	210.00	104.78	32.85	1.70	0.20	44.69	2.95	33.25	

generation. Nonetheless, since all the TEMs share a common TPCT, there exists an optimum in the generation. In the case of *Islote Hilario*, the optimized GTEG generates 68.07 W with 16 TEMs, while in *Casa de los Camelleros*, the optimum number of TEMs is 28, which leads to a generation of 43.23 W. If a solid bar had been used as hot side heat exchanger and fin dissipators as cold side ones, generation will respectively be 97% and 81% lower, while if only the cold side heat exchangers are modified the reduction is of around 30%, thus reaffirming that passive heat exchangers based on phase change are the most adequate ones for GTEGs. Thanks to these GTEGs and their scalability, it would be possible to generate 681.53 MWh of electricity in one year.

CRediT authorship contribution statement

Leyre Catalan: Methodology, Software, Validation, Formal analysis, Investigation, Writing - original draft, Writing - review & editing, Visualization. **Miguel Araiz:** Methodology, Software, Writing - review & editing. **Patricia Aranguren:** Writing - review & editing, Supervision. **David Astrain:** Conceptualization, Writing - review & editing, Supervision.

Declaration of Competing Interest

The authors declare that they have no known competing financial interests or personal relationships that could have appeared to influence the work reported in this paper.

Acknowledgments

We would like to acknowledge the support of the Spanish State Research Agency and FEDER–UE under the grant RTC-2017-6628-3; as well as the FPU Program of the Spanish Ministry of Science, Innovation, and Universities (FPU16/05203).

References

[1] Zuo W, Li Q, He Z, Li Y. Numerical investigations on thermal performance enhancement of hydrogen-fueled micro planar combustors with injectors for micro-thermophotovoltaic applications. Energy 2020;194:116904 https://doi.org/10.1016/j.energy.2020.116904.
[2] Li Q, Zuo W, Zhang Y, Li J, He Z. Effects of rectangular rib on exergy efficiency of a hydrogen-fueled micro combustor. Int J Hydrogen Energy 2020;45(16):10155–63. https://doi.org/10.1016/j.ijhydene.2020.01.221.
[3] Zuo W, Li J, Zhang Y, Li Q, Jia S, He Z. Multi-factor impact mechanism on combustion efficiency of a hydrogen-fueled micro-cylindrical combustor. Int J Hydrogen Energy 2020;45(3):2319–30. https://doi.org/10.1016/j.ijhydene.2019.11.012.
[4] REN21. Renewables Now, Why is renewable energy important? URL:https://www.ren21.net/why-is-renewable-energy-important/.
[5] REN21, Renewables 2019 Global Status Report, Tech. rep., Paris; 2019.
[6] Li K, Bian H, Liu C, Zhang D, Yang Y. Comparison of geothermal with solar and wind power generation systems. Renew Sustain Energy Rev 2015;42:1464–74. https://doi.org/10.1016/j.rser.2014.10.049.
[7] Astrain D, Vián JG, Martínez A, Rodríguez A. Study of the influence of heat exchangers' thermal resistances on a thermoelectric generation system. Energy 2010;35(2):602–10. https://doi.org/10.1016/j.energy.2009.10.031.
[8] Elghool A, Basrawi F, Ibrahim TK, Habib K, Ibrahim H, Idris DMND. A review on heat sink for thermo-electric power generation: classifications and parameters affecting performance. Energy Conv Manage 2017;134:260–77. https://doi.org/10.1016/j.enconman.2016.12.046.
[9] Wang K, Liu J, Wu X. Downhole geothermal power generation in oil and gas wells. Geothermics 2018;76(October):141–8. https://doi.org/10.1016/j.geothermics.2018.07.005.
[10] Wang K, Wu X. Downhole thermoelectric generation in unconventional horizontal wells. Fuel 2019;254(March):115530 https://doi.org/10.1016/j.fuel.2019.05.113.
[11] Suter C, Jovanovic ZR, Steinfeld A. A 1kWe thermoelectric stack for geothermal power generation – modeling and geometrical optimization. Appl Energy 2012;99:379–85. https://doi.org/10.1016/j.apenergy.2012.05.033.
[12] Suter C, Jovanovic Z, Steinfeld A. A 1 kWel thermoelectric stack for geothermal power generation-Modeling and geometrical optimization. AIP Conf Proc 2012;1449:540–3. https://doi.org/10.1063/1.4731613.
[13] Liu C, Chen P, Li K, A 1 KW thermoelectric generator for low-temperature geothermal resources. In: Thirty-Ninth Workshop on Geothermal Reservoir Engineering, no. 2001; 2014. p. 1–12.
[14] Liu C, Chen P, Li K. Geothermal power generation using thermoelectric effect. GRC Trans 2013;37.
[15] Liu C, Chen P, Li K. A 500 W low-temperature thermoelectric generator: design and experimental study. Int J Hydrogen Energy 2014;39(28):15497–505. https://doi.org/10.1016/j.ijhydene.2014.07.163.
[16] Niu X, Yu J, Wang S. Experimental study on low-temperature waste heat thermoelectric generator. J Power Sources 2009;188(2):621–6. https://doi.org/10.1016/j.jpowsour.2008.12.067.
[17] Ahiska R, Mamur H. Design and implementation of a new portable thermoelectric generator for low geothermal temperatures. IET Renew Power Gen 2013;7(6):700–6. https://doi.org/10.1049/iet-rpg.2012.0320.
[18] Ahiska R, Mamur H. Development and application of a new power analysis system for testing of geothermal thermoelectric generators. Int J Green Energy 2016;13(7):672–81. https://doi.org/10.1080/15435075.2015.1017102.
[19] Banerjee A, Chakraborty T, Matsagar V. Evaluation of possibilities in geothermal energy extraction from oceanic crust using offshore wind turbine monopiles. Renew Sustain Energy Rev 2018;92(May):685–700. https://doi.org/10.1016/j.rser.2018.04.114.
[20] Catalan L, Aranguren P, Araiz M, Perez G, Astrain D. New opportunities for electricity generation in shallow hot dry rock fields: a study of thermoelectric generators with different heat exchangers. Energy Conv Manage 2019;200:112061https://doi.org/10.1016/j.enconman.2019.112061.
[21] Brown D. The enormous potential for hot dry rock geothermal energy. In: Mining the Earth's heat: hot dry rock geothermal energy. Springer-Verlag, Berlin Heidelberg; 2012, Ch. 2. arXiv:1107.2286, doi:10.1007/978-3-.
[22] Remeli MF, Tan L, Date A, Singh B, Akbarzadeh A. Simultaneous power generation and heat recovery using a heat pipe assisted thermoelectric generator system. Energy Conv Manage 2015;91:110–9. https://doi.org/10.1016/j.enconman.2014.12.001.
[23] Aranguren P, Astrain D, Rodriguez A, Martinez A. Net thermoelectric power generation improvement through heat transfer optimization. Appl Therm Eng 2017;120:496–505. https://doi.org/10.1016/j.applthermaleng.2017.04.022.
[24] Brito F, Goncalves L, Martins J, Antunes N, Sousa D. Thermoelectric exhaust heat recovery with heat pipe-based thermal control. J Electr Mater 2015.
[25] Pacheco N, Brito FP, Vieira R, Martins J, Barbosa H, Goncalves LM. Compact automotive thermoelectric generator with embedded heat pipes for thermal control. Energy 2020;197:117154 https://doi.org/10.1016/j.energy.2020.117154.
[26] Orr B, Akbarzadeh A, Mochizuki M, Singh R. A review of car waste heat recovery systems utilising thermoelectric generators and heat pipes. Appl Therm Eng 2016;101:490–5. https://doi.org/10.1016/j.applthermaleng.2015.10.081.
[27] Date A, Date A, Dixon C, Akbarzadeh A. Theoretical and experimental study on heat pipe cooled thermoelectric generators with water heating using concentrated solar thermal energy. Sol Energy 2014;105:656–68. https://doi.org/10.1016/j.solener.2014.04.016.
[28] Huang Y, Li W, Xu D, Wu Y. Spatiotemporal rule of heat transfer on a soil/finned tube interface. Sensors (Switzerland) 2019;19(5). https://doi.org/10.3390/s19051159.
[29] Huang Y, Xu D, Kan J, Li W. Study on field experiments of forest soil thermoelectric power generation devices. PLoS ONE 2019;14(8):1–13. https://doi.org/10.1371/journal.pone.0221019.
[30] Dell R, Unnthorsson R, Wei C, Sidebotham G, Jonsson M, Foley W, Ginzburg E, Paul S, Kim S, Morris A. Thermoelectric-based power generator for powering microcontroller based security camera. ASME international mechanical engineering congress and exposition. 2012. p. 635–42.
[31] Dell R, Wei CS, Petralia MT, Gislason G, Unnthorsson R. Thermoelectric powered security systems in iceland using a geothermal steam pipe as a heat source. Proceedings 2(8):2018;440. doi: 10.3390/ICEM18-05309. URL: http://www.mdpi.com/2504-3900/2/8/440.
[32] Diez-Gil J, Araña V, Ortiz R, Yuguero J. Stationary convection model for heat transfer by means of geothermal fluids in post eruptive systems. Geothermics 1987;16(1):77–89.
[33] Ziapour BM, Shaker H. Heat transfer characteristics of a two-phase closed thermosyphon using different working fluids. Heat Mass Transfer/Waerme- und Stoffuebertragung 2010;46(3):307–14. https://doi.org/10.1007/s00231-009-0570-1.
[34] Ebeling J-C, Kabelac S, Luckmann S, Kruse H. Simulation and experimental validation of a 400 m vertical CO2 heat pipe for geothermal application; 2016. p. 218–25.
[35] Elghool A, Basrawi F, Ibrahim H, Ibrahim TK, Ishak M, Yusof TM, Bagaber SA. Enhancing the performance of a thermo-electric generator through multi-objective optimisation of heat pipes-heat sink under natural convection. Energy Conv Manage 2020;209(February):112626 https://doi.org/10.1016/j.enconman.2020.112626.
[36] Fraisse G, Ramousse J, Sgorlon D, Goupil C. Comparison of different modeling approaches for thermoelectric elements. Energy Conv Manage 2013;65:351–6. https://doi.org/10.1016/j.enconman.2012.08.022.
[37] Rodríguez A, Vián JG, Astrain D, Martinez A. Computational model and test bench for thermoelectric power generation, for thermoelectric parameters dependent. Proceedings on the temperature, International Conference on Thermoelectrics, ICT 2006. p. 300–4. https://doi.org/10.1109/ICT.2006.331374.
[38] Aranguren P, Araiz M, Astrain D, Martínez A. Thermoelectric generators for waste heat harvesting: a computational and experimental approach. Energy Conv Manage 2017;148:680–91. https://doi.org/10.1016/j.enconman.2017.06.040.
[39] Araiz M, Martínez A, Astrain D, Aranguren P. Experimental and computational study on thermoelectric generators using thermosyphons with phase change as heat exchangers. Energy Conv Manage 2017;137:155–64. https://doi.org/10.1016/j.enconman.2017.01.046.
[40] Araiz M, Casi Á, Catalán L, Martínez Á, Astrain D. Prospects of waste-heat recovery

from a real industry using thermoelectric generators: Economic and power output analysis. Energy Conv Manage 2019;205(November 2019):112376https://doi.org/10.1016/j.enconman.2019.112376.
[41] Brito FP, Martins J, Goncalves LM, Sousa R. Modelling of thermoelectric generator with heat pipe assist for range extender application. IECON proceedings (Industrial electronics conference) 2011:4589–95. https://doi.org/10.1109/IECON.2011.6120066.
[42] Brito FP, Alves A, Pires JM, Martins LB, Martins J, Oliveira J, Teixeira J, et al. Analysis of a temperature-controlled exhaust thermoelectric generator during a driving cycle. J Electr Mater 2016;45(3):1846–70. https://doi.org/10.1007/s11664-015-4258-7.
[43] Chapman AJ. Fundamentals of heat transfer. New York: Macmillan Publishing Company; 1987.
[44] Incropera FP, Witt DPD. Fundamentals of heat transfer. 4th ed., Prentice Hall.
[45] Forster H, Zuber N. Dynamics of vapour bubbles and boiling heat transfer. Am Inst Chem Eng J 1955;1:531–5.
[46] Rohsenow W, Hartnett J, Cho Y. Handbook of heat transfer. 3rd ed. McGraw-Hill Handbooks; 1998.
[47] Lee S, Song S, Au V, Moran KP. Constriction/spreading resistance model for electronics packaging. In: 4th ASME/JSME thermal engineering conference, vol. 4; 1995. p. 199–206. URL:http://www.digikey.it/WebExport/SupplierContent/Aavid_59/PDF/Aavid_ConstrictionModel.pdf.
[48] Lemmon EW, Bell IH, Huber, ML, McLinden MO. NIST Standard Reference Database 23: Reference Fluid Thermodynamic and Transport Properties-REFPROP, Version 10.0, National Institute of Standards and Technology (2018). doi:10.18434/T4JS3C. URL:https://www.nist.gov/srd/refprop.
[49] Filippov L, Novoselova N. Vestnik Moscov. Univ Gas 1955;10.
[50] Gambill W. Chem. Eng 66(151):1959.
[51] Graham T. On the motion of gases. Philos Trans 1846;136:573–631.
[52] Shah MM. An improved and extended general correlation for heat transfer during condensation, Hvac&R Research 15(September 2009):2009;37–41. doi: 10.1080/10789669.2009.10390871.
[53] Hoke JL, Clausing AM, Swofford TD. An experimental investigation of convective heat transfer from wire-on-tube heat exchangers. J Heat Transfer 1997;119(2):348–56. https://doi.org/10.1115/1.2824231.
[54] Araiz M, Catalan L, Herrero O, Perez G, Rodriguez A. Bringing thermoelectricity into reality. IntechOpen 2018. https://doi.org/10.5772/intechopen.71354. URL:https://www.intechopen.com/books/bringing-thermoelectricity-into-reality/the-importance-of-the-assembly-in-thermoelectric-generators.
[55] Rodríguez A, Pérez-Artieda G, Beisti I, Astrain D, Martínez A. Influence of temperature and aging on the thermal contact resistance in thermoelectric devices. J Electr Mater 2020. https://doi.org/10.1007/s11664-020-08015-y.
[56] Gorse C, Johnston D, Pritchard M. A dictionary of construction. Surveying and Civil Engineering, Oxford University Press; 2012.
[57] II-VI Marlow, Technical Data Sheet for TG12-8. URL:https://cdn2.hubspot.net/hubfs/547732/Data_Sheets/TG12-8.pdf.
[58] Coleman H, Steele W. Experimentation, validation and uncertainty. Analysis for Engineers, 3rd ed., Wiley.
[59] Instituto Geológico Minero Español, Evaluación del potencial geotérmico superficial de Montañas de Fuego como Sistema de Roca Caliente Seca, Tech. rep.; 1992.
[60] Gomez-Ortiz D, Blanco-Montenegro I, Arnoso J, Martin-Crespo T, Solla M, Montesinos FG, et al. Imaging thermal anomalies in hot dry rock geothermal systems from near-surface geophysical modelling. Remote Sens 2019;11:(6). https://doi.org/10.3390/rs11060675.
[61] Instituto para la Diversificación y Ahorro de Energía (IDAE), Guía técnica. Condiciones climáticas exteriores de proyecto., 2010. URL:http://www.idae.es/uploads/documentos/documentos_12_Guia_tecnica_condiciones_climaticas_exteriores_de_proyecto_e4e5b769.pdf.
[62] Meteoblue, Clima lanzarote. URL:https://www.meteoblue.com/es/tiempo/historyclimate/climatemodelled/lanzarote_espana_2515699.

Chapter 4

Design, Construction and Characterization of a Geothermal Thermoelectric Generator for Timanfaya National Park

Chapter 3 has studied the influence of different parameters in a geothermal thermoelectric generator with a two phase closed thermosyphon as hot side heat exchanger and loop thermosyphons as cold side ones. Based on those results, this chapter takes a step forward, addressing the construction and characterization of real devices.

As derived from the state of the art, most of the existing geothermal thermoelectric generators limit their study to a computational model, and occasionally, also include a prototype at the laboratory. The field installation of medium–scale geothermal thermoelectric generators cannot be found in the literature. Field experiments are of great interest for the development of this technology since they permit testing the behavior of these complex systems under real conditions. Nonetheless, previous to their installation, the design process needs to take into account several aspects that influence the installation and operation on field. This chapter considers such requisites with the objective of developing and characterizing a real thermoelectric generator to be installed on field.

For this purpose, Section 4.1 explains the previous considerations that apply for Timanfaya National Park, Section 4.2 describes the developed design according to the previous aspects, and Section 4.3 deals with the construction and characterization of the device. Finally, Section 4.4 summarizes the main conclusions obtained.

4.1 Previous Considerations

As exposed in the introduction, the geothermal anomalies of Timanfaya National Park have been studied since the 1980s. As a result of these studies, there exist a series of boreholes such as the one depicted in Figure 4.1 with diameters between 50 and 305 mm, and depths ranging from 29 to 71 m.

Figure 4.1: Borehole located at Timanfaya National Park.

As a first approximation to the installation of real prototypes at Timanfaya National Park, in this chapter the area of *Casa de los Camelleros* has been selected due to the lower temperatures available, which lead to a smaller internal pressure in the hot side heat exchanger and permit using a wider variety of materials. Figure 4.2 shows again the temperature of the geothermal gases with respect to the depth for the boreholes located at *Casa de los Camelleros*. As can be observed, in the boreholes S–1, S–2 and S–3, the temperature of the gases increases linearly during the first meters. In contrast, in borehole S–4, the temperature remains practically constant down to 12 m. Apart from presenting a different behavior, this last borehole also presents a higher temperature. Therefore, it will be the one taken as reference for the design of the generator. The dimensions of this borehole are 305 mm of diameter and a depth of 31 m, of which 7 are intubated.

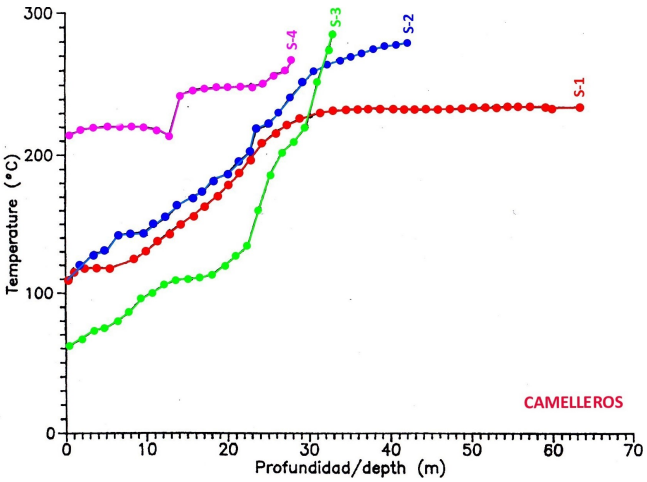

Figure 4.2: Temperature of the geothermal gases with respect to the depth for the boreholes located at *Casa de los Camelleros*. *Reprinted with the permission of [IGME1992].*

Drilling the boreholes is a quite complicated and expensive task. Therefore, the design of the generators should try to maximize the power generation per borehole. As derived from the previous chapter, for this purpose it is of utmost importance to develop heat exchangers with low thermal resistances. According to the heat transfer equations, bigger areas lead to lower thermal resistances. Nonetheless, larger heat exchangers entail a higher weight and cost.

In order to obtain low thermal resistances while maintaining the compactness of the heat exchangers, auxiliary equipment, such as fans and pumps, are commonly used. Nevertheless, as has been emphasized throughout the present Ph. D. dissertation, these components consume energy, decreasing net generation, and besides introduce moving parts in the whole system, forfeiting one of the main advantages of thermoelectric modules. Moreover, this auxiliary equipment also provokes noise. Taking into account that the thermoelectric generator to be designed and constructed in this chapter is going to be installed in a natural reserve, it is necessary to obtain a completely noiseless device without moving elements so that it does not pose a risk to the wildlife nor the several tourists that visit the park each year. Hence, the thermoelectric generator to be developed will include completely passive heat exchangers. Nonetheless, despite being passive, they will benefit from the windy climate characteristic of Lanzarote island and the considerable velocity of the gases that ascend from the boreholes, which are considered of such magnitude that equate forced convection conditions naturally. Additionally, another restriction that exists as a consequence of the installation of the device in a natural reserve is that only innocuous working fluids can be used, so that if a leak occurs, no environmental damage is caused.

4.2 Design of a GTEG for *Casa de los Camelleros*

Based on the previous requirements, this section proceeds with the design of a complete thermoelectric generator for *Casa de los Camelleros*, taking into account all the elements necessary to make it a reality: hot side heat exchangers, cold side heat exchangers, and the assembly between the different components. In the design, it will be important to commit to the simplicity of assembly and construction.

The thermoelectric generator studied in Chapter 3 for *Casa de los Camelleros* was composed of a cylindrical two phase closed thermosyphon with fins in the evaporator part as hot side heat exchanger. In the upper part of this tube, the thermoelectric modules, each one with its own loop thermosyphon as cold side heat exchanger, were assembled placing two per level. Figure 4.3 depicts the 3D rendering of seven generators like that inserted in the borehole under consideration in this chapter. As can be observed, the two phase closed thermosyphon requires curving so that the cold side loop thermosyphons do not touch with each other, while a pipe needs to be installed to divert the geothermal gases without influencing the thermoelectric modules nor the cold side heat exchangers.

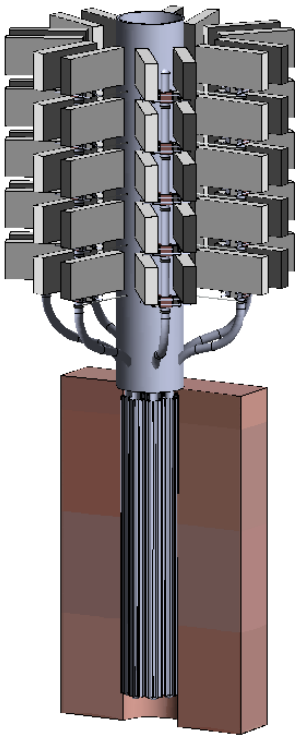

Figure 4.3: 3D rendering of seven thermoelectric generators with a two phase closed thermosyphon as hot side heat exchanger and loop thermosyphons as cold side ones.

Although the former design is completely scalable, one of the main limitations detected is that, due to the size of the cold side heat exchangers, an increase in the number of thermoelectric modules entails a considerable rise of the overground height, specifically, 250 mm in the case of the 6 levels loop thermosyphon and 365 mm in the case of the 8 levels one. Taking into account the results obtained in the previous chapter, even with the shortest inserted length of the two phase closed thermosyphon studied, at least 10 thermoelectric modules are required, which implies a minimum height of 1.25 m, to which is necessary to add the curved part of the tube. Since the objective is to generate as much as possible, the final design would require an excessive height and therefore, the visual impact would be elevated, its installation would be complicated, and very tough moorings would be needed to resist the wind impact. Consequently, it is preferred to look for other geometries of phase change heat exchangers for the cold side.

In the application under consideration, the cold side heat exchangers are responsible for releasing the heat not transformed into electricity by the thermoelectric modules into the environment, and need to do it passively while being as compact as possible. The phase change heat exchangers available commercially do not meet these requirements, since they focus on their operation in conjunction with a fan. Therefore, the present Ph. D. dissertation has opted for designing and manufacturing its own heat exchangers. Figure 4.4 depicts the design of the cold side heat exchanger developed in this chapter, which is composed of four heat pipe tubes inserted by pressure in holes drilled in the base of a fin dissipator, leading a supplementary system for heat dissipation, and additional aluminum fins inserted in the condensation area of the tubes. Thanks to the insertion of the round tubes inside the base of the dissipator, a good thermal contact with the planar thermoelectric generators is ensured, better than the alternative of introducing the pipes in semicircular channels and pressing them afterwards, which lead to a surface finish with noticeable irregularities [Catalan2020]. For compactness, the heat pipe tubes have been placed horizontally and subsequently bent, permitting a separation of only 60 mm between two consecutive levels as shown in Figure 4.5. More details about the assembly, the dimensions, and the characterization of this heat exchanger are described in Subsection 4.3.1.

In Figure 4.5, it can also be observed the assembly between the different components of the generator. This aspect has great importance and can negatively affect generation. According to Araiz el al., it is recommended to tighten the thermoelectric modules individually, ensuring a good pressure distribution [Araiz2018]. Therefore, in order to fulfill that premise, in each level a pair of cold side heat exchangers have been tightened against each other with four screws, comprising between them the hot side two phase closed ther-

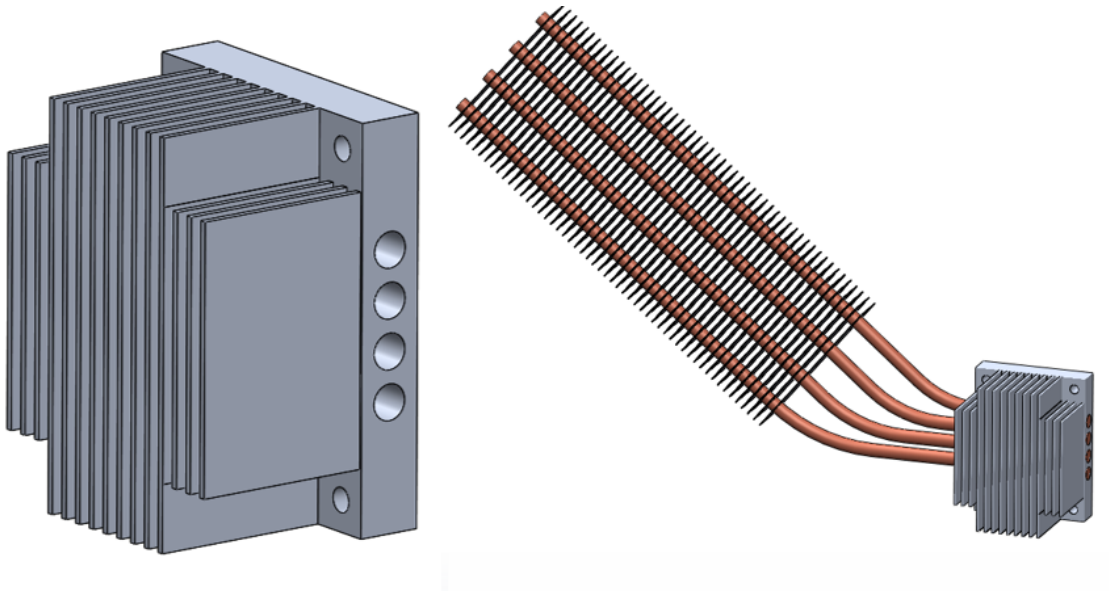

Figure 4.4: Cold side heat exchanger developed for this application, composed of a fin dissipator and four heat pipes.

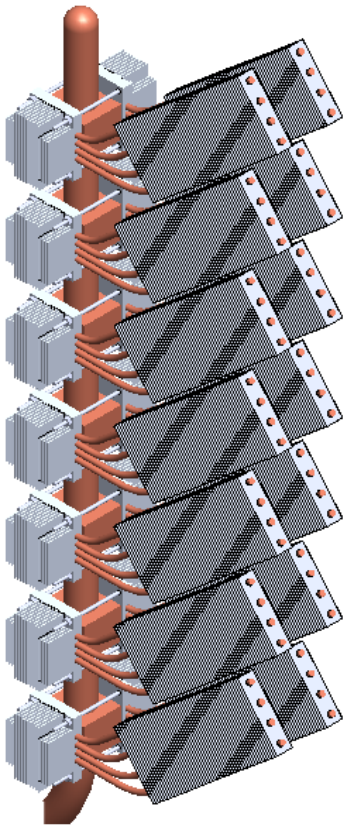

Figure 4.5: Overground part of a thermoelectric generator with the more compact heat exchangers developed in the present Ph. D. dissertation.

mosyphon and the thermoelectric modules. Due to the round shape of this hot side heat exchanger, it has also been necessary to insert a copper block that ensures a planar surface in contact with the thermoelectric modules. Copper is a highly conductive material, but also presents a high density. Hence, the dimensions of the block will need to be in concordance with the size of the thermoelectric modules to avoid an increase of the weight, while permitting a tight assembly with the hot side two phase closed thermosyphon. More details about its geometry and dimensions are described in Subsection 4.3.3.

4.3 Construction and Characterization of the Designed Prototype

Thanks to the previous design, the requirements of compactness, easiness of construction and assembly, and absence of moving parts, noise, and auxiliary equipment are satisfied. Hence, this section deals with the real construction and the characterization of the designed generator, detailing the followed procedure. More specifically, two prototypes will be built and studied, one with 10 thermoelectric modules, and another one with 6.

4.3.1 Cold Side Heat Exchanger

Figure 4.6 shows the constructed cold side heat exchanger, formed of four 500 mm long sintered heat pipes with a diameter of 8 mm inserted in a 70 x 90 mm^2 fin dissipator with a base 14.5 mm thick and fifteen 40 x 1.5 mm^2 corrugated fins. In order to ensure a good thermal contact between the heat pipes and the dissipator, the construction methodology was performed as follows: firstly, four holes with a diameter slightly smaller than that of the tubes were drilled with a reamer in the base of the fin dissipator with a separation of 3 mm; afterwards, the dissipator was heated up so that it expanded; meanwhile, the heat pipes were cooled down so that they contracted; once the expansion and contraction were considered enough, the heat pipes were inserted by pressure in the holes and the whole assembly was cooled down. When the assembly got cold, the heat pipes could not be taken out, which indicates a good thermal contact.

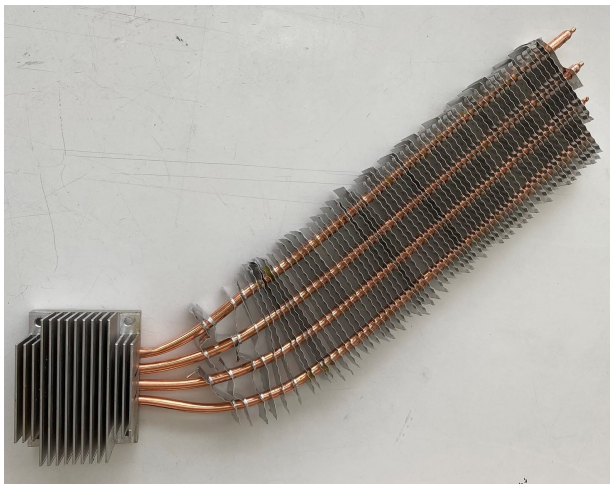

Figure 4.6: Cold side heat exchanger constructed to release heat from the thermoelectric modules. It is composed of four heat pipes inserted in the base of a fin dissipator.

The next step consisted in bending the heat pipes with the desired curvature and adding commercial aluminum 104 x 27.5 x 0.3 mm^3 fins with a separation of 5 mm, trying to cover the longer length of the tubes as possible. Nonetheless, since one of the main uncertainties of the design was the influence of having a horizontal section in the pipes, the thermal resistance of this cold side heat exchanger was characterized for different heat fluxes during the assembly procedure, before adding the fins. Figure 4.7 shows the 4 configurations studied: completely vertical, completely horizontal, with bent tubes, and the final configuration with bent tubes and fins.

The methodology followed to determine the thermal resistance of each case is similar to the one followed in Chapter 2 and it is summarized in the schematics of Figure 4.8. Hence, cartridge heaters supplied the heat flux of each experiment by Joule effect. Rockwool insulation was added around these heaters so that heat flowed through the heat exchanger. The temperature at the base of the heat exchanger T_{ev} and in the climatic chamber T_{amb} were measured, based on which the thermal resistance was calculated according to Equation 4.1,

$$R_{CHE} = \frac{T_{ev} - T_{amb}}{\dot{Q}} = \frac{T_{ev} - T_{amb}}{V \cdot I - \dot{Q}_{losses}} \tag{4.1}$$

where the heat flux $\dot{Q}$ is indeed calculated as the subtraction between the heat provided by the heat source $(V \cdot I)$ and the heat flux that is dissipated in the insulating material $\dot{Q}_{losses}$. These thermal losses are obtained as detailed in Equation 4.2, thanks to the temperature difference between the external part of the insulation (T_{ins}) and the ambient (T_{amb}), the insulation area (A_{ins}), and a convection coefficient h derived from Equation 4.3 [Parmelee1947].

$$\dot{Q}_{losses} = h \cdot A_{ins} \cdot (T_{ins} - T_{amb}) \tag{4.2}$$

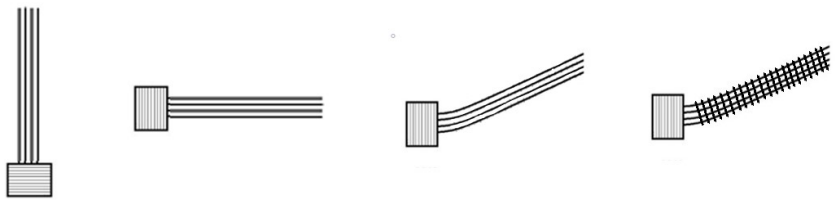

Figure 4.7: Configurations for which the thermal resistance of the developed cold side heat exchanger has been characterized.

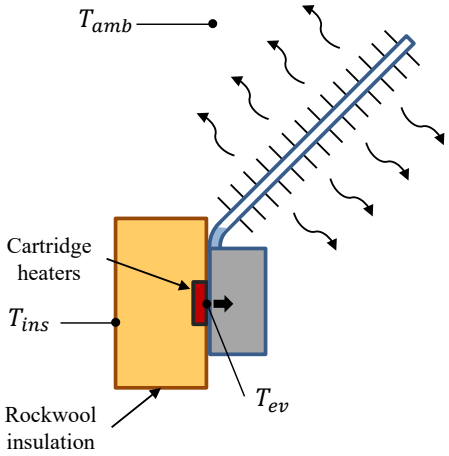

Figure 4.8: Schematics of the test to determine the thermal resistance of the cold side heat exchangers.

$$Nu_L = 0.664 \cdot Pr^{1/3} \cdot Re_L^{1/2} \qquad \begin{bmatrix} 0.6 \leq Pr \leq 50 \\ Re < Re_{x,c} \approx 5 \cdot 10^5 \end{bmatrix} \tag{4.3}$$

The obtained results are shown in Figure 4.9, exhibiting the characteristic decrease of thermal resistance with increasing heat fluxes of phase change heat exchangers. As can be observed, the highest thermal resistances are achieved when the tubes are completely horizontal, presenting values of 1.08 K/W with a heat flux of 20 W that decrease to 0.91 K/W with 100 W. If the heat pipes are bent, the thermal resistance of the heat exchanger improves, leading to values similar to those obtained with the vertical configuration and that suppose a reduction of 12.4 % on average with respect the completely horizontal case. Hence, having a horizontal section in the pipes, bending the rest, barely affects its behavior.

The configuration in which the heat exchanger will work, i.e. bent and with fins, presents values that decrease from 0.42 K/W with a heat flux of 20 W to 0.4 K/W with 140 W. Although these values are slightly higher than the ones obtained with the loop thermosyphons used in Chapters 2 and 3, the developed configuration is more compact, permitting the addition of more thermoelectric modules per unit of length of the hot side heat exchanger, leading to a lower visual impact, and easing the assembly and installation on field.

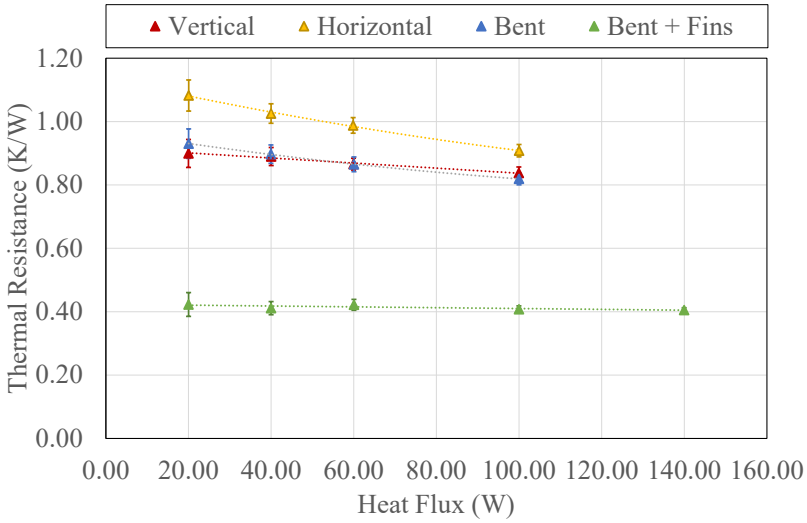

Figure 4.9: Thermal resistance with respect to different heat fluxes for the four studied configurations.

4.3.2 Hot Side Heat Exchanger

The designed hot side heat exchanger is also based on phase change, but in the configuration known as two phase closed thermosyphon, which basically consists of a closed tube with a fluid in its interior. In this case, a copper tube with a diameter of 41.27 mm, a thickness of 1.25 mm and water as working fluid has been used. As exposed at the beginning of this section, only two prototypes will be built. Therefore, for simplicity, the bending curve of the design developed in Section 4.2 will not be performed.

The two constructed prototypes are similar except for the number of thermoelectric modules installed. Hence, the inserted length of both heat exchangers is 2 m, out of which a quarter is filled with distilled water. The exterior length varies with the number of modules, with a height of 1 m in the case of the prototype with 10 modules and 600 mm the one with only 6.

Copper was chosen as the material because apart from its good thermal properties, it is malleable and easy to solder. Moreover, copper components are widely available because of their use in the cooling sector. Therefore, the construction of each two phase closed thermosyphon has been simply based on a commercial copper tube, two lids, and an obus valve.

In the operation of this type of heat exchanger, it is important to guarantee that only water is inside. Thus, in the filling process, it is necessary to remove all the air inside. For this purpose, an amount of water slightly higher than required was introduced and the valve

was closed. The device was heated up so that the interior water increased its temperature and consequently its pressure. Since this pressure was higher than the atmospheric one, when the valve was opened, the vapor went out sweeping along the air inside the tube.

In Chapter 3 the importance of including fins in the hot side heat exchanger of *Casa de los Camelleros* to improve the heat transfer with the geothermal gases was highlighted. One possibility to add these fins simply consists in soldering them to the tube. Nevertheless, due to the thin thickness of the tube, there exists the risk of leaking. As shown in Figure 4.10, the chosen option is based on a extruded aluminum profile with 31 fins 17 mm high and 2 mm thick. This solution permits a higher number of fins and it is easier to assemble to the thermosyphon since the profile is open and some space has been left for its tightening, so that a good thermal contact is ensured.

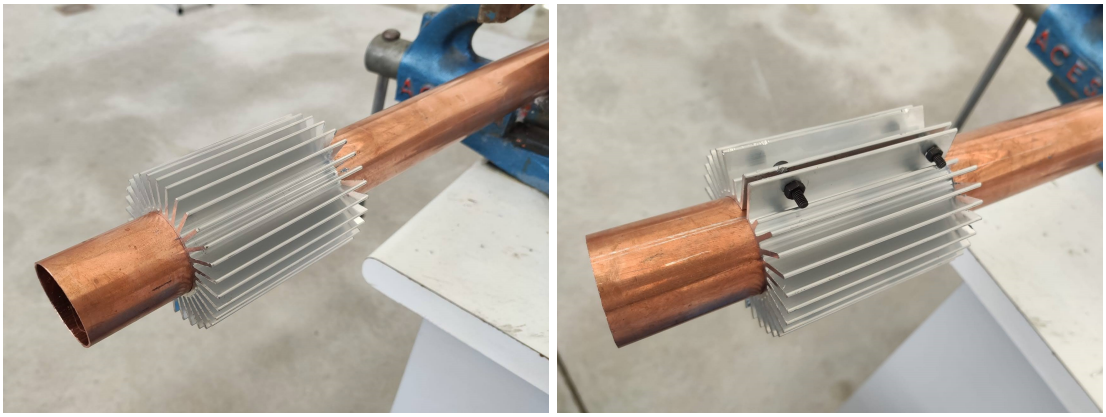

Figure 4.10: Detail of the fin profile to be attached to the hot side copper tube, showing also the assembly procedure.

Similarly to the cold side heat exchanger, the hot side one has also been tested at the laboratory to analyze its performance, although without the fin profile. Hence, as shown in Figure 4.11, rope heaters have been coiled around the inserted length of the two phase closed thermosyphon, and covered with rockwool as insulation. The temperature has been measured at two different heights in the liquid (T_{liq1} and T_{liq2}) and in the vapor (T_{vap1} and T_{vap2}), as well as in the overground area at the position in which the thermoelectric modules will be installed considering the prototype composed of 10 thermoelectric modules, this is 5 levels (T_{L1}, T_{L2}, T_{L3}, T_{L4} and T_{L5}).

Figure 4.12 depicts the results obtained for five different temperatures of the heat source. As can be observed, the temperature suffers a slight decrease with the increase of height that presents a linear tendency with a similar slope regardless of the heat source temperature. Nonetheless, the temperature loss between the evaporator and the highest level is of just 14 °C on average, 50 % less than those obtained in Chapter 2.

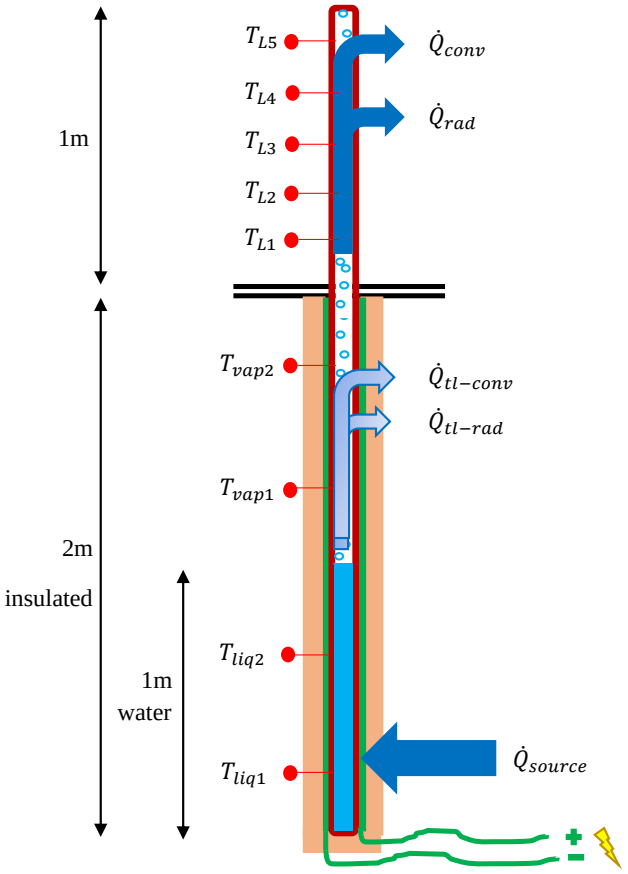

Figure 4.11: Schematics for the individual characterization of the hot side heat exchanger.

Apart from the temperature distribution, it is also interesting to determine the thermal resistance of the hot side heat exchanger. Equation 4.4 shows the expression necessary for its calculation. In this equation, since the temperature at each height varies, average temperatures will be considered both at the liquid section T_{liq} (average of T_{liq1} and T_{liq2}) and in the overground part of the tube T_{tube} (average of T_{L1}, T_{L2}, T_{L3}, T_{L4} and T_{L5}).

$$R_{HHE} = \frac{T_{liq} - T_{tube}}{\dot{Q}} \tag{4.4}$$

Regarding the heat flux $\dot{Q}$, the heat flux that goes through the prototype needs to be considered. According to Equation 4.5, this heat equals the heat supplied by the heat source $(V \cdot I)$ minus the thermal losses $\dot{Q}_{losses}$ that occur both by convection $\dot{Q}_{tl-conv}$ and by radiation $\dot{Q}_{tl-rad}$. In turn, the heat that goes through the prototype also equals the

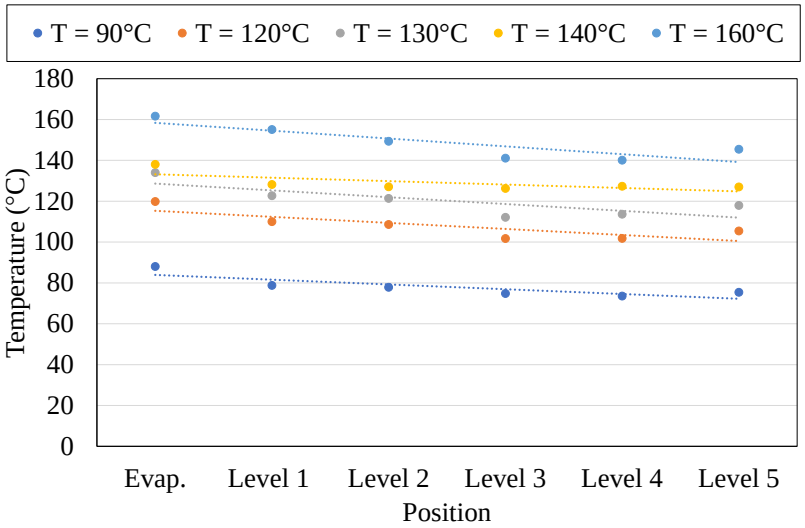

Figure 4.12: Temperature distribution in 5 different levels for five temperatures of the heat source.

heat dissipated by convection and by radiation in the upper part of the tube, $\dot{Q}_{conv}$ and $\dot{Q}_{rad}$ respectively.

$$\dot{Q} = V \cdot I - \dot{Q}_{losses} = V \cdot I - \dot{Q}_{tl-conv} - \dot{Q}_{tl-rad} = \dot{Q}_{conv} + \dot{Q}_{rad} \tag{4.5}$$

Equation 4.6 depicts the calculation of the convective heat, either the dissipated in the upper part or the one associated with the thermal losses, where h_{conv} is the convective heat transfer coefficient, A is the external area, T_{ext} is the surface temperature of the tube or the insulating material, and T_{amb} is the ambient temperature.

$$\dot{Q}_{conv} = h_{conv} \cdot A \cdot (T_{ext} - T_{amb}) \tag{4.6}$$

The convective heat transfer coefficient h_{conv} considers both natural and forced conditions, weighted by the parameter φ, as shown in Equation 4.7, in which k is the thermal conductivity of air, L_c is the characteristic length of the considered part, and $Nu_{natural}$ and Nu_{forced} are the Nusselt numbers calculated with the correlations detailed in Equations 4.8 and 4.9 [Bejan2003, Rohsenow1998, Dincer2018], which in turn depend on Grashof Gr, Prandtl Pr, and Reynolds Re numbers, as well as on the length L, the external diameter

D, and the constants C, n and s that vary depending on Reynolds and Prandtl numbers.

$$h_{conv} = \varphi \cdot h_{natural} + (1-\varphi) \cdot h_{forced} = \varphi \cdot \frac{Nu_{natural} \cdot k}{L_c} + (1-\varphi) \cdot \frac{Nu_{forced} \cdot k}{L_c} \quad (4.7)$$

$$Nu_{natural} = \frac{4}{3} \cdot \left[\frac{7 \cdot Gr \cdot Pr^2}{5 \cdot (20 + 21 \cdot Pr)} \right]^{1/4} + \frac{4 \cdot (272 + 315 \cdot Pr) \cdot L}{35 \cdot (64 + 63 \cdot Pr) \cdot D} \quad (4.8)$$

$$Nu_{forced} = C \cdot Re^n \cdot Pr^s \cdot \left(\frac{Pr_\infty}{Pr_{sup}} \right)^{1/4} \quad (4.9)$$

On its behalf, the heat dissipated by radiation, either in the upper part or the one associated with the thermal losses, is calculated with the corrected equation of Stefan–Boltzmann for a non–black body (Equation 4.10), where ϵ is the emissivity of the surface, σ is the Stefan–Boltzmann constant that equals 5.67 x 10^{-8} W/m$^2 \cdot$ K^4, and similarly than before, A is the external area, T_{ext} is the surface temperature of the tube or the insulating material, and T_{amb} is the ambient temperature.

$$\dot{Q}_{rad} = \epsilon \cdot \sigma \cdot A \cdot (T_{ext}^4 - T_{amb}^4) \quad (4.10)$$

For the considered geometry, Table 4.1 summarizes the parameters used in the calculation of the former equations both for the heat dissipated in the upper part, and the one lost to the environment. In the determination of these parameters it has been taken into account that the upper part is more exposed to the conditions of the laboratory, being more affected by forced convection, while the lower part is protected due to the structure used for holding the thermosyphon during the experiments. Moreover, their materials are also different: pure copper in the upper part and rockwool in the lower one, where the thermal losses occur, and therefore present a different emissivity.

Once calculated the actual heat flux that goes through the hot side heat exchanger, its thermal resistance has been calculated, leading to the results depicted in Figure 4.13. As can be observed, this heat exchanger also follows the characteristic decrease of thermal resistance of the heat exchangers based on phase change when the heat flux increases, diminishing from a thermal resistance of 0.16 K/W with 68 W to 0.07 K/W with 157 W. In comparison with the two phase closed thermosyphon developed in Chapter 2, the obtained values are more than 75 % lower than before for similar heat fluxes. The main differences

Table 4.1: Summary of the parameters used in the calculation of the heat fluxes, either the heat dissipated in the upper part or the one corresponding to thermal losses.

Upper part		Thermal losses		Constants	
ϵ	0.02	ϵ	0.75	C	0.26
φ	0.3	φ	0.8	n	0.6
v (m/s)	0.4	v (m/s)	0.3	s	0.37
L (m)	1	L (m)	2		
D (m)	0.048	D (m)	0.11		

between the new and the previous thermosyphons are the shape, being initially squared and round now; the length, which has been tripled; the thickness, which has been reduced 75 %; the condensation area, which has been increased; and the material, substituting the initial stainless steel by copper. Neglecting the length that does not have a significant influence in phase change heat exchangers, the other four changes have favorably contributed to the reduction of the thermal resistance of this heat exchanger. Thus, the round shape permits a reduction of the thickness due to its better resistance of the internal pressures. This fact added to the better thermal conductivity of copper in comparison with stainless steel and the increased condensation area reduces the conductive and condensation components of the thermal resistance of this thermosyphon, leading to a decrease in its total thermal resistance.

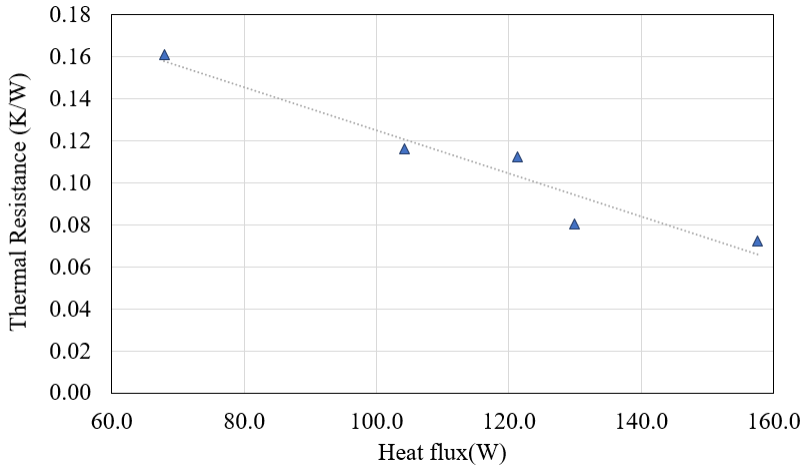

Figure 4.13: Thermal resistance of the hot side biphasic thermosyphon for different heat fluxes.

4.3.3 Copper Block

Since the hot side heat exchanger is round and the thermoelectric modules are planar, it is necessary to add an intermediate piece that ensures a good thermal contact between them. Figure 4.14 shows the copper block designed for this purpose. Its dimensions are 70 x 50 x 60 mm^3. The tightening of this piece is performed by six screws located parallel to the heat flux direction that besides ensuring a good thermal contact, guarantee an adequate grabbing to the hot side heat exchanger, so that it does not fall down.

Figure 4.14: Copper block used to ensure a good thermal contact between the round hot side two phase closed thermosyphon and the planar thermoelectric modules.

4.3.4 Moorings

Apart from the individual components of the generator, it is also important to design a resistant mooring that holds the prototypes in the correct position with respect to ground level and that is capable of resisting the momentum exerted by the wind. The design of this piece is also important to facilitate the installation on field, and to guarantee that the geothermal gases are diverted, not affecting the operation of the thermoelectric modules nor the cold side heat exchangers.

Figure 4.15 depicts the piece designed to be screwed up to the flange located at the borehole. It has been divided into two parts to facilitate installation. Thus, first, the upper half is installed, permitting the individual insertion of the two prototypes in the borehole and their tightening. Figure 4.16 details the piece responsible for holding the prototype to this base. As can be observed, it is based on a block similar to the one described in Subsection 4.3.3, but made of steel due to its better mechanical capabilities. This piece is first tightened to the two phase closed thermosyphon and afterwards fixed to the base. Once fixed, the deflector is placed and tightened.

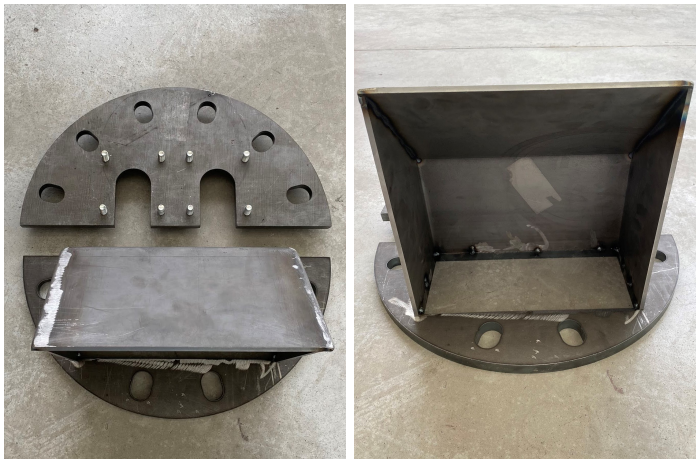

Figure 4.15: Support for holding the two developed prototypes (left) and detail of the deflector of geothermal gases.

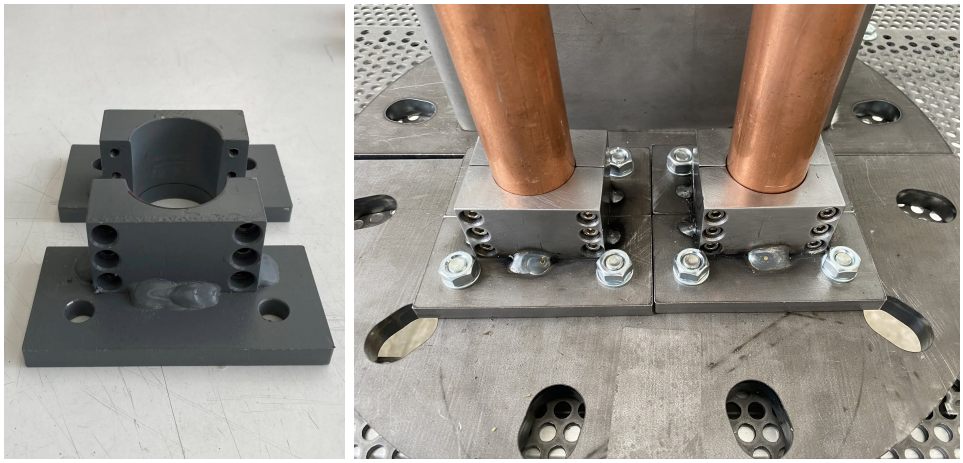

Figure 4.16: Detail of the steel piece responsible for holding the prototype, and detail of its assembly with the support and the hot side two phase loop thermosyphons.

4.3.5 Whole Assembly

Once described all the elements that compose the generator and after checking the good performance of the heat exchangers, it is the turn of assembling the whole devices. Figure 4.17 depicts this whole assembly installed in an structure built at the laboratory that simulates the borehole. In order to resemble the geothermal heat at the laboratory, rope heaters have been coiled around the inserted length of the two phase closed thermosyphon, and covered first with rockwool and afterwards with neoprene as insulation. With a similar purpose of avoiding thermal losses, the upper part of the hot side heat exchanger has been

also insulated to ensure that condensation occurs on the thermoelectric modules. This insulation has been performed with rockwool and covered with aluminum waterproofing tape. Other details that can be observed in the figure are the obus valve at the top of the two phase closed thermosyphon, a box for all the electronics systems necessary for the characterization of the device prior to its installation on field, and finally a meteorological station that will also be installed.

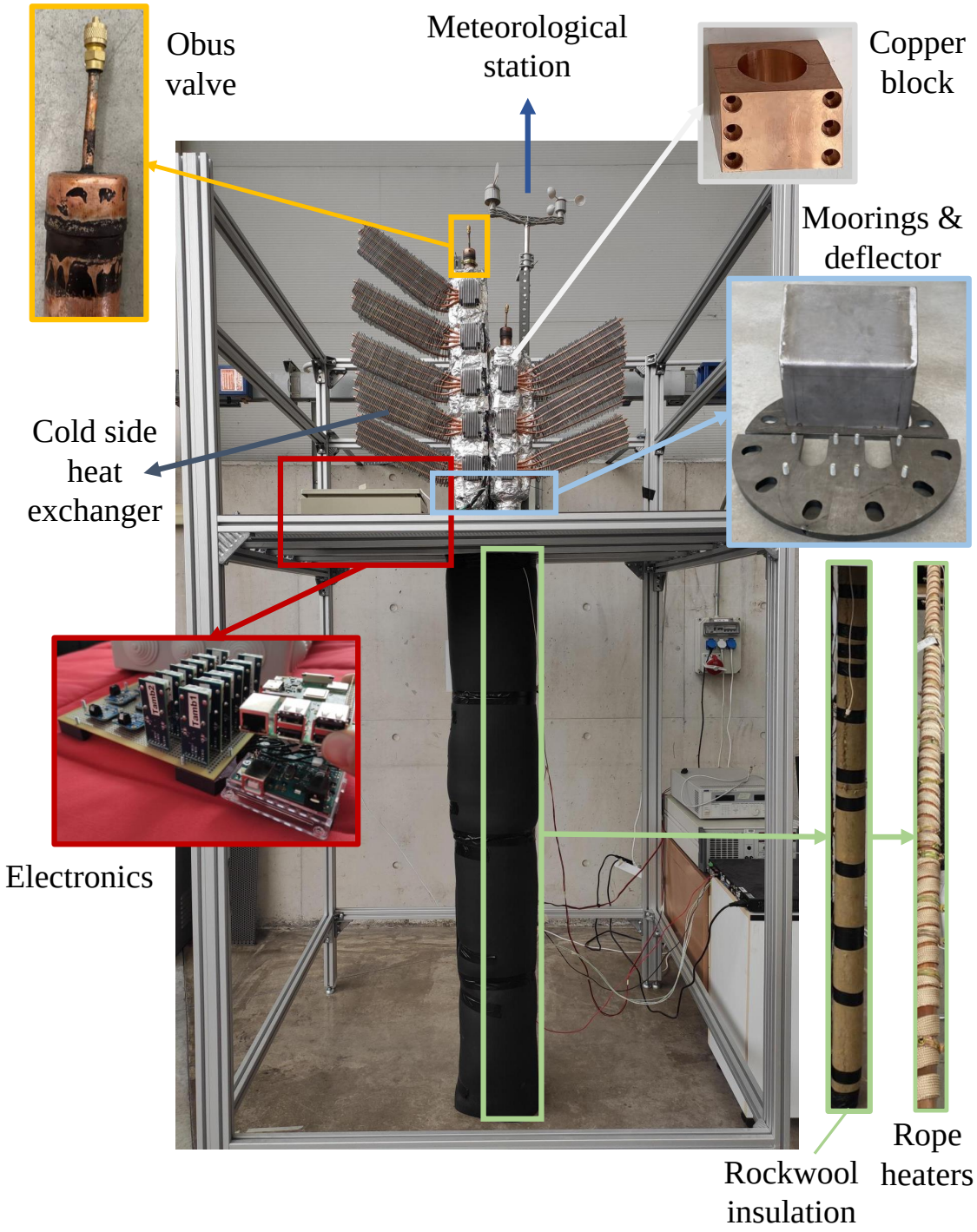

Figure 4.17: Whole assembly of the two prototypes of geothermal thermoelectric built for *Casa de los Camelleros*, detailing some of their components.

4.3.6 Characterization of the Whole Geothermal Thermoelectric Generator

Based on the previous assembly, this subsection deals with the characterization of the whole geothermal thermoelectric generators at the laboratory. More specifically, it focuses on the study of their generation capabilities for different operating conditions. In order to differentiate the two generators, from now on, the prototype with 10 thermoelectric modules is denoted Prototype A, while the 6 modules' one, Prototype B.

Figure 4.18 shows the installed sensors in order to perform the previous study. Thus, 8 power P measurements (by sensing voltage V and current intensity I) and 20 temperature readings have been performed by means of Adafruit INA210 breakout boards at each level [Adafruit2020], where there are two thermoelectric modules connected in series. On their behalf, temperatures have been sensed with Maxim Integrated MAX31855PMB1 peripheral modules with type K thermocouples at those points that were considered of interest [Maxim2020]. Hence, in each device, the temperature of the external part of the tube has been measured at different heights, two in the section that intends to be inserted underground, one in the liquid part T_{liq} and the other in the vapor T_{vap} one; and another two overground, close to the first T_{tube1} and last T_{tube2} levels. At this first and last levels, the temperature of the hot T_H and the cold T_C side of the thermoelectric modules have also been measured. Moreover, the temperature at the external part of the insulating material at two different points T_{los1} and T_{los2} and two ambient temperatures T_{amb1} and T_{amb2} have also been monitored. These sensors were controlled by means of an Arduino Mega that sent the information in JSON format to a Raspberry Pi 3 B + that stored the measured data in an Influx database that was synchronized with a server that represented the information in Grafana.

The first experiment that was performed intended to determine the optimal load resistance. For this purpose, the temperature of the heat source, i.e. the rope heaters, was maintained at an approximately constant value of 120 °C by varying the supplied power, and different load resistances were connected to each level. More specifically, open–circuit, 4 Ω, 6.6 Ω, 12 Ω and 22.6 Ω were tested.

Figure 4.19 shows the obtained results after the stabilization of all the variables for Prototype A, with 5 levels (10 thermoelectric modules), on the left; and Prototype B, with 3 levels (6 thermoelectric modules), on the right. As can be observed, both prototypes present a similar behavior, rapidly increasing the power generated with low load resistances until an optimal generation is reached, from which the power generated decreases slowly as the load resistance increases. In both prototypes, the optimal load resistance is 6.6 Ω, i.e.

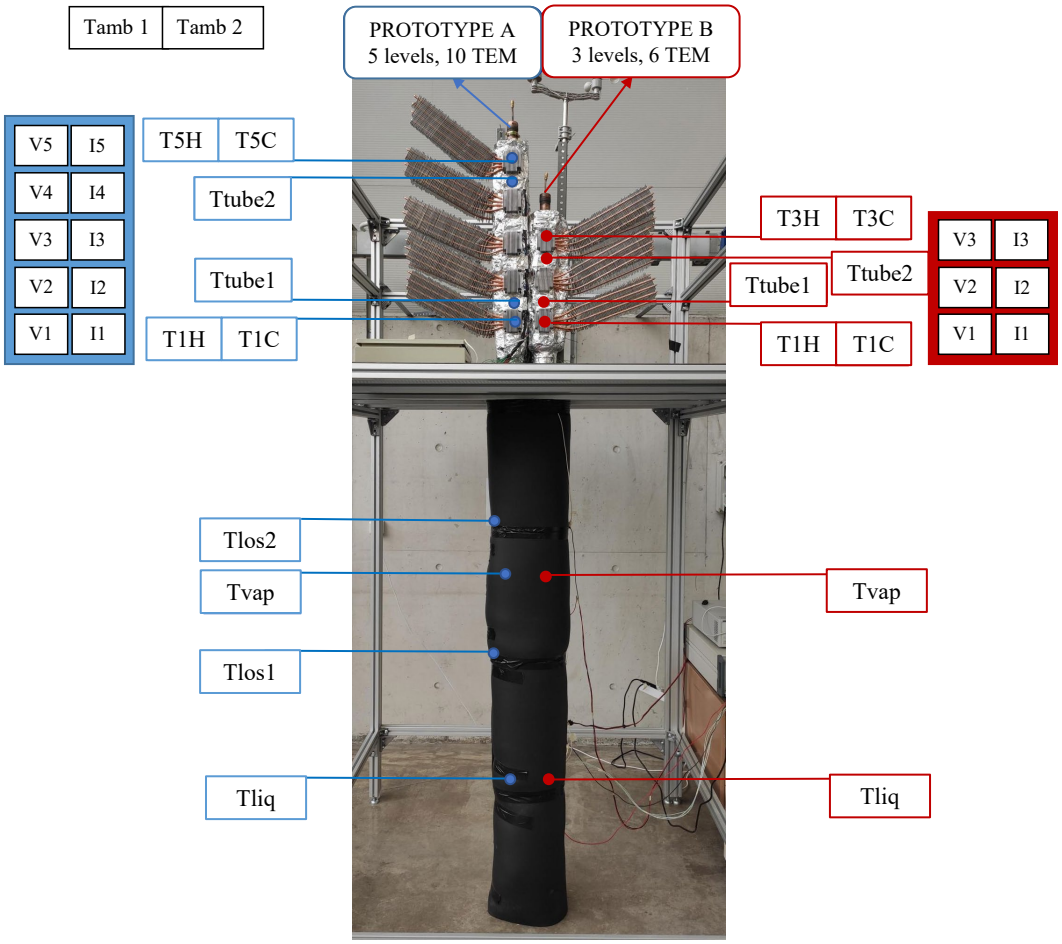

Figure 4.18: Disposition of the K-type thermocouples and the power generation sensors installed for the characterization of the thermoelectric generators.

3.3 Ω per module, which coincides with the results obtained in Chapter 2. With this load resistance, the power generated varies depending on the level and on the prototype. Thus, the generation is higher for the lower levels, as their temperature is higher. Level 3 of Prototype A is the exception of the former statement, leading to the lowest generation due to a poor thermal contact derived from the assembly. When comparing the results obtained with Prototype A and B, it can be observed that, as derived in Chapter 3, the prototype with less thermoelectric modules presents a higher generation because, since a common hot side heat exchanger is being used, the temperature of the hot side and the gradient of the thermoelectric modules increase with less thermoelectric modules. Hence, the power generated by Prototype B is higher than the Prototype A's one, reaching 1.26 W in the first level versus the 0.86 W produced at the same level in Prototype A, a 50 % increase.

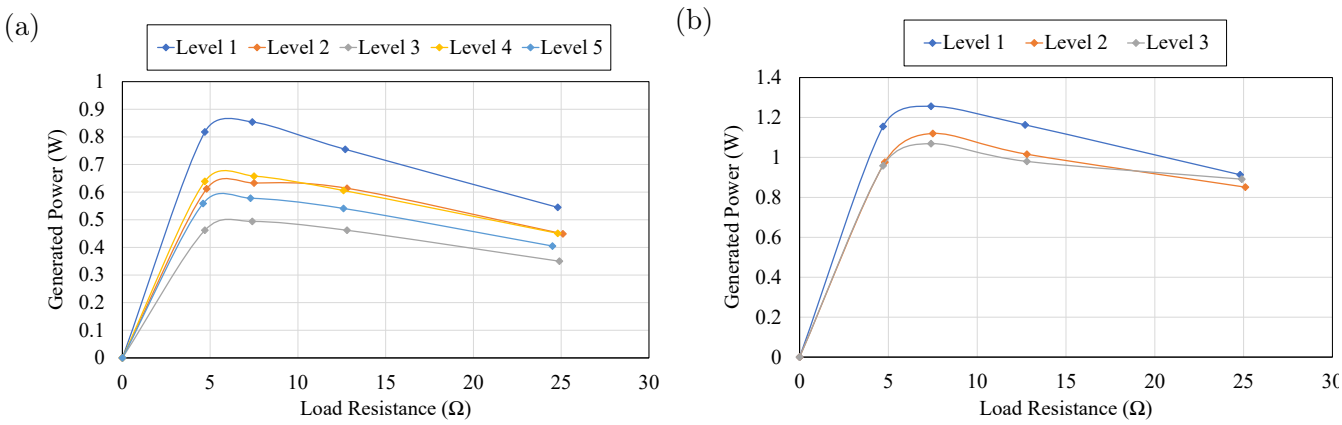

Figure 4.19: Power generated per level for different load resistances (a) in Prototype A and (b) in Prototype B.

Once determined the optimal load resistance, the maximum generation was measured for different temperatures of the heat source (from 110 to 180 °C), and ambient conditions (in natural and forced convection, the latter with a wind speed of 1.5 m/s). Figure 4.20 depicts the obtained results, representing the maximum power generated in each level versus the temperature difference between the source and the ambient for both natural convection (empty markers) and forced one (filled ones), considering again Prototype A in the left and Prototype B in the right. As can be observed, in all cases, the power generation increases with higher gradients between the heat source and the ambient temperatures, leading to an almost linear correlation, and under forced convection conditions. Similarly than before, this generation is higher for lower levels and differs from Prototype A and B. Thus, if the first level of each generator is again considered and if forced convection conditions are taken into account, it can be seen that in Prototype A generation increases from 2.1 W with a temperature difference between sources of 103 °C to 4.1 W with a 159 °C gradient, while in the case of Prototype B, the values ascend from 3.65 W to 6.9 W with a temperature difference a bit higher than before, 118 to 166 °C. These results entail a power generation per thermoelectric module of up to 3.45 W, higher than in Chapter 2, thanks to the developed heat exchangers with low thermal resistances that permit maximizing the temperature difference between the sides of the thermoelectric modules.

Figure 4.21 depicts the total generation per prototype in order to analyze the influence of natural and forced convection conditions. Hence, it can be observed that the slope of the linear tendency, as well as their values, are higher for forced convection conditions, increasing the generation rate as the heat source temperature increases. When working under forced convection conditions, the thermal resistance of the cold side heat exchangers decreases, increasing the heat flux and the temperature gradient in the thermoelectric

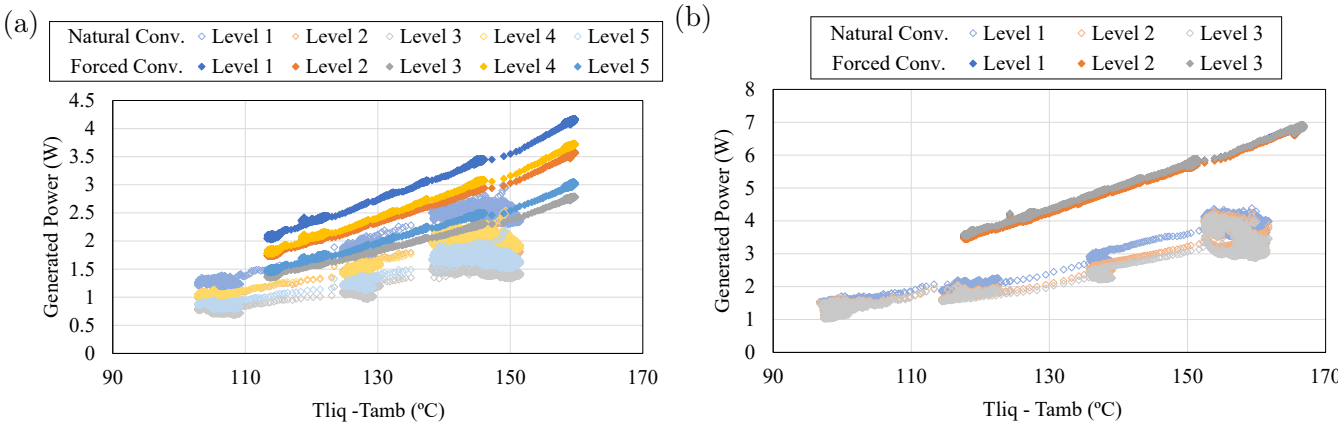

Figure 4.20: Power generated per level for different temperature gradients between the liquid section and the ambient considering both natural and forced convection (a) in Prototype A and (b) in Prototype B.

modules, and therefore the generation. Moreover, in contrast to natural convection conditions, the heat dissipated by the lower levels is rapidly released, not affecting the behavior of the higher ones, which also favors an increased generation. Another effect caused by forced convection is a reduced dispersion of the values, leading to a more uniformity in the experiments.

When comparing the generation of both prototypes, it can be seen that although the two prototypes present a different number of thermoelectric modules, their generation is quite similar, leading to around 10 W with a temperature difference of 120 °C, that increases to almost 20 W with a 160 °C gradient. According to Chapter 3, when increasing the number of thermoelectric modules, the generation per level decreases but total generation is higher until a maximum point is reached. With the studied conditions, the optimum point was reached with a higher number of thermoelectric modules. Therefore, there may be some contact issues in Prototype A, due to the more complicated assembly.

Nonetheless, despite having a total generation a bit lower than in theory, the expectations for the installation of the prototypes at *Casa de los Camelleros* are promising. Timanfaya National Park is characterized by considerable wind velocities that will permit reducing even more the thermal resistance of the cold side heat exchangers, compensating the low heat transfer mechanism between the geothermal gases and the prototypes, which was not considered in the laboratory experiments. The field installation of these generators is expected for early September 2020, which will be key in order to definitely understand the behavior of the design devices and determine the generation possibilities. This knowledge will also permit the design of a new prototype that encompasses all the detected upgrades, approaching to a future scenario of medium–scale generation by simply

reproducing several devices, thanks to the scalability of this technology.

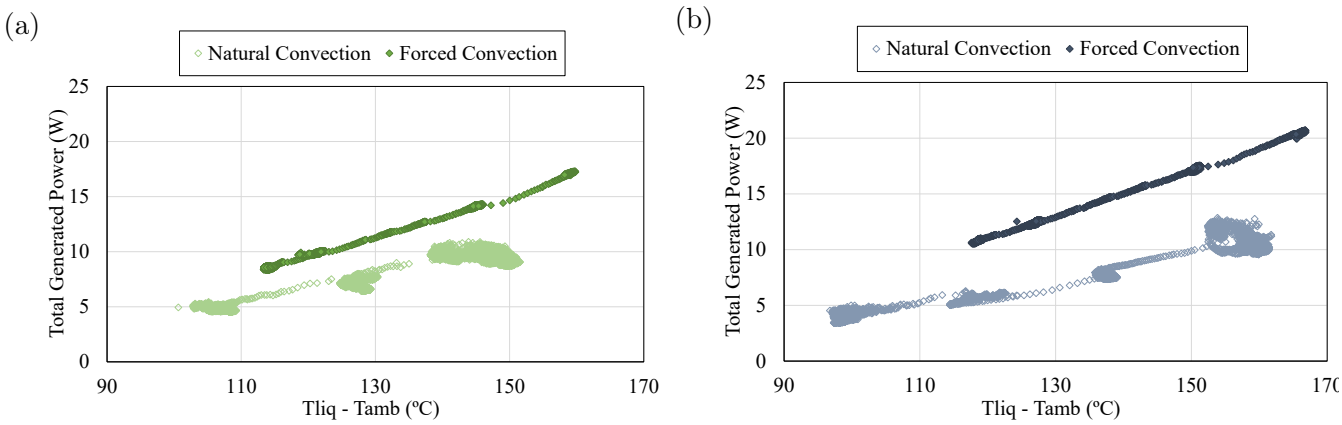

Figure 4.21: Total generation of (a) Prototype A and (b) Prototype B, for different temperature gradients between the liquid section and the ambient, considering both natural and forced convection conditions.

4.4 Conclusions of Chapter 4

In conclusion, this chapter has dealt with the design, construction and characterization of two prototypes of thermoelectric generators to be installed in due course at Timanfaya National Park; more specifically at the area known as *Casa de los Camelleros* where the gases emerge at a temperature of more than 200 °C.

Firstly, the design of the devices has been conducted, for which it has been necessary to take into consideration that apart from having heat exchangers with low thermal resistances, it is of utmost importance to avoid moving parts, auxiliary consumption, noise, and harmful working fluids, while being compact, modular, and easy to assembly. Due to the lack of commercial products with such characteristics, the manufacturing process of the heat exchangers has been developed, leading to an inexpensive and quick methodology that permits obtaining good values of the thermal resistances of around 0.4 K/W in the case of the cold side heat exchanger and less than 0.16 K/W in the case of the hot side one.

After the design process, the two prototypes have been built ensuring a good thermal contact between the different components and insulating the devices to avoid undesirable thermal losses. Afterwards, the two generators have been characterized at the laboratory under different operating conditions. Hence, considering the optimal load resistance, a linear correlation between the power generated and the gradient between the heat source and the ambient temperatures has been obtained. This generation is higher for lower levels, forced convection conditions, as well as in the prototype with less thermoelectric modules. In total, the prototype with 10 thermoelectric modules has led to a maximum generation of 17.1 W given a temperature difference of 160 °C and a wind speed of 1.5 m/s, while the prototype with 6 thermoelectric modules has produced a maximum of 20 W with the same velocity and a gradient of 166 °C. Based on these results, the viability and the potential of the developed devices has been demonstrated, showing promising expectations for their due course installation on field.

4.5 Bibliography

[Adafruit2020] Adafruit. INA219 High Side DC Current Sensor Breakout - 26V ±3.2A Max .

[Araiz2018] M. Araiz, L. Catalan, O. Herrero, G. Perez, and A. Rodriguez. The Importance of the Assembly in Thermoelectric Generators. In Patricia Aranguren, editor, *Bringing Thermoelectricity into Reality*, chapter 7, pages 123–144. IntechOpen, 2018.

[Bejan2003] Adrian Bejan and Allan D. Kraus. *Heat Transfer Handbook*. Wiley, 2003.

[Catalan2020] L. Catalan, M. Araiz, P. Aranguren, G.D. Padilla, P.A. Hernandez, N.M. Perez, C. Garcia de la Noceda, J.F. Albert, and D. Astrain. Prospects of Autonomous Volcanic Monitoring Stations: Experimental Investigation on Thermoelectric Generation from Fumaroles. *Sensors*, 20(3547), 2020.

[Dincer2018] Ibahim Dincer and Osamah Siddiqui. *Comprehensive Energy Systems*. Elsevier Inc., 2018.

[IGME1992] Instituto Geológico Minero Español. Evaluación del potencial geotérmico superficial de Montañas de Fuego como Sistema de Roca Caliente Seca. Technical report, 1992.

[Maxim2020] Maxim. MAX31855PMB1 Peripheral Module.

[Parmelee1947] G.V. Parmelee and R.G. Huebscher. Heat transfer by forced convection along a smooth flat surface. *Heat Piping Air Conditioning*, 19(8):115, 1947.

[Rohsenow1998] W.M. Rohsenow, J.P. Hartnett, and Y.I. Cho. *Handbook of heat transfer*. McGraw-Hill Handbooks, 3rd edition, 1998.

Chapter 5

Thermoelectric Generation from Volcanic Fumaroles

The studies performed hitherto in the present Ph. D. dissertation have been focused on medium–scale geothermal thermoelectric generation in shallow hot dry rock fields. Hereinafter, the other application under consideration in this thesis, the stand–alone power supply of volcanic monitoring stations, is analyzed.

Volcanoes are considered one of the most dangerous natural hazards. And even though volcanic eruptions cannot be avoided, it is possible to reduce their damage by measuring the so–called precursors, which permit predicting when a volcanic eruption is going to occur. For this purpose, it is necessary to install a sensor network to measure diverse parameters such as the seismic movements, the temperature and composition of the volcanic products or changes in the gravitational forces among others. Nevertheless, the power supply of such sensors constitutes a challenge due to the absence of power grid, the access difficulties, the climatology, and the acidic environment associated with volcanoes.

Nowadays, energy supply is fulfilled by means of photovoltaic panels and, consequently, batteries, so that power supply is ensured during nights, periods of absence of sun, or episodes of volcanic ashes. However, this solution is not valid for all the locations. This is the case of those volcanoes that record severe snowfalls during long periods in winter, or that are located at extreme latitudes, where there is no sun during months. In these cases, it is not possible to monitor the activity of the volcano, with its consequent risk.

As a solution, the present Ph. D. dissertation proposes the utilization of thermoelectric generators to transform the heat emitted by fumaroles, one of the most evident signs of the activity of the volcanoes, into electricity. Hence, this fifth chapter represents the first

approximation to this solution, studying the viability of fumaroles as heat source. For this purpose, a thermoelectric generator was installed at Teide volcano (Canary Islands, Spain), where there exist 83 °C fumaroles. Taking into account the studies developed in the previous chapters, the installed thermoelectric generator was composed of heat exchangers based on phase change.

The obtained results are gathered in the publication "Prospects of Autonomous Volcanic Monitoring Stations: Experimental Investigation on Thermoelectric Generation from Fumaroles" published in the journal *Sensors* 20 (2020) 3547. These results led to very valuable information about the heat transfer with the fumaroles and the harsh conditions that the device needs to withstand, which become essential for the development of future devices, carried out in the next chapter.

sensors

MDPI

Article

Prospects of Autonomous Volcanic Monitoring Stations: Experimental Investigation on Thermoelectric Generation from Fumaroles

Leyre Catalan [1,*], Miguel Araiz [1], Patricia Aranguren [1], German D. Padilla [2,3], Pedro A. Hernandez [2,3,4], Nemesio M. Perez [2,3,4], Celestino Garcia de la Noceda [5], Jose F. Albert [6] and David Astrain [1]

1 Department of Engineering, Institute of Smart Cities, Public University of Navarre, 31006 Pamplona, Spain; miguel.araiz@unavarra.es (M.A.); patricia.arangureng@unavarra.es (P.A.); david.astrain@unavarra.es (D.A.)
2 Instituto Volcanologico de Canarias (INVOLCAN), 38320 San Cristobal de La Laguna, Spain; german@iter.es (G.D.P.); phdez@iter.es (P.A.H.); nperez@iter.es (N.M.P.)
3 Instituto Tecnologico y de Energias Renovables (ITER), 38600 Granadilla de Abona, Spain
4 Agencia Insular de Energia de Tenerife (AIET), 38612 Granadilla de Abona, Spain
5 Instituto Geologico y Minero de España (IGME), 28003 Madrid, Spain; c.garcia@igme.es
6 GAIA Geotermia y Aguas Minerales S.L., 28029 Madrid, Spain; j.albert@gaiarecursos.es
* Correspondence: leyre.catalan@unavarra.es; Tel.: +34-948-16-84-41

Received: 26 May 2020; Accepted: 20 June 2020; Published: 23 June 2020

Abstract: Fumaroles represent evidence of volcanic activity, emitting steam and volcanic gases at temperatures between 70 and 100 °C. Due to the well-known advantages of thermoelectricity, such as reliability, reduced maintenance and scalability, the present paper studies the possibilities of thermoelectric generators, devices based on solid-state physics, to directly convert fumaroles heat into electricity due to the Seebeck effect. For this purpose, a thermoelectric generator composed of two bismuth-telluride thermoelectric modules and heat pipes as heat exchangers was installed, for the first time, at Teide volcano (Canary Islands, Spain), where fumaroles arise in the surface at 82 °C. The installed thermoelectric generator has demonstrated the feasibility of the proposed solution, leading to a compact generator with no moving parts that produces a net generation between 0.32 and 0.33 W per module given a temperature difference between the heat reservoirs encompassed in the 69–86 °C range. These results become interesting due to the possibilities of supplying power to the volcanic monitoring stations that measure the precursors of volcanic eruptions, making them completely autonomous. Nonetheless, in order to achieve this objective, corrosion prevention measures must be taken because the hydrogen sulfide contained in the fumaroles reacts with steam, forming sulfuric acid.

Keywords: thermoelectric generator; geothermal; volcano; power generation; autonomous; thermoelectricity; heat pipe

1. Introduction

Volcanoes are one of the most evident manifestations of geothermal energy. In active volcanoes, one way in which this geothermal energy is revealed is in the form of fumaroles, i.e., vents in the Earth's surface from which steam and volcanic gases are emitted, normally at temperatures between 70 and 100 °C [1]. Monitoring these fumaroles in conjunction with other precursors is of great importance in order to predict volcanic eruptions [2–4]. Nevertheless, the power supply of the required equipment is a challenge due to the habitual remoteness of volcanoes.

Geothermal energy has the potential to be transformed into electricity [5], for which, traditionally, cycles have been used provided that the temperature of the geothermal field is greater than 70 °C [6,7]. In the low enthalpy range (70 to 150 °C approximately), in which fumaroles are encompassed, power is typically generated by means of binary cycles, closed cycles that convert heat from a geothermal fluid into electricity by transferring the heat to another low boiling point working fluid that drives a turbine [8]. This fluid can be an organic fluid, leading to an Organic Rankine Cycle (ORC), or ammonia, in which case the cycle is known as Kalina. Nowadays, some of the existing binary plants are already working with inlet temperatures between 70 and 100 °C, presenting capacities up to 0.5 MW and efficiencies lower than 3% [9]. Nevertheless, binary cycles are not suitable for the considered application, since a compact, autonomous, and robust stand-alone device to supply low power is required.

One alternative in order to generate electricity from geothermal heat consists in the use of thermoelectric generators, solid-state devices that directly convert heat flux into electricity due to the Seebeck effect. For this purpose, thermoelectric generators are composed of thermoelectric modules and heat exchangers. The conversion itself takes place in the thermoelectric modules, a group of thermocouples connected electrically in series and thermally in parallel protected with ceramic sheets, while the heat exchangers are necessary in order to maximize the temperature difference between the sides of the modules, since the greater the temperature difference, the higher the generation.

Fin dissipators, liquid-based heat exchangers, heat pipes, and thermosyphons are the most common heat exchangers used in thermoelectric generators [10]. Fin dissipators stand out due to their simplicity, robustness, and low price, achieving low thermal resistances when working as active cooling systems, i.e., aided by a fan so that forced convection conditions are obtained [11,12]. On their behalf, liquid-based heat exchangers present better convection coefficients, improving the performance of the system. However, the pumps necessary to propel the liquid through the circuit require a higher auxiliary consumption and therefore reduce net generation [13,14]. Finally, heat pipes and thermosyphons are gaining attention in the last years. Making use of the latent heat of an internal fluid that cyclically vaporizes and condensates, these heat exchangers obtain low thermal resistances without requiring auxiliary equipment [15–17].

Thermoelectric generators present numerous advantages [18]: Direct energy conversion, avoiding the intermediate conversion of thermal energy into mechanical energy in order to generate electricity with an alternator; long lifespan, especially when working with constant reservoirs, as it has been demonstrated in spatial applications; ability to generate electricity with any temperature difference; scalability; and static and noiseless operation of the thermoelectric modules, which neither use working fluids. Nevertheless, they present an important drawback that has prevented their utilization in civil applications: Their efficiency is very low, between 2 and 5% depending on the temperature range [18,19], an efficiency very similar to the one obtained with binary plants in the temperature range considered with fumaroles.

In their application to geothermal heat, thermoelectric generators have been identified as one of the ways to speed up the installation of geothermal power [20], and therefore there exist various proposals that combine thermoelectric generators and geothermal energy. Most of them try to maximize power generation from low-medium enthalpy geothermal fields ($T < 150$ °C) incorporating for this purpose liquid-based heat exchangers, similarly to their competitors, binary cycles. Some of these proposals demonstrate their feasibility by simulation, such as Suter et al., who optimized a 1 kW thermoelectric generator with a 100 °C temperature difference [21], or Wang et al., who proposed integrating these thermoelectric generators downhole in oil and gas wells, being able to obtain 8.5 kW in a vertical well with a 100 °C gradient, and 128 kW in the case of a horizontal one with a temperature difference of 156 °C [22,23]. In contrast, others do it with real prototypes at the laboratory, such as Liu et al. who built a 160 W thermoelectric generator composed of 96 thermoelectric modules that operated with an 80 °C gradient [24–26], or Ahiska and Mamur, who produced 41.6 W with 20 thermoelectric modules

and a temperature difference of 67 °C [27,28], or finally, Trip et al., who, with a gradient of 72 °C and 40 modules, generated 0.4 W [29].

Due to the utilization of liquid-based heat exchangers, all the previous examples obtain low values of thermal resistance. However, they present an extra electrical consumption because of the pump, which reduces net generation. Catalan et al. experimentally demonstrated that passive heat exchangers based on phase change are more adequate for geothermal thermoelectric generators [30]. These heat exchangers also present low values of thermal resistance, but they do not include mobile parts nor auxiliary consumption, thus maximizing power generation and reducing maintenance requirements. While they proposed their use for a high temperature hot dry rock field, they can be extrapolated to fumaroles. In fact, Xie et al. already demonstrated the feasibility of a thermoelectric generator with a heat pipe as hot side heat exchanger in hydrothermal vents, the equivalent of fumaroles underwater, obtaining a maximum of 3.9 W with 4 thermoelectric modules from a 379 °C vent located at a depth of 2765 m.

The objective of the present paper is to study, for the first time, the viability of thermoelectric generators in volcanic fumaroles. For this purpose, a prototype with heat exchangers based on phase change has been installed at Teide volcano. Teide is a stratovolcano located in Tenerife (Canary Islands, Spain), a volcanic island in the Atlantic Ocean whose landscape is molded by different volcanoes. Teide is not only the highest volcano on the island, with an altitude of 3718 m, but also the third highest volcano in the world from its base on the seafloor. Due to its activity, Teide volcano presents constant fumaroles at a temperature of 82 °C, which corresponds with water vaporization temperature at that height [31,32]. These fumaroles will represent the heat source for the installed thermoelectric generator.

The interest in generating electricity from fumaroles resides in the possibility of supplying energy to the volcanic monitoring stations that aim to measure the precursors of volcanic eruptions. Most active volcanoes of the world incorporate this kind of vigilance stations, which measure different parameters such as the variation in temperature or composition of the fumaroles, or the seismic activity. The power requirements of these stations depend on the installed equipment. Nonetheless, it is normally of a few watts, with punctual peaks during communication [33,34], and with Internet of Things (IoT) technologies, it can be diminished to a few milliwatts [35]. Hence, given this low energy consumption, the proposal of thermoelectric generators with phase change heat exchangers could become the perfect energy supplier and make the stations completely autonomous: Power would be generated continuously during day and night, even improving with adverse weather conditions, the device would use passive heat exchangers that do not require auxiliary consumption nor present mobile parts, reducing maintenance requirements in locations that normally are difficult to access, and it would be very compact and easy to install.

The use of thermoelectricity for micro-generation oriented to sensors is widely available in the literature [36–38]. Regarding its combination with geothermal energy, two faint tendencies can be found. On the one hand, some proposals combine traditional geothermal plants with thermoelectric generators installed on the pipes to power different sensors or actuators [39–41]. On the other hand, others use the temperature difference between forest soil and the environment to power sensors, as proposed by Stokes et al. [42] and put into practice by Huang et al. using heat pipes as heat exchangers [43–45]. Nonetheless, the use of fumaroles as heat source is proposed for the first time in the present paper.

Section 2 details the thermoelectric generator installed at Teide volcano. Section 3 describes the monitoring system used. Section 4 analyzes the obtained results as well as the arisen problems. Finally, Section 5 presents the conclusions and future lines.

2. Thermoelectric Generator for Teide Volcano

While the most important element of a thermoelectric generator are the thermoelectric modules, heat exchangers become essential in order to maximize power generation. A reduction of 10% in the thermal resistance of the heat exchangers leads to an 8% higher generation [46]. In accordance

with Catalan et al. [30], who demonstrated that heat exchangers based on phase change are the most recommended ones for geothermal thermoelectric generators, the present paper includes heat pipes at both sides of the thermoelectric modules.

Figure 1 depicts an exploded view of the geothermal thermoelectric generator (GTEG) installed at Teide's fumaroles, whose mode of operation is patented under number WO 2019/202180 A1 [47]. In this view, a cut has been performed in the ground to emphasize the construction and positioning of the hot side heat exchanger, which is in direct contact with the ground in reality. Thus, geothermal heat is absorbed by means of eight 450 mm long grooved tubes made of nickel-plated copper containing water in their interior (Figure 2a). 350 mm of these tubes are in direct contact with the ground, causing the vaporization of the internal fluid, which ascends to the upper part of the pipe, where it condensates releasing heat to the thermoelectric modules. In order to obtain a planar contact surface between the tubes and the thermoelectric modules, the tubes are inserted in semicircular channels milled in a $150 \times 90 \times 15\,mm^3$ aluminum plate, and pressed afterward, as detailed in Figure 2c.

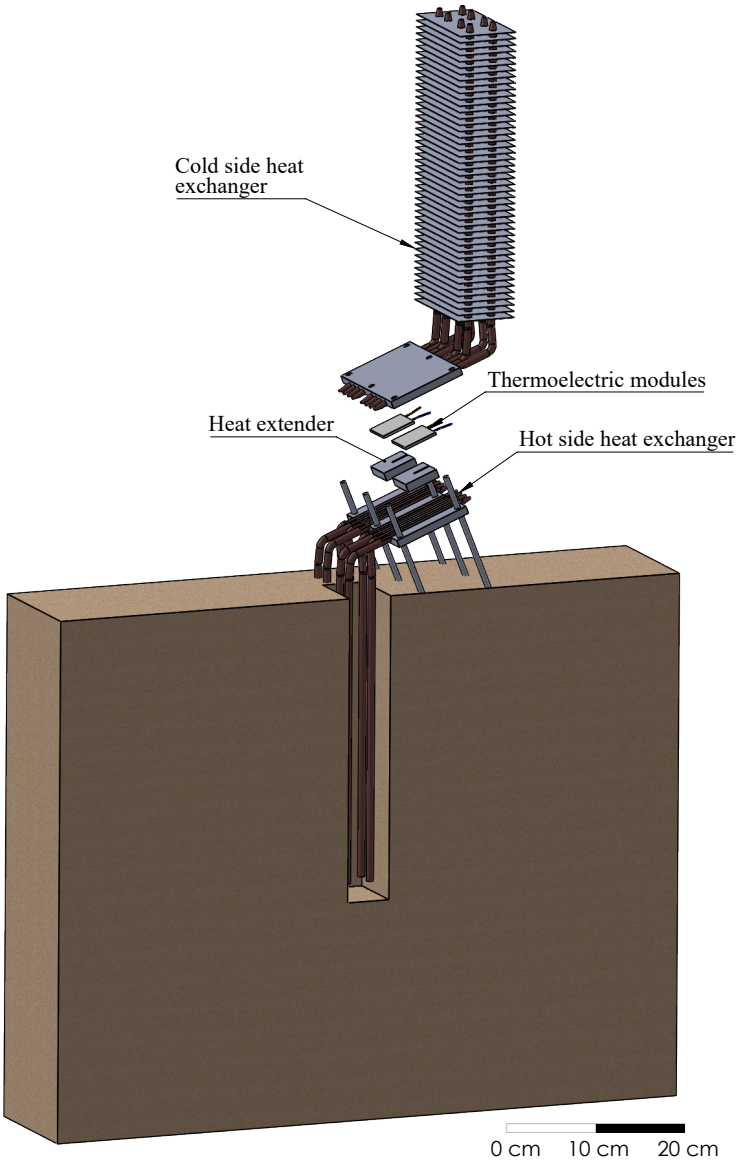

Figure 1. Exploded view of the geothermal thermoelectric generator installed at Teide volcano.

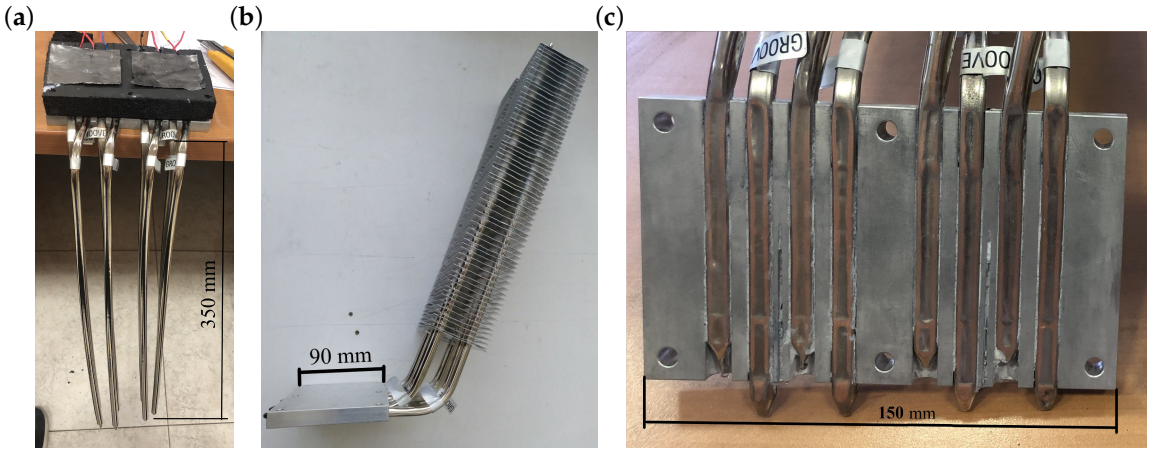

Figure 2. (**a**) Hot side heat exchanger. (**b**) Cold side heat exchanger. (**c**) Detail of the fitting between the heat pipe tubes and the aluminum plate.

Two bismuth-telluride thermoelectric modules partially convert the incident heat, which is provided by condensation inside the hot side heat exchanger, into electricity. The remaining heat is released on the other side of the TEG by the cold side heat exchanger. The installed modules are one Marlow TG12-8-01L and one Marlow TG12-8-01LS [48]. The only difference between them is that the latter is sealed with silicone for protection. Furthermore, as shown in Figure 1, a $40 \times 40 \times 10$ mm^3 aluminum heat extender was added between the hot side heat exchanger and each thermoelectric module since a slight separation of the heat exchangers reduces thermal losses due to thermal bridges [49].

The heat released by the thermoelectric modules is transmitted to the cold side heat exchanger, which is similar to the hot side one, except for the inclusion of 62 aluminum fins with a distance of 5 mm (Figure 2b). In this case, vaporization takes place in the lower part of the heat exchanger, in contact with the thermoelectric modules. The vapor ascends and condensates in the finned part of the tube. Since these fins allow increasing the exchange area with the windy environment, thus its thermal resistance decreases.

This cold side heat exchanger has been characterized in order to determine its thermal resistance with respect to the heat flux for different environmental conditions. For this purpose, as shown in Figure 3, cartridge heaters embedded in two 40×40 mm^2 copper blocks have been used as heat source, simulating the heat released by the thermoelectric modules. In order to ensure that all the heat provided by the power supply goes through the heat exchanger, it has been necessary to add rockwool insulation so that thermal losses into the environment are minimized.

In the experiments, it has been studied the influence of different heat fluxes (75, 100 and 125 W per block) and environmental conditions (pure natural convection as well as 1.6 and 2.9 m/s wind velocities reproduced with a fan). In each case, the thermal resistance per thermoelectric module has been calculated with Equation (1), in which T_{ev} is the temperature measured at the base of the evaporator, T_{amb} is the ambient temperature and $\dot{Q}$ is the useful heat flux per block provided by the power supply, which is in turn calculated as the subtraction of the power ($V \times I$) minus the estimated thermal losses $\dot{Q}_{losses}$, for which the estimation of the convective heat transfer coefficient is necessary similarly to [30]. Each experiment has been repeated three times and the uncertainties have been calculated according to [50], leading to an average uncertainty of 4.3%.

$$R = \frac{T_{ev} - T_{amb}}{\dot{Q}} = \frac{T_{ev} - T_{amb}}{V \times I - \dot{Q}_{losses}} = \frac{T_{ev} - T_{amb}}{V \times I - h_{ins} \times A_{ins} \times (T_{ins} - T_{amb})} \quad (1)$$

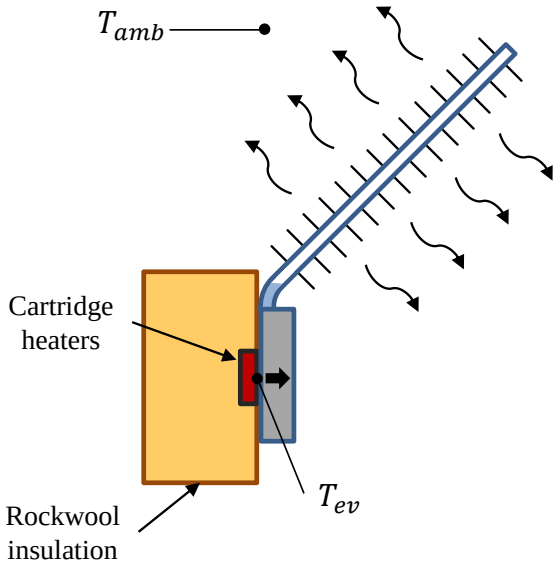

Figure 3. Schematics of the characterization of the cold side heat exchanger.

Figure 4 depicts the results of thermal resistance obtained for the different heat fluxes and environmental conditions studied. As can be observed, in all cases the thermal resistance decreases with increasing heat fluxes. This is the conventional behavior of phase change heat exchangers, since the properties of their internal working fluid improve with temperature, leading to a lower thermal resistance. Nonetheless, the biggest influence on the thermal resistance is caused by the exterior conditions, decreasing with higher wind velocities. In forced convection, thermal resistance is practically constant, presenting values of 0.22 and 0.18 K/W with wind velocities of 1.6 and 2.9 m/s respectively. In contrast, in natural convection a more pronounced dependency with respect to the heat flux can be observed, decreasing from a thermal resistance of 0.61 K/W with 75 W to 0.55 K/W with 125 W. The thermal resistance of the cold side heat exchanger can be divided into all the processes that occur within it: Conduction in the lower part of the tubes, boiling, condensation, conduction in the upper part of the tubes and the fins, and convection.

$$R = R_{k1} + R_b + R_{cond} + R_{k2} + R_{conv} = \frac{ln(D_e/D_i)}{2\pi Lk} + \frac{1}{h_b A_b} + \frac{1}{h_{cond} A_{cond}} + \frac{ln(D_e/D_i)}{2\pi Lk} + \frac{1}{h_{conv} A_{conv} \eta_{fins}} \quad (2)$$

It is the latter the one that is influenced by wind velocity. As derived from the Nusselt expressions, in forced convection the convective coefficient h_{conv} depends on Reynolds and Prandtl numbers exclusively and therefore, this coefficient mainly depends on the air velocity, while in natural convection Grashof number also has influence [51]. As shown in Equation (3), Grashof number is directly proportional to the gravity g, the coefficient of thermal expansion β that equals to $1/T$ for ideal gases, the temperature difference between the surface and the ambient $T_s - T_{amb}$ and the cube of the characteristic length, and inversely proportional to the square of the kinematic viscosity ν. Hence, if the temperature difference between the external part of the tube and the ambient increases, so does Grashof number, resulting in a greater Nusselt number and consequently a better convective heat transfer coefficient that causes a lower convective thermal resistance. In the experiments, when the heat flux increases, the temperature difference between the surface of the tubes and the heat sink also increases, leading to a lower convective thermal resistance and consequently, to a smaller total thermal resistance of the cold side heat exchanger. Nonetheless, Teide, due to its altitude, is generally windy, so forced convection conditions will be predominant and the heat exchanger's thermal resistance is expected to be lower than 0.3 K/W.

$$Gr = \frac{g \times \beta \times (T_s - T_{amb}) \times l^3}{\nu^2} \quad (3)$$

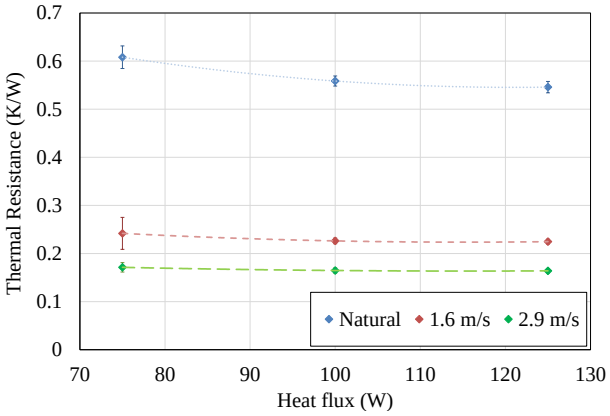

Figure 4. Thermal resistance per thermoelectric module of the cold side heat exchanger for different external conditions. Each experiment has been repeated three times and the uncertainties have been calculated according to [50].

All the aforementioned components were assembled by means of six M6 threaded rods that permit holding the prototype in the ground and provide stability. For this purpose, the heat pipe tubes were bent an angle of 69° with respect to the vertical. In order to improve the thermal contact between the thermoelectric modules and the heat exchangers, Panasonic pyrolytic graphite sheets 0.1 mm thick were included [52]. Finally, neoprene layers (10 and 15 mm thick) covered all the exposed parts of the aluminum plates, forcing condensation and vaporization of the hot and cold side heat exchangers respectively, to occur on the thermoelectric modules (Figure 5). This is especially important in the hot side heat exchanger, since it is desirable that all the absorbed geothermal heat goes through the thermoelectric modules, and it is not lost before its transformation into electricity. While the neoprene cover the thermoelectric modules, their position, as well as the heat extenders and graphite sheets one, has been detailed in Figure 5.

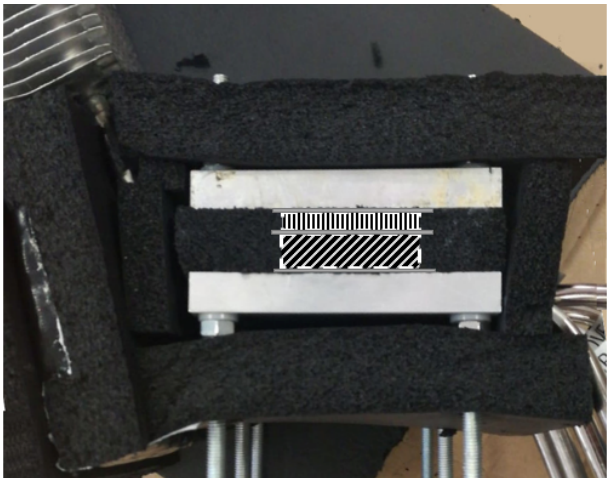

Figure 5. Detail of the neoprene layers installed covering the aluminum plates. On the figure, a drawing of the position of the heat extenders (with diagonal lines), the thermoelectric modules (with vertical lines) and the graphite sheets (in filled gray) has also been added.

The prototype was installed on 15th March 2019 at Teide volcano, the most emblematic volcano at the Canary Islands (Spain). In particular, it was installed closed to "La Fortaleza" lookout, located at an altitude of approximately 3500 m, facing the northern part of the island (Figures 6 and 7). In this location, there exist fumaroles with a temperature of 82 °C [31,32].

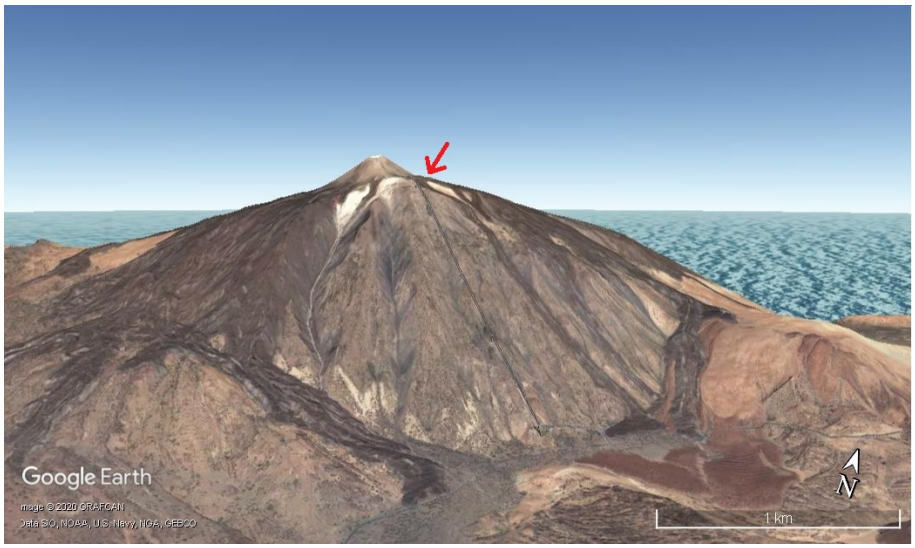

Figure 6. Location of the installed prototype closed to "La Fortaleza" lookout. © Google Earth.

Figure 7. Prototype installed at Teide volcano.

3. Monitoring System

In order to study the viability of thermoelectric generators in volcanic fumaroles, monitoring the prototype installed at Teide volcano becomes indispensable. Hence, 18 thermocouples, four humidity sensors, and two power sensors have been installed.

Figure 8 details the position of the thermocouples, most of which have been duplicated: T_{ground_40cm0} and T_{ground_40cm1} are buried in the ground, at an approximate depth of 40 cm; T_{ground_10cm} and T_{ground_5cm} are also buried in the ground, but at 10 cm and 5 cm deep respectively; T_{hhe_inf0} and T_{hhe_inf1} measure two of the tubes (one corresponding to each module) of the hot side heat exchanger in their lower part, at an approximate depth of 35 cm (neoprene isolation avoids the influence of ground temperature); T_{hhe_sup0} and T_{hhe_sup1} are located on the same tubes than the latter, but in its superior part, out of the ground, close to the aluminum plate, and are also protected with neoprene; T_{ht0} and T_{ht1} represent the temperature of the aluminum plate of the hot side heat exchanger, measured thanks to the grooves that can be appreciated in Figure 2c; T_{h0} is the hot side temperature of the Marlow TG12-8-01L thermoelectric module, while T_{h1} refers to the sealed Marlow TG12-8-01LS module; T_{c0} and T_{c1} are the cold side temperature of the thermoelectric modules, measured in the grooves of the cold side aluminum plate; and T_{che0} and T_{che1} indicate the temperature of two tubes of the cold side heat exchanger in the upper part (again each tube corresponds to one module and neoprene isolation has been added).

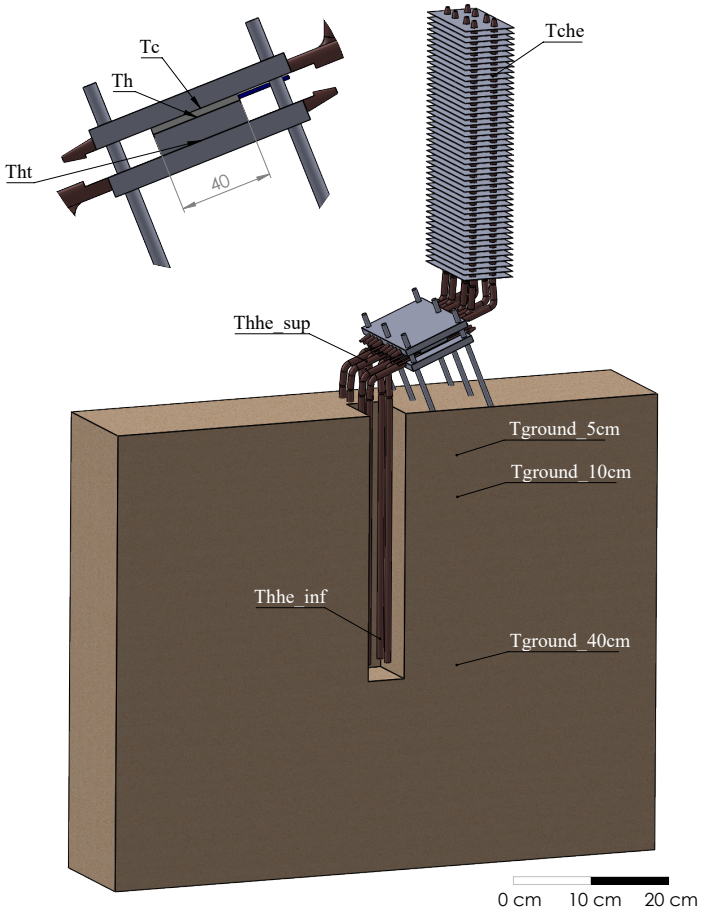

Figure 8. Positioning of the K-type thermocouples.

All the previous temperatures have been measured by means of K-type thermocouples with epoxy coated tips and ±2 °C accuracy. Each thermocouple was connected to a MAX31855, an Adafruit breakout board responsible for the amplification of the thermocouples' signal with cold compensation

reference [53]. For protection, all the thermocouples were coated with heat shrink tubing and those buried in the ground were also inserted in a 2 mm brass tube.

In addition, two shielded DTH22 sensors [54] measured the ambient temperature (T_{amb0} and T_{amb1}) as well as the humidity (Hum_{amb0} and Hum_{amb1}). Ground humidity was also measured by means of two soil moisture sensors buried at a depth of 40 cm [55].

The previous sensors were used in order to monitor the conditions at which the installed thermoelectric generator was working. Nonetheless, it is of utmost importance to determine the power generation of the thermoelectric modules. For this purpose, the thermoelectric modules were individually connected to a 3.2 Ω load resistance as a first approximation. The objective of the present paper is to study the viability of thermoelectric generation from fumaroles, and therefore, a constant load resistance has been connected and its generation has been measured with Adrafuit INA219 breakout boards, with 1% precision [56]. However, in case the viability is demonstrated and these devices are used for a real application, maximum power point trackers will be required, with their associated efficiency that will slightly reduce total generation. Actual MPPTs achieve efficiencies higher than 85% even in ultralow-power applications [57,58].

All the temperature, humidity, and power generation sensors were connected to an Arduino Mega 2560, which did a measurement scan every 10 s. This Arduino formatted the measured values into a JSON structure that was sent by RS485 protocol to a Raspberry PI 3 Model B+. RS485 protocol was chosen because the distance between the Arduino and the Raspberry was greater than 5 m, more than the maximum distance supported by USB. The Raspberry stored the received data into InfluxDB, a time series database. This Raspberry was in turn connected to a GSM Router so that its database was synchronized with a private server through MQTT protocol, allowing to see the info in a Grafana dashboard. Figure 9 details the communication between the Arduino and the Raspberry, including the MAX485 converter configured as transmitter in the Arduino and as receptor in the Raspberry [59], as well as the BSS138 logic level converter to adapt the received signal to Raspberry's GPIO requirements [60]. The schematics also shows the PV panel, including its MPPT and storage system, that was part of the existing volcanic vigilance station located at "La Fortaleza" lookout, and that supplied power to the Arduino, the Raspberry and the GSM router.

In order to protect the electronics from ambient conditions, all the circuits were placed in plastic boxes.

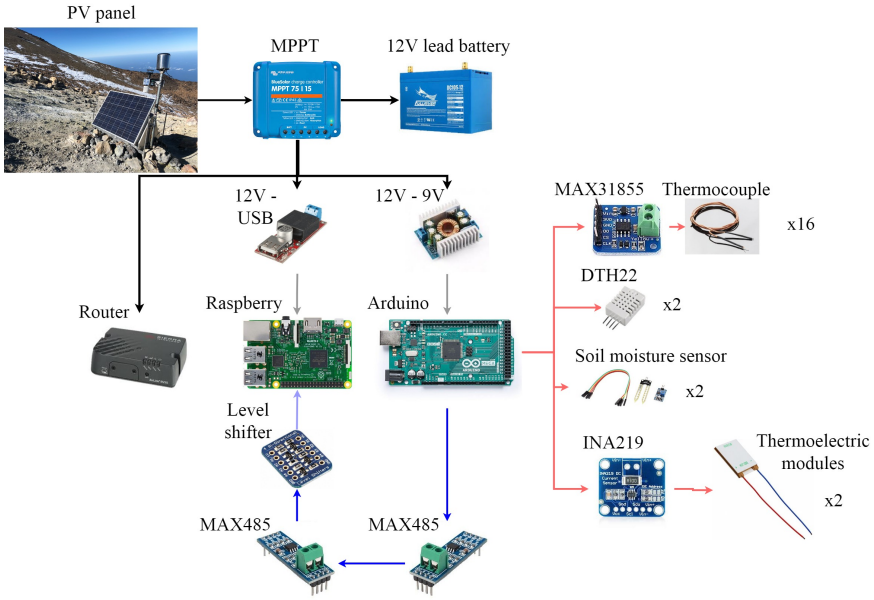

Figure 9. Diagram of the monitoring system including the power supply (black), the RS485 communication (blue), and the sensors (red).

4. Results and Discussion

Once the prototype and the monitoring system have been described, the present section shows the results obtained on the 16th and 17th March 2019, after the stabilization of the different variables.

On the one hand, Figure 10 depicts the conditions of temperature and humidity of the heat source, the fumaroles. The temperature has been measured at a depth of 5, 10, and 40 cm (brown lines). As can be observed, at very low depths, the ground temperature is influenced by ambient conditions. Nonetheless, as depth is increased, ground temperature stabilizes and presents an approximately constant value of 82 °C. Considering that it is necessary to transport geothermal heat from a considerable depth underground to the thermoelectric modules located overground, the selected heat pipes represent an excellent solution since they are capable of transmitting great amounts of heat with a minimum temperature drop as they are based on phase change. Soil moisture, depicted in the right axis of the figure and measured at a depth of 40 cm, also follows a constant tendency, with almost 90% of relative humidity. Since this value is greater than 30%, a good heat transfer from the soil is expected [45].

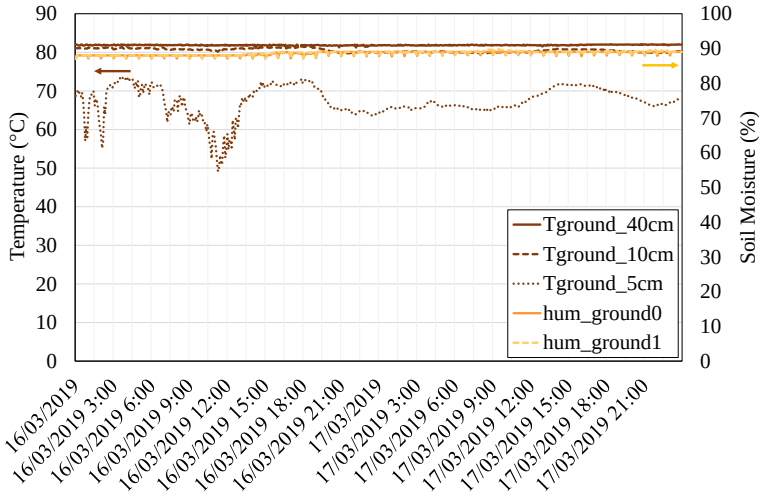

Figure 10. Ground temperature at a depth of 5 cm (dotted brown line), 10 cm (dashed brown line), and 40 cm (filled brown line) on the left axis, and soil moisture at a depth of 40 cm on the right axis (orange and yellow lines).

On the other hand, the conditions of the heat sink are shown in Figure 11. Ambient temperature (Figure 11a, left axis) varies throughout the day, with temperatures below zero during the night and up to 12 °C during the day. Slight variations between the sensors are due to their different locations. Figure 11a also depicts the relative ambient humidity in its right axis. Humidity does not follow a clear tendency and differs depending on the considered date. Hence, on 16th March, humidity constantly oscillates between 20 and 50%, while on 17th March, it stabilizes to an approximately constant value of 15%. In order to completely characterize the heat sink conditions, wind velocity has been represented in Figure 11b. These values of wind velocity were obtained from a weather station located nearby, which measured this value every hour. While it would be desirable to have more frequent measurements, the available data shows a typical variant smooth-moderate breeze with wind velocities that oscillate between 1 and 9 m/s, leading to forced convection in the cold side heat exchanger.

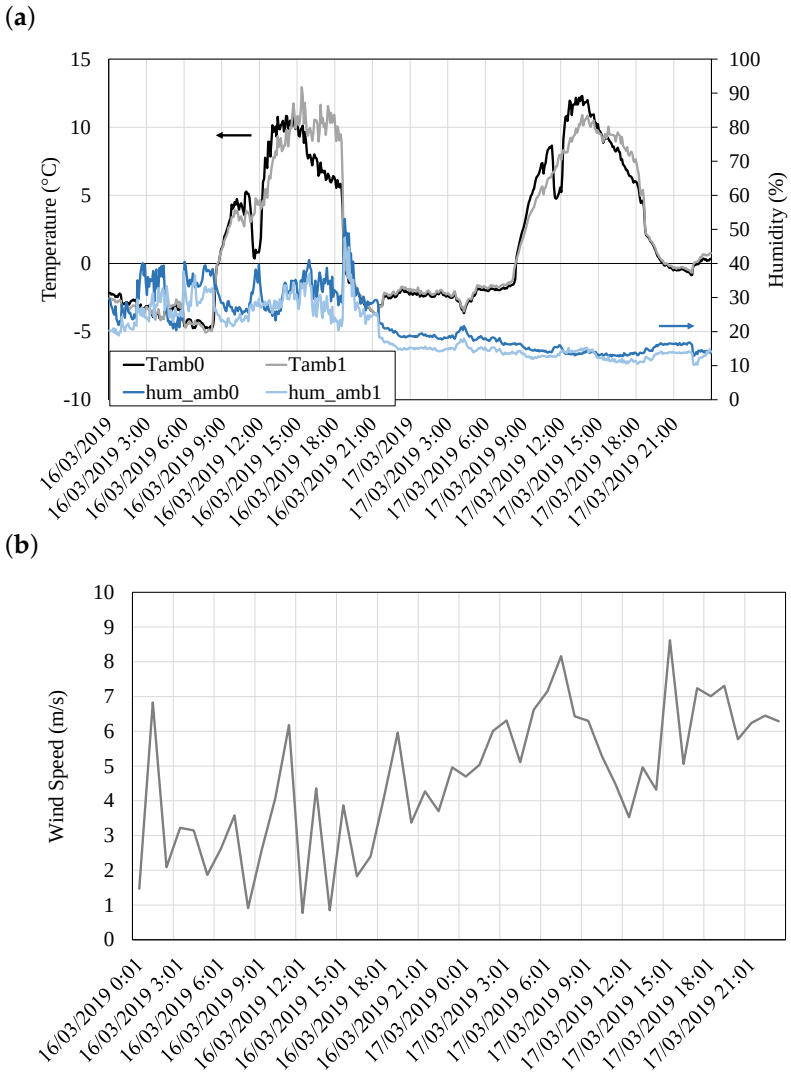

Figure 11. (**a**) Ambient temperature (left axis) and relative humidity (right axis) measured every 10 s. (**b**) Wind velocity measured every hour at a weather station nearby.

The maximum temperature difference achievable between the sides of the thermoelectric modules would equal the subtraction of ground temperature minus ambient temperature ($T_{ground} - T_{amb}$). Nevertheless, the real temperature difference of the thermoelectric modules is always lower. The discrepancy between the real and the ideal values depends on the installed heat exchangers. Thus, the lower the thermal resistance of the heat exchangers, the higher the temperature difference of the thermoelectric modules.

In this case, the two thermoelectric modules installed, the unsealed and the sealed Marlow TG12-8, have been assembled with the same heat exchangers. Hence, as shown in Figure 12, their temperature difference is similar and it is encompassed in the 36 to 46 °C range, depending on the ambient conditions. A slightly higher temperature difference can be appreciated in the case of the sealed module (3.6 °C more on average), which is believed to be because of thermal contact and assembly disparities rather than due to the sealant, since the manufacturer states the same behavior regardless of the addition or not of the protection sealant [48].

The effect of the importance of having heat exchangers with low thermal resistance can be also appreciated in Figure 12 comparing the temperature difference between the ground and the hot side of the module ($T_{ground} - T_h$) versus the difference between the cold side of the module and the ambient temperature ($T_c - T_{amb}$), this is the temperature difference in the hot and the cold side heat pipes.

Both heat exchangers had the same structure, but the cold side one included a series of fins. These fins increase the heat transfer area with the environment, which leads to a lower thermal resistance and therefore to a lower temperature difference in the cold side heat exchanger. Hence, the cold side heat pipe has a temperature difference between 8 and 21 °C while the hot side one presents a difference in the 15 to 27 °C range.

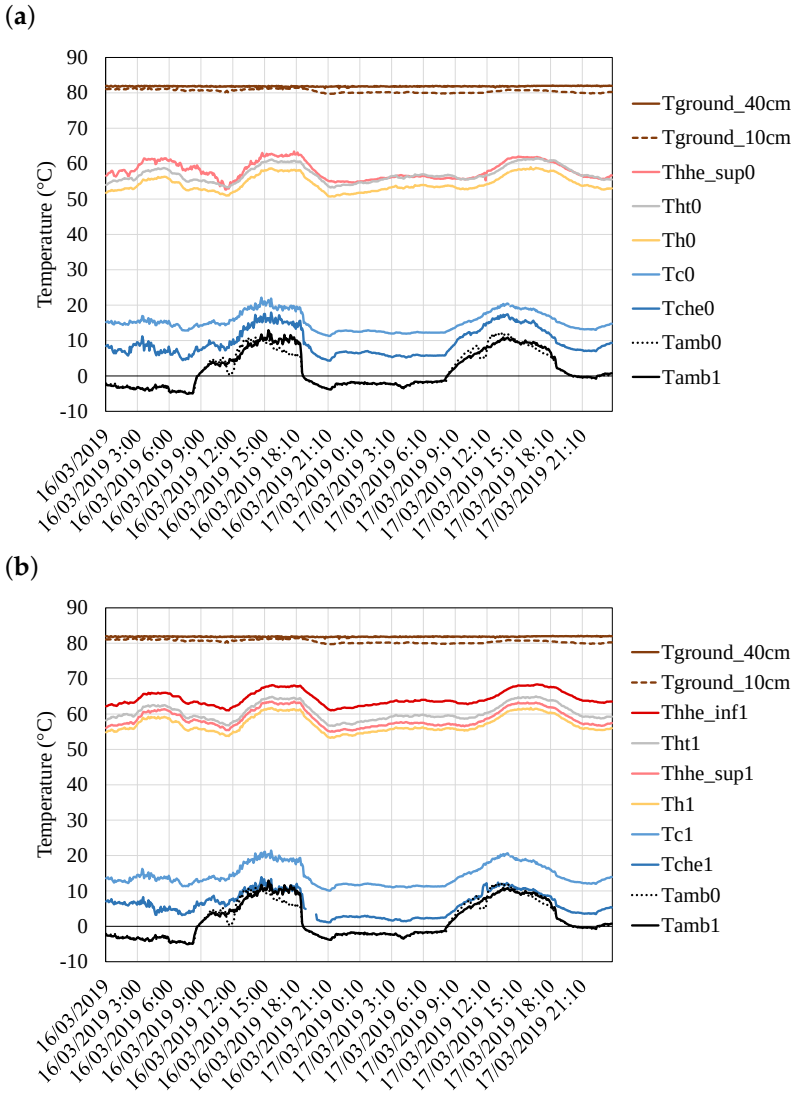

Figure 12. Temperature distribution of the prototype, separated into (**a**) the unsealed thermoelectric module and (**b**) the sealed one. T_{ground} represents the ground temperature measured at depths of 40, 10 and 5 cm; T_{hhe_inf} and T_{hhe_sup} are the temperatures in the lower and upper part of the hot side heat exchanger's tubes respectively; T_{ht} is the temperature of the aluminum plate of the hot side heat exchanger; T_h and T_c represent the hot and cold side of the modules; T_{che} is the temperature at the tubes of the cold side heat exchanger; and finally T_{amb} measures the ambient temperature.

Apart from the ground, the ambient as well as the modules' hot and cold side temperatures, more thermocouples have been installed in order to monitor the temperature at other interesting points. In the case of the cold side heat exchanger, T_{che} measured the temperature on the surface of two of the heat pipe tubes (one corresponding to each module), in the upper finned part. As can be seen in Figure 12, these temperatures are approximately in the middle of T_{che} and T_{amb}, showing that the convective component of the cold side heat pipe has the same weight in the thermal resistance that all the resting processes (conduction, boiling, and condensation).

In the case of the hot side heat exchanger, two tubes were selected (again one per each module) and thermocouples were located in their lower and upper parts, at a depth of 35 cm in the ground ($T_{hhe-inf}$) and in the bent part respectively ($T_{hhe-sup}$). In addition, two thermocouples measured the temperature T_{ht} at the base of this heat exchanger, before the heat extender introduced between the heat exchanger and the thermoelectric modules. These temperatures are also depicted in Figure 12. Firstly, it can be observed that the introduction of the heat extender causes a slight temperature loss in the hot side of the thermoelectric module, which is quantified at an average of 3 °C. In the case of not introducing it, the temperature of the hot side of the thermoelectric modules would slightly increase, but heat losses through thermal bridges will be higher, reducing total efficiency [49].

Secondly, regarding the temperatures of the tubes, when comparing the thermocouples corresponding to each module, it can be seen that the temperature of the upper part $T_{hhe-sup}$ is similar in both cases, with a tendency clearly affected by the ambient conditions and really close to T_{ht}. In the lower part, only $T_{hhe-inf-1}$ could be registered. This temperature is again influenced by the ambient conditions, and it is quite close to $T_{hhe-sup}$. Hence, heat transfer with the ground is the most critical component of the thermal resistance of the hot side heat exchanger. An increase of area, including vertical fins, would improve this heat transfer, leading to a lower thermal resistance and therefore an increase of the temperature difference of the modules and their generation.

Once the temperature distribution has been analyzed, Figure 13 (left axis) shows the generation of the two thermoelectric modules, being P_0 the power generated by the unsealed module and P_1 the power corresponding to the sealed one. The sealed module had a greater temperature difference between its sides that translates into a slightly higher generation in comparison with the unsealed one. Apart from this slight difference, both modules follow a similar generation tendency, increasing their generation during the night and decreasing it during the day. In order to have a better perception of this fact, the ambient temperature and the temperature difference accross both modules ΔT have been also represented in the right axis of Figure 13. During the night, ambient temperature decreases and therefore, the temperature difference of the modules increases, leading to a higher generation, which in the sealed module reached up to 0.33 W while in the unsealed one, 0.326 W. During the day, the temperature difference decreases, and so does the generation, with values of around 0.32 W. This effect occurs with a small delay due to the thermal inertia of the different components. Furthermore, it can be also observed that a lower temperature does not necessarily imply a greater generation. During the night of 16th March, the ambient temperature was lower than on the 17th of March. However, generation on the latter is greater due to the higher wind velocity, which improves the convection of the cold side heat exchanger, leading to a lower thermal resistance.

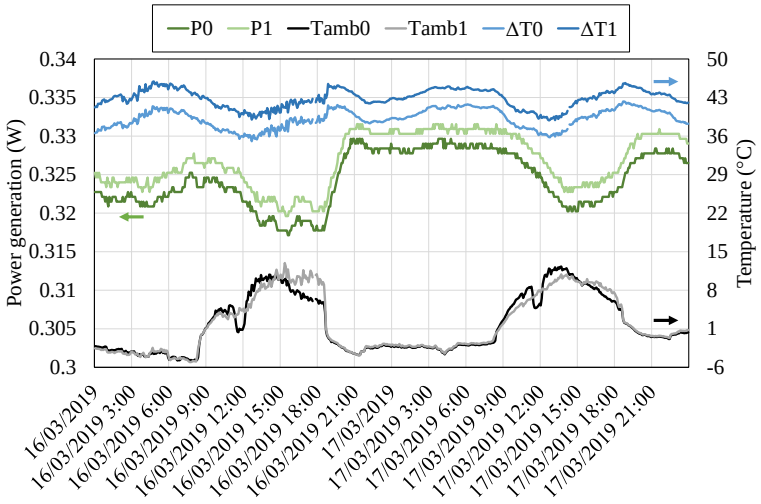

Figure 13. Power generated by the thermoelectric modules (left axis) and ambient temperature (right axis).

While the generation values could seem scarce, the obtained results are considered of great interest, since this generation can be used to supply power to volcanic monitoring stations, making them completely autonomous. As stated in the introduction, the power requirement of these stations is of just a few watts, and in some cases even of only milliwatts. The latter is the case of Awadallah et al., who required a power consumption of 0.34 mW on average [35]. Thus, the prototype developed in this paper would generate 1000 times more power than required, permitting the installation of more sensors. In those cases that present a higher consumption, one of the main advantages of the proposed device is that, due to the utilization of a constant heat source, the capacity of the required batteries can be greatly reduced, something really interesting since the installed batteries usually have really high capacities [61]. Moreover, the device is very compact and uses passive heat exchangers, reducing maintenance to a minimum due to the absence of mobile parts, aspects of great importance in the application under consideration. Its cost is neither an issue, as thermoelectric generators have demonstrated to be competitive in comparison with other technologies [62].

In order to fully demonstrate its viability, measures against corrosion need to considered. The monitoring of the different variables stopped after three days, on 19 March 2019. Three weeks later it was possible to examine the prototype, and it was discovered that corrosion had severely affected the electronics, as shown in Figure 14. Volcanic fumaroles present a composition of gases that includes hydrogen sulfide (H_2S). Water vapor reacts with hydrogen sulfide, leading to sulfuric acid, which highly corrodes metals, especially copper [63]. The plastic boxes where the electronics was introduced were not sealed, permitting the entry of gases and humidity, and causing corrosion.

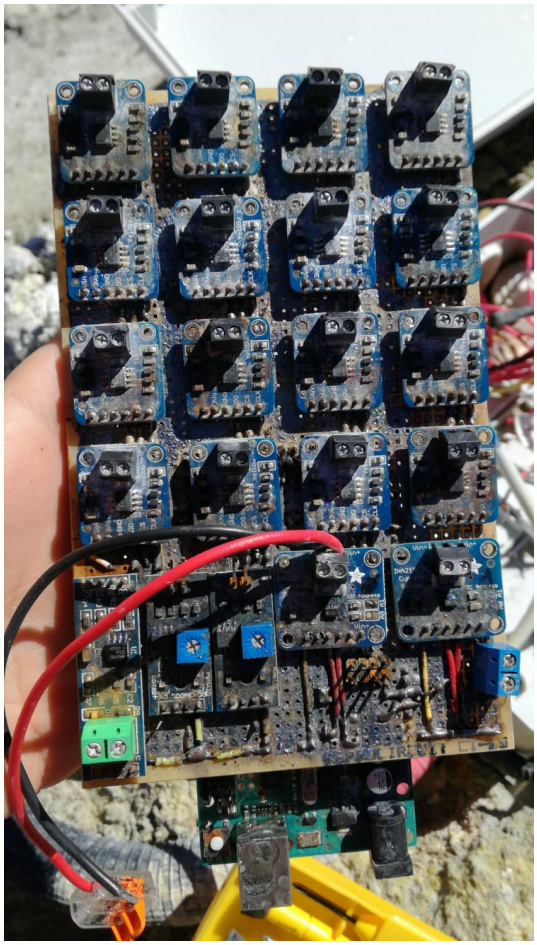

Figure 14. Corroded Printed Circuit Board (PCB) after one month of operation under volcanic conditions at Teide.

The heat pipe tubes that compose the prototype were also made of copper (nickel-plated), and therefore, signs of corrosion were also perceptible. Figure 15 shows the aluminum plate of the cold side heat exchanger after approximately one month of exposure to Teide's volcanic environment. As can be observed, excepting the graphite sheet where the thermoelectric modules were placed, all the surface is covered by yellowish deposits of sulfur, despite the fact that it was protected with neoprene and adhesive tape. Hence, in order to achieve the objective of autonomous volcanic monitoring stations, it is important to take measures against the corrosion, protecting better the electronics with a protection of at least IP64 [64], as well as using heat pipes made of more resistant materials such as steel or titanium [65,66], or with protective coatings [67], so that they can resist better in this acidic environment.

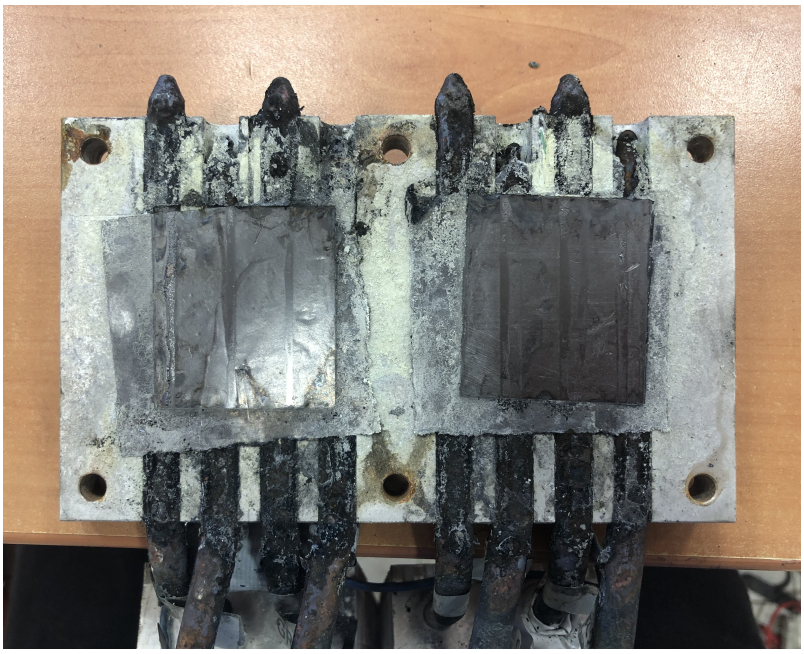

Figure 15. Corrosion of the cold side heat exchanger.

5. Conclusions

In conclusion, the present paper has experimentally demonstrated, for the first time, the feasibility of thermoelectric generators to generate electricity from fumaroles taking as reference Teide volcano (Canary Islands, Spain), which present 82 °C fumaroles. The installed thermoelectric generator is capable of generating between 0.32 and 0.33 W per module with a temperature difference between the heat reservoirs of 69 to 86 °C that includes ambient temperatures below 0 °C. This generation, thanks to the heat pipes used as heat exchangers, based on phase change, is obtained with no auxiliary consumption nor moving parts, leading to a robust generator. This result is especially interesting because the produced electricity could serve in order to supply energy to the volcanic monitoring stations that measure the precursors of the eruptions, making them completely autonomous. Nonetheless, for this purpose, it is necessary to protect the generator against the corrosion provoked by hydrogen sulfide reacting with steam and forming sulfuric acid, which virulently attacks metals, especially copper.

6. Patents

The mode of operation of the developed thermoelectric generation is patented under number WO 2019/202180 A1 [47].

Author Contributions: The main and most important part of this work has been carried out by L.C. with the supervision of D.A. In detail, the different parts have been developed as follows: Conceptualization, L.C., M.A., P.A., J.F.A. and D.A.; Data curation, L.C. and D.A.; Funding acquisition, P.A.H., N.M.P., C.G.d.l.N., J.F.A. and D.A.; Investigation, L.C. and M.A.; Methodology, L.C., M.A., G.D.P. and D.A.; Project administration, G.D.P., P.A.H. and

N.M.P.; Software, L.C.; Supervision, D.A.; Visualization, L.C.; Writing—original draft, L.C.; Writing—review & editing, L.C., P.A. and D.A. All authors have read and agreed to the published version of the manuscript.

Funding: This research was funded by the Spanish State Research Agency with FEDER–UE funds under grants number RTC-2017-6628-3 and RTI-2018-093501-B-C22.

Acknowledgments: We would like to acknowledge the support of FPU Program of the Spanish Ministry of Science, Innovation, and Universities (FPU16/05203). We also would like to ackcnowledge the technical support of Carlos Pérez (Constante Solar), Miguel Vera (Constante Solar), Vidal Dominguez (INVOLCAN), Ana Carolina Montañez (INVOLCAN) and José Barrancos (ITER).

Conflicts of Interest: The authors declare no conflict of interest.

Abbreviations

The following nomenclature has been used in this manuscript:

A	Area (m^2)
D	Diameter (m)
g	Gravity (m/s^2)
Gr	Grashof number
h	Heat transfer coefficient (W/m^2K)
Hum	Relative humidity (%)
I	Intensity (A)
k	Thermal conductivity (W/mK)
l	Characteristic length (m)
L	Length (m)
P	Power (W)
$\dot{Q}$	Heat flux (W)
R	Thermal resistance (K/W)
T	Temperature (°C)
V	Voltage (V)
ΔT	Temperature difference across the thermoelectric modules
η_{fins}	Efficiency of the fins
ν	Kinematic viscosity (m^2/s)

The following subscripts have been used in this paper:

0	Relative to the unsealed Marlow TG12-8-01L thermoelectric module
1	Relative to the sealed Marlow TG12-8-01LS thermoelectric module
amb	Ambient
b	Boiling
c	Cold side of the thermoelectric module
che	In the finned part of the cold side heat exchanger
cond	Condensation
conv	Convection
e	External
ev	Evaporator's base
ground_40cm	Buried in the ground at a depth of 40 cm
ground_5cm	Buried in the ground at a depth of 5 cm
ground_10cm	Buried in the ground at a depth of 10 cm
h	Hot side of the thermoelectric module
hhe_inf	In the lower part of the hot side heat exchanger
hhe_sup	In the upper part of the hot side heat exchanger
ht	In the aluminum plate of the hot side heat exchanger, before the heat extender
i	Internal
ins	In the exterior part of the insulation material
k	Conductive
losses	Thermal losses
s	Superficial

References

1. Definition of Fumarole. Available online: https://www.britannica.com/science/fumarole (accessed on 16 January 2020).
2. Inguaggiato, S.; Diliberto, I.S.; Federico, C.; Paonita, A.; Vita, F. Review of the evolution of geochemical monitoring, networks and methodologies applied to the volcanoes of the Aeolian Arc (Italy). *Earth-Sci. Rev.* **2018**, *176*, 241–276. [CrossRef]
3. Mori, T.; Hernandez, P.A.; Salazar, J.M.L.; Perez, N.M.; Notsu, K. An in situ method for measuring CO_2 flux from volcanic-hydrothermal fumaroles. *Chem. Geol.* **2001**, *177*, 85–99. [CrossRef]
4. Somma, R.; Troise, C.; Zeni, L.; Minardo, A.; Fedele, A.; Mirabile, M.; De Natale, G. Long-Term Monitoring with Fiber Optics Distributed Temperature Sensing at Campi Flegrei: The Campi Flegrei Deep Drilling Project. *Sensors* **2019**, *19*. [CrossRef]
5. Parri, R.; Lazzeri, F. Larderello: 100 years of geothermal power plant evolution in Italy. In *Geothermal Power*; DiPippo, R., Ed.; Elservier: Amsterdam, The Netherlands, 2016; pp. 537–590.
6. Gudmundsson, J.; Freeston, D.; Lienau, P. The Lindal Diagram. *GRC Trans.* **1985**, *9*, 15–17.
7. Operacz, A.; Chowaniec, J. Perspectives of geothermal water use in the Podhale Basin according to geothermal step distribution. *Geol. Geophys. Environ.* **2017**, *44*, 379–389. [CrossRef]
8. DiPippo, R. *Geothermal Power Plants. Principles, Applications, Case Studies and Environmental Impact*, 3rd ed.; Butterworth-Heinemann: Oxford, UK, 2012; ISBN 9780080982069.
9. Zarrouk, S.J.; Moon, H. Efficiency of geothermal power plants: A worldwide review. *Geothermics* **2014**, *51*, 142–153. [CrossRef]
10. Elghool, A.; Basrawi, F.; Ibrahim, T.K.; Habib, K.; Ibrahim, H.; Idris, D.M.; Nafiz, D. A review on heat sink for thermo-electric power generation: Classifications and parameters affecting performance. *Energy Convers. Manag.* **2017**, *134*, 260–277. [CrossRef]
11. Martinez, A.; Astrain, D.; Aranguren, P. Thermoelectric self-cooling for power electronics: Increasing the cooling power. *Energy* **2016**, *112*, 1–7. [CrossRef]
12. Tzeng, S.C.; Jeng, T.M.; Lin, Y.L. Parametric study of heat-transfer design on the thermoelectric generator system. *Int. Commun. Heat Mass Transf.* **2014**, *52*, 97–105. [CrossRef]
13. Aranguren, P.; Astrain, D.; Perez, M.G. Computational and experimental study of a complete heat dissipation system using water as heat carrier placed on a thermoelectric generator. *Energy* **2014**, *74*, 346–358. [CrossRef]
14. Aranguren, P.; Araiz, M.; Astrain, D. Auxiliary consumption: A necessary energy that affects thermoelectric generation. *Appl. Therm. Eng.* **2018**. [CrossRef]
15. Shabgard, H.;Allen, M.J.; Sharifi, N.; Benn, S.P.; Faghri, A.; Bergman, T.L. Heat pipe heat exchangers and heat sinks: Opportunities, challenges, applications, analysis, and state of the art. *Int. J. Heat Mass Transf.* **2015**, *89*, 138–158. [CrossRef]
16. Remeli, M.F.; Tan, L.; Date, A.; Singh, B.; Akbarzadeh, A. Simultaneous power generation and heat recovery using a heat pipe assisted thermoelectric generator system. *Energy Convers. Manag.* **2015**, *91*, 110–119. [CrossRef]
17. Araiz, M.; Martinez, A.; Astrain, D.; Aranguren, P. Experimental and computational study on thermoelectric generators using thermosyphons with phase change as heat exchangers. *Energy Convers. Manag.* **2017**, *137*, 155–164. [CrossRef]
18. Champier, D. Thermoelectric generators: A review of applications. *Energy Convers. Manag.* **2017**, *140*, 167–181. [CrossRef]
19. Yang, L.; Chen, Z.; Dargusch, M.S.; Zou, J. High Performance Thermoelectric Materials: Progress and Their Applications. *Adv. Energy Mater.* **2018**, *8*, 1701797. [CrossRef]
20. Li, K.; Bian, H.; Liu, C.; Zhang, D.; Yang, Y. Comparison of geothermal with solar and wind power generation systems. *Renew. Sustain. Energy Rev.* **2015**, *42*, 1464–1474. [CrossRef]
21. Suter, C.; Jovanovic, Z.R.; Steinfeld, A. A 1 kWe thermoelectric stack for geothermal power generation-Modeling and geometrical optimization. *Appl. Energy* **2012**, *99*, 379–385. [CrossRef]
22. Wang, K.; Wu, X. Downhole thermoelectric generation in unconventional horizontal wells. *Fuel* **2019**, *254*. [CrossRef]
23. Wang, K.; Wu, X. Downhole geothermal power generation in oil and gas wells. *Geothermics* **2018**, *76*, 141–148. [CrossRef]

24. Liu, C.; Chen, P.; Li, K. Geothermal Power Generation Using Thermoelectric Effect. *GRC Trans.* **2013**, *37*, 733–738.
25. Liu, C.; Chen, P.; Li, K. A 500 W low-temperature thermoelectric generator: Design and experimental study. *Int. J. Hydrog. Energy* **2014**, *39*, 15497–15505. [CrossRef]
26. Liu, C.; Chen, P.; Li, K. A 1 KW Thermoelectric Generator for Low-temperature Geothermal Resources. In Proceedings of the Thirty-Ninth Workshop on Geothermal Reservoir Engineering, Stanford, CA, USA, 24–26 February 2014; pp. 1–12; ISBN 9781634394673.
27. Ahiska, R.; Mamur, H. Design and implementation of a new portable thermoelectric generator for low geothermal temperatures. *IET Renew. Power Gener.* **2013**, *7*, 700–706. [CrossRef]
28. Ahiska, R.; Mamur, H. Development and application of a new power analysis system for testing of geothermal thermoelectric generators. *Int. J. Green Energy* **2016**, *13*, 672–681. [CrossRef]
29. Trip, N.D.; Burca, A.; Morgos, L. Considerations on the use of thermoelectric generators at low temperatures to recover waste geothermal energy. In Proceedings of the 14th International Conference on Engineering of Modern Electric Systems, EMES 2017, Oradea, Romania, 1–2 June 2017; pp. 248–251. [CrossRef]
30. Catalan, L.; Aranguren, P.; Araiz, M.; Perez, G.; Astrain, D. New opportunities for electricity generation in shallow hot dry rock fields: A study of thermoelectric generators with different heat exchangers. *Energy Convers. Manag.* **2019**, *200*. [CrossRef]
31. Melian, G.; Tassi, F.; Perez, N.M.; Hernandez, P.A.; Sortino, F.; Vaselli, O.; Padron, E.; Nolasco, D.; Barrancos, J.; Padilla, G.; et al. A magmatic source for fumaroles and diffuse degassing from the summit crater of Teide Volcano (Tenerife, Canary Islands): A geochemical evidence for the 2004–2005 seismic-volcanic crisis. *Bull. Volcanol.* **2012**, *74*, 1465–1483. [CrossRef]
32. Perez, N.M.; Hernandez, P.A.; Padron, E.; Melian, G.; Nolasco, D.; Barrancos, J.; Padilla, G.; Calvo, D.; Rodriguez, F.; Dionis, S.; et al. An increasing trend of diffuse CO_2 emission from Teide volcano (Tenerife, Canary Islands): Geochemical evidence of magma degassing episodes. *J. Geol. Soc.* **2013**, *170*, 585–592. [CrossRef]
33. Peci, L.M.; Berrocoso, M.; Fernandez-Ros, A.; Garcia, A.; Marrero, J.M.; Ortiz, R. Embedded ARM System for Volcano Monitoring in Remote Areas: Application to the Active Volcano on Deception Island (Antarctica). *Sensors* **2014**, *14*, 672–690. [CrossRef] [PubMed]
34. Moure, D.; Torres, P.; Casas, B.; Toma, D.; Blanco, M.J.; Del Rio, J.; Manuel, A. Use of Low-Cost Acquisition Systems with an Embedded Linux Device for Volcanic Monitoring. *Sensors* **2015**, *15*, 20436–20462. [CrossRef] [PubMed]
35. Awadallah, S.; Moure, D.; Torres-Gonzalez, P. An Internet of Things (IoT) Application on Volcano Monitoring. *Sensors* **2019**, *19*. [CrossRef]
36. Seyoun, B.B.; Rossi, M.; Brunelli, D. Energy Neutral Wireless Bolt for Safety Critical Fastening. *Sensors* **2017**, *17*. [CrossRef]
37. Magno, M.; Sigrist, L.; Gomez, A.; Cavigelli, L.; Libri, A.; Popovici, E.; Benini, L. SmarTEG: An Autonomous Wireless Sensor Node for High Accuracy Accelerometer-Based Monitoring. *Sensors* **2019**, *19*. [PubMed]
38. Saraereh, O.; Alsaira, A.; Khan, I.; Choi, B.J. A Hybrid Energy Harvesting Design for On-Body Internet-of-Things (IoT) Networks. *Sensors* **2020**, *20*. [CrossRef] [PubMed]
39. Foley, W.; Dell, R.; Wei, C.S.; Unnthorsson, R. Point of use thermoelectric powered automated irrigation system for an intesive shallow bottom heat system using waste geothermal hot water and steam condensate in Iceland. *Trans. Geotherm. Resour. Counc.* **2015**, *2015*, 117–124.
40. Dell, R.; Unnthorsson, R.; Wei, C.S.; Mitchell, N. A Thermoelectric Powered Quadruped Robotic System for Remote Monitoring of Geothermal Open Field Heated Gardens in Iceland. *GRC Trans.* **2016**, *40*, 173–180.
41. Dell, R.; Wei, C.S.; Petralia, M.T.; Gislason, G.; Unnthorsson, R. Thermoelectric Powered Security Systems in Iceland Using a Geothermal Steam Pipe as a Heat Source. *Proceedings* **2018**, *2*, 440. [CrossRef]
42. Stokes, C.D.; Duff, E.; Mantini, M.J.; Grant, B.; Venkatasubramanian, R. Nanostructured thermoelectric material and device technology for energy harvesting applications. In Proceedings of the 2010 IEEE Nanotechnology Materials and Devices Conference, Monterey, CA, USA, 12–15 October 2010; pp. 154–159. [CrossRef]
43. Wang, N.; Xu, D.; Li, W.; Chen, C.; Huang, Y. Feasibility study of a new thermoelectric conversion device utilizing the temperature differences in forest soil. *Acta Tech. CSAV (Ceskoslovensk Akademie Ved)* **2017**, *62*, 1–12.

44. Huang, Y.; Xu, D.; Kan, J.; Li, W. Study on field experiments of forest soil thermoelectric power generation devices. *PLoS ONE* **2019**, *14*, 1–13. [CrossRef]
45. Huang, Y.; Li, W.; Xu, D.; Wu, Y. Spatiotemporal rule of heat transfer on a soil/finned tube interface. *Sensors* **2019**, *19*. [CrossRef]
46. Astrain, D.; Vian, J.G.; Martinez, A.; Rodriguez, A. Study of the influence of heat exchangers' thermal resistances on a thermoelectric generation system. *Energy* **2010**, *35*, 602–610. [CrossRef]
47. Astrain, D.; Catalan, L.; Aranguren, P.; Araiz, M. Thermoelectric Generator with no Moving Parts Applied to Geothermal Energy. WO Patent 2019/202180 A1, 24 October 2019.
48. II-VI Marlow. Technical Data Sheet for TG12-8. Available online: https://cdn2.hubspot.net/hubfs/547732/Data_Sheets/TG12-8.pdf (accessed on 10 November 2018).
49. Araiz, M.; Catalan, L.; Herrero, O.; Perez, G.; Rodriguez, A. The importance of the assembly in thermoelectric generators. In *Bringing Thermoelectricity into Reality*; Aranguren, P., Ed.; IntechOpen: London, UK, 2018; pp. 123–144; ISBN 978-1-78923-440-4. [CrossRef]
50. Coleman, H.W.; Steele, W.G. *Experimentation, Validation and Uncertainty. Analysis for Engineers*, 3rd ed.; Wiley: Hoboken, NJ, USA, 2009.
51. Incropera, F.P.; DeWitt, D.P. *Principles of Heat and Mass Transfer (Spanish version)*, 4th ed.; Prentice Hall: Mexico, 1999.
52. Panasonic Industry. Thermal Protection: Pyrolitic Graphite Sheet (PGS). Available online: https://eu.industrial.panasonic.com/products/circuit-thermal-protection/thermal-protection/pyrolytic-graphite-sheet-pgs (accessed on 16 December 2019).
53. Adafruit. Thermocouple Amplifier MAX31855 Breakout Board. Available online: https://www.adafruit.com/product/269 (accessed on 7 January 2020).
54. K-Electronica. Temperature and Humidity Sensor DTH22. Available online: http://k-electronica.es/complementos/235-sensor-de-temperatura-y-humedad-dht22-compatible-arduino-en-tenerife-canarias-la-laguna-8436545519684.html?search_query=humedad&results=10 (accessed on 14 January 2020).
55. K-electronica. Soil Humidity Sensor. Available online: http://k-electronica.es/complementos/244-sensor-de-humedad-del-suelo-para-arduino-en-tenerfie-canarias-la-laguna-8436545519769.html?search_query=humedad&results=10 (accessed on 14 January 2020).
56. Adafruit. INA219 High Side DC Current Sensor Breakout. Available online: https://www.adafruit.com/product/904 (accessed on 17 January 2020).
57. Lopez-Lapeña, O.; Penella, M.T.; Gasulla, M. A New MPPT Method for Low-Power Solar Energy Harvesting. *IEEE Trans. Ind. Electron.* **2010**, *57*, 3129–3138. [CrossRef]
58. Rawy, K.; Yoo, T.; Kim, T.T. An 88% Efficiency 0.1–300-µW Energy Harvesting System with 3-D MPPT Using Switch Width Modulation for IoT Smart Nodes *IEEE J. Solid-State Circuits* **2018**, *53*, 2751–2762. [CrossRef]
59. K-electronica. MAX485CSA Converter RS-485 TTL to RS485 for Arduino. Available online: http://k-electronica.es/complementos/274-convertidor-max485csa-max485-rs-485-ttl-a-rs485-para-arduino-en-tenerife-canarias-la-laguna-8436545520000.html?search_query=RS485&results=1 (accessed on 17 January 2020).
60. Adafruit. 4-Channel I2C-Safe Bi-Directional Logic Level Converter. Available online: https://www.adafruit.com/product/757 (accessed on 29 January 2020).
61. Terray, L.; Royer, L.; Sarramia, D.; Achard, C.; Bourdeau, E.; Chardon, P.; Claude, A.; Fuchet, J.; Gauthier, P.J.; Grimbichler, D.; et al. From Sensor to Cloud: An IoT Network of Radon Outdoor Probes to Monitor Active Volcanoes. *Sensors* **2020**, *20*. [CrossRef]
62. Araiz, M.; Casi, A.; Catalan, L.; Martinez, A.; Astrain, D.; Prospects of waste-heat recovery from a real industry using thermoelectric generators: Economic and power output analysis. *Energy Convers. Manag.* **2020**, *205*. [CrossRef]
63. Watanabe, M.; Hokazono, A.; Handa, T.; Ichino, T.; Kuwaki, N. Corrosion of copper and silver plates by volcanic gases. *Corros. Sci.* **2006**, *48*, 3759–3766. [CrossRef]
64. International Electrotechnical Commission. *IEC 60529: Degrees of Protection Provided by Enclosures (IP Code)*; National Electrical Manufacturers Association: Rosslyn, VA, USA, 2004.
65. Htun, K.M. *Materials Compatibility with the Volcanic Environment. Technical Report.* U.S. Department of Energy: Nevada, NV, USA, 1984.

66. Mohan, P.S.; Sundaram, M.; Guruviah, S. Corrosion of metals in sulphur dioxide atmosphere—A laboratory study. *Key Eng. Mater.* **1991**, *20–28*, 179–184. [CrossRef]
67. Hempel. Hempadur 85671 Data Sheet. Available online: https://www.hempel.es/es-ES/products/hempadur-85671 (accessed on 7 October 2019).

Chapter 6

Stand–alone Power Supply of Volcanic Monitoring Stations with Thermoelectric Generators

The previous publication has demonstrated that thermoelectric generation from fumaroles is possible, obtaining values one order of magnitude higher than the typical ones available in the literature with other geothermal thermoelectric generators oriented to sensors. Nevertheless, it became evident the harsh conditions that need to be withstood by the device. In order to obtain completely autonomous volcanic vigilance stations powered by thermoelectric generators, it will be necessary to deal with these conditions, taking the actions deemed appropriate.

Based on the knowledge acquired with the first prototype, in this chapter, an optimized device has been designed and constructed, including several corrosion protection measures. This prototype is again composed of phase change heat exchangers due to their low thermal resistances without moving parts nor auxiliary equipment, which removes maintenance requirements. Furthermore, apart from the development of the generator itself, this chapter also takes a step forward, developing the electronic system required to obtain a completely autonomous volcanic vigilance station, which includes maximum power point trackers (MPPTs), a small storage system, a microcontroller, several sensors and a communication system to send the measured data to a center located various kilometers away.

The device has been perfectly characterized at the laboratories of the Public University of Navarre, obtaining the thermal resistance of the heat exchangers, the optimal generation

of the device, and the consumption of the developed electronic system. After this characterization, the device was installed again at Teide volcano, where it has been on operation for more than six months.

The attainment of this milestone has been reflected in the paper "Experimental evidence of the viability of thermoelectric generators to power volcanic monitoring stations" published in the journal *Sensors* 20 (2020) 4839. This paper analyze the results obtained in the period from 18^{th} December 2019 to 20^{th} August 2020. Nonetheless, on the date of presentation of this Ph. D. dissertation the prototype was still on operation.

sensors

MDPI

Article

Experimental Evidence of the Viability of Thermoelectric Generators to Power Volcanic Monitoring Stations

Leyre Catalan *, Amaia Garacochea, Alvaro Casi, Miguel Araiz, Patricia Aranguren and David Astrain

Department of Engineering, Institute of Smart Cities, Public University of Navarre, 31006 Pamplona, Spain; amaia.garacochea@unavarra.es (A.G.); alvaro.casi@unavarra.es (A.C.); miguel.araiz@unavarra.es (M.A.); patricia.arangureng@unavarra.es (P.A.); david.astrain@unavarra.es (D.A.)

* Correspondence: leyre.catalan@unavarra.es; Tel.: +34-948-16-84-41

Received: 27 July 2020; Accepted: 23 August 2020; Published: 27 August 2020

Abstract: Although there is an important lack of commercial thermoelectric applications mainly due to their low efficiency, there exist some cases in which thermoelectric generators are the best option thanks to their well-known advantages, such as reliability, lack of maintenance and scalability. In this sense, the present paper develops a novel thermoelectric application in order to supply power to volcanic monitoring stations, making them completely autonomous. These stations become indispensable in any volcano since they are able to predict eruptions. Nevertheless, they present energy supply difficulties due to the absence of power grid, the remote access, and the climatology. As a solution, this work has designed a new integral system composed of thermoelectric generators with high efficiency heat exchangers, and its associated electronics, developed thanks to Internet of Things (IoT) technologies. Thus, the heat emitted from volcanic fumaroles is transformed directly into electricity with thermoelectric generators with passive heat exchangers based on phase change, leading to a continuous generation without moving parts that powers different sensors, the information of which is emitted via LoRa. The viability of the solution has been demonstrated both at the laboratory and at a real volcano, Teide (Canary Islands, Spain), where a compact prototype has been installed in an 82 °C fumarole. The results obtained during more than eigth months of operation prove the robustness and durability of the developed generator, which has been in operation without maintenance and under several kinds of meteorological conditions, leading to an average generation of 0.49 W and a continuous emission over more than 14 km.

Keywords: thermoelectric generator; volcano surveillance; power supply; geothermal; LoRa; autonomous; heat pipe

1. Introduction

Volcanoes are considered one of the most dangerous natural hazards [1]. Nowadays, more than 10% of the global population lives within 100 km of a volcano that has the potential to erupt [2]. Therefore, volcanic vigilance becomes indispensable in any volcanic system of the world, so that the damage caused by the inevitable eruptions can be reduced.

Normally, volcanic eruptions are preceded by anomalous signals, known as precursors [3,4]. Volcanic vigilance consists in the monitoring of these signals in order to, together with knowledge of past activity, predict when, where, and how the next volcanic eruption will occur. For this purpose, due to the diverse nature of the different manifestations of volcanic activity, volcano surveillance requires the combination of different techniques, the data of which needs to be analyzed together.

Seismology studies the earthquakes and other generating events of seismic waves [5]; geodesy focuses on the variations in the shape and dimensions of the Earth [6]; geochemistry studies the change in temperature and composition of the volcanic products [7]; gravimetry deals with variations of the gravitational forces [8]; and magnetotellurics analyzes the fluctuations in the electromagnetic fields of the Earth [9].

In order to obtain data, most of the previous techniques use local measurements. There exist some remote methodologies such as GPS, GNSS, InSAR or satellite temperature monitoring [10,11]. Nevertheless, local measurements are preferred due to their better accuracy and the coverage of all techniques [12]. Among local measurements, two trends can be in turn distinguished: continuous and discontinuous data acquisition [13]. In the former, permanent vigilance stations are installed in key locations, while the latter consists in performing in situ manual measurements. In general, if possible, continuous monitoring is more recommended, due to its lower cost (does not require several people taking measurements) and more information provided. Nevertheless, power supply and communication systems of such stations constitute a challenge [12], since volcanic areas are usually remote, inaccessible, and lack a power grid. This causes that only 30% of active volcanoes have instrumentation to measure their activity [14].

In order to face the previous situation, the most common alternative consists in using photovoltaic panels and, consequently, batteries, so that power supply is ensured during nights, periods of absence of sun, or episodes of volcanic ashes [15,16]. However, sometimes, depending on the climatology and the specific conditions, the required capacity of the batteries is so high that it is preferred to lose data during some periods, rather than deal with the installation difficulties of an enormous battery in a remote and inaccessible location. This is the case of those volcanoes that record severe snowfalls during long periods in winter such as Mt. Fuji in Japan [17], or that are located at extreme latitudes where the sun does not shine for months, like Deception Island in Antarctica [18].

In the last years, with the purpose of reducing the capacity of the batteries, low-energy devices have proliferated, focusing on both data acquisition and communications. Hence, it stands out the use of systems with embedded Linux, which permit real-time monitoring with a power consumption lower than 2.5 W [16,18,19]. These systems are usually combined with communication technologies normally associated with Internet of Things (IoT). For instance, Awadallah et al. developed a wireless network of thermometers to measure soil temperatures in volcanic areas based on LoRa [20]. LoRaWAN protocol was also chosen by Terray et al., but in this case to control soil radon emissions [21].

Apart from reducing the consumption of the different elements that compose a vigilance station, another solution consists in using an alternative energy source, such as geothermal energy, which presents the advantage of being always available independently of weather. In active volcanoes, the most evident manifestation of geothermal energy coincides with one of the signs of active volcanism: fumaroles, vents in the Earth's surface from which steam and volcanic gases are emitted, normally at temperatures between 70 and 100 °C [22]. Hence, this solution fits in the proverb "*if you cannot beat them, join them*".

Traditional geothermal cycles are not suitable for low-scale power generation from volcanic fumaroles. Nonetheless, thermoelectric generators could become an alternative. Thermoelectric generators are devices based on solid state physics whereby heat (i.e., temperature difference) is directly transformed into electricity by means of the Seebeck effect. Thanks to these devices, the operation of which is more deeply described in Section 2, it is possible to generate electricity continuously from geothermal heat [23,24], even improving with adverse meteorological conditions, thus permitting a reduction in the capacity of the batteries or the utilization of other storage technologies such as supercapacitors. Furthermore, these devices are modular, compact, and have demonstrated their reliability and durability without maintenance requirements in spatial applications [25].

Considering the former advantages, the use of thermoelectric generators have already been proposed to power ground sensors. Due to the difference in heat capacity and conduction rate between the air and the ground, there normally exists a temperature difference between them [26].

Lawrence [27] and Stevens [28] demonstrated that this temperature difference can be transformed into electricity by means of thermoelectric generators, permitting the power supply of remote sensors. As indicated by Stokes et al., this type of self-sufficient power source could serve for unattended ground sensors (UGS) in defense and security [29]. They experimented with this proposal at the laboratory, developing a complete sensor consisting of a thermoelectric generator, a DC-DC boost converter, a wireless sensor transmitter, and supercapacitors, which presented good performance with temperature differences as low as 1 °C.

Forest monitoring is another possible application. Similarly to volcano surveillance, forests are also monitored in order to analyze the impact of droughts or fires, to uncover their structure, and to study variations of their biota, for which wireless sensors are used [30–32]. Nevertheless, these sensors also present energy supply problems due to their remoteness. As a solution, Wang et al. proposed the utilization of thermoelectric generators to provide a stable power supply, taking advantage of the mentioned temperature difference between the ground and the air [33]. Huang et al. improved the previous micro-generator and performed field experiments under natural conditions in two different locations [34]. The results obtained over six months reveal that the location influences the power generation that can be obtained. Hence, in Harbin an average of 0.335 mW were generated, while in Beijing, only 0.076 mW could be produced. In a later article, they concluded that in order to efficiently harvest micro-energy from shallow soil, the thermoelectric generator needs to be placed where the soil moisture is greater than 30% [35].

Roadway and bridge infrastructures also require energy harvesting in order to power a multitude of data collection and communication applications [36]. For this purpose, it is considered that thermoelectric generators are one of the most readily available methods [37], transforming the heat absorbed from the exposure to solar radiation into electricity. For instance, Tahami et al. fabricated a system to embed into asphalt pavements, so that with the temperature difference between the pavement surface and the soil below it, electricity could be generated. They optimized and tested a prototype in the field, obtaining 29 mW [38]. Another alternative consists in making use of the temperature difference between road surface and ambient air, as proposed by Jiang et al., who obtained up to 45 mW [39].

Thermoelectric generators can also represent a solution for the power supply of volcanic monitoring stations. In comparison with the previous examples, this application presents the advantage of having a heat source with higher temperature, which is beneficial for the efficiency improvement of thermoelectric generators. In contrast, the device needs to operate in a harsher environment and requires to be more robust, being able to work without maintenance, for which moving parts should be avoided.

The objective of the present paper is to develop an autonomous and robust volcanic monitoring station powered by thermoelectric generators. For this purpose, Section 2 details the operation of thermoelectric generators in their application to volcanic fumaroles; Section 3 describes the thermoelectric generator that has been developed; Section 4 characterizes the previous generator at the laboratory; Section 5 details the electronics of the device, also analyzing alternative communication systems typically associated with Internet of Things (IoT); Section 6 examines the behavior of the complete system in a real volcano; Section 7 studies supplying power to a real vigilance station; and finally Section 8 summarizes the main contributions of the present paper.

2. Operation of a Geothermal Thermoelectric Generator (GTEG)

As exposed in the introduction, thermoelectric generators are devices based on solid state physics whereby heat (i.e., temperature difference) is directly transformed into electricity by means of the Seebeck effect. This transformation is held in the so-called thermoelectric modules, the efficiency of which is proportional to the temperature difference between their sides. In order to maximize this temperature difference, the introduction of heat exchangers with low thermal resistances becomes indispensable, so that the temperature of the hot side of the thermoelectric modules approaches to

the temperature of the heat source, and the temperature of the cold side does the same with respect the dissipation sink (normally the environment). An 8% higher generation can be obtained with a reduction of 10% in the thermal resistance of the heat exchangers [40]. Fin dissipators, heat exchangers with a fluid as heat carrier, heat pipes, and thermosyphons are the most common heat exchangers used in thermoelectric generators [41].

Thanks to these devices, it is possible to generate electricity directly, avoiding the intermediate conversion of thermal energy into mechanical energy; regardless of the source temperature, only a temperature gradient is required; durably, as demonstrated in spatial applications; with scalability possibilities, increasing the installed power just by adding more thermoelectric modules; and without moving parts, working fluids and noise in the operation of their main element, the thermoelectric modules [42]. As a drawback, they present a very low efficiency, which can be rated between 2 and 5% depending on the temperature range. Nevertheless, as derived from the introduction, there exist some applications in which the benefits of thermoelectric generators counteract their main disadvantage, becoming the best alternative. This is the case of supplying power to volcanic monitoring stations, the application under consideration in the present paper.

In this application, fumaroles represent the heat source. These fumaroles, in their emergence to the surface, heat up and moisten the soil. Hence, due to the low heat transfer coefficient of gases, the thermoelectric generator responsible for the power supply will be directly in contact with the hot and wet soil. For depths higher than 10% it is considered that the temperature of the soil equals the fumaroles' one and that the soil moisture is close to 90%, thus a good heat transfer from the soil is expected [35].

The purpose of the hot side heat exchanger consists of absorbing the volcanic heat underground and transmitting it, with a minimal temperature difference to the thermoelectric modules located overground, so that the hot side of the thermoelectric modules approaches the temperature of the fumaroles. Catalan et al. demonstrated that heat exchangers based on phase change are the most adequate ones for this task [43], and therefore, will be the ones considered in this paper. As depicted in Figure 1, this type of heat exchanger is made of one or several tubes with an internal fluid in their interior. In contact with the heat source, the internal fluid vaporizes, occupying all the available space. Afterward, this vapor condensates releasing heat to the thermoelectric modules. If the condensed fluid returns to the evaporator part only due to gravity, the heat exchanger is known as thermosyphon, while if a wick material is introduced so that it can work in any position, the term heat pipe is used. Lawrence, Wang et al., and Huang et al. also used phase change heat exchangers, specifically heat pipes, to absorb heat from the soil and transfer it to the thermoelectric modules [27,33–35].

The heat that is not transformed into electricity by the thermoelectric modules needs to be dissipated into the environment, again with a heat exchanger with a minimal thermal resistance so that the cold side of the thermoelectric modules approach the ambient temperature. In the previous examples [27,33–35], fin dissipators in natural convection were used due to their simplicity and low cost. Nonetheless, in this case, heat exchangers based on phase change will be again used since they have demonstrated to be the most suitable ones for the cold side of the modules, leading to low thermal resistances without requiring auxiliary consumption [43,44]. Their mode of operation is similar to the hot side one, with cyclic vaporization and condensation of the internal fluid, although in this case heat is absorbed from the thermoelectric modules and released into the environment (Figure 1). The main difference between them is that in the cold side heat exchangers, in order to improve convection between the exterior part of the tube and the ambient, fins are normally added, so that the heat exchange area is increased.

Altogether, the use of heat exchangers based on phase change leads to a noiseless, compact, robust, and modular generator, with no auxiliary consumption nor moving parts, and therefore without maintenance requirements. Furthermore, since a constant temperature heat source is being used, a continuous power supply is obtained.

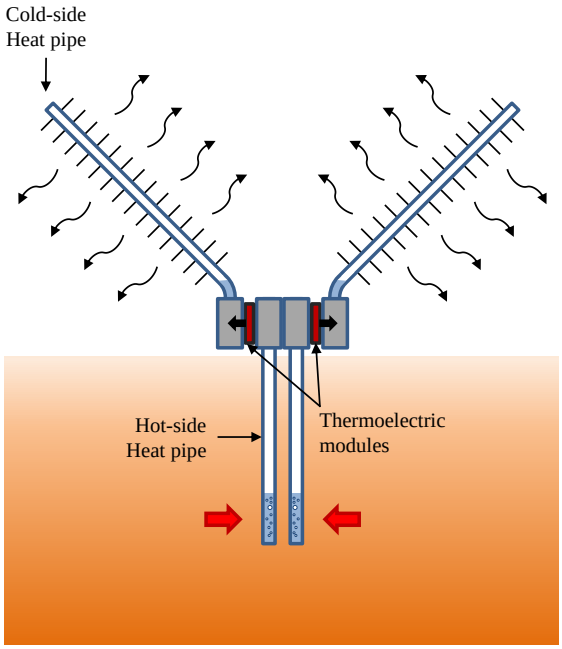

Figure 1. Schematics of a geothermal thermoelectric generator (GTEG) with heat pipes as heat exchangers.

3. Prototype Description

Figure 2 depicts the thermoelectric generator developed in the present paper to be installed in volcanic fumaroles and supply power to volcanic monitoring stations. The prototype is composed of two thermoelectric modules, each of them with its own heat exchangers.

Figure 2. Designed thermoelectric generator composed of two thermoelectric modules and heat pipes as heat exchangers.

The hot side heat exchanger of each module is composed of four 450 mm long copper sintered heat pipes with an external diameter of 8 mm. The tubes have been inserted in an $82 \times 50 \times 20\,mm^3$ aluminum plate in which four holes with a slightly smaller diameter than the heat pipes have been drilled with a separation of 3 mm, so that a good thermal contact is ensured.

Each cold side heat exchanger has also been manufactured with the former procedure. Nonetheless, in this case, 500 mm long heat pipes have been inserted in the base of an aluminum fin dissipator. This dissipator has a base of $82 \times 50 \times 14.5\,mm^3$ and seventeen $40 \times 1.5\,mm^2$ corrugated fins. Fins have also been inserted on the heat pipe tubes in order to increase the heat exchange area and therefore, improve heat dissipation to the environment. More specifically, 72 aluminum $104 \times 27.5 \times 0.3\,mm^3$ fins have been added with a separation of 5 mm.

The hot and cold heat exchangers are assembled by means of four M5 threaded rods, which due to their closeness, ensure a good pressure distribution in the thermoelectric modules and therefore a suitable thermal contact [45]. For compactness, the same threaded rods are used to assembly a generator with two thermoelectric modules, as shown in Figure 2. In this paper, commercial bismuth telluride modules have been used. More specifically, Marlow TG12-8-01LS [46]. These modules are sealed with silicone, so that the thermocouples are protected, something especially important in this application due to the harsh volcanic environment.

The heat exchangers also need to be protected. Hence, the heat pipes of the hot side heat exchanger have been coated with an epoxy-based primer [47], while the cold side ones with a marine primer [48]. Furthermore, the weakest parts, such as the ends of the heat pipes and the inter-phases with the aluminum plates or the fin dissipators, have been protected with an epoxy adhesive [49].

4. Laboratory Characterization

This section details the characterization of the previous prototype at the laboratory. First, it describes the characterization of the cold side heat exchanger. Afterward, the complete characterization of the whole thermoelectric generator is developed.

The characterization of the cold side heat exchanger (CHE) refers to the determination of its thermal resistance for different heat fluxes. For this purpose, a $40 \times 40\,mm^2$ heating plate has been used to provide the desired heat flux $\dot{Q}_{CHE}$ in each experiment, and the temperature at the base of the heat exchanger T_b and in the climatic chamber T_{amb} have been measured. Thanks to these measurements, the thermal resistance has been calculated according to Equation (1). Each experiment has been repeated three times and the uncertainties have been obtained with [50], considering thermocouples with precision $\pm 1\,°C$. Insulation was also added to ensure that all the heat flux went through the heat exchanger.

$$R_{CHE} = \frac{T_b - T_{amb}}{\dot{Q}_{CHE}} = \frac{T_b - T_{amb}}{V \cdot I} \quad (1)$$

Figure 3 shows the thermal resistance of the heat exchanger with respect to the heat flux for the two conditions studied: natural and forced convection, the latter with a wind velocity of 4 m/s. As can be observed, in both cases the thermal resistance decreases as the heat flux increases. This occurs because the properties of the internal working fluid, which is cyclically experimenting phase change, improve with temperature, thus decreasing the thermal resistance for higher heat fluxes.

The former decrease is more noticeable for natural convection, where the thermal resistance diminishes from 0.68 K/W with 20 W, to 0.49 K/W with 100 W. In contrast, for forced convection the thermal resistance barely decreases 0.01 K/W from 20 to 120 W, presenting an average value of 0.24 K/W. The heat transfer coefficient in natural convection strongly depends on the temperature difference between the surface of the heat exchanger and the environment, improving with higher gradients. Nevertheless, in forced convection, this effect blurs in favor of the influence of wind velocity. Considering that this paper considers an outdoor application, the values of thermal resistance with forced convection are more representative.

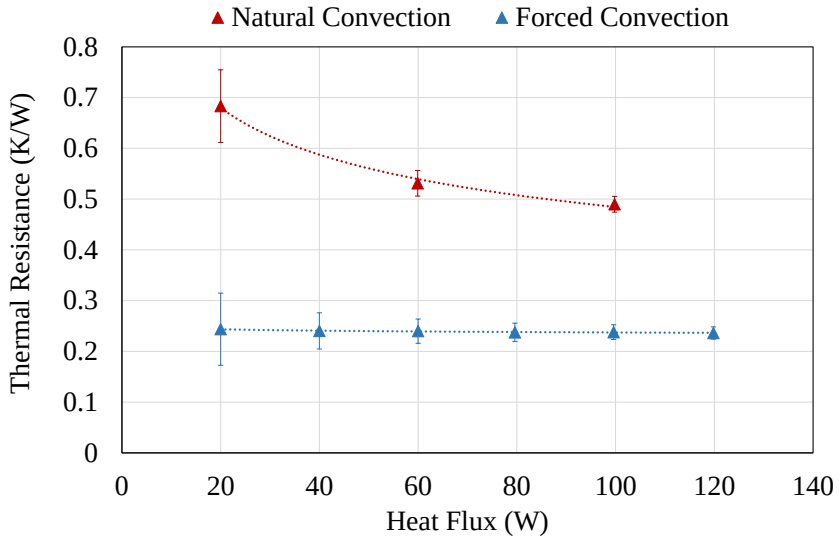

Figure 3. Thermal resistance of the cold side heat exchanger for different heat fluxes, considering natural and forced convection.

Apart from the characterization of the cold side heat exchanger, it is important to determine how much power can be generated with the designed prototype. At the laboratory, the experiments have been performed using the thermal bath depicted in Figure 4 as the heat source, while its analysis under real conditions is detailed in Section 6. This thermal bath is composed of a 10 L water heater, an insulated 30 L container, and a pump for the recirculation of the water used as the heat carrier. The designed prototype has been introduced in the insulated container, in direct contact with the water, which has been maintained at a practically constant temperature of 75 °C.

Figure 4. Thermal bath used as heat source in the laboratory experiments to determine the power generated by the designed prototype.

Utilizing the previous temperature constant heat source and with an ambient temperature of 16.5 °C, each thermoelectric module has been individually connected to an electrical load resistance and its voltage and intensity have been measured for the calculation of the power generated. More specifically, short-circuit, 1 Ω, 2.2 Ω, 3.2 Ω, 4.7 Ω and open-circuit conditions have been experimented and the uncertainties calculated again with [50]. In the experiments, the temperatures of the heat source T_{source}, the hot and the cold side of the thermoelectric modules T_H and T_C, and the ambient temperature T_{amb} have also been measured.

Figure 5 depicts, for the two thermoelectric modules M1 and M2, the voltage (left axis) and the power generated (right axis) with respect to the intensity. From left to right, the values correspond to open-circuit (OC), 4.7 Ω, 3.2 Ω, 2.2 Ω, 1 Ω and short-circuit (SC). As can be observed, the behavior of both thermoelectric modules is quite similar. As the load electrical resistance decreases, the intensity increases and the voltage decreases, with a linear relationship between them. In both cases, the open-circuit voltage is approximately 1.89 V while the short-circuit intensity presents a value of around 0.71 A (0.68 A M1, and 0.74 A M2).

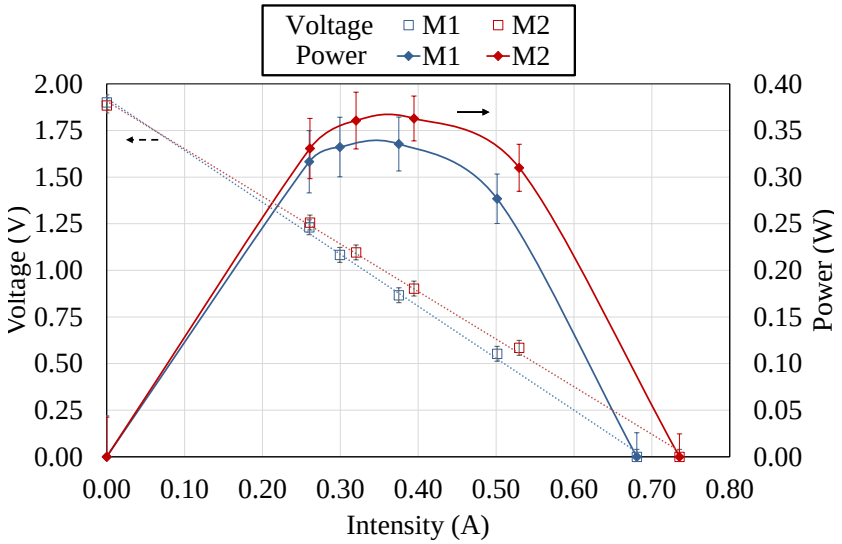

Figure 5. Voltage (**left** axis) and power generated (**right** axis) of the two thermoelectric modules studied, M1 and M2, with respect the intensity. The values correspond, from left to right, to open-circuit (OC), 4.7 Ω, 3.2 Ω, 2.2 Ω, 1 Ω and short-circuit (SC).

Regarding power generation, depending on the electrical load resistance connected to the thermoelectric modules, generation varies, obtaining its maximum with a load resistance equal to the electrical internal resistance of the thermoelectric module. Hence, given an available temperature difference between sources of 58.81 °C on average, module 1 (M1) generates a maximum of 0.34 W with a 2.2 Ω load resistance, which corresponds with a current of 0.38 A. On its behalf, module 2 (M2) presents a slightly higher maximum generation, 0.36 W, also with a load resistance of 2.2 Ω, that in this case corresponds with an intensity of 0.40 A. The small disparities between both thermoelectric modules are due to the different thermal contacts arisen from the assembly as well as to the differences in the heat exchangers, which were manually manufactured.

These disparities can be seen with more detail in Table 1. This table firstly displays, for each case, the temperatures of the heat source T_{source}, the hot and the cold side of the thermoelectric modules T_H and T_C, and the ambient temperature T_{amb}. Based on the temperature difference of the cold side heat exchanger ($T_C - T_{amb}$) and its characterization, it is possible to make an iterative process and obtain the heat flux that is being released to the environment $\dot{Q}_{CHE}$ (Equation (1)). With this heat flux and the generated power P, from the energy balance shown in Equation (2) the heat absorbed from the heat source $\dot{Q}$ can be obtained, permitting the calculation of the efficiency of the thermoelectric modules (Equation (3)). Thus, it can be observed that the heat flux that goes through M2 is 4.75%

higher than the one that goes through M1. This explains the higher generation of M2, which works with an efficiency of 1% with the optimal load resistance.

$$\dot{Q} = P + \dot{Q}_{CHE} \tag{2}$$

$$\eta = \frac{P}{\dot{Q}} \tag{3}$$

Thanks to the calculated heat flux and the measured temperatures, the thermal resistance of the hot side heat exchanger (HHE) has also been calculated (Equation (4)). Hence, the hot side heat exchanger of M1 presents a thermal resistance of 0.36 K/W on average, while the one of M2 is a bit smaller, 0.35 K/W. In comparison with the cold side heat exchanger (CHE), the value of which remains practically constant at 0.24 K/W, these resistances are 33 and 30.9% higher respectively. As a consequence, the temperature difference in the hot side heat exchangers is higher than in the cold ones (12.26 versus 8.15 °C on average).

$$R_{HHE} = \frac{T_{source} - T_H}{\dot{Q}} \tag{4}$$

Table 1. For each thermoelectric module (M1 and M2) and load electrical resistance R_{load}, temperatures of the heat source T_{source}, the hot and cold side of the thermoelectric modules T_H and T_C, and ambient T_{amb}, power generated P, heat flux extracted from the source $\dot{Q}$, efficiency of the thermoelectric modules η, and thermal resistances of the hot and cold side heat exchangers (HHE and CHE respectively).

Thermoelectric Module	R_{load} (Ω)	T_{source} (°C)	T_H (°C)	T_C (°C)	T_{amb} (°C)	P (W)	$\dot{Q}$ (W)	η (%)	R_{HHE} (K/W)	R_{CHE} (K/W)
M1	SC	74.23	61.90	25.47	16.53	0.00	37.01	0.00%	0.33	0.24
	1	76.23	62.50	24.96	16.42	0.28	35.34	0.78%	0.39	0.24
	2.2	75.08	62.75	24.85	16.57	0.34	34.22	0.97%	0.36	0.24
	3.2	75.40	63.19	24.64	16.56	0.33	33.38	0.99%	0.36	0.24
	4.7	75.92	63.73	24.51	16.44	0.32	33.36	0.94%	0.36	0.24
	OC	74.82	64.01	23.76	16.31	0.00	30.75	0.00%	0.35	0.24
M2	SC	74.23	61.53	26.11	16.53	0.00	39.72	0.00%	0.32	0.24
	1	76.23	62.32	25.37	16.42	0.31	37.07	0.83%	0.37	0.24
	2.2	75.08	62.51	25.21	16.57	0.36	35.76	1.00%	0.35	0.24
	3.2	75.40	63.02	25.01	16.56	0.36	34.96	1.02%	0.35	0.24
	4.7	75.92	63.59	24.84	16.44	0.33	34.77	0.94%	0.35	0.24
	OC	74.82	63.84	24.05	16.31	0.00	31.95	0.00%	0.34	0.24

5. Electronics

The objective of the present paper is to develop an autonomous and robust volcanic monitoring station. Hence, since the generator part has already been analyzed, this section focuses on the electronic part associated to it prior to the installation of the whole system in a real volcano. These electronics, in order to resemble a real station, include a system to process the generated signal, as well as devices for acquiring data and emitting it wirelessly to a receptor. Their description will be based on the diagram shown in Figure 6, with the generation on the left side (with green arrows) and the consumption in the right one (with red ones). As can be observed, a prototype with four thermoelectric modules, this is two devices such as the one depicted in Figure 2, are considered to ensure a sufficient generation under real conditions, given that the heat transfer with the fumaroles is one of the greatest unknowns.

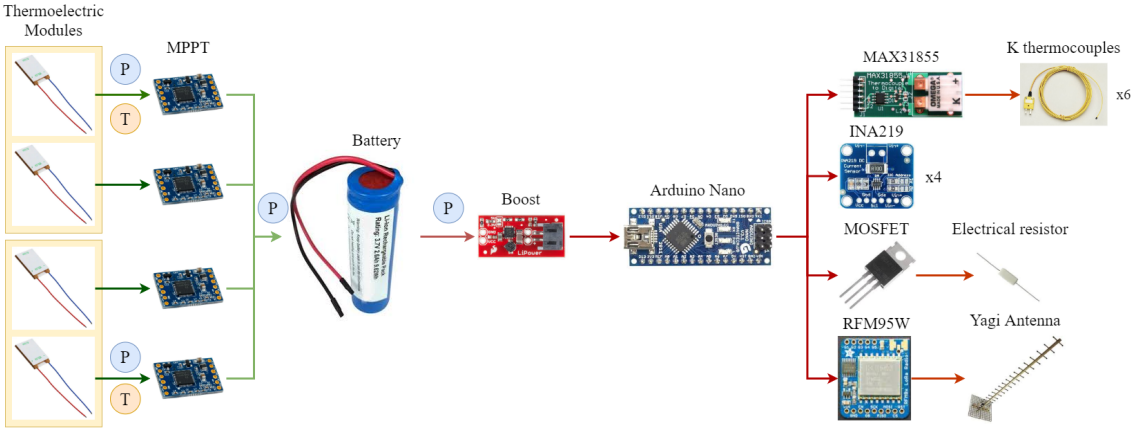

Figure 6. Diagram of the electronics installed with the prototype, which represents the node of the LoRa communication system.

According to the previous section, it is important that the thermoelectric modules are connected to the optimal load electrical resistance. For this purpose, there exist some devices known as Maximum Power Point Trackers (MPPT) that perform this task. In thermoelectricity, the most common MPPT devices, which are also the simplest ones, adjust the output voltage of the thermoelectric modules to a value half of the open-circuit one [51]. In the present paper, each thermoelectric module has been individually connected to a Cypress MB39C831-EVB-03 Ultra Low Voltage Boost PMIC Energy Harvesting Evaluation Board [52], which works given an input voltage in the range between 0.3 and 4.75 V. As depicted in Figure 6, these boost converters are connected to a Li-ion battery. Hence, when the converter can obtain sufficient electric power from the thermoelectric modules, the charge is stared to the Li-ion battery until it reaches 4 V, when the charge is stopped. Charge restarts once the battery voltage has decreased to 3.7 V approximately. The RS Pro 18650 26H Li-ion battery pack has been used in this work [53].

On the demand side, data acquisition and communication systems are considered. In order to control them, it is necessary to include a microcontroller. In this case, Arduino Nano has been chosen because, presenting enough computational capacity, it has a very low energy consumption. Moreover, since all these components require a constant voltage of 5 V, which is higher than the battery's one, a boost converter is required. This paper has installed a SparkFun PRT 10255 Boost Converter [54].

The monitoring system is in turn composed of two different parts. On the one hand, active sensing of six temperatures and four power generations is performed, thus simulating the existence of sensors in a real station while monitoring the operating conditions of the prototype. These measurements are taken every 4 min thanks to Maxim Integrated MAX31855PMB1 peripheral modules (with type K thermocouples) and Adafruit INA219 breakout boards respectively [55,56]. In order to avoid errors, these measurements are repeated 15 times, and the average of all the valid ones is stored. On the other hand, there is an extra consumption simulated passively with electrical resistors that includes peaks of demand, which are typical in vigilance stations. Hence, there is a constant power requirement of 0.3 W and every 12 min, a peak of consumption of 0.5 W occurs during 2 min. For this purpose, one of the outputs of the Arduino is connected to a MOSFET, so that an electrical resistor is directly connected to the battery when determined by the microcontroller.

All the data registered by the active sensors needs to be emitted to a reception center. Nevertheless, this process usually requires a high energy consumption [18]. Therefore, the present paper investigates low energy communication systems that, while being able to communicate wirelessly over a considerable distance, facilitate thermoelectric generation as the power supplier. Low-Power Wide-Area Network (LPWAN) standards, typically associated with Internet of Things (IoT), meet these requirements. Hence, this work analyzes the five technologies that seem to have the widest market potential: SigFox, LoRaWAN (Long Range WAN), IEEE 802.15 promoted by Wi-SUN (Wireless Smart Ubiquitous Network), and 3GPP standards: LTE-M (LTE for M2M) and NB-IoT (Narrow Band IoT) [57].

Table 2 summarizes the main characteristics of the former technologies in relation to their frequency band, maximum data rate, range (or coverage) and power usage [58–63]. As can be observed, within the table two categories can be distinguished. On the one hand, there is a category composed of LTE-M and NB-IoT, which use the current cellular telecommunications bands, since they are indeed extensions of the 4G network infrastructure. As a consequence, their range is extensive, but present a medium power usage, leading to their discard for the application under consideration in this paper.

Table 2. Comparison of some Low-Power Wide-Area Network (LPWAN) technologies [58–63].

Technology	Frequency Band	Maximum Data Rate	Range	Power Usage
SigFox	Sub-GHz ISM	600 bbps	10 km (urban), 50 km (rural)	Low
LoRaWAN	Sub-GHz ISM	50 kbps	5 km (urban), 15 km (rural)	Low
Wi-SUN	Sub-Ghz ISM & 2.4 GHz	300 kbps	5 km	Low
LTE-M	Cellular Bands	1 Mbps	Several km	Medium
NB-IoT	Cellular Bands	100 kbps	Several km	Medium

On the other hand, SigFox, LoRaWAN, and Wi-SUN use the unlicensed ISM frequency bands and present low power usage. SigFox was one of the pioneers in the LPWAN market and it targets the very low power and low bandwidth applications, while offering very good coverage characteristics. Nevertheless, it is not available everywhere and it requires the payment of a royalty. On its behalf, LoRa is completely open and permits faster data rates, although the coverage range is curbed. Finally, Wi-SUN is focused on applications within public utilities, smart homes and smart cities, and therefore presents a reduced range of 5 km.

The present paper represents the first approximation for an autonomous volcanic monitoring station. Hence, the remoteness of volcanoes leads to the discard of Wi-SUN. Among SigFox and LoRa, the latter is preferred because, although it has a smaller coverage, it permits a higher data rate, it is completely free and it can be implemented everywhere. Due to these advantages, LoRa was also the technology chosen by Awadallah et al. and Terray et al. for their volcano surveillance applications, emitting the information up to 8.5 and 1.7 km, respectively [20,21].

Figure 7 details the complete solution provided by LoRa. Thus, the data acquired by the sensors is sent to a gateway located on a place with internet connection. For this purpose, it is necessary to install a transceiver and an antenna both at the node and at the gateway. In this paper, Adafruit RFM95W LoRa Radio Transceiver Breakout boards in conjunction with Yagi antennas have been used [64,65]. In the case of the gateway, a Raspberry Pi 3 B+ has been used as microcontroller, so that the received data is stored in an Influx database and synchronized with a server by means of MQTT protocol, so that the data can be represented with Grafana.

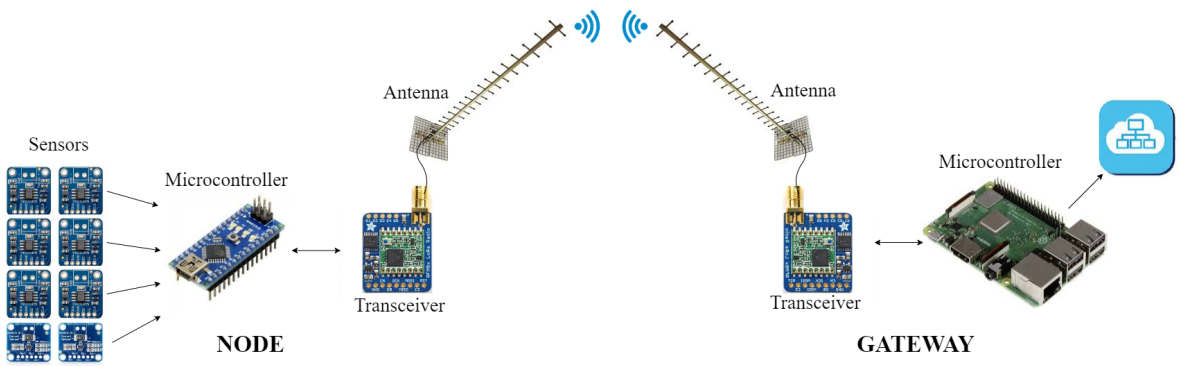

Figure 7. Schematics of a communication system implemented with LoRa.

The power consumption in the node will depend on the frequency of emission, the distance, the size of the measured data, and the used sensors, transceiver, and microcontroller. Nonetheless,

in order to have an approximation of the power requirement of such a system, a simplified experiment has been performed in this paper. Hence, a node composed of an Arduino Nano as microcontroller took, every 4 min, six temperature measurements with MAX31855 boards and two power measurements with Adafruit INA219s. The measured data was sent to a gateway located 13 km away by means of the mentioned Adafruit RFM95W board and Yagi antenna. As a result, the power demand in the node was 0.11 W on average, reaching peaks of 0.246 W during the emission. Therefore, LoRa is definitely chosen as the communication system in this paper, since it is able to emit wirelessly the measured data over a considerable distance while presenting a minimal energy consumption, thus facilitating thermoelectric generation as the power supplier.

The emission of data from the prototype node to the gateway has been programmed to be bi-directional and encrypted. Thus, the prototype emits, every four minutes, the measured data and waits for the confirmation of reception of the message. This process is performed with an initial spreading factor of nine. If the confirmation is not received after 60 s, a second attempt starts. In case neither confirmation is received, a third and last attempt is performed with a spreading factor of 10, so that the range is increased. If the confirmation from the gateway is received, the prototype node sends a new message to the gateway and both nodes update their encrypted key.

Finally, similarly to the prototype, and due to the harsh volcanic environmental conditions, it is necessary to protect the electronics to stand severe conditions. Figure 8 depicts the protection measures that have been taken. Thus, the PCB with all the electronics has been introduced in an IP67 plastic box and covered with Raytech magic power gel [66]. This box has been closed and introduced in another IP67 plastic box. Since the different cables need to be taken out of the boxes, cable glands have been installed with a Nylon conduit contractor, and the connections have been protected with self-amalgamating tape and polyurethane foam.

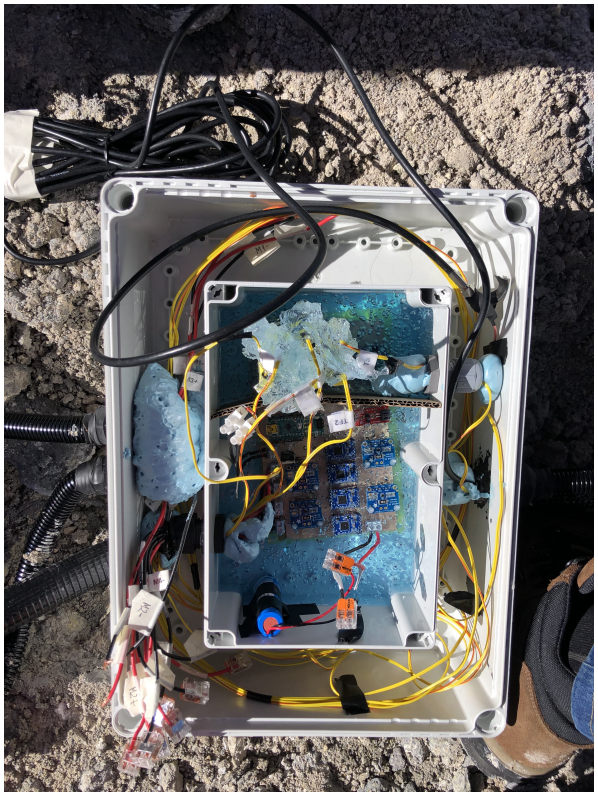

Figure 8. Detail of the protection boxes to avoid corrosion in the PCB.

6. Behavior on a Real Volcano

On 18th December 2019, the prototype was installed at Teide volcano (Canary Islands, Spain) with its associated electronics (Figure 9) and on the submission date of this manuscript, the prototype was still in operation. Teide is a stratovolcano located in the Canary Islands (Spain), an archipelago of volcanic origin that emerges in the Atlantic Ocean. With an altitude of 3718 m, Teide is one of the most evident manifestations of the active volcanism of the islands, and therefore, it is widely monitored. Figure 10 details the location of the prototype, in the northern side of the volcano at an approximate altitude of 3500 m, as well as the position of the gateway, 14 km away with direct vision. As shown in Figure 9, in its installation, aluminum deflectors were added so that the volcanic gases are diverted, not coming into contact with the thermoelectric modules nor the cold side heat exchangers. Polyurethane foam was used for sealing the joints. Furthermore, polyethylene was also added in order to insulate the aluminum block of the hot side heat exchanger and the thermoelectric modules from the influence of ambient conditions.

Figure 9. Prototype installed at Teide volcano on December 2019, composed of 4 thermoelectric modules.

Figure 11 depicts the typical operation of the prototype, taking as reference the variables measured between 29 December 2019 and 2 January 2020. More specifically, Figure 11a shows the temperature of the ground T_{ground}, the hot and the cold side of two thermoelectric modules $M1\_T_H$, $M1\_T_C$, $M2\_T_H$ and $M2\_T_C$, and the ambient temperature T_{amb}. Each monitored thermoelectric module belongs to one of the individual generators installed.

As can be observed, ground temperature T_{ground} remains practically constant with an average value of 81.82 °C. At the opposite side of the prototype, the ambient temperature T_{amb} presents the typical fluctuations of day and night. Hence, since the considered values correspond to winter, during the night, temperatures close to 0 °C are found, while during the day, the temperatures rise up to an average of 10 °C.

The difference between the ground and the ambient temperatures ($T_{ground} - T_{amb}$) represents the maximum temperature difference achievable by the thermoelectric modules, although, in reality,

the temperature difference between the hot and the cold side of the modules will be lower. The approximation of the temperature difference of the thermoelectric modules ($T_H - T_C$) to the maximum available one ($T_{ground} - T_{amb}$) depends on the heat exchangers installed. The lower the thermal resistances of the heat exchangers, the closer the temperature differences.

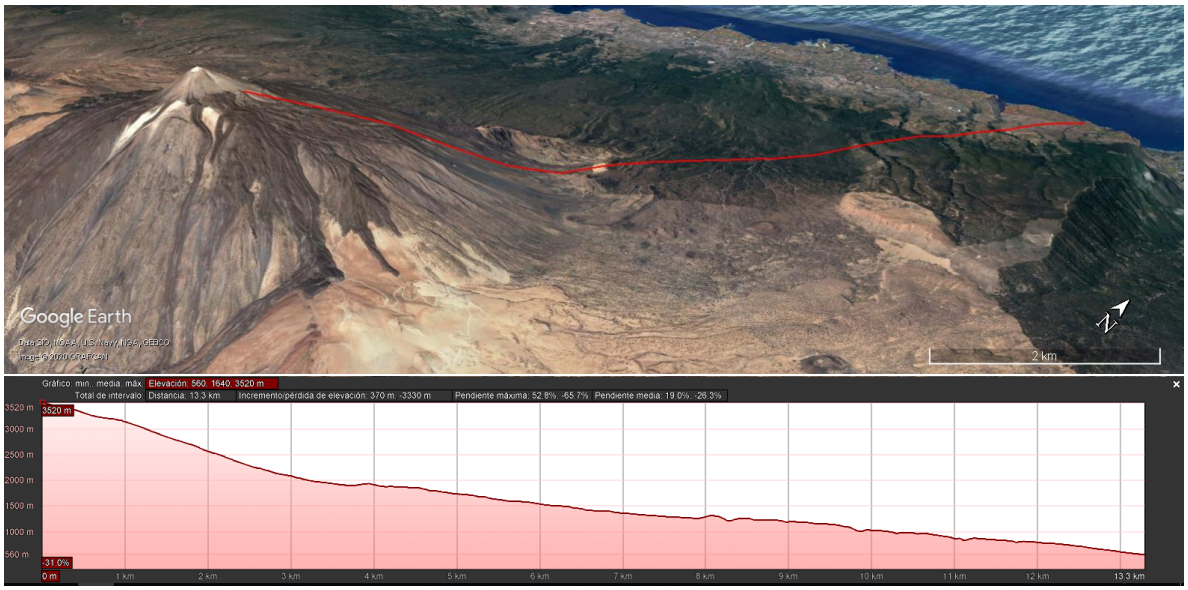

Figure 10. Location of the prototype node and the gateway, and their associated elevation profile. Images taken from Google Earth ©.

In the considered hot side heat exchangers, there exists an average temperature difference of 13.5 °C, while this difference is of 10.5 °C in the case of the cold side ones. Thus, the thermoelectric modules work under a gradient of 54 °C, which is similar for the two thermoelectric modules that are being monitored. This gradient is slightly influenced by the ambient conditions, decreasing during the day and increasing during the night, which will affect generation.

Figure 11b–d show the values associated with the measurements performed by means of the INA219s: power, voltage, and intensity respectively. In particular, these sensors, as shown in Figure 6, have been installed monitoring the individual power generated by the thermoelectric modules M1 and M2 of which the temperatures are also being measured (before the MPPT), the generation of all the thermoelectric modules (after the MPPTs and before the battery), and the consumption of the different devices (at the battery output).

As explained before, the consumption profile presents a cyclic oscillation, with a fixed power requirement of 0.3 W and peaks of 0.5 W during 120 s every 12 min. Since the measurement of the different variables is performed every four minutes, the consumption profile is shown as peaky rather than pulsed, as can be observed in green in Figure 11b. The measurement of this consumption is being performed at the output of the battery, or in other words, at the input of the PRT boost converter that adapts the battery voltage to 5 V, so that the consumption of all the charges is considered. Thus, the voltage of the consumption coincides with the battery one in Figure 11c.

In order to satisfy the previous demand, four thermoelectric modules were installed. Nevertheless, the generation supplied by only one module is enough for this purpose. As can be observed in Figure 11b, the generation of the four thermoelectric modules, in red, is slightly lower than the generation of M2, in dark blue, while the generation of M1, in light blue, is null. This means that out of the four thermoelectric modules installed, only M2 is in operation. The generation of the individual modules is measured before the MPPT. Therefore, the difference between the total generation and the individual generation of M2 is due to the conversion efficiency of the MPPT, which can be rated as 85.7% in this case.

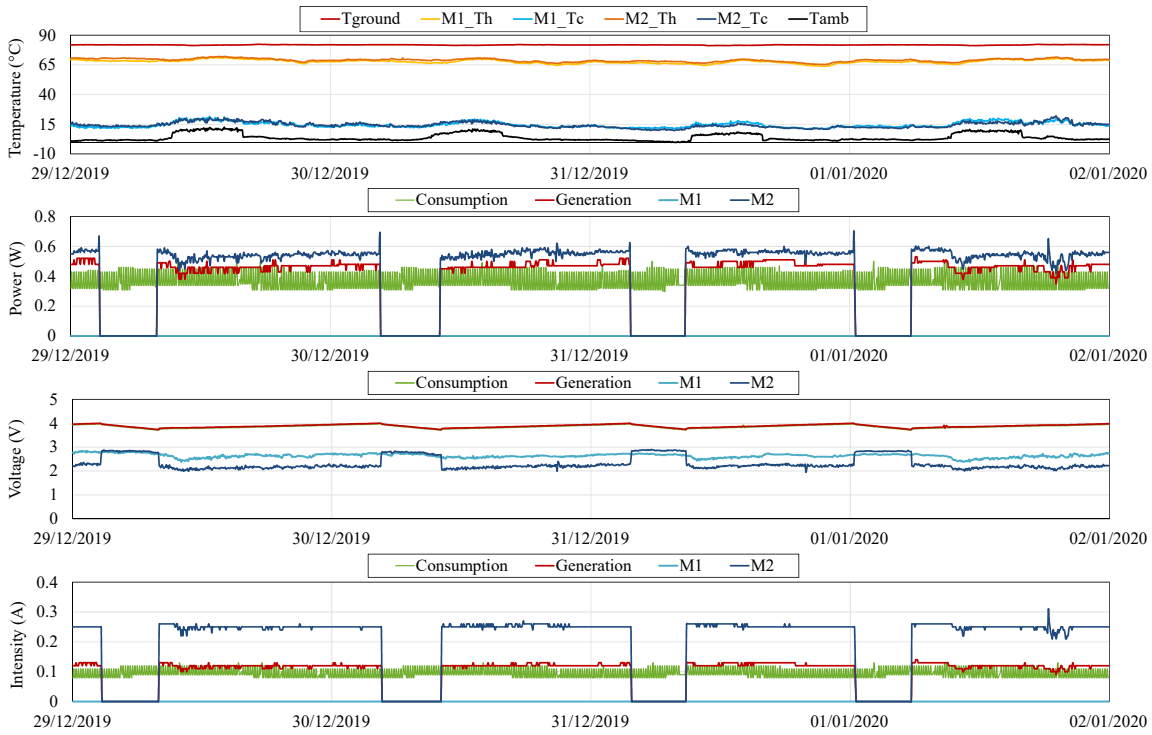

Figure 11. **(a)** Temperature of the ground T_{ground}, the hot and the cold side of two thermoelectric modules M1 and M2 (T_H and T_C) and the ambient T_{amb}, **(b)** power, **(c)** voltage and **(d)** intensity measurements during typical operation.

The total generation is around 0.47 W, higher than the consumption, which presents an average value of 0.37 W. Hence, the battery is charged with the excess of energy produced, until it reaches 4 V (Figure 11c). At this moment, the MPPT opens the circuit of M2 for security reasons, leading to a null intensity and increasing the voltage of M2 from 2.18 to 2.82 V approximately. This open-circuit value is very similar to the one displayed by M1.

When all the modules are in open-circuit, the battery is progressively discharged, reducing its voltage. When this voltage reaches 3.74 V, M2 activates again, starting a new cycle. The threshold at which the thermoelectric modules activate is determined by the MPPT. Nonetheless, there exist slight differences in the used boards. M2 has the highest threshold and therefore, it is the first one that starts its operation. It would be necessary to have a battery voltage lower than 3.74 V for the activation of other thermoelectric modules.

If the ambient temperature increases, the available temperature difference decreases, as so does the gradient between the sides of the thermoelectric modules, and therefore, the generation. Figure 12 depicts the variables measured between 19 and 23 May 2020, when temperatures close to the typical maximums at Teide volcano were recorded [67]. In this period, the ambient temperature presents values of around 8 °C during the night and up to 22 °C during the day. Consequently, the temperature difference between the sides of the modules has decreased from the previous case, with an average of 49 °C.

As shown in Figure 12, the total generation obtained with the former gradient is of just 0.35 W, lower than the average consumption. Therefore, the battery is gradually discharged although one thermoelectric module is in operation. When the voltage of the battery is lower than 3.73 V, another thermoelectric module starts its operation. The individual generation of this module is not being monitored, but it can be seen that the total generation, in red, exceeds the individual generation of M2, while M1 remains in open-circuit. When the battery voltage reaches 3.99 V, this second thermoelectric module switches to open-circuit, and again M2 is the only module in operation. On 20th May, the total generation with only M2 was higher than the consumption, completely charging the battery a couple

of hours after the disconnection of the second module. Nevertheless, on the 21st, when the second module switched to open-circuit, total generation with M2 was similar to the consumption. Hence, an equilibrium between generation and consumption can be observed, discharging the battery during the day and charging it during the night, but without reaching the upper nor the lower thresholds to switch to open-circuit or force the operation of a new module respectively. During this equilibrium period, the influence of ambient temperature in generation can be perfectly seen. This influence is more detailed in Figure 13, which shows the ambient temperature T_{amb} (left axis), the total power generation and the power generated by M2 (right axis) between 21st and 23rd May 2020. Thus, during the day temperature increases, diminishing the available temperature difference and therefore reducing generation. During the night, this temperature decreases and generation increases.

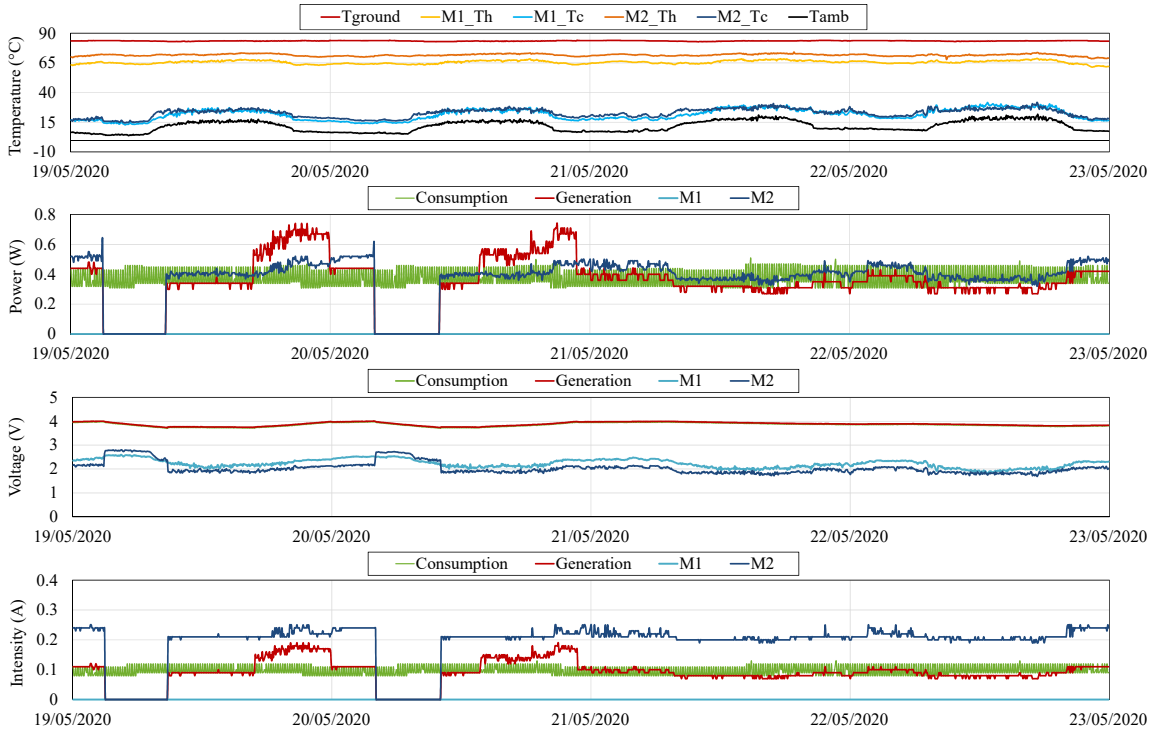

Figure 12. **(a)** Temperature, **(b)** power, **(c)** voltage and **(d)** intensity measurements during several hot days.

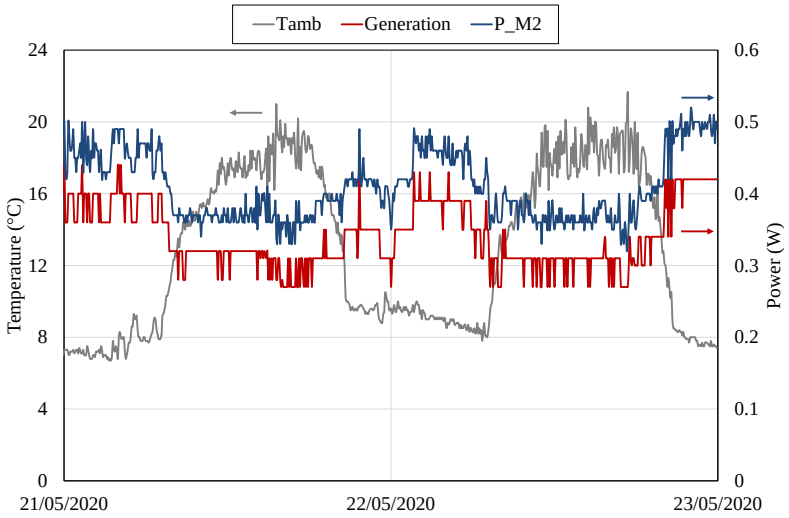

Figure 13. Ambient temperature T_{amb} (left axis), power generated by M2 and total generation (right axis) between 21st and 23rd May 2020.

The ambient temperature during the days depicted in Figure 12 is very similar to the one used in the laboratory characterizations. Hence, assuming that the wind conditions at Teide are similar to the laboratory ones (in forced convection), an estimation of the heat flux, the thermal resistance of the heat exchangers, and the efficiency can be performed.

Table 3 summarizes the average results of M2 on 19 May between 11:00 and 20:00 h. As can be observed, at Teide, ground temperature is almost 10 °C higher than the laboratory's heat source's one. Consequently, the heat flux increases, reaching 40 W in this case and raising the hot side temperature to 72.5 °C. Since the gradient between the sides of the module is higher, so is generation, with an average value of 0.41 W, which entails an efficiency of 1.02%.

Based on the previous data, it is also possible to calculate the thermal resistance of the hot side heat exchanger. Hence, with Equation (4) a value of 0.27 K/W is obtained, 23 % lower than at the laboratory, where natural convection with water was the heat transfer mechanism. Heat transfer between the ground and the hot side heat exchanger was one of the greatest unknowns, complicating its simulation at the laboratory. Nonetheless, it has been experimentally demonstrated that this heat transfer is really acceptable, with a thermal resistance quite similar to the cold side one. The fumaroles heat up and moisten the ground in their ascent to the surface. Thus, heat transfer is not produced by convection with the gaseous fumaroles but by conduction with the hot and wet ground, which permits obtaining better heat transfer coefficients.

Table 3. Average temperatures, generation and thermal resistances of M2 during 19 May 2020 between 11:00 and 20:00 h.

Temperatures		Generation		Thermal Resistances	
T_{ground}	83.44 °C	P	0.41 W	R_{HHE}	0.27 K/W
T_H	72.53 °C	$\dot{Q}$	40.00 W	R_{CHE}	0.24 K/W
T_C	24.77 °C	η	1.02%		
T_{amb}	15.12 °C				

Since its installation in December 2019, the prototype has undergone multiple kinds of meteorological conditions, from severe snowfalls and frosts to days with the typical Saharan air layer. On the one hand, Figure 14 shows its operation between 21 and 24 January 2020, when ambient temperature reached values down to −10 °C. As can be seen, due to the greater difference between ground and ambient temperature, the gradient between the sides of the thermoelectric modules increases, also raising the generation, which reaches values of up to 0.66 W in the case of M2. Despite its operation with temperatures below 0 °C, the cold side heat exchanger does not present signs of freezing, except a very punctual moment. The night between 22 and 23 January, an uncoupling between the ambient and the modules' cold side temperature can be observed, which could be due to the freezing of the cold side heat exchangers. Nevertheless, this fact only causes a slight reduction in the power generated, which is not even enough to reduce the total generation below the demand.

On the other hand, the prototype has also dealt with other extreme meteorological conditions such as the typical Saharan air layer. This phenomenon, also known as *Calima* in the Canary Islands, is characterized by a hot, dry, and dust-laden atmosphere. As shown before, high temperatures are not a problem for the operation of the prototype. The most critical aspect of this phenomenon is the reduced visibility caused by dust plumes, which could affect the communication with the gateway, located 14 km away. Nevertheless, since its installation, there have not been data losses. Not even in February, when one of the worst *Calima* episodes in the last 30 years affected the Canary Islands [68].

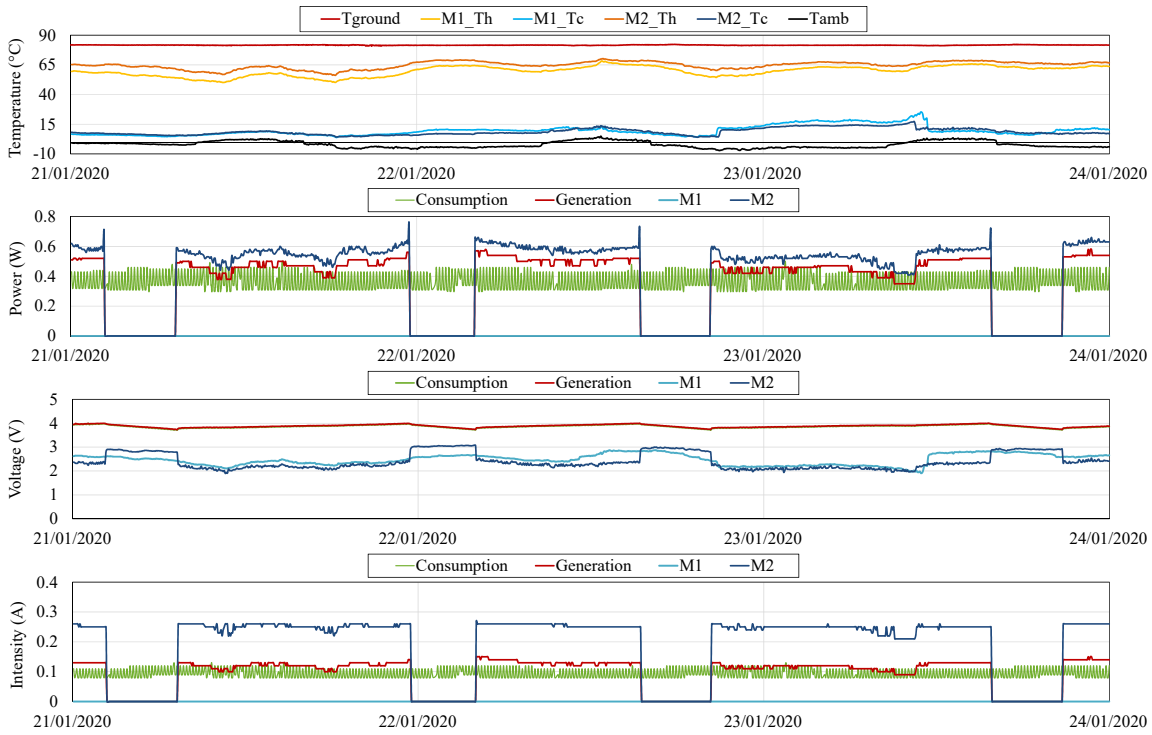

Figure 14. **(a)** Temperature, **(b)** power, **(c)** voltage and **(d)** intensity measurements during several cold days.

The visibility loss can also occur due to the formation of clouds between the emitter and the gateway. At Teide, it is common to observe a temperature inversion that leads to the so-called *sea of clouds* due to its appearance from above. Nevertheless, despite occurring quite often, this phenomenon neither affects the communication system. Thus, the prototype, and its associated electronics, have demonstrated to withstand several types of meteorological conditions, being able to supply the required energy mostly with only one thermoelectric module and ensuring communication at every moment.

Table 4 summarizes the number of hours that each thermoelectric module has been in operation between 19 December 2019 and 20 August 2020. As can be observed, M2 is the thermoelectric module that leads generation, with more than 4400 h of operation. M3 is the other module that supplies power occasionally, with less than 270 h being active, while M1 and M4 are never necessary. On average, M2 is in operation 86.2% of the time, being in open-circuit the rest of the time. Nonetheless, depending on the ambient conditions, this percentage of time in operation can vary. In the table, apart from the average values, it is also represented by the percentage under the typical conditions shown in Figure 11, under the hot days depicted in Figure 12, and under the cold days considered in Figure 14. Hence, when the ambient temperature decreases, due to the higher generation of the thermoelectric modules, M2 needs to be active a shorter period of time, while in hot days, the operation time increases. It is in these hot days when it is sometimes required that another thermoelectric module, M3, starts its operation, when the generation of M2 is lower than the consumption and the battery is being discharged. Nevertheless, the rest of the time is in open circuit, leading to an average of 0.9% of the time in operation. Thus, it can be seen that during 93.95% of the time that the prototype has been installed at Teide volcano, the generation of M2 has been enough to supply the required power.

Table 4. Total hours in operation and percentage of time active of the four thermoelectric modules installed, considering the average between 19 December 2019 and 20 August 2020, as well as their behavior under typical conditions (Figure 11), hot days (Figure 12) and cold days (Figure 14).

Thermoelectric Module	Total Time in Operation (h)	Percentage of Time in Operation (%)			
		Average	Typical	Hot Days	Cold Days
M1	0	0%	0%	0%	0%
M2	4441.4	86.2%	78.2%	87.6%	73.4%
M3	269.1	5.2%	0%	16.8%	0%
M4	0	0%	0%	0%	0%

Finally, Figure 15 shows the power generated by M2 with respect to the temperature difference between its sides $\Delta T = T_H - T_C$ during the previous period. As can be observed, there exists a linear correlation between the generated power and the temperature difference between its sides. This correlation has remained unaltered during the eigth months analyzed, presenting an average value of 0.49 W with a 51.5 °C gradient that supposes 2.2 kWh of energy produced. Therefore, the robustness and the resistance of the developed prototype to the harsh volcanic conditions has been evidenced, even more taking into account that no maintenance has been carried out.

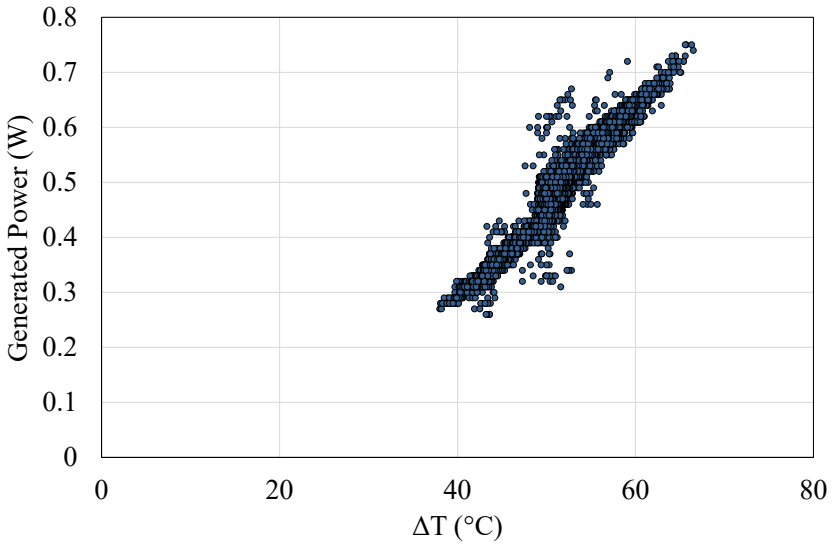

Figure 15. Power generated by M2 versus the temperature difference between their sides $\Delta T = T_H - T_C$ between 19 December 2019 and 20 August 2020.

7. Supplying Power to a Real Vigilance Station

In this last section the viability of supplying power to a real station is analyzed. Clearly, depending on the station under consideration, with its associated equipment, a different power supply will be necessary. Nonetheless, since one of the main advantages of thermoelectricity is its scalability, an increase in the generated power can be simply achieved by installing more thermoelectric modules (with their associated heat exchangers).

This section considers as reference one of the vigilance stations located at Teide volcano. More specifically, the one located at "La Fortaleza" lookout, which is next to the installed prototype and belongs to the Volcanological Institute of the Canary Islands [69]. The station is composed of a seismograph, a WEST continuous monitoring flux unit that measures the concentration of several gases (CO_2, H_2S, CH_4), soil moisture and temperature, as well as various meteorological parameters [70], and a GSM router to emit the measured data to the control center.

The power consumption of the station was monitored over two days. As a result, it was obtained that both the seismograph and the router present a practically uniform power consumption of 1.86 W

and 3.77 W on average respectively. In contrast, the flux unit presents an average demand of 1.5 W that is not constant but with peaks of demand once an hour.

Nowadays, this consumption is powered by means of a 175 W photovoltaic panel of dimensions $1306 \times 991 \times 40\,mm^3$. This panel is connected to a Victron BlueSolar MPPT 75|15 [71], a charge controller that maximizes energy harvesting from the panel and stores it in a 1260 Wh lead-acid battery. The system is over-dimensioned in order to ensure the vigilance of the volcano despite snow periods up to 3.7 days. Nevertheless, it complicates maintenance due to its size and weight.

The solution proposed in the present paper, based on a geothermal thermoelectric generator, permits a more uniform generation that even improves with adverse meteorological conditions. Therefore, it would be possible to reduce the energy storage requirements or replace it with other technologies such as supercapacitors. Nonetheless, in order to make it possible, it is desirable to reduce the power demand to a minimum due to the low efficiency of the thermoelectric modules. In the power measurements, the high power demand of the router stands out, which is two and three times the average consumption of the seismograph and the flux unit respectively, while being the least critical for the volcano vigilance and the easiest one to be modified.

As explained in Section 5, LoRa is able to communicate wirelessly over a considerable distance with a minimal consumption of just 0.11 W, which supposes a reduction of 97 % in the power requirement of the communication system, leading to a reduced number of thermoelectric modules necessary in order to obtain a completely autonomous volcanic monitoring station. More specifically, taking into account all the previous information, in order to supply an average power of 3.24 W, seven thermoelectric modules would be necessary, that is, two devices such as the one depicted in Figure 9. Therefore, the solution proposed in this paper will be perfectly viable to power a real volcanic monitoring station.

8. Conclusions

In conclusion, the present paper has demonstrated the viability of obtaining autonomous volcanic vigilance stations. Volcano surveillance is essential in order to predict volcanic eruptions and be able to reduce their damage. However, due to the usual remoteness of volcanoes, power supply generally constitutes a challenge.

As a solution, this work has developed a novel system composed of thermoelectric generators as power suppliers, as well as all their related electronics, for which technologies typically associated with Internet of Things (IoT) have been used. Thus, thanks to the heat emitted in volcanic fumaroles, which is indeed a sign of activity of the volcanoes, electricity can be directly generated by means of the Seebeck effect. Since fumaroles are a constant temperature heat source, a continuous generation is obtained regardless of the weather conditions, permitting a drastic reduction in the capacity of the required batteries. Thanks to this generation, it is possible to measure different variables and emit the results via LoRa to a gateway located several kilometers away.

In order to analyze the viability of this solution, a prototype formed by heat pipes as heat exchangers has been characterized at the laboratory and installed afterward at Teide volcano (Canary Islands, Spain), where there exists 83.5 °C fumaroles. In more than eigth months of operation, the device has demonstrated that only one module is enough to cover the demand of data acquisition and communication over 14 km. On average, this thermoelectric module has generated 0.49 W with a temperature difference of 51.5 °C.

During its operation, the prototype has resisted, without any maintenance, several kinds of adverse meteorological conditions in a very harsh environment. Therefore, the viability of the solution has been demonstrated, evidencing all its advantages: durability, reliability, lack of maintenance, scalability, absence of moving parts, noiseless operation, robustness, and compactness.

9. Patents

The mode of operation of the developed thermoelectric generator is patented under number WO 2019/202180 A1.

Author Contributions: Conceptualization: L.C., A.G., A.C., M.A., P.A., D.A.; investigation: L.C., A.G., A.C., M.A.; construction and characterization: L.C., A.G., A.C., M.A.; monitoring and communication systems: L.C., A.G.; software: L.C., A.G.; installation: L.C., A.G., A.C., M.A., D.A.; analysis of results: L.C., A.G., D.A.; supervision: D.A.; writing—original draft: L.C.; writing—review and editing: L.C., P.A., D.A. All authors have read and agreed to the published version of the manuscript.

Funding: This research was funded by the Spanish State Research Agency with FEDER–UE funds under grant number RTC-2017-6628-3.

Acknowledgments: We would like to acknowledge the support of FPU Program of the Spanish Ministry of Science, Innovation, and Universities (FPU16/05203) and the Official School of Industrial Engineers of Navarre with the scholarship *Fuentes Dutor*. Moreover, we would also like to acknowledge the logistical support of Nemesio M. Perez, German D. Padilla, Pedro A. Hernandez, Jose Barrancos, Vidal Dominguez, Carlos Perez, Miguel Vera, Celestino Garcia de la Noceda and Pepe Albert from INVOLCAN, ITER, AIET, Constante Solar, IGME and GAIA Geotermia y Aguas Minerales S.L..

Conflicts of Interest: The authors declare no conflict of interest. The funders had no role in the design of the study; in the collection, analyses, or interpretation of data; in the writing of the manuscript, or in the decision to publish the results.

Abbreviations

The following abbreviations are used in this manuscript:

CHE	Cold side heat exchanger
GTEG	Geothermal Thermoelectric Generator
HHE	Hot side heat exchanger
IoT	Internet of Things
LPWAN	Low Power Wide Area Network
MPPT	Maximum Power Point Tracker
M1	Thermoelectric module 1
M2	Thermoelectric module 2
OC	Open-circuit
SC	Short-circuit
I	Intensity (A)
P	Power (W)
$\dot{Q}$	Heat flux (W)
R	Thermal resistance (K/W)
R_{load}	Load electrical resistance (Ω)
T	Temperature (°C)
V	Voltage (V)
η	Efficiency (%)
amb	Ambient
b	Base of the heat exchanger
C	Cold side of the thermoelectric module
H	Hot side of the thermoelectric module
source	Heat source

References

1. TMW. 7 Most Dangerous Natural Disasters. Available online: https://themysteriousworld.com/most-dangerous-natural-disasters/ (accessed on 28 May 2020).
2. Global Volcano Model; International Association of Volcanology; Chemistry of the Earth's Interior. *Global Volcanic Hazards and Risk: Summary Background Paper for the Global Assessment Report on Disaster Risk Reduction 2015*; In United Nations Office for Disaster, *Global assessment report on disaster risk reduction 2015*, Geneva, Switzerland, 2015.

3. Sherburn, S.; Scott, B.J.; Olsen, J.; Miller, C. Monitoring seismic precursors to an eruption from the Auckland volcanic field, New Zealand. *N. Z. J. Geol. Geophys.* **2007**, *50*, 1–11, doi:10.1080/00288300709509814.
4. López, C.; Blanco, M.J.; Abella, R.; Brenes, B.; Cabrera Rodríguez, V.M.; Casas, B.; Domínguez Cerdea, I.; Felpeto, A.; De Villalta, M.F.; Del Fresno, C.; et al. Monitoring the volcanic unrest of El Hierro (Canary Islands) before the onset of the 2011-2012 submarine eruption. *Geophys. Res. Lett.* **2012**, *39*, 1–7, doi:10.1029/2012GL051846.
5. Chastin, S.F.; Main, I.G. Statistical analysis of daily seismic event rate as a precursor to volcanic eruptions. *Geophys. Res. Lett.* **2003**, *30*, 1–4, doi:10.1029/2003GL016900.
6. Gottsmann, J.; Neuberg, J.; Scheu, B. *Volcanic Unrest*; Springer: Cham, Switzerland, 2019.
7. Frondini, F.; Chiodini, G.; Caliro, S.; Cardellini, C.; Granieri, D.; Ventura, G. Diffuse CO_2 degassing at Vesuvio, Italy. *Bull. Volcanol.* **2004**, *66*, 642–651, doi:10.1007/s00445-004-0346-x.
8. Greco, F.; Currenti, G.; D'Agostino, G.; Germak, A.; Napoli, R.; Pistorio, A.; Del Negro, C. Combining relative and absolute gravity measurements to enhance volcano monitoring. *Bull. Volcanol.* **2012**, *74*, 1745–1756, doi:10.1007/s00445-012-0630-0.
9. Slezak, K.; Jozwiak, W.; Nowozynski, K.; Orynski, S.; Brasse, H. 3-D studies of MT data in the Central Polish Basin: Influence of inversion parameters, model space and transfer function selection. *J. Appl. Geophys.* **2019**, *161*, 26–36, doi:10.1016/j.jappgeo.2018.11.008.
10. Laiolo, M.; Coppola, D.; Barahona, F.; Benítez, J.E.; Cigolini, C.; Escobar, D.; Funes, R.; Gutierrez, E.; Henriquez, B.; Hernandez, A.; et al. Evidences of volcanic unrest on high-temperature fumaroles by satellite thermal monitoring: The case of Santa Ana volcano, El Salvador. *J. Volcanol. Geotherm. Res.* **2017**, *340*, 170–179, doi:10.1016/j.jvolgeores.2017.04.013.
11. Stephens, K.J.; Wauthier, C. Satellite geodesy captures offset magma supply associated With Lava Lake appearance at Masaya Volcano, Nicaragua. *Geophys. Res. Lett.* **2018**, *45*, 2669–2678, doi:10.1002/2017GL076769.
12. Instituto Geográfico Nacional. Técnicas de Vigilancia Volcánica. Available online: https://www.ign.es/resources/docs/IGNCnig/TecnicasDeVigilancia_v8.pdf (accessed on 5 June 2020).
13. Inguaggiato, S.; Diliberto, I.S.; Federico, C.; Paonita, A.; Vita, F. Review of the evolution of geochemical monitoring, networks and methodologies applied to the volcanoes of the Aeolian Arc (Italy). *Earth-Sci. Rev.* **2018**, *176*, 241–276, doi:10.1016/j.earscirev.2017.09.006.
14. McGuire, W. Monitoring active volcanoes: An introduction. In *Monitoring Active Volcanoes: Strategies, Procedures and Techniques*, 1st ed.; McGuire, W., Kilburn, C., Murray, J., Eds.; Routledge: London, UK, 1995; pp. 1–21.
15. Teschner, M.; Vougioukalakis, G.E.; Faber, E.; Poggenburg, J.; Hatziyannis, G. Real time monitoring of gas-geochemical parameters in Nisyros fumaroles. *Dev. Volcanol.* **2005**, *7*, 247–254, doi:10.1016/S1871-644X(05)80044-0.
16. Moure, D.; Torres, P.; Casas, B.; Toma, D.; Blanco, M.J.; Río, J.D.; Manuel, A. Use of low-cost acquisition systems with an embedded linux device for volcanic monitoring. *Sensors* **2015**, *15*, 20436–20462, doi:10.3390/s150820436.
17. Pérez-Guillén, C.; Tsunematsu, K.; Nishimura, K.; Issler, D. Seismic detection and tracking of avalanches and slush flows on Mt. Fuji, Japan. *Earth Surf. Dyn. Discuss.* **2019**, 1–29, doi:10.5194/esurf-2019-25.
18. Peci, L.M.; Berrocoso, M.; Fernández-Ros, A.; García, A.; Marrero, J.M.; Ortiz, R. Embedded ARM system for volcano monitoring in remote areas: Application to the active volcano on Deception Island (Antarctica). *Sensors* **2014**, *14*, 672–690, doi:10.3390/s140100672.
19. Lopes Pereira, R.; Trindade, J.; Gonçalves, F.; Suresh, L.; Barbosa, D.; Vazão, T. A wireless sensor network for monitoring volcano-seismic signals. *Nat. Hazards Earth Syst. Sci.* **2014**, *14*, 3123–3142, doi:10.5194/nhess-14-3123-2014.
20. Awadallah, S.; Moure, D.; Torres-González, P. An internet of things (IoT) application on volcano monitoring. *Sensors* **2019**, *19*, doi:10.3390/s19214651.
21. Terray, L.; Royer, L.; Sarramia, D.; Achard, C.; Bourdeau, E.; Chardon, P.; Claude, A.; Fuchet, J.; Gauthier, P.J.; Grimbichler, D.; et al. From sensor to cloud: An IoT network of radon outdoor probes to monitor active volcanoes. *Sensors* **2020**, *20*, 2755, doi:10.3390/s20102755.
22. Encyclopedia Britannica. Definition of Fumarole. Available online: https://www.britannica.com/science/fumarole (accessed on 16 January 2016).

23. He, W.; Zhang, G.; Zhang, X.; Ji, J.; Li, G.; Zhao, X. Recent development and application of thermoelectric generator and cooler. *Appl. Energy* **2015**, *143*, 1–25, doi:10.1016/j.apenergy.2014.12.075.
24. Suter, C.; Jovanovic, Z.; Steinfeld, A. A 1 kWel thermoelectric stack for geothermal power generation-Modeling and geometrical optimization. *AIP Conf. Proc.* **2012**, *1449*, 540–543, doi:10.1063/1.4731613.
25. Woerner, D. A Progress Report on the eMMRTG. *J. Electron. Mater.* **2016**, *45*, 1278–1283, doi:10.1007/s11664-015-3998-8.
26. Stevens, J.W. Optimal placement depth for air-ground heat transfer systems. *Appl. Therm. Eng.* **2004**, *24*, 149–157, doi:10.1016/j.applthermaleng.2003.09.004.
27. Lawrence, E.E.; Snyder, G.J. A study of heat sink performance in air and soil for use in a thermoelectric energy harvesting device. In Proceedings of the Twenty-First International Conference on Thermoelectrics, Long Beach, CA, USA, 25–29 August 2002; pp. 446–449.
28. Stevens, J.W. Performance factors for ground-air thermoelectric power generators. *Energy Convers. Manag.* **2013**, *68*, 114–123, doi:10.1016/j.enconman.2012.12.029.
29. Stokes, C.D.; Duff, E.A.; Mantini, M.J.; Grant, B.A.; Venkatasubramanian, R. Nanostructured thermoelectric material and device technology for energy harvesting applications. In Proceedings of the 2010 IEEE Nanotechnology Materials and Devices Conference, Monterey, CA, USA, 12–15 October 2010; pp. 154–159.
30. Yan, X.; Cheng, H.; Zhao, Y.; Yu, W.; Huang, H.; Zheng, X. Real-time identification of smoldering and flaming combustion phases in forest using a wireless sensor network-based multi-sensor system and artificial neural network. *Sensors* **2016**, *16*, doi:10.3390/s16081228.
31. Norman, S.P.; Koch, F.H.; Hargrove, W.W. Review of broad-scale drought monitoring of forests: Toward an integrated data mining approach. *For. Ecol. Manag.* **2016**, *380*, 346–358, doi:10.1016/j.foreco.2016.06.027.
32. Cale, J.A.; Klutsch, J.G.; Erbilgin, N.; Negrón, J.F.; Castello, J.D. Using structural sustainability for forest health monitoring and triage: Case study of a mountain pine beetle (Dendroctonus ponderosae)-impacted landscape. *Ecol. Indic.* **2016**, *70*, 451–459, doi:10.1016/j.ecolind.2016.06.020.
33. Wang, N.; Xu, D.; Li, W.; Chen, C.; Huang, Y. Feasibility study of a new thermoelectric conversion device utilizing the temperature differences in forest soil. *Acta Tech. CSAV* **2017**, *62*, 1–12.
34. Huang, Y.; Xu, D.; Kan, J.; Li, W. Study on field experiments of forest soil thermoelectric power generation devices. *PLoS ONE* **2019**, *14*, e0221019, doi:10.1371/journal.pone.0221019.
35. Huang, Y.; Li, W.; Xu, D.; Wu, Y. Spatiotemporal rule of heat transfer on a soil/finned tube interface. *Sensors* **2019**, *19*, doi:10.3390/s19051159.
36. Wang, H.; Jasim, A.; Chen, X. Energy harvesting technologies in roadway and bridge for different applications—A comprehensive review. *Appl. Energy* **2018**, *212*, 1083–1094, doi:10.1016/j.apenergy.2017.12.125.
37. Gholikhani, M.; Roshani, H.; Dessouky, S.; Papagiannakis, A.T. A critical review of roadway energy harvesting technologies. *Appl. Energy* **2020**, *261*, 114388, doi:10.1016/j.apenergy.2019.114388.
38. Tahami, S.A.; Gholikhani, M.; Nasouri, R.; Dessouky, S.; Papagiannakis, A.T. Developing a new thermoelectric approach for energy harvesting from asphalt pavements. *Appl. Energy* **2019**, *238*, 786–795, doi:10.1016/j.apenergy.2019.01.152.
39. Jiang, W.; Yuan, D.; Xu, S.; Hu, H.; Xiao, J.; Sha, A.; Huang, Y. Energy harvesting from asphalt pavement using thermoelectric technology. *Appl. Energy* **2017**, *205*, 941–950, doi:10.1016/j.apenergy.2017.08.091.
40. Astrain, D.; Vián, J.G.; Martínez, A.; Rodríguez, A. Study of the influence of heat exchangers' thermal resistances on a thermoelectric generation system. *Energy* **2010**, *35*, 602–610, doi:10.1016/j.energy.2009.10.031.
41. Elghool, A.; Basrawi, F.; Ibrahim, T.K.; Habib, K.; Ibrahim, H.; Idris, D.M.N.D. A review on heat sink for thermo-electric power generation: Classifications and parameters affecting performance. *Energy Convers. Manag.* **2017**, *134*, 260–277, doi:10.1016/j.enconman.2016.12.046.
42. Champier, D. Thermoelectric generators: A review of applications. *Energy Convers. Manag.* **2017**, *140*, 167–181, doi:10.1016/j.enconman.2017.02.070.
43. Catalan, L.; Aranguren, P.; Araiz, M.; Perez, G.; Astrain, D. New opportunities for electricity generation in shallow hot dry rock fields: A study of thermoelectric generators with different heat exchangers. *Energy Convers. Manag.* **2019**, *200*, 112061, doi:10.1016/j.enconman.2019.112061.

44. Elghool, A.; Basrawi, F.; Ibrahim, H.; Ibrahim, T.K.; Ishak, M.; Yusof, T.M.; Bagaber, S.A. Enhancing the performance of a thermo-electric generator through multi-objective optimisation of heat pipes-heat sink under natural convection. *Energy Convers. Manag.* **2020**, *209*, 112626, doi:10.1016/j.enconman.2020.112626.
45. Araiz, M.; Catalan, L.; Herrero, O.; Perez, G.; Rodriguez, A. *Bringing Thermoelectricity into Reality*; IntechOpen: London, UK, 2018; pp. 123–144.
46. II-VI Marlow. Technical Data Sheet for TG12-8. Available online: https://cdn2.hubspot.net/hubfs/547732/Data_Sheets/TG12-8.pdf (accessed on 10 November 2018).
47. Titanlux. Epoxy Primer. Available online: https://www.titanlux.es/es/productos/producto/imprimacion-anticorrosiva-epoxi (accessed on 9 October 2018).
48. Titanlux. Marine Primer. Available online: https://www.titanlux.es/es/productos/producto/imprimacion-marina-spray (accessed on 9 October 2018).
49. Multicomp. Medium Cure Thermally Conductive Adhesive, Flowable. Available online: https://es.farnell.com/multicomp/mc002976/adhesivo-epoxi-jeringa-25ml-negro/dp/2917625?ost=2917625 (accessed on 9 October 2018).
50. Coleman, H.; Steele, W. *Experimentation, Validation and Uncertainty. Analysis for Engineers*, 3rd ed.; John Wiley & Sons: Hoboken, NJ, USA, 2018.
51. Mamur, H.; Ahiska, R. Application of a DC-DC boost converter with maximum power point tracking for low power thermoelectric generators. *Energy Convers. Manag.* **2015**, *97*, 265–272, doi:10.1016/j.enconman.2015.03.068.
52. Cypress. Embedded in Tomorrow. MB39C831-EVB-03 Ultra Low Voltage Boost PMIC Energy Harvesting Evaluation Board. Available online: https://www.mouser.es/ProductDetail/Cypress-Semiconductor/MB39C831-EVB-03?qs=%2Fha2pyFadujg6FCDuilZeC4uCIlnLbGlfI4VPcTwKpbX13BO8p6KNQ%3D%3D (accessed on 24 September 2018).
53. RS Pro. 18650 26H Li-ion Battery Pack. Available online: https://es.rs-online.com/web/p/baterias-recargables-de-tamanos-especiales/1449406/?relevancy-data=636F3D3126696E3D4931384E525353746F636B4E756D626572266C753D656E266D6D3D6D61746368616C6C26706D3D5E2828282872737C5253295B205D3F293F285C647B337D5B5C2D5C735D3F5C647B332C347D5B705061415D3F29297C283235285C647B387D7C5C647B317D5C2D5C647B377D2929292426706F3D3126736E3D592673723D2673743D52535F53544F434B5F4E554D4245522677633D4E4F4E45267573743D3134342D39343036267374613D3134343934303626&searchHistory=%7B%22enabled%22%3Atrue%7D (accessed on 25 September 2018).
54. Sparkfun. LiPower—Boost Converter. PRT-10255 ROHS. Available online: https://www.sparkfun.com/products/10255 (accessed on 26 September 2018).
55. Maxim. MAX31855PMB1 Peripheral Module. Available online: http://www.farnell.com/datasheets/2025616.pdf?_ga=2.166306554.590905385.1591082285-1433754008.1590608561 (accessed on 10 February 2018).
56. Adafruit. INA219 High Side DC Current Sensor Breakout—26 V ±3.2 A Max . Available online: https://www.adafruit.com/product/904 (accessed on 17 January 2018).
57. Tadayoni, R.; Henten, A.; Falch, M. Internet of Things—The battle of standards. In Proceedings of the Joint 13th CTTE and 10th CMI Conference on Internet of Things—Business Models, Users, and Networks, Copenhagen, Denmark, 23–24 November 2017; pp. 1–7.
58. Raza, U.; Kulkarni, P.; Sooriyabandara, M. Low power wide area networks: An overview. *IEEE Commun. Surv. Tutor.* **2017**, *19*, 855–873, doi:10.1109/COMST.2017.2652320.
59. Frenzel, L. Long-Range IoT on the Road to Success. Available online: https://www.electronicdesign.com/technologies/embedded-revolution/article/21805055/longrange-iot-on-the-road-to-success (accessed on 4 February 2019).
60. Harada, H.; Mizutani, K.; Fujiwara, J.; Mochizuki, K.; Obata, K.; Okumura, R. IEEE 802.15.4g based Wi-SUN communication systems. *IEICE Trans. Commun.* **2017**, *E100B*, 1032–1043, doi:10.1587/transcom.2016SCI0002.
61. Accent Systems. Diferencias Entre NB-IoT y LTE-M. Available online: https://accent-systems.com/es/blog/diferencias-nb-iot-lte-m/ (accessed on 7 February 2019).
62. Wi-SUN Alliance. Comparing IoT Networks at a Glance; Available online: https://www.wi-sun.org/wp-content/uploads/Wi-SUN-Alliance-Comparing_IoT_Networks-r1.pdf (accessed on 6 May 2020)
63. Postscapes. IoT Standards and Protocols. Available online: https://www.postscapes.com/internet-of-things-protocols/ (accessed on 4 May 2020).

64. Adafruit. RFM95W LoRa Radio Transceiver Breakout—868 or 915 MHz—RadioFruit . Available online: https://www.adafruit.com/product/3072 (accessed on 10 January 2019).
65. RF Solutions. Antenna 2G (GSM/GPRS), ISM Band, 23 dBi, SMA Connector. Available online: https://es.rs-online.com/web/p/antenas-gsm-y-gprs/7620070/ (accessed on 10 March 2019).
66. RayTech. Magic Power Gel. Available online: https://www.raytech.it/es/producto/baja-tension/rellenos/gel-es/magic-power-gel(accessed on 14 April 2019).
67. Castro-Almazán, J.A.; Muñoz-Tuñón, C. Climatological study for the Cherenkov telescope array north site at the Canary Islands I: Temperature, precipitation, and relative humidity. *Publ. Astron. Soc. Pac.* **2018**, *130*, 115002, doi:10.1088/1538-3873/aadf77.
68. Tagoror Meteo. Islas Canarias. La Verdad Oculta Sobre el Episodio HistóRico de Calima de Febrero de 2020. Available online: https://tagorormeteo.es/episodio-historico-de-calima-de-febrero-de-2020/ (accessed on 3 May 2020).
69. Volcanological Institute of the Canary Islands INVOLCAN. Available online: http://www.involcan.org/ (accessed on 7 February 2017).
70. WEST Systems. Available online: https://www.westsystems.com/ (accessed on 18 January 2018).
71. Victron Energy. SmartSolar MPPT 75/10, 75/15, 100/15 & 100/20. Solar Charge Controller. Available online: https://www.victronenergy.com/solar-charge-controllers/smartsolar-mppt-75-10-75-15-100-15-100-20 (accessed on 22 January 2019).

Chapter 7

Conclusions and Future lines

This last chapter summarizes the most relevant conclusions and results obtained in the studies and developments performed during the attainment of the present Ph. D. dissertation, in which two novel applications of thermoelectric generators based on geothermal energy have been analyzed: medium–scale generation from Hot Dry Rock fields, and stand–alone power supply of volcanic monitoring stations.

Section 7.1 includes the general conclusions of the thesis, which have been divided into conclusions derived from the state of the art in Subsection 7.1.1, conclusions of the development of thermoelectric generators for medium–scale geothermal power generation in Subsection 7.1.2, and conclusions of the stand–alone volcanic monitoring stations powered by thermoelectric generators in Subsection 7.1.3.

Afterwards, Section 7.2 presents the most relevant scientific contributions made during the time devoted to the fulfillment of this Ph. D. dissertation, including not only the results directly related to the thesis but also other contributions performed during the same period.

Finally, Section 7.3 comprises the recommendations for future works intended to continue with this research line. Most of these recommendations will be accomplished within the research project ELECTROVOLCAN (RTC–2017–6628–3) funded by the Spanish Ministry of Science, Innovation, and Universities, which finishes in June 2021. Furthermore, the second application related to autonomous volcanic vigilance station has also received extra funding, thanks to a grant awarded to the Ph. D. candidate by the Official School of Industrial Engineers of Navarre in the *Fuentes Dutor* call.

7.1 Conclusions

The main conclusions reached after the completion of this Ph. D. dissertation are described below, starting with those derived from the state of the art, and followed by the outcomes of the two applications under consideration in the present thesis. Moreover, the attainment of the different specific objectives of the thesis is also pointed out.

7.1.1 Conclusions Derived from the State of the Art

The conclusions relative to the state of the art address the research necessities derived from the bibliographic review, which have led to the development of the present Ph. D. dissertation.

1. Although thermoelectricity has demonstrated to be a robust, reliable, durable, and scalable technology that does not require moving parts, working fluids nor auxiliary equipment, there is a lack of real applications. Therefore, there is an interest to find new applications in which thermoelectric generators can finally be made a reality despite their low efficiency.

2. In order to improve the efficiency of thermoelectric generators, apart from the development of new thermoelectric materials, it is of utmost importance to optimize the heat exchangers due to their influence in the robustness and efficiency of the generators. In this sense, heat exchangers that obtain low values of thermal resistance without moving parts nor auxiliary consumption are gaining attention.

3. In the last years, computational models have emerged as an indispensable tool for the design and optimization of thermoelectric generators. Nonetheless, in order to obtain a reliable instrument, it is necessary that these models take into account all thermoelectric effects, consider temperature–dependent properties, and incorporate the modeling of the heat exchangers and the heat reservoirs.

4. Geothermal energy has recently been proposed as heat source for thermoelectric generators. In comparison with other renewable sources, geothermal energy stands out because it is not affected by weather, it is stable, it has a high capacity factor, and it can be used as base–load power.

5. Hot Dry Rock fields are one of the most abundant geothermal fields in the world. Nevertheless, despite their high temperatures, their exploitation is not being conducted

due to the seismicities induced by the only method existing nowadays, Enhanced Geothermal Systems.

6. Volcanic vigilance stations are indispensable in any volcanic system of the world. However, the power supply of such stations is often a challenge, so it is usually decided not to monitor the volcanoes, with its consequent risk. These stations require an autonomous and robust generator, that does not require maintenance, and that can withstand all kinds of meteorological conditions.

7.1.2 Conclusions of Medium–Scale Geothermal Thermoelectric Generation from Hot Dry Rock Fields

The first application subject of study of the present Ph. D. dissertation proposes the utilization of thermoelectric generators for Hot Dry Rock fields. The study, optimization, development, and characterization of such devices have been performed in the Chapters 2, 3 and 4, obtaining results that also lay the foundations for the second application under consideration in this thesis. The most relevant conclusions can be summarized as follows:

1. Thermoelectric generators can become an environmentally–friendly alternative to Enhanced Geothermal Systems in Hot Dry Rock fields because rock fracture can be avoided if solid or phase change heat exchangers are used on the hot side. Among both types of heat exchangers, the latter has demonstrated to be more appropriate since lower thermal resistances can be obtained.

2. A first prototype composed of a two–phase closed thermosyphon with a thermal resistance of 0.31 K/W as hot side heat exchanger and two bismuth–telluride thermoelectric modules was built and characterized at the laboratory considering fin dissipators and loop thermosyphons with different geometries as cold side heat exchangers.

3. The thermal resistance of the different types and geometries of cold side heat exchangers was experimentally determined with respect to different heat fluxes and fan voltages (the latter only in the case of fin dissipators; loop thermosyphons were completely passive and did not include any auxiliary equipment). The obtained results show that the thermal resistance of fin dissipators is mainly dependent on the fan voltage, decreasing with higher voltages since force convection improves. Hence, values of 0.37 K/W were obtained with 6 V, which diminished to 0.27 K/W when doubling the fan voltage. In the case of loop thermosyphons, their thermal resistance depends on both the heat flux and the size of the condensation area. Thus,

lower thermal resistances were obtained with higher heat fluxes and increased condensation areas. The 8 levels loop thermosyphon showed the best values, decreasing from 0.29 K/W with 20 W to 0.16 K/W with 140 W, while the 6 levels one presented slightly higher values, decreasing from 0.4 to 0.24 K/W for the same heat flux range.

4. After the characterization of the cold side heat exchangers, the whole thermoelectric generator was experimented to determine the power generated by the modules considering different heat source temperatures and load resistances. The lower thermal resistance of the 8 levels loop thermosyphon led to the highest generation. Thus, for a 200 °C heat source, a generation of 3.3 W per module was obtained, while with the 6 levels one 2.4 W were generated. The latter value is comparable with the results of total generation with fin dissipators as cold side heat exchangers. Nevertheless, it is necessary to take into account the consumption of the auxiliary equipment. If net generation is considered, the maximum power generation obtained with fin dissipators was 1.5 W, 54.5 % and 37.5 % less than with the previous loop thermosyphons respectively.

5. Considering the previous results, the importance of using passive heat exchangers, with no auxiliary consumption, and presenting low thermal resistances became evident. The best configuration of a geothermal thermoelectric generator is therefore composed of heat exchangers based on phase change at both sides of the thermoelectric modules. With this statement, the specific objective 2 is considered fulfilled.

6. Based on the former affirmation, a computational model based on the thermo–electrical analogy was developed. This model simulates the performance of an entire thermoelectric generator, including the heat exchangers, the heat source and sink; does not neglect any thermoelectric effect; and takes into consideration the influence of temperature in the properties, as well as the thermal and electrical effects. The model was programmed to facilitate the study of different configurations and permits the discretization of the heat exchangers including all the involved phenomena. Thus, in the case of heat exchangers based on phase change, conduction, boiling, condensation, and convection resistances are considered.

7. The novelty of the model, besides the application for it was conceived, is that it simulated for the first time a thermoelectric generator with phase change heat exchangers at both sides of the thermoelectric modules. Furthermore, the model is so versatile that it serves for any thermoelectric application, being a design and optimization tool in and of itself.

8. The developed model was validated thanks to the aforementioned experiments. Hence, firstly the ability of the model to estimate the thermal resistance of the cold side heat exchanger was determined, leading to a relative error encompassed in the [−9.08 %, 8.21 %] interval in the 95 % of the cases for the habitual heat fluxes in this application. Regarding the whole thermoelectric generator, the generation values predicted by the model were in a ±6 % error range in comparison with the experimental ones considering load resistances higher than 2 Ω, and in a ±8 % one when estimating the temperature difference across the thermoelectric modules. Hence, these results lead to the attainment of the specific objective 1.

9. Based on the model, an analysis of the influence of different parameters on a geothermal thermoelectric generator was performed taking as reference two locations within Timanfaya National Park: *Islote Hilario*, where the geothermal gases emerge at a temperature of 480 °C and with a velocity of 11.15 m/s, and *Casa de los Camelleros*, with 200 °C and 6.03 m/s respectively. More specifically, for a geometry composed of a two phase closed thermosyphon with water as working fluid as hot side heat exchanger and loop thermosyphons for the cold side one, the influence of the size of both heat exchangers and of the number of thermoelectric modules were studied. As a result, the importance of having low thermal resistances was again evidenced, since the lower the thermal resistances the higher the generation. Nonetheless, for each configuration, there was an optimal number of thermoelectric modules due to the fact that the proposed design used a unique two phase closed thermosyphon for all the modules and cold side heat exchangers. This optimal number of modules increased with higher thermal resistances of the cold side heat exchanger.

10. Among the studied cases, the optimal geothermal thermoelectric generator for *Islote Hilario* generated 68.07 W with 16 thermoelectric modules, when the hot side two phase closed thermosyphon was inserted 3 m in the ground and 8 levels loop thermosyphons were used as cold side heat exchangers. The same size of heat exchangers led to the optimal generator in *Casa de los Camelleros* too. Nevertheless, due to the lower heat source temperature, the maximum generation of this device was of 43.23 W, achieved with 28 thermoelectric modules.

11. Another alternative that also fulfills the requirements of absence of moving parts and auxiliary consumption but it is simpler, consists of using a solid bar as hot side heat exchanger and fin dissipators working under natural convection as cold side ones. This configuration was also studied, obtaining a huge detriment in the generation that was quantified in 97 % for *Islote Hilario* and 81 % in Casa de los Camelleros. If the hot side heat exchanger was modified and a two phase closed

thermosyphon was again used, but fin dissipators were maintained at the cold side, the decrease in the generation was quantified in 31.9 % and 27.1 % respectively in comparison with loop thermosyphons. Apart from the decrease in generation, the utilization of fin dissipators as cold side heat exchangers also required a higher number of thermoelectric modules to reach the optimal value, which would increase the size and cost of the generator. Therefore, it was reaffirmed that the best configuration for a geothermal thermoelectric generator is composed of phase change heat exchangers at both sides of the thermoelectric modules.

12. With the optimized geothermal thermoelectric generators with phase change heat exchangers, and taking into account the extension of the areas of *Islote Hilario* and *Casa de los Camelleros* (3000 and 2000 m^2 respectively), the average ambient conditions, and the amount of energy that can be extracted from the ground per unit of time without affecting the geothermal field, an estimation of the annual electricity generation that can be achieved was performed. Thus, it was obtained that up to 470.87 MWh can be generated in *Islote Hilario* and 210.66 MWh in *Casa de los Camelleros*, which sums up an annual electricity generation of 681.53 MWh. This result entails the achievement of the specific objective 4.

13. Based on the previous results, two prototypes with phase change heat exchangers were designed to be installed on field at the geothermal anomalies of *Casa de los Camelleros* considering constructional aspects. In the process, it was taken into account that apart from having heat exchangers with low thermal resistances, it is also important to avoid moving parts, auxiliary consumption, noise, and harmful working fluids, while being compact, modular, and easy assembly.

14. Due to the lack of commercial products with the previous characteristics, the manufacturing process of the heat exchangers was also developed, leading to an inexpensive and quick methodology that permits obtaining low values of thermal resistances. In the case of the cold side heat exchanger, it was experimentally determined that its value is of around 0.4 K/W, while in the hot side one, thermal resistances lower than 0.16 K/W were obtained.

15. After the complete design process, the two real size prototypes were built at the laboratories of the Public University of Navarre, where their characterization was performed for different operating conditions prior to their installation on field.

16. The obtained results show that, for the optimal load resistance, there exists a linear correlation between the power generated and the gradient between the heat source and the ambient temperatures. This generation is higher for lower levels, forced

convection conditions, as well as in the prototype with less thermoelectric modules. In total, the prototype with 10 thermoelectric modules led to a maximum generation of 17.1 W given a temperature difference of 160 °C between sources and a wind speed of 1.5 m/s, while the prototype with 6 thermoelectric modules produced a maximum of 20 W with the same velocity and a gradient of 166 °C. These results suppose the accomplishment of the specific objective 3, whose scope will be enlarged in the upcoming installation at Timanfaya National Park.

7.1.3 Conclusions of the Stand–Alone Power Supply of Volcanic Monitoring Stations

The second application under consideration in the present Ph. D. dissertation deals with the development of autonomous volcanic monitoring stations powered by thermoelectric generators. Chapters 5 and 6 have analyzed their prospects, for which two different prototypes were installed at Teide volcano (Canary Islands, Spain). The main conclusions obtained in this application are described below.

1. Firstly, the fumaroles available at Teide volcano were characterized regarding their temperature and humidity. These fumaroles represent the heat source for the thermoelectric generators, heating up and moistening the soil in their emergence to the surface. Hence, it was measured that for depths higher than 10 cm the temperature of the ground presents a constant value of 82 °C, while for shallower depths the ambient conditions influence. The soil moisture also presents a stable value of around 90 %, which ensures a good heat transfer with the generator.

2. A first prototype composed of two thermoelectric modules and heat pipes as heat exchangers was installed at Teide volcano in March 2019. Similarly to the previous application, this configuration permits obtaining a generator without moving parts nor auxiliary consumption. The cold side heat exchanger of this prototype presented a thermal resistance lower than 0.3 K/W under forced convection conditions, the typical ones in the volcano.

3. This first prototype produced a net generation between 0.32 and 0.33 W per module given a temperature difference between the heat reservoirs of 69 to 86 °C that includes ambient temperatures below 0 °C. The average temperature of the hot and cold sides of the thermoelectric modules was 55 and 15 °C respectively.

4. This first prototype served for the demonstration of the feasibility of thermoelectric generation from fumaroles. Nevertheless, it also exhibited the harsh conditions that

the device needs to withstand. The hydrogen sulfide contained in the fumaroles reacts with steam forming sulfuric acid, which virulently attacks metals, especially copper. This caused the failure of the electronics after only two days of installation.

5. Thanks to all the knowledge learned from the previous experience, a new prototype was developed. This second prototype was also composed of heat pipes as heat exchangers, thus leading to a robust device that does not require maintenance, and incorporated four thermoelectric modules. Nonetheless, in comparison with the previous one, several improvements were introduced: protective coatings against corrosion, new assembly method for the heat exchangers, and reduced thermal resistance of the cold side heat exchangers thanks to an increase of area.

6. This second prototype was firstly characterized in the laboratory. Hence, it was obtained a thermal resistance of 0.24 K/W for the cold side heat exchanger under forced convection conditions with an ambient temperature of 15 °C and an air velocity of 4 m/s. In the case of the hot side heat exchanger, the average value was 0.35 K/W under natural convection in a 75 °C thermostatic bath with water. The generation of the prototype was also measured for different electrical load resistances. Thus, the obtained results led to a maximum power generation of 0.36 W per module with a 2.2 Ω load resistance, equivalent to an efficiency of 1 %.

7. Apart from the generator itself, the development of the electronic part necessary to achieve a completely autonomous volcanic monitoring station was also one of the specific objectives of the present Ph. D. dissertation, that was completely developed. Thus, a complete system composed of MPPTs that ensure that the thermoelectric modules work in their optimum point and store the generated energy in a low–capacity battery, a boost converter that elevates the battery voltage to the one required by the consuming elements, several sensors that monitor different temperatures and electrical powers, an electrical resistor that simulates peaks in the consumption, and a communication system based on LoRa to emit the measured data to a gateway located several kilometers away was also developed. The modification of the communication technology from a GSM router to the Internet of Things (IoT) technology LoRa permitted a reduction of 97 % in the energy demand.

8. The prototype was installed at Teide volcano in December 2019 and on the date of submission of this Ph. D. dissertation it is still in operation. During 93.95 % of the time only one thermoelectric module has been necessary to power the data acquisition and communication systems. This thermoelectric module has generated between 0.27 and 0.75 W with a temperature difference across it in the range of 38 to 66 °C; on

average 0.49 W with a temperature gradient of 51.5 °C. With the measured data, it was possible to calculate the thermal resistance of the heat exchangers, leading to 0.27 and 0.24 K/W for the hot and cold side respectively, which evidences that conduction is the heat transfer mechanism dominant in the heat transfer with the ground. Hence, the other specific objective related to the stand–alone power supply of volcanic monitoring stations, the fifth specific objective, is also considered fulfilled.

9. Since its installation, the prototype has resisted all kind of meteorological conditions, from severe snowfalls and frost to days with the typical Saharan air layer, and neither the generator nor the electronic system have failed, being still in operation after more than 8 months and always ensuring the communication over 14 km every 4 minutes. Therefore, it can be concluded that autonomous volcanic vigilance stations powered by thermoelectric generators can become a reality.

7.2 Scientific Contributions

The research carried out during the fulfillment of this thesis has been presented in different formats: patents, publications in JCR journals, books, book chapters, publications in conference proceedings, communications in conferences, or Bachelor's Thesis supervised. This section enumerates these scientific contributions distinguishing into those contributions directly related to the present Ph. D. dissertation, and those performed at the same time due to the participation of the Ph. D. candidate in other research projects. In addition to this information, the scholarships obtained and the research stays accomplished during the thesis are also mentioned.

Scholarships

- The research presented in this Ph. D. dissertation was awarded public funding for the whole period of the thesis by means of a predoctoral scholarship for the training of university teachers given by the Spanish Ministry of Science, Innovation, and Universities. The call was published in the Spanish State Official Newsletter (BOE) on Thursday 22^{nd} December 2016, and the awarded scholarship code is FPU 16/05203.
- On 3^{rd} December 2018, a three months research stay was initiated at the Institute of Technology and Renewable Energies (ITER) located in Tenerife (Spain), thanks to the predoctoral mobility program funded by the Government of Navarre.
- Furthermore, in May 2020, another scholarship was obtained to continue with the development of volcanic vigilance stations powered by thermoelectric generators. This scholarship is funded by the Official School of Industrial Engineers of Navarre.

Research stays

- As exposed previously, between December 2018 and March 2019, a research internship was performed at the Institute of Technology and Renewable Energies (ITER). This institution is the coordinator of ELECTROVOLCAN project and has its headquarters in Tenerife island (Canary Islands, Spain).
- Between March and June 2020, another research stay was programmed at Cardiff University under the supervision of professor Gao Min. Nevertheless, with the coronavirus pandemic, it could not be attended in person and only those tasks that could be developed remotely were completed.

Patents

The configuration of a geothermal thermoelectric generator with biphasic thermosyphons at both sides of the thermoelectric modules has been patented under the number WO 2019/202180 A1, whose authors are D. Astrain, L. Catalan, P. Aranguren and M. Araiz.

Publications in JCR Journals

The publications in JCR Journals directly related to the thesis are the four articles that endorse the present Ph. D. dissertation as a compendium.

- L. Catalan, P. Aranguren, M. Araiz, G. Perez, D. Astrain. "New opportunities for electricity generation in shallow hot dry rock fields: a study of thermoelectric generators with different heat exchangers". *Energy Conversion and Management* 200 (2019) 112061. DOI: 10.1016/j.enconman.2019.112061
- L. Catalan, M. Araiz, P. Aranguren, D. Astrain. "Computational study of geothermal thermoelectric generators with phase change heat exchangers". *Energy Conversion and Management* 221 (2020) 113120. DOI: 10.1016/j.enconman.2020.113120
- L. Catalan, M. Araiz, P. Aranguren, G.D. Padilla, P.A. Hernandez, N.M. Perez, C. Garcia de la Noceda, J.F. Albert, D. Astrain. "Prospects of Autonomous Volcanic Monitoring Stations: Experimental Investigation on Thermoelectric Generation on Fumaroles". *Sensors* 20 (2020), 3547. DOI: 10.3390/s20123547
- L. Catalan, A. Garacochea, A. Casi, M. Araiz, P. Aranguren, D. Astrain. "Autonomous volcanic monitoring stations: combination of thermoelectric generators and Internet of Things (IoT)". *Sensors* 20 (2020) 4839. DOI: 10.3390/s20174839

Besides them, the Ph. D. candidate has also published the following articles in JCR journals. These publications are also related to thermoelectricity, encompassed in other research projects developed by the Thermal and Fluids Engineering Research Group from the Public University of Navarre, in which, as exposed later, the Ph. D. candidate has participated.

- M. Araiz, A. Casi, L. Catalan, A. Martinez, D. Astrain. "Prospects of waste-heat recovery from a real industry using thermoelectric generators: Economic and power output analysis". *Energy Conversion and Management* 205 (2020) 112376. DOI: 10.1016/j.enconman.2019.112376

- D. Astrain, A. Merino, L. Catalan, P. Aranguren, M. Araiz, D. Sanchez, R. Cabello, R. Llopis. "Improvements in the cooling capacity and the COP of a transcritical CO2 refrigeration plant operating with a thermoelectric subcooling system". *Applied Thermal Engineering* 155 (2019) 110-122. DOI: 10.1016/j.applthermaleng.2019.03.123

Books and book chapters

During this period, a book chapter and a book have also been published parallel to the development of the thesis.

- M. Araiz, L. Catalan, O. Herrero, G. Perez, A. Rodriguez. "The importance of the assembly in thermoelectric generators" in the book "Bringing Thermoelectricity into Reality". P. Aranguren, *IntechOpen*: London, UK, 2018. pp. 123–144. ISBN: 978-1-78923-440-4. DOI: 10.5772/intechopen.71354
- J. Samanes, J. Pascual, A. Berrueta, M. Araiz, L. Catalan, P. Aranguren, D. Arricibita. "Energía sostenible: sin malos humos" The Spanish adaption of David MacKay's "Sustainable Energy: without the hot air". UPNA and UIT Cambridge: Pamplona, Spain. 2019. ISBN: 978-84-9769-353-0.

Publications in Conference Proceedings

The conference proceedings directly related to the thesis are:

- L. Catalan, M. Araiz, P. Aranguren, D. Astrain. "Design of a passive geothermal thermoelectric generator for shallow hot dry rock fields: application to Timanfaya National Park". *XI National and II International Engineering Thermodynamics Congress Proceeding Book* 2019. ISBN: 978-84-09-11635-5.
- L. Catalan, D. Astrain, P. Aranguren, M. Araiz. "Comparative analysis of different cooling systems for geothermal thermoelectric generators". *IX Iberian and VII Ibero-American Congress in Cooling Science and Techniques Proceedings (CYTEF 2018)* 2018. ISBN: 978-84-09-01619-8.

Moreover, the following proceedings have also been published:

- P. Aranguren, I. San Martin, L. Catalan, A. Martinez, A. Jurio, S. Diaz, G. Perez, M. Gomez, E. Barrenechea. "Initiative to Increment the number of women in STEM

degrees: Women, Science and Technology Chair of the Public University of Navarre". *IEEE Global Engineering Education Conference EDUCON* 2020. ISBN: 978-1-7281-0930-5.

- A. Jurio, L. Catalan, I. San Martin, P. Aranguren, A. Martinez, S. Diaz, E. Barrenechea, M. Gomez, G. Perez. ""Yo quiero ser cientifica" a creative way to inspire girls in science". *IEEE Global Engineering Education Conference EDUCON* 2020. ISBN: 978-1-7281-0930-5.

- M. Araiz, D. Astrain, P. Aranguren, A. Martinez, L. Catalan, A. Casi. "Thermoelectric generator with passive heat exchangers for waste-heat recovery in a manufacturing plant". *XI National and II International Engineering Thermodynamics Congress Proceeding Book* 2019. ISBN: 978-84-09-11635-5.

- P. Aranguren, D. Sanchez, A. Casi, M. Araiz, L. Catalan. "ITF CAN COOLER: A tailored vapor compression cooling system designed to be used at practice sessions". *XI National and II International Engineering Thermodynamics Congress Proceeding Book* 2019. ISBN: 978-84-09-11635-5.

- M. Araiz, P. Aranguren, L. Catalan, A. Martinez, D. Astrain. "Passive heat exchanger with no moving parts for thermoelectric generators". *IX Iberian and VII Ibero-American Congress in Cooling Science and Techniques Proceedings (CYTEF 2018)* 2018. ISBN: 978-84-09-01619-8.

- D. Astrain, L. Catalan, P. Aranguren, M. Araiz, A. Merino, D. Sanchez, R. Llopis, R. Cabello, J. Catalan-Gil. "Computational Study of a CO2 Cooling System with Thermoelectric Subcooling". *IX Iberian and VII Ibero-American Congress in Cooling Science and Techniques Proceedings (CYTEF 2018)* 2018. ISBN: 978-84-09-01619-8.

Communications in Conferences

During the fulfillment of the thesis, the Ph. D. candidate has assisted to 14 international conferences. The contributions directly related to this Ph. D. dissertation are detailed below, indicating the type of contribution (oral, poster, or invited).

- Oral: L. Catalan, A. Garacochea, A. Casi, M. Araiz, P. Aranguren, D. Astrain, G.D. Padilla, N.M. Perez, P.A. Hernandez, J.F. Albert, C. Garcia de la Noceda. "Autonomous volcanic monitoring stations: combination of thermoelectric generators and Internet of Things (IoT)". Virtual Conference on Thermoelectrics (Online, 2020).

- Oral: P. Alegria, L. Catalan, M. Araiz, D. Astrain. "Design and optimization of a thermoelectric generator for the high enthalpy superficial geothermal anomalies of Timanfaya National Park". Virtual Conference on Thermoelectrics (Online, 2020).
- Invited: L. Catalan. "Study of the degradation of different thermoelectric modules at Teide volcano". Seminar on Climatic Reliability of Electronics: Global Challenges and Perspectives. (Lyngsby, Denmark, 2020).
- Oral: L. Catalan, M. Araiz, P. Aranguren, A. Garacochea, D. Astrain, V. Dominguez, A.C. Montañez, G.D. Padilla, N.M. Perez, P.A. Hernandez, J. Barrancos, J.F. Albert, C. Garcia de la Noceda. "Autonomous volcanic monitoring stations at Teide National Park (Spain)". 17th European Conference on Thermoelectrics (Limassol, Cyprus, 2019).
- Poster: L. Catalan, M. Araiz, P. Aranguren, D. Astrain. "Study of different heat exchangers for thermoelectric generators for Timanfaya National Park (Spain)". 17th European Conference on Thermoelectrics (Limassol, Cyprus, 2019).
- Poster: L. Catalán, G. Pérez, C. Berlanga, A. Garacochea, D. Astrain, P. Aranguren, M. Araiz. "Study of the degradation of different thermoelectric modules in acidic environment". 17th European Conference on Thermoelectrics (Limassol, Cyprus, 2019).
- Oral: L. Catalan, G. Perez, C. Berlanga, D. Astrain, A. Garacochea, P. Aranguren, M. Araiz, V. Dominguez, A.C. Montañez, G.D. Padilla. "Study of the degradation of different thermoelectric modules at Teide National Park". EUROCORR 2019 "The annual event of the European Federation of Corrosion" (Sevilla, Spain, 2019).
- Poster: L. Catalan, G. Perez, C. Berlanga, A. Garacochea, A. Rodriguez, V. Dominguez, A.C. Montañez, G.D. Padilla, N.M. Perez. "Study of the degradation of heat exchanger materials in the acidic environment of Teide National Park". EUROCORR 2019 "The annual event of the European Federation of Corrosion" (Sevilla, Spain, 2019).
- Oral: L. Catalan, A. Garacochea, M. Araiz, P. Aranguren, D. Astrain, V. Dominguez, A.C. Montañez, G.D: Padilla, N.M. Perez, J.F. Albert, C. Garcia de la Noceda, P.A. Hernandez, J. Barrancos. "Development of a thermoelectric generator to supply energy to volcanic vigilance stations". 2nd Iberian Thermoelectric Workshop (Ciudad Real, Spain, 2019).

- Poster: L. Catalan, M. Araiz, A. Casi, P. Aranguren, D. Astrain. "Computational optimization of a geothermal thermoelectric generator for high enthalpy superficial hot dry rock fields". 2nd Iberian Thermoelectric Workshop (Ciudad Real, Spain, 2019).
- Poster: A. Garacochea, L. Catalan, A. Casi, E. Gubia, D. Astrain. "The promising combination of thermoelectric generators with IoT technologies for autonomous monitoring systems". 2nd Iberian Thermoelectric Workshop (Ciudad Real, Spain, 2019).
- Poster: L. Catalan, D. Astrain, P. Aranguren, M. Araiz. "Geothermal Thermoelectric Generator for Timanfaya National Park". 38th International Conference on Thermoelectrics and 4th Asian Conference on Thermoelectrics (Gyeongju, South Korea, 2019).
- Oral: L. Catalan, M. Araiz, P. Aranguren, D. Astrain. "Design of a passive geothermal thermoelectric generator for shallow hot dry rock fields: application to Timanfaya National Park". XI National and II International Engineering Thermodynamics Congress (Albacete, Spain, 2019).
- Co-Invited: D. Astrain, L. Catalan. "Generation of electricity by the thermoelectric effect using superficial geothermal anomalies of volcanic origin". IEA International Workshop on Geothermal Energy (Pozo Izquierdo, Spain, 2019).
- Oral: L. Catalan, D. Astrain, P. Aranguren, M. Araiz. "Comparative Analysis of Different Cooling Systems for Geothermal Thermoelectric Generators". 37th International and 16th European Conference on Thermoelectrics (Caen, France, 2018).
- Oral: L. Catalan, D. Astrain, P. Aranguren, M. Araiz. "Comparative analysis of different cooling systems for geothermal thermoelectric generators". IX Iberian and VII Ibero-American Congress in Cooling Science and Techniques Proceedings. (Valencia, Spain, 2018).
- Oral: L. Catalan, P. Aranguren, D. Astrain, M. Araiz, A. Martinez, A. Casi. "Computational Model and Experimental Validation of a Thermoelectric Generation System based on Geothermal Energy". 15th European Conference on Thermoelectrics (Padua, Italy, 2017).
- Oral: L. Catalan, D. Astrain, P. Aranguren, M. Araiz, G. Perez, A. Casi. "Thermoelectric generation based on high enthalpy geothermal resources using high efficiency heat exchangers". 15th European Conference on Thermoelectrics (Padua, Italy, 2017).

Other contributions in which the Ph.D. candidate has participated in the same period are:

- Oral: P. Aranguren, I. San Martin, L. Catalan, A. Martinez, A. Jurio, S. Diaz, G. Perez, M. Gomez, E. Barrenechea. "Initiative to Increment th number of women in STEM degrees: Women, Science and Technology Chair of the Public University of Navarre". 2020 IEEE Global Engineering Education Conference EDUCON (Porto, Portugal, 2020).
- Oral: A. Jurio, L. Catalan, I. San Martin, P. Aranguren, A. Martinez, S. Diaz, E. Barrenechea, M. Gomez, G. Perez. ""Yo quiero ser cientifica" a creative way to inspire girls in science". 2020 IEEE Global Engineering Education Conference EDUCON (Porto, Portugal, 2020).
- Oral: M. Araiz, D. Astrain, P. Aranguren, A. Martinez, L. Catalan, A. Casi. "Thermoelectric Generator Design and Experimentation for Waste-Heat Recovery in a Manufacturing Plant". 17th European Conference on Thermoelectrics (Limassol, Cyprus, 2019).
- Poster: P. Aranguren, D. Astrain, M. Araiz, L. Catalan, A. Casi, D. Sanchez, R. Llopis, R. Cabello. "Influence of the design parameters of a thermoelectric subcooler on the COP of a transcritical CO2 refrigeration system". 17th European Conference on Thermoelectrics (Limassol, Cyprus, 2019).
- Invited: D. Astrain, A. Rodriguez, A. Martinez, G. Perez, P. Aranguren, M. Araiz, L. Catalan, A. Casi, A. Garacochea. "Thermoelectric Applications: looking for new possibilities". 2nd Iberian Thermoelectric Workshop (Ciudad Real, Spain, 2019).
- Oral: D. Astrain, L. Catalan, P. Aranguren, M. Araiz, A. Merino, D. Sanchez, R. Llopis, R. Cabello, J. Catalan-Gil. "Design of a thermoelectric subcooling system to improve the efficiency of a CO2 vapour compression refrigeration system". 38th International Conference on Thermoelectrics and 4th Asian Conference on Thermoelectrics (Gyeongju, South Korea, 2019).
- Oral: P. Aranguren, D. Sanchez, M. Araiz, L. Catalan, D. Astrain. "Operation enhancement of a transcritical CO2 cooling machine using thermoelectric subcooling". 38th International Conference on Thermoelectrics and 4th Asian Conference on Thermoelectrics (Gyeongju, South Korea, 2019).
- Poster: A. Rodriguez, G. Perez, I. Beisti, L. Catalan. "Influence of temperature and aging on the thermal contact resistance in thermoelectric generators". 38th Interna-

tional Conference on Thermoelectrics and 4th Asian Conference on Thermoelectrics (Gyeongju, South Korea, 2019).

- Oral: M. Araiz, D. Astrain, P. Aranguren, A. Martinez, L. Catalan, A. Casi. "Thermoelectric generator with passive heat exchangers for waste-heat recovery in a manufacturing plant". XI National and II International Engineering Thermodynamics Congress (Albacete, Spain, 2019).
- Oral: P. Aranguren, D. Sanchez, A. Casi, M. Araiz, L. Catalan. "ITF CAN COOLER: A tailored vapor compression cooling system designed to be used at practice sessions". XI National and II International Engineering Thermodynamics Congress (Albacete, Spain, 2019).
- Invited: L. Catalan. "APERNA: a student initiative for the promotion of renewable energies". Euro-Mediterranean Cooperation on Education Research & Business in Solar Energy Workshop (Pamplona, Spain, 2019).
- Poster: M. Araiz, D. Astrain, P. Aranguren, A. Martinez, L. Catalan. "Passive Thermoelectric Generator for Waste Heat Recovery from a Combustion Chamber". 37th International and 16th European Conference on Thermoelectrics (Caen, France, 2018).
- Poster: P. Aranguren, M. Araiz, L. Catalan, O. Herrero, G. Perez, A. Rodriguez. "The importance of the assembly in thermoelectric generators". 37th International and 16th European Conference on Thermoelectrics (Caen, France, 2018).
- Oral: M. Araiz, P. Aranguren, L. Catalan, A. Martinez, D. Astrain. "Passive heat exchanger with no moving parts for thermoelectric generators". IX Iberian and VII Ibero-American Congress in Cooling Science and Techniques Proceedings. (Valencia, Spain, 2018).
- Oral: D. Astrain, L. Catalan, P. Aranguren, M. Araiz, A. Merino, D. Sanchez, R. Llopis, R. Cabello, J. Catalan-Gil. "Computational Study of a CO2 Cooling System with Thermoelectric Subcooling". IX Iberian and VII Ibero-American Congress in Cooling Science and Techniques Proceedings (Valencia, Spain, 2018).
- Invited: L. Catalan. "Geothermal electrical generation". Workshop on the Possibilities of geothermal energy in Navarre (Pamplona, 2018).
- Oral: F.J. Iñigo, L. Catalan, A. Martinez, P. Aranguren, D. Astrain. "Design and optimization of a cooling system for the manufacturing of hot melt adhesives by

means of the development and validation of a computational model". 10th National Engineering Thermodynamics Congress (Lleida, Spain, 2017).

Participation in research projects

As stated before, the research project in which the present Ph. D. dissertation has been encompassed is ELECTROVOLCAN: "Design and experimental development of thermoelectric generators for geothermal anomalies of volcanic origin: application to the volcanic systems of Timanfaya (Lanzarote) and Teide (Tenerife)" funded by the Spanish Ministry of Science, Innovation, and Universities (RTC-2017-6628-3) with 1 254 649 € for the period between January 2018 and June 2021.

Apart from this project, the Ph. D. candidate has also taken part in the following research public projects:

- LOWTEWI: "Greenhouse attenuation in stand-alone refrigeration systems" funded by the Spanish Ministry of Science, Innovation, and Universities (RTI2018-093501-B-C22). January 2019 – December 2021.
- TERMOFLEX: "Flexible Thermoelectric Devices" funded by the Government of Navarre (PC023-024). March 2018 – December 2019.
- REHEAT: "Advanced thermoelectric generators to make use of waste heat" funded by the Government of Navarre (0011-1365-2018-000101). March 2018 – December 2019.
- MEDSOL: "Strengthening Capacities of South-Mediterranean Higher Education Institutions in the field of Solar Energy" funded in the Erasmus+ Program (573722-EPP-1-2016-1-FR-EPPKA2-CBHE-JP).
- Bi-Al: "Aluminum integral forks by the combination of injection in semi solid state and high pressure" funded by the Government of Navarre (0011-1365-2018-000098). March 2018 - December 2019.
- SIGER: "Systems for electrical generation from waste heat: application to the hot gases from houses and industries" funded by the Spanish Ministry of Economy and Competitiveness (DPI2014-53158-R). January 2015 – December 2018.
- HOTMELT: "New Flexible Technologies for the Manufacture of Hot Melt Adhesives" funded by the Government of Navarre (0011-1365-2016-000094) July 2016 – April 2018.

Supervision of Bachelor's Thesis

During the fulfillment of the thesis, the following Bachelor's thesis have been supervised:

- A. Azcona, "Estudio y diseño del intercambiador del lado frío de un prototipo de generación termoeléctrica geotérmico", September 2020.
- J.M. Fernandez, "Caracterización y diseño de generadores termoeléctricos para abastecimiento de estaciones de vigilancia volcánica", June 2020.
- "Diseño de un generador termoeléctrico geotérmico: optimización del intercambiador del lado caliente", June 2020.
- A. Yabar, "Caracterización térmica de intercambiadores de calor bifásicos en condiciones extremas", June 2019.
- D. Alonso, "Estudio de sistemas de intercambio de calor aplicados a la generación termoeléctrica a partir de calor geotérmico", June 2018.

7.3 Future Lines

As exposed before, the work developed in the present Ph. D. dissertation has continuity within the research project ELECTROVOLCAN and the Fuentes Dutor scholarship. Therefore, most of the recommendations proposed in this last section are indeed considered in the objectives of these projects.

The proposed recommendations have been divided into the two applications analyzed. Hence, for the medium–scale geothermal power generation, the future lines to be developed are:

1. Once the prototypes have been characterized at the laboratory, it is necessary to install them at Timanfaya National Park, so that their behavior under real conditions, with the hot geothermal gases, can be characterized. The estimated installation date is September 2020.

2. The previous prototypes were oriented to the location known as *Casa de los Camelleros* within Timanfaya National Park. Therefore. it is also necessary to design, build, characterize, and install a device in *Islote Hilario*, where the temperature and velocity of the gases are greater, which suggests a higher generation.

3. Due to the higher temperatures available at Hilario, it is also interesting to study the use of other thermoelectric modules more suitable for these conditions and that permit obtaining a higher generation.

4. The field installation of the prototypes will permit figuring out improvements to be made in the prototypes, similar to what occurred with the Teide's devices. Based on this knowledge, a final design for each location needs to be developed.

5. With the final design of the generators, the ELECTROVOLCAN project has the objective to reach a power installation of 1 kW by installing several prototypes. Moreover, it also contemplates the estimation of its cost and its comparison with other existing technologies.

6. Lastly, it is expected to complement the former geothermal plant with photovoltaic panels so that the visitor's center located at Timanfaya National Park can entirely be powered with renewable sources, avoiding using fossil fuels as occurs nowadays. The procedure for this future project is already in operation.

On its behalf, in the case of autonomous volcanic monitoring stations, the proposed recommendations are summarized as follows:

1. In spite of the fact that the prototype has been in operation for more than 8 months without showing signs of degradation, a study of the environmental stresses on the performance of thermoelectric modules of different materials is recommended, especially due to the harsh volcanic environment. Hence, accelerated corrosion methods that simulate the conditions available at the volcanoes would need to be combined with techniques of characterization of the thermoelectric modules, such as the impedance spectroscopy. This line is expected to be performed in collaboration with Cardiff University.

2. Apart from the study of thermoelectric modules degradation, the resistance of different materials and coatings also needs to be studied. For this purpose, accelerated corrosion techniques such as the Kesternich test would be again required.

3. Since in the case of fumaroles, the geothermal anomalies are located just a few centimeters deep, it could be interesting to study other alternatives for the hot side heat exchanger, the most critical one regarding corrosion. Thus, one possibility could be to analyze the behavior of a solid bar as hot side heat exchanger, examining if the corrosion resistance gain compensates with respect to the expected thermal resistance loss.

4. The viability of stand–alone volcanic vigilance stations powered by thermoelectric generators was proven by simulating the power consumption of their devices. Therefore, a step further would be to supply power to a real monitoring station.

5. The last future line that arises from the second application of this Ph. D. dissertation deals with the installation of the developed device in an even more extreme environment, as it is the case of Deception Island, a volcanic island located in Antarctica where the absence of sun is a reality during several months and extremely low temperatures are registered. Spain has a military base on this island, which permits the development of several research projects during the austral summer. Therefore, it is intended to request a project in this regard.

This thesis has been subsidized by the program for Training University Teachers of the Spanish Ministry of Science, Innovation and Universities with the scholarship FPU 16/05203. Moreover, funding from the same ministry has been used under the research and development project RTC–2017–6628–3.